Raquel Patrícia Gomes Silvestre Vinhas

Mestre em Biologia Celular

Gold nanoparticles for nanotheranostics in leukemia – Addressing Chronic Myeloid Leukemia

Dissertação para obtenção do Grau de Doutor em

Biociências Moleculares

Orientador: Prof. Doutor Pedro Miguel Ribeiro Viana Baptista, Professor Catedrático, Faculdade de Ciências e Tecnologia da Universidade Nova de Lisboa
Co-orientadora: Prof. Doutora Maria Alexandra Núncio de Carvalho Ramos Fernandes, Professora Auxiliar, Faculdade de Ciências e Tecnologia da Universidade Nova de Lisboa

Júri:

Presidente: Prof. Doutor Paulo Manuel Assis Loureiro Limão-Vieira
Vogais: Prof. Doutora Cecília Maria Pereira Rodrigues
Prof. Doutor José Alexandre de Gusmão Rueff Tavares
Prof. Doutor Pedro Miguel Ribeiro Viana Baptista
Prof. Doutor João Nuno Sereno de Almeida Moreira

FACULDADE DE CIÊNCIAS E TECNOLOGIA
UNIVERSIDADE NOVA DE LISBOA

Maio 2018

ACKNOWLEDGEMENTS

This thesis was most definitely a joint effort. Each person that crossed my path during this journey had a part in it and the following words cannot express the amount of gratitude I share with you.

First, I acknowledge my supervisors, Prof. Pedro Baptista and Prof. Alexandra Fernandes, for having accepted me for a lab rotation, four years ago, without knowing the first thing about me. That week turned into four fruitful years, which could not have happened if it was not for your trust and belief in my abilities. I still feel very lucky to be in the intersection of your work and for all the autonomy and opportunities you gave me. Though our discussions on scientific issues were enlightening, our best conversations far surpassed the limits of science and occasionally involved a glass of wine, which, as we all know, I never refuse!

Prof. Pedro Baptista, thank you for taking a chance on me, pushing me further and, most of all, for the ambitious directions you always envisioned for this project. Your positivity was paramount and throughout the years that same positivity and scientific spirit passed on to me.

Prof. Alexandra Fernandes, thank you for looking at this project with such joy. Most of all, thank you for the many conversations that made me persevere. You always had the right words at the right time. More than a supervisor, you were a guiding friend.

I express my gratitude to the staff at Hospital dos Capuchos: Dr. Aida Botelho de Sousa, Dr. Patrícia Ribeiro, Alexandra Lourenço and Susana Santos. The clinical perspective you provided during this thesis made me look at results in a different way. It is all about the patients! The most rewarding feeling I could have found through these years is that our collaboration might have helped a few people.

I acknowledge all collaborators at CEMOP and CENIMAT, specially Prof. Hugo Águas and Pedro Alves, for providing all the required resources and knowledge for the microfluidics experiments. Pedro Alves, thank you as well for your kindness, advice and, above all, I praise your patience.

"Friends are family you choose!" This is the best cliché to describe how I feel about the people I have met since I came to Caparica. Fábio, Bruno, Milton, Pedrosa, Fabiana, Ana Sofia "Catraia", Rita M., Sara, Catarina, Luís, Letícia, Larguinho and Rita C., you are very unique! I remember how lost I was at the start (and other times!) of this thesis, and somehow you stopped everything to help me. I cannot forget, as well, all the young brains I had the pleasure to meet: Beatriz C., Andreia C., Bárbara, Inês, Beatriz O., Catarina B. and Cynthia.

Andreia, the time that we have known each other has taught me many things. One of them is that comfort can come from the most unusual places. Never had I thought that we would be flatmates for this long and how much fun we were going to have together. I am sure many adventures are still yet to come.

I thank my family and closest friends for always expressing how proud they are of me. This achievement is mostly yours. It is almost impossible to fail when one is surrounded by such caring, strong and resilient people. I thank my father for the enormous support along the way. I emphasize, as well, the major part my sister Cláudia had in this period, particularly when I doubted everything. You know me better than anyone. After all, you have 34 years of experience on the job. Thank you so much!

Throughout the course of these PhD thesis, I have learnt a lot on cancer genetics and nanotechnology, however I have to confess that my most important knowledge has been given to me by my mother since the very beginning. You showed me how to be kind and independent. You are my best role model.

RESUMO

A leucemia é um tipo de cancro que se inicia na medula óssea e resulta na produção desregulada de glóbulos brancos imaturos (células leucémicas). A leucemia mieloide crónica (LMC) é o seu subgrupo mais homogéneo, afetando aproximadamente 1.5 milhões de pacientes no mundo. Praticamente todos os casos apresentam a translocação t(9;22)(q34.1;q11.2) e a consequente fusão genética *BCR-ABL1*, que codifica a tirosina cinase BCR-ABL1. O sucesso do tratamento da LMC advém do seu diagnóstico precoce e do desenvolvimento de inibidores de tirosina cinase eficazes.

A nanotecnologia apresenta um enorme potencial para suprimir as lacunas dos procedimentos convencionais usados no combate à LMC. As nanopartículas de ouro (AuNPs), em particular, possuem propriedades óticas relevantes para deteção *ex vivo* de biomarcadores, mas podem funcionar também *in vivo* numa estratégia de teranóstico, combinando tratamento e diagnóstico de acordo com o perfil molecular do paciente.

Neste estudo, foi otimizado um ensaio colorimétrico, usando nanossondas de ouro, para a deteção da isoforma mais frequente de *BCR-ABL1* (e14a2), tendo sido posteriormente validado em amostras clínicas. Este método simples e direto permitiu a deteção de amostras de RNA que expressam e14a2, com precisão e especificidade. O ensaio foi ainda incorporado num chip de microfluídica, traduzindo-se em resultados mais rápidos recorrendo a volumes mais baixos de amostra, devido à escala e estrutura do dispositivo.

Adicionalmente, foi desenhada uma nova estratégia terapêutica para combater os mecanismos de resistência ao tratamento de primeira linha para LMC: imatinib (IM). O silenciamento *in vitro* de *BCR-ABL1* foi eficaz, usando AuNPs funcionalizadas com polietilenoglicol e oligonucleotídos de DNA em cadeia simples, *antisense* e em formato *hairpin*. A nanoformulação permitiu redução da dose de IM, numa estratégia combinada, e potenciou um decréscimo da viabilidade de células K562 resistentes a IM.

Os resultados desta tese demonstram a adequação e flexibilidade das AuNPs como ferramentas para nanoteranóstico, diagnóstico e tratamento personalizado de LMC.

Termos chave:

Leucemia, LMC, BCR-ABL1, nanopartículas de ouro, nanoteranóstico

ABSTRACT

Leukemia is a type of cancer that initiates in the bone marrow and results in the unregulated production of immature white blood cells (leukemic cells). The most homogenous subgroup of the disease is chronic myeloid leukemia (CML) accounting for nearly 1.5 million patients worldwide. Virtually all cases harbor the genetic translocation t(9;22)(q34.1;q11.2) resulting in the *BCR-ABL1* gene fusion, that encodes for BCR-ABL1 tyrosine kinase. CML treatment success relies on an early diagnosis and the intense research towards developing effective tyrosine kinase inhibitors (TKI).

Nanotechnology offers unprecedent advantages to tackle the shortcomings of conventional procedures for the management of CML. Gold nanoparticles (AuNPs) have unique optical properties suitable for *ex vivo* biosensing applications, but can also function *in vivo* as nanocarriers in a theranostic approach that links treatment with diagnosis according to patient's molecular profile.

A gold nanoprobe (Au-nanoprobe) colorimetric assay was optimized for the detection of the most frequent *BCR-ABL1* isoform (e14a2) and was validated on fully characterized clinical samples. This simple and cheap method enabled the direct detection of e14a2-expressing RNA samples, with accuracy and high specificity. The Au-nanoprobe assay was translated onto a microfluidics chip, resulting in a faster outcome with smaller sample volumes, due to the scale and design of the device.

Additionally, a new therapeutic strategy was designed to overcome CML resistance to first line therapy, such as imatinib (IM). *BCR-ABL1* gene silencing was effectively achieved *in vitro*, using AuNPs functionalized with polyethylene glycol and a hairpin-shaped antisense single stranded DNA (ssDNA) oligonucleotide. Furthermore, the nanoconstruct allowed to reduce the dose of IM, when tested in a combined approach, and potentiated a viability decrease of K562 cells resistant to IM.

The results of this thesis strongly suggest that AuNPs are a suitable and flexible tool for CML nanotheranostics, improving detection and a personalized treatment strategy.

Keywords:

Leukemia, CML, BCR-ABL1, gold nanoparticles, nanotheranostics

x

LIST OF PUBLICATIONS

Included in this thesis:

- **Vinhas R**, Cordeiro M, Carlos FF, Mendo S, Fernandes AR, Figueiredo S, Baptista PV. 2015. Gold nanoparticle-based theranostics: disease diagnostics and treatment using a single nanomaterial. Nanobiosensors in Disease Diagnosis. 4:11-23.

- Larguinho M, Canto R, Cordeiro M, Pedrosa P, Fortuna A, **Vinhas R**, Baptista PV. 2015. Gold nanoprobe-based non-crosslinking hybridization for molecular diagnostics. Expert Review of Molecular Diagnostics. 15(10):1355-1368.

- Pedrosa P, **Vinhas R**, Fernandes AR, Baptista PV. 2015. Gold nanotheranostics: proof-of-concept or clinical tool? Nanomaterials. 5(4):1853-1879.

- **Vinhas R**, Tolmatcheva A, Canto R, Ribeiro P, Lourenço A, Sousa AB, Baptista PV, Fernandes AR. 2016. A novel mutation in *CEBPA* gene in a patient with acute myeloid leukemia. Leukemia & Lymphoma. 57(3):711-713.

- **Vinhas R**, Correia C, Ribeiro P, Lourenço A, Sousa AB, Fernandes AR, Baptista PV. 2016. Colorimetric assessment of *BCR-ABL1* transcripts in clinical samples via gold nanoprobes. Analytical and Bioanalytical Chemistry. 408(19):5277-5284.

- Veigas B, Pinto J, **Vinhas R**, Calmeiro T, Martins R, Fortunato E, Baptista PV. 2017. Quantitative real-time monitoring of RCA amplification of cancer biomarkers mediated by a flexible ion sensitive platform. Biosensors and Bioelectronics. 91:788-795.

- **Vinhas R**, Cordeiro M, Pedrosa P, Fernandes AR, Baptista PV. 2017. Current trends in molecular diagnostics of chronic myeloid leukemia. Leukemia & Lymphoma. 58(8):1791-1804.

- **Vinhas R**, Fernandes AR, Baptista PV. 2017. Gold nanoparticles for *BCR-ABL1* gene silencing: Improving tyrosine kinase inhibitor efficacy in chronic myeloid leukemia. Molecular Therapy - Nucleic Acids. 7:408-416.

- **Vinhas R**, Mendes R, Fernandes AR, Baptista PV. 2017. Nanoparticles – Emerging potential for managing leukemia and lymphoma. Frontiers in Bioengineering and Biotechnology. 5(79):1-10.

- Alves PU, **Vinhas R**, Fernandes AR, Birol SZ, Trabzon L, Bernacka-Wojcik I, Igreja R, Lopes P, Baptista PV, Águas H, Fortunato E, Martins R. 2018. Multifunctional microfluidic chip for optical

nanoprobe based RNA detection – application to Chronic Myeloid Leukemia. Scientific reports. 8(1):381.

- Matias AS, **Vinhas R**, Mendes R, Fernandes AR, Baptista PV. 2018. Nanoparticles as emerging diagnostic tools in liquid tumours. European Medical Journal. 2(1):80-87.

- **Vinhas R**, Lourenço A, Santos S, Ribeiro P, Silva M, Sousa AB, Baptista PV, Fernandes AR. A double Philadelphia chromosome-positive chronic myeloid leukemia patient, co-expressing P210$^{BCR-ABL1}$ and P195$^{BCR-ABL1}$ isoforms. [Submitted to Haematologica]

- **Vinhas R**, Lourenço A, Santos S, Lemos M, Ribeiro P, Sousa AB, Baptista PV, Fernandes AR. A novel *BCR-ABL1* mutation in a patient with Philadelphia chromosome-positive B-cell acute lymphoblastic leukemia. [Submitted to Leukemia and Lymphoma]

LIST OF ABBREVIATIONS AND SYMBOLS

ABC – ATP-binding-cassette

ABL1 − Abelson murine leukemia 1 gene

Abs – absorbance

AFC − 7-amino-4-trifluoromethyl coumarin

ALL – acute lymphocytic leukemia

AlloSCT – allogeneic stem cell transplantation

AML – acute myeloid leukemia

AP – accelerated phase

AUC – area under the curve

Au-nanobeacon – gold nanobeacon

Au-nanoconjugate – gold nanoconjugate

Au-nanoprobe – gold nanoprobe

AuNP – gold nanoparticle

AuNP@PEG – gold nanoparticles functionalized with polyethylene glycol

AuNP@PEG@e14a2 – gold nanoparticles functionalized with polyethylene glycol and e14a2 antisense ssDNA oligonucleotide

AuNP@PEG@MYC – gold nanoparticles functionalized with polyethylene glycol and *c-MYC* antisense ssDNA oligonucleotide

B-ALL – B-cell acute lymphocytic leukemia

BAX – Bcl-2-associated X gene

BC – blast crisis

BCL-2 – B-cell lymphoma 2 gene

BCR − breakpoint cluster region gene

bZIP − basic leucine zipper domain

C/EBPα − CCAAT/enhancer binding protein α

CCyR – complete cytogenetic response

CEBPA – CCAAT/enhancer binding protein α gene

CEMOP − Center of Excellence in Microelectronics Optoelectronics and Processes

CENIMAT – Materials Research Center

CHLC – Centro Hospitalar de Lisboa Central

CHR – complete hematologic response

CLL – chronic lymphocytic leukemia

CML – chronic myeloid leukemia

c-MYC – avian myelocytomatosis viral oncogene homolog

CP – chronic phase

CT – computed tomography

Ct – threshold cycle

CTC – circulating tumor cell

dB – decibel

DEPC – diethyl pyrocarbonate

DLS – dynamic light scattering

DMEM – Dulbecco's modified Eagle medium

DMR – deep molecular response

DMSO – dimethyl sulfoxide

DTT – dithiothreitol

EDTA – ethylenediaminetetraacetic acid

EGF – epithelial growth factor

ELN – European LeukemiaNet

EMA – European Medicines Agency

EPR – enhanced permeability and retention

FBS – fetal bovine serum

FDA – US food and drug administration

FISH – fluorescence *in situ* hybridization

FRET - Förster resonance energy transfer

GRP – gastrin-releasing peptide

IM – imatinib

IR – infrared

IRIS – Study of Interferon and STI571

IS – international scale

K562-IM – K562 cells resistant to imatinib

LED – light-emitting diode

LOD – limit of detection

MB – methylene blue

MCyR – major cytogenetic response

MDR – multidrug resistance

MMR – major molecular response

MRD – minimal residual disease

MRI – magnetic resonance imaging

MTS – (3-(4,5-dimethylthiazol-2-yl)-5-(3-carboxymethoxyphenyl)-2-(4-sulfophenyl)-2H-tetrazolium)

NCCN – National Comprehensive Cancer Network

NCL – non-crosslinking

NGS – next generation sequencing

NIR – near infrared

NNI – National Nanotechnology Initiative

NP – nanoparticle

NPV – negative predictive value

OCT1 – organic cation transporter 1 gene

PAT – photoacoustic tomography

PBS – phosphate buffer saline

PDMS – polydimethylsiloxane

PDT – photodynamic therapy

PEG – polyethylene glycol

PET – positron emission tomography

Ph – Philadelphia chromosome

pHLIP – pH low insertion peptides

PI – polydispersity index

PMSF – phenylmethylsulfonyl fluoride

PNB – plasmonic nanobubbles

POC – point-of-care

PPV – positive predictive value

PS – photosensitizer

PTT – photothermal therapy

PTD – photodynamic therapy

QD – quantum dot

qPCR – quantitative polymerase chain reaction

rAbs – absorbance ratio

RCA – rolling circle amplification

RGD – arginylglycylaspartic acid

rhTNF – recombinant human tumor necrosis factor

RPMI – Roswell Park Memorial Institute medium

R_s – detection response

RT-PCR – reverse transcription polymerase chain reaction

SDS-PAGE – sodium dodecyl sulfate polyacrylamide gel electrophoresis

SERS – surface-enhanced Raman scattering

SLL – small lymphocytic leukemia

SNP – single nucleotide polymorphism

SNR – signal-to-noise ratio

SPECT – single-photon positron emission tomography

SPIO – super-paramagnetic iron oxide

SPR – surface plasmon resonance

SSC – side scatter intensity

SSC-A – side scatter peak area

TAD – transactivation domain

TBST – tris-buffered saline with tween 20

TEM – transmission electron microscopy

Tf – transferrin

TKI – tyrosine kinase inhibitors

UCIBIO – Research Unit on Applied Molecular Biosciences

US – ultrasound

UV – ultraviolet

UV-Vis – ultraviolet-visible

WHO – World Health Organization

TABLE OF CONTENTS

LIST OF FIGURES

LIST OF TABLES

Para aquela que me ensinou a rir, Mãe

"Well I can ease your pain
Get you on your feet again
Relax
I'll need some information first
Just the basic facts."

Comfortably Numb, Pink Floyd, 1979

CHAPTER 1 – **INTRODUCTION**

Part of the literature review presented in this chapter has been published, whole or in part, elsewhere. The author of this thesis reviewed and critically discussed the references cited in the text.

- **Vinhas R**, Cordeiro M, Carlos FF, Mendo S, Fernandes AR, Figueiredo S, Baptista PV. 2015. Gold nanoparticle-based theranostics: disease diagnostics and treatment using a single nanomaterial. Nanobiosensors in Disease Diagnosis. 4:11-23.

- Larguinho M, Canto R, Cordeiro M, Pedrosa P, Fortuna A, **Vinhas R**, Baptista PV. 2015. Gold nanoprobe-based non-crosslinking hybridization for molecular diagnostics. Expert Review of Molecular Diagnostics. 15(10):1355-1368.

- Pedrosa P, **Vinhas R**, Fernandes AR, Baptista PV. 2015. Gold nanotheranostics: proof-of-concept or clinical tool? Nanomaterials. 5(4):1853-1879.

- **Vinhas R**, Cordeiro M, Pedrosa P, Fernandes AR, Baptista PV. 2017. Current trends in molecular diagnostics of chronic myeloid leukemia. Leukemia & Lymphoma. 58(8):1791-1804.

- **Vinhas R**, Mendes R, Fernandes AR, Baptista PV. 2017. Nanoparticles – Emerging potential for managing leukemia and lymphoma. Frontiers in Bioengineering and Biotechnology. 5(79):1-10.

- Matias AS, **Vinhas R**, Mendes R, Fernandes AR, Baptista PV. 2018. Nanoparticles as emerging diagnostic tools in liquid tumours. European Medical Journal. 2(1):80-87.

1

1.1 Leukemia

Hematologic malignancies are the most common type of cancer among children and young adults, and comprise diseases such as leukemia, lymphoma and myeloma, which affect the bone marrow, lymphatic system and blood cells.[1] The sequential stages of hematopoietic differentiation provide multiple occasions for the occurrence of mutations and other disruptive events that lead to distinct tumor subtypes and clinical presentations.[2] In fact, the heterogeneity of tumors of the hematopoietic system presents unique challenges for current diagnosis and treatment.[3–6]

Leukemia is a clonal disorder originated in the bone marrow during hematopoiesis and is characterized by the unregulated proliferation of poorly differentiated white blood cells. Prognosis and treatment of the disease depend highly on the type of leukemia, the extent of the disease, age and patient history. Most patients are treated with chemotherapy/targeted therapy, although a small portion ultimately undergoes radiation therapy and/or bone marrow transplantation.[7]

Though hematological malignances constitute no more than 10 % of all cancers worldwide, leukemia research has attracted considerable attention. This is believed to result from the combination of several factors: 1) the blood-borne nature of the disease and accessibility of relevant tissues; 2) the fact that hematopoiesis has been thoroughly dissected, thus prompting modelling of leukemogenesis; 3) the emotional impact of a lethal cancer of childhood, since acute leukemia is the most common pediatric cancer in developed societies, which engrossed massive funding opportunities; and 4) the early identification of chromosomal translocations and fusion genes in leukemia karyotypes.[7]

1.1.1 Classification

Classification of leukemia is based on the type of cell affected (myeloid or lymphoid) and the degree of cell proliferation (acute or chronic), resulting in four main categories.[2] Acute myeloid leukemia (AML) is the most common type in adults and acute lymphocytic leukemia (ALL) is more prevalent among pediatric patients.[1] Chronic myeloid leukemia (CML) is a myeloproliferative disorder with an annual incidence of 1-2 cases per 100 000 adults, accounting for 15-20 % of newly diagnosed cases of leukemia in adults.[1,8]

The distinction between lymphomas and lymphoid leukemias (both included in lymphoid-derived neoplasms) should be carefully addressed since they are closely related. In fact, chronic lymphocytic leukemia (CLL) and small lymphocytic lymphoma (SLL) are essentially the same disease, where the only difference is the location of the primarily occurrence of cancer. In CLL, a significant number of the anomalous lymphocytes are found in the blood, bone marrow and lymphoid tissue; in SLL, the bulk of the disease is in the lymph nodes, bone marrow, and other lymphoid tissues, but is rarely detected in peripheral blood. Both conditions are tackled the same way, using immunomodulating agents, monoclonal antibodies or kinase inhibitors.[9]

Following clinical, morphological and immunophenotypic diagnosis,[10] genetics plays an important role in the classification of these diseases and commonly assist risk stratification, from poor to favorable prognosis (Table 1.1).[11,12]

AML is the most clinically and biologically heterogeneous group of leukemias. Many of the variations that underlie the pathogenesis of the disease include chromosomal additions, deletions, and translocations, as well as small-scale mutations in oncogenes (Table 1.1). Since disease progression and treatment response are largely dependent on these genetic events, proper cytogenetic and molecular testing is imperative for patient evaluation and provide insights into critical pathways involved in AML pathogenesis. Small-scale mutations on genes encoding for nucleophosmin 1 (*NMP1*), fms-related tyrosine kinase 3 (*FLT3*) and CCAAT/enhancer-binding protein α (*CEBPA*) are in fact used to define AML sub-classes according to World Health Organization (WHO) guidelines. *CEBPA* encodes for a transcription factor that is critical for myeloid differentiation. Point mutations on this gene confer a relatively good prognosis for AML patients, but this seems only true for cases with biallelic variations.[13–16]

CML is a good example of how hematological diseases have greatly benefited from the advance of cytogenetic and molecular methodologies. It was the first cancer in which a unique chromosomal abnormality was identified, t(9;22)(q34.1;q11.2) – Philadelphia chromosome (Ph) - and the associated *BCR-ABL1* gene, providing a specific target for disease treatment (Table 1.1).[17] Tyrosine kinase inhibitors (TKIs) target the dysregulated kinase activity of the fusion protein encoded by *BCR-ABL1*.[18,19]

Table 1.1 Common genetic abnormalities associated to leukemia.[11,20]

Subtype	Frequent genetic biomarkers
AML	- t(8;21)(q22;q22); *RUNX1-RUNX1T1* - inv(16)(p13q22) or t(16;16)(p13;q22); *CBFB-MYH11* - t(15;17)(q22;q12); *PML-RARA* - t(9;11)(p21;q23); *MLLT3-KMT2A* - t(6;9)(p23;q34); *DEK-NUP214* - inv(3)(q21q26) or t(3;3)(q21;q26); *RPN-EVI1, GATA2, MECOM* - t(1;22)(p13;q13); *RBM15-MKL1* - t(9;22)(q34;q11); *BCR-ABL1* - *CEBPA, NPM1, and FLT3* mutations predict response to chemotherapy for cytogenetically normal AML patients
CML	- t(9;22)(q34;q11); *BCR-ABL1*

B-cell ALL	- t(9;22)(q34;q11)*; BCR-ABL1*
	- t(v;11q23)*; KMT2A*
	- t(12;21)(p13;q22)*; ETV6-RUNX1*
	- t(5;14)(q31;q32); *IL3-IGH*
	- t(1;19)(q23;p13)*; TCF3-PBX1*
	- Hyperdiploidy
	- Hypodiploidy
T-cell ALL	- *TAL1* gene rearrangements (1p32)
	- *TLX1* gene rearrangements (10q24)
	- *LMO2* gene rearrangements (11p13)
	- t(5;14)(q35;q32)*; TLX3- BCL11B*
	- t(10;11)(p12;q14)*; PICALM- MLLT10*
	- *NUP214- ABL1* fusion and amplification
	- *KMT2A* gene rearrangements (11q23)
CLL (or SLL)	- del(13q)
	- trisomy 12
	- del(11q); *ATM*
	- del(17p); *TP53*

ALL, acute lymphocytic leukemia; AML, acute myeloid leukemia; CLL, chronic lymphocytic leukemia; CML, chronic myeloid leukemia; SLL, small lymphocytic leukemia.

Genes: *ABL1*, Abelson murine leukemia 1; *ATM*, ataxia-telangiectasia mutated; *BCL11B*, B-cell lymphoma/leukemia 11B; *BCR*, breakpoint cluster region; *CBFB*, core-binding factor ß; *CEBPA,* CCAAT/enhancer-binding protein α; *DEK,* DEK proto-oncogene; *ETV6*, erythroblast transformation-specific translocation variant 6; *EVI1*, ecotropic virus integration site 1; *FLT3,* fms-related tyrosine kinase 3; *GATA2*, GATA-binding factor 2; *IGH*, Immunoglobulin heavy-chain; *IL3*, interleukin-3; *KMT2A*, lysine methyltransferase 2A; *LMO2*, LIM-domain only 2; *MECOM,* MDS1 and EVI1 complex locus; *MKL1*, megakaryoblastic leukemia 1; *MLLT10*, histone lysine methyltransferase DOT1L cofactor; *MLLT3*, super elongation complex subunit; *MYH11*, myosin heavy chain 11; *NPM1*, nucleophosmin 1; *NUP214*, nucleoporin 214; *PBX1*, pre B cell leukemia homeobox 1; *PICALM*, phosphatidylinositol binding clathrin assembly protein; *PML*, promyelocytic leukemia; *RARA,* retinoic acid receptor α; *RBM15,* RNA binding motif protein 15; *RPN*, ribophorin I; *RUNX1*, runt related transcription factor 1; *RUNX1T1,* RUNX1 translocation partner 1; *TAL1*, TAL bHLH transcription factor 1, erythroid differentiation factor; *TCF3*, transcription factor 3; *TLX1/3*, T-cell leukemia homeobox 1 or 3; *TP53*, tumor protein p53.

1.1.2 Chronic myeloid leukemia

Originally named chronic granulocyte leukemia, the first documented cases of CML are believed to date back to 1840s.[21,22] Since then, there has been a solid evolution in the strategies for laboratorial diagnostics of the disease, from cytogenetics to molecular characterization that support therapeutic decisions, which ought to be tailored so as to enhance therapy success. CML is also paradigmatic in the straightforward relation between early and accurate hematologic, cytogenetic and molecular characterization, and patients' prognosis.[17]

1.1.2.1 Molecular biology and disease progression

The molecular hallmark of CML is the Ph chromosome - a shortened and truncated version of chromosome 22 present in at least 95 % of patients.[23] This abnormality occurs in the myeloid lineage of hematopoiesis and results in the reciprocal translocation of genetic material between the long arms of chromosomes 9 and 22 - t(9;22)(q34.1;q11.2). The subsequent fusion of the Abelson murine leukemia (*ABL1*) gene on chromosome 9 (region q34) with the breakpoint cluster region (*BCR*) gene on chromosome 22 (region q11), results in the *BCR-ABL1* oncogene.[23,24] This chimeric version of ABL1 has unregulated activity and triggers a cascade of events that culminate in malignant cell transformation. The constitutive expression of the active protein kinase leads to the phosphorylation of a series of intracellular substrates, perturbing multiple signaling pathways, including the Ras/mitogen-activated protein kinases (Ras/MAPK), phosphatidylinositol-3-kinase/protein kinase B (PI3K/Akt), and Janus kinase 2/signal transducer and activator of transcription 5 (Jak2/Stat5) pathways. This phosphorylation cascade promotes cell growth, survival advantage, cytokine independence, protection against apoptosis and causes the clonal expansion of fully differentiated myeloid cells.[25–27]

Although CML molecular hallmarks have been deeply studied, chromosome instability originates a range of *BCR-ABL1* variants. Due to three well-defined breakpoint regions in the *BCR* gene (*m-BCR*, *M-BCR* and *μ-BCR*), the product of the *BCR-ABL1* fusion oncogene may exist in three principal forms of molecular weight: 190, 210, and 230 kDa, containing the same region of the ABL1 tyrosine kinase at the C-terminal but including different portions of BCR sequence at the N-terminal.[28,29] This reciprocal translocation during hematopoiesis combined with alternative splicing events may result in multiple *BCR-ABL1* transcripts, all encoding proteins with high tyrosine kinase activity (Figure 1.1).[30] Nevertheless, the majority of Ph-positive (Ph+) CML patients (~95 % harbor the 210 kDa protein (P210$^{BCR-ABL1}$) translated from either the e13a2 (b2a2) or e14a2 (b3a2) fusion transcripts. Less frequent in CML is the 190 kDa fusion protein (P190$^{BCR-ABL1}$) translated from an e1a2 junction (<5 %). *ABL1* breakpoints can occur anywhere over a larger area at its 5' end but occur invariably between exon 1a and exon 2 (Figure 1.1).[29] Additional rare *BCR–ABL1* fusion transcripts (<1 %) characterized by particular phenotypes have been described, such as e14a3 (P210), e13a3 (P210), e1a3 (P190), e19a3 (P230), e6a2 (P195), e8a2 (P200) and e18a2 (P225) (Figure 1.1).[30–32]

There is a high controversy between the various published studies concerning the type of fusion transcript (e.g., e13a2 *vs* e14a2) and its influence in CML phenotype.[29,33–35] Balatzenko *et al* demonstrated that CML patients with high levels of expression of the multidrug resistance 1 gene (*MDR1*) and presenting the e14a2 transcript had a significantly higher platelets count and a lower white blood cell count compared to e13a2 patients.[33] More recently, Hanfstein *et al* stated that e13a2 and e14a2 CML might represent distinct biological entities but the clinical outcome under treatment was comparable and no risk prediction could be made according to *BCR-ABL1* transcript type at diagnosis.[34]
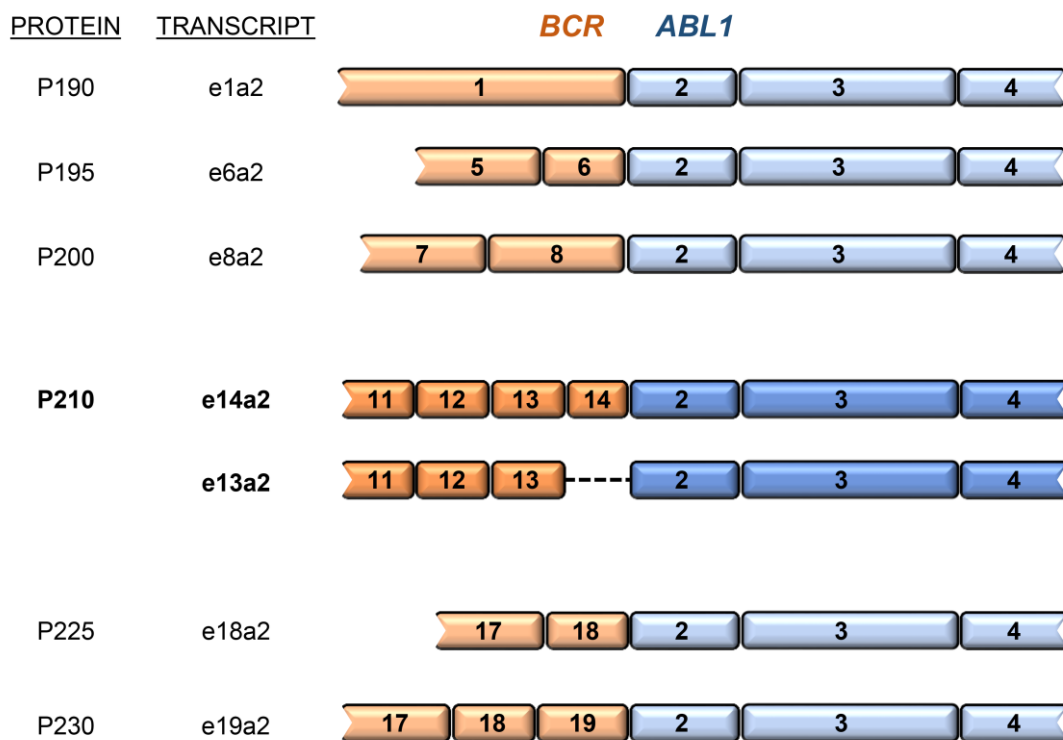
Figure 1.1 Structure of *BCR-ABL1* isoforms. P210[BCR-ABL1] isoforms represent 95 % of Ph+ CML cases and may derive from two transcript types (e14a2 or e13a2) due to alternative splicing events. Alternative splicing may also occur to *ABL1* exons 2 or 3, thus originating additional (rare) isoforms of the gene. Nomenclature of BCR-ABL1 protein isoforms relates to their final protein size (e.g. P210 = 210 kDa).[29–31]

CML onset comprises three distinct phases: chronic (CP), accelerated (AP) and blast crisis (BC).[36] The disease is usually diagnosed in CP (85 % of newly diagnosed cases), which is relatively long-lasting (three to five years, without treatment) and is characterized by the accumulation of myeloid progenitors

(blast cells) in the blood, bone marrow and spleen.[36] Despite being generally asymptomatic, there are common symptoms in this stage, such as fatigue, weight loss, illness and general pain, due to anemia and splenomegaly (enlarged spleen - detected in 50-60 % of cases).[37] Over the years it may progress into AP with a rapid expansion of circulating myeloid elements. Ultimately, CML may evolve to BC, which is characterized by differentiation retention in the myeloid or lymphoid lineage, resembling an acute leukemia with a predominant myeloid phenotype (~70 %).[38,39] BC occurs when over 30 % immature blasts, myeloid or lymphoid, are present in blood or bone marrow, resulting in the increase of *BCR-ABL1* mRNA and protein levels.[38] This terminal phase usually leads to metastasis, organ failure and death, presenting a poor prognosis and worsening symptoms, bleeding, fever and infections.[37] The median survival of patients with BC without treatment is 3 months.[40]

The mechanisms underlying CML triphasic model of progression can be partially explained by the genetic instability characteristic of blast cells, resulting in the acquisition of additional genomic alterations, such as trisomy 8, isochromosome 17, double Ph+, c-MYC amplification and activation of pathways that block myeloid differentiation and inactivation of tumor suppressor genes such as phosphoprotein 53 gene (*p53*) and retinoblastoma gene *(RB)*. These molecular events extend leukemic stem cells (LSCs) replicative lifespan.[24, 26,41] Therefore, LSCs and related pathways may serve as key targets for curing CML.[26]

1.1.2.2 Diagnostics and disease follow-up

Clinical manifestations of CML are often non-specific, and many patients diagnosed with CML are asymptomatic (30-50 % in the US alone). CML is frequently detected when an elevated white blood cell count is revealed by a routine blood test or when splenomegaly is detected on a general physical examination.[37] After hematological characterization, bone marrow biopsy is mandatory to confirm diagnosis. In a case of persistent unexplained leukocytosis, CML diagnosis consists of probing for the presence of the Ph chromosome by routine cytogenetics (karyotype); or the Ph-related molecular *BCR-ABL1* abnormalities by fluorescence *in situ* hybridization (FISH); or by molecular biology screening.[8,38]

The Ph chromosome is present in 95 % of CML patients (typical t(9;22) from chromosome banding analysis of at least 20 marrow cells metaphases) as the sole chromosomal abnormality. The remaining patients show additional chromosomal alterations (clonal evolution), such as trisomy 8, isochromosome 17, deletions in the 22q, or other Ph-variants (involving chromosome 22 or 9 or involving other chromosomes in addition to chromosomes 9 and 22). These are treated as standard Ph+ patients since Ph-variant patients present similar responses to therapy and prognosis.[8,38]

FISH analysis relies on analyzing at least 200 nuclei for the co-localization of DNA probes designed to hybridize specifically to the *BCR* and *ABL1* genes.[38] FISH may be performed in bone marrow and/or blood samples with high concordance (false positive range of 1–10 % depending on the probes used).[8] CML characterization at diagnostic is imperative but CML patients must be monitored continuously to assess their response to therapy (Table 1.2) to achieve an optimal response and a deeper, stable,

8

treatment-free remission.[38] For disease follow up, peripheral blood samples should be used in place of bone marrow.[42]

The success of precise therapy for CML depends greatly on its diagnosis, but also on disease follow-up. Three key parameters should be considered when monitoring CML patients' response to therapeutics: hematologic response or normalization of blood counts; cytogenetic response, which relates to the percentage of Ph+ cells in the bone marrow; and molecular response, defined by the expression level of *BCR-ABL1* transcript in a bone marrow or blood sample. The European LeukemiaNet (ELN) established milestones for hematologic, cytogenetic, and molecular responses to be achieved at specific time-points after therapy initiation for improved clinical outcome (Table 1.2). Beginning treatment with imatinib (IM), the first TKI for CML treatment released after the interferon era (additional information in section 1.1.2.3 – *CML therapeutics*), the following events are expected: complete hematologic response (CHR) with major cytogenetic response (MCyR) after 3 months; complete cytogenetic response (CCyR) after 6 months; and major molecular response (MMR) after 12 months of therapy. Therefore, follow-up is crucial for disease monitoring. It is recommended that these patients perform a peripheral blood collection and analysis every 3 months after starting TKI treatment. Patients who do not achieve these milestones should be immediately considered for an alternative TKI/therapy (Tables 1.2 and 1.3).[38,42,43]

Table 1.2 Expected levels of CML patients response after TKI therapy initiation (ELN guidelines).[38,42] Additional information on different TKIs can be accessed in section 1.1.2.3 – *CML therapeutics*.

Time point for IM	Time point for dasatinib and nilotinib	Optimal response	FISH (Ph+)	*BCR-ABL1* levels (IS)
n/a	3 months	CHR	≤ 65 %	≤ 10 %
3 months	6 months	CHR, MCyR	≤ 35 %	≤ 10 %
6 months	12 months	CCyR	0 %	≤ 1 %
12 months	>12 months	MMR	0 %	≤ 0.1 %
>12 months	n/a	DMR	0 %	≤ 0.01 %*

*Expected result in two consecutive blood samples (assay sensitivity > 10^{-4})

CCyR, complete cytogenetic response; CHR, complete cytogenetic response; CML, chronic myeloid leukemia; DMR, deep molecular response; ELN, European LeukemiaNet; IM, imatinib; IS, international scale; MCyR, major cytogenetic response; MMR, major molecular response; n/a, not applicable; Ph+, Philadelphia chromosome-positive cells; TKI, tyrosine kinase inhibitors.

CML molecular monitoring

BCR-ABL1 mRNA transcripts typically remain detectable after CCyR. Reverse transcriptase polymerase chain reaction (RT-PCR) is thus far the only tool capable of monitoring responses after patients reach CCyR.[43] This methodology has become an integral part of CML management since 1999 due to its sensitivity levels.[44] The low levels of minimal residual disease (MRD) normally achieved during therapy call for a sensitive monitoring assay for reliable detection and quantitation.[8,43] Currently, two PCR-based modalities can be performed to detect the *BCR-ABL1* transcript in CML patient samples: RT-nested PCR, a qualitative approach; or reverse transcriptase quantitative polymerase chain reaction (RT-qPCR), a quantifiable assay.

Nested PCR is a modification of PCR that was designed to improve its sensitivity and specificity. Basically, two pairs of primers target the same region: the first pair (outer primers) amplifies a fragment in a conventional PCR reaction; the second set (inner primers) anneals to sites within the first amplicon. In CML, RT-nested PCR provides characterization of the transcript allowing the identification of the more frequent transcripts: e13a2 or e14a2. This approach also allows for identification of one of the atypical fusion transcripts that are not amplified by the standard primer sets.[44] As previously mentioned, there is a high controversy among the various published studies concerning the type of fusion transcript and its influence in CML phenotype and/or response to therapy.[29,33–35] Recently, the ELN expert panel acknowledged that the transcript type (e13a2 *vs* e14a2 or other more atypical variants) may influence response to therapy and disease outcome, which demonstrates the relevance of performing this molecular screening.[38]

RT-qPCR provides data on the actual percentage of *BCR-ABL1* mRNA transcripts in peripheral blood or bone marrow, and is capable to detect one CML cell in a background of 100 000 normal cells.[43,45] It also provides a strong correlation between the results obtained from peripheral blood and bone marrow, allowing molecular monitoring without the necessity of obtaining bone marrow aspirations.[38,43] RT-qPCR is definitely the current method of choice for CML molecular detection and quantification, and should be performed before initiation of specific TKI therapy to establish a baseline for *BCR-ABL1* mRNA levels for each individual patient.[38] As such, several efforts have been made to optimize and standardize this methodology to reduce the heterogeneity of *BCR-ABL1* expression results amongst different clinical laboratories.[42,46,47] According to guidelines from the National Comprehensive Cancer Network (NCCN) and the ELN, results are now conveyed as the ratio of *BCR-ABL1* transcript numbers to the number of control gene transcripts (typically, *ABL1* gene).[42] This value is then compared to a standardized baseline representing 100 % IS (International Scale, defined by the median value of *BCR-ABL1* mRNA at the time of diagnosis in 30 patients with CML as established in the Study of Interferon and STI571 - IRIS), that is independent of individual patient-specific *BCR-ABL1* baseline values.[48]

Deep molecular response (DMR) is defined as the 4-log reduction or more from the standardized baseline (*BCR-ABL1* transcripts = 0.01 % IS). A MMR corresponds to a 3-log reduction in the *BCR-*

ABL1 transcripts from the baseline and is fixed at 0.1 % IS. These correlate to minimal risk of transformation to advanced phases of disease with 100 % probability of remaining progression-free at 24 months. Generally, a 2-log reduction (*BCR-ABL1* transcripts = 1 % IS) and 1-log reduction (*BCR-ABL1* transcripts = 10 % IS) correlate with CCyR (defined as absence of Ph+ chromosomes) and MCyR, respectively (Table 1.2).[38,42]

Another integral part of molecular diagnosis and therapy management in CML is the assessment of the chimeric gene mutational status. Kinase domain mutation profile plays a minor role in selecting an initial TKI, but becomes highly relevant for patients where no *ab initio* response to the TKI is obtained, or in relapsed cases. Indeed, BCR-ABL1 mutations range from 25 % to 30 % of early CP patients on first-line IM to approximately 70 % to 80 % of BC patients.[38,49] Due to the clonal diversity of *BCR-ABL1*-expressing cells, mutational screening is conventionally performed via Sanger sequencing that is capable to detect a point mutation if the clone accounts for more than 15 % of all Ph+ cells.[49]

1.1.2.3 Therapeutics

Treatment depends on the type of leukemia, the disease stage, prior history of treatment, age and health of the patient, as well as the genetic profile. Most patients are treated with chemotherapy, while some may also undergo radiation therapy, stem cell transplantation or targeted therapy.[37,39,40]

Up until the 1990s, the best nontransplant options for CML-CP management were nonspecific agents such as busulfan, hydroxyurea and interferon-alfa, which provide for temporary disease control. In fact, IFN-α is capable of reducing the proportion of the Ph chromosome but with multiple side effects.[50,51] From the 1990s onwards, the treatment of choice resulting in curatives interventions, was the allogeneic stem cell transplantation (AlloSCT). However, AlloSCT not only carries high risks of morbidity and mortality, but also requires relatively young patients and an appropriate stem cell donor.[52,53] CML treatment strategies and outcomes boosted with the design and development of small molecules capable of interfering and inhibiting the kinase activity of the BCR-ABL1 protein – TKIs.[54–57] TKI therapy is considered the standard first-line treatment for patients with newly diagnosed CML-CP. As shown in table 1.3, five TKIs are available and recommended in the management of CML patients: IM (first generation), dasatinib, nilotinib (second generation), bosutinib (second/third generation) and ponatinib (third generation).[57–62]

IM is usually well tolerated and constitutes the preferable option due to its high efficacy with durable hematological and cytogenetic responses.[64,65] It retains the BCR-ABL1 protein in its inactive conformation, via competitive inhibition at the ATP-binding site and consequently blocking the downstream signal transduction pathways, preventing the phosphorylation of substrates.[64] Although this first generation TKI demonstrates the ability to induce complete hematologic response in CML-CP patients, IM monotherapy is not curative for several patients. Early relapse, primary and acquired TKI resistance remain an important concern mainly due to the incomplete eradication of BCR-ABL1

expressing leukemic cells.[27, 57,66–68] Besides IM, dasatinib and nilotinib have indication for first-line therapy in CML. The choice of the most appropriate TKI is based on several factors such as blood counts at diagnosis, patient age, drug cost, comorbidities and drug toxicity profile. This ensures that the treatment is the most adequate, target-oriented and well tolerated by each patient, with minimal impact on quality of life.[57,69,70] These molecules (dasatinib and nilotinib) are more potent inhibitors than IM (*in vitro*) and have demonstrated the ability to induce more rapid and deeper responses in newly diagnosed patients. However, their impact on long-term overall survival remains undetermined.[71–74]

Table 1.3 TKIs in CML management. Adapted from Leach, 2016.[63]

TKIs	Indications	FDA approved
IM	First line therapy for CML-CP	5/2001
	After failure of interferon-alpha therapy in CML-CP, AP, or BC	4/2003
Dasatinib	For patients resistant or intolerant to prior therapy (at any CML phase)	6/2006
	First line therapy for CML-CP	10/2010
Nilotinib	For patients resistant or intolerant to prior therapy (CML-CP and AP)	10/2007
	As first line therapy in CML-CP	6/2010
Bosutinib	For patients resistant or intolerant to prior therapy (CML-CP and AP), except for cases with detectable V299L and T315I BCR-ABL1 mutations	9/2012
Ponatinib	As second-line therapy or beyond when no other TKI is indicated, or when a T315I mutation in BCR-ABL1 is identified	3/2013

AP, advanced phase; BC, blast crisis; CML, chronic myeloid leukemia; CP, chronic phase; IM, imatinib; TKI, tyrosine kinase inhibitor

Overcoming TKI resistance

It is known that 15 % to 40 % of CML patients will develop resistance or intolerance to first-line TKI treatment, with a need for a second-line TKI.[57,75] This limited therapeutic potential is mainly due to TKIs resistance mechanisms that can be BCR-ABL1 dependent or independent. BCR-ABL1 dependent TKIs resistance mechanisms rely mostly on the overexpression of the *BCR-ABL1* oncogene and mutational events.[76] The most studied ones are the mutations occurring on the kinase domain of BCR-ABL1, generally point mutations, impairing TKIs activity, mainly by preventing the fusion protein from adopting the inactive conformation. It has been demonstrated that the majority of these IM-resistant mutations are related to substitutions of amino acids that play a crucial role on specific IM

binding. The most recurrent alterations can occur at three different regions and seven specific residues: in the docking site for phosphate moieties of ATP named P-loop (M244V, G250E, Y253F/H and E255K/V); in the contact site related to selective BCR-ABL1 inhibition by IM (T315I); and in the catalytic domain (M351T and F359V).[77,78]

Generally, second generation TKIs are active against most of the IM-resistant mutations, however, CML patients harboring T315I, F317L or V299L mutations usually do not respond to dasatinib, whereas patients harboring the E255K/V, T315I, F359C/V or Y253H mutations have a lower response to nilotinib.[79,80] More recently, bosutinib appeared as the newest second-generation TKI, and have been proved to be highly effective in CML patients with BCR-ABL1 kinase mutations that lead to IM failure (exceptions are the V299L and T315I mutations).[81–85] The T315I mutation displays resistance to all current available TKIs, except for ponatinib, a third generation TKI that was recently approved for patients resistant or intolerant to prior TKI therapy (Table 1.3).[83,86] Therefore, mutational screening could lead to a better and informed selection of second and third line TKI therapy to be applied in patients who failed first or second line treatment, providing clinical benefit for those involved.[49, 85,87] Upon resistance to a first-line TKI, BCR-ABL1 mutation analysis is then recommended according to the NCCN and ELN guidelines.[58] Patients that fail all current TKIs regimens are eligible for AlloSCT.[38,88]

BCR-ABL1 independent TKIs resistance mechanisms have been reported. These include patient compliance and drug metabolism.[89,90] Other mechanisms are linked to drug transport and its intracellular influx. IM cell uptake is mediated by the human organic cation transporter 1 (OCT1). When its activity is high there is an improvement on overall survival and response rates [91]. Conversely, patients with lower OCT1 activity are associated with sub-optimal responses and they are more likely to undergo leukemic transformation.[91,92]

IM exposure can also lead to a multidrug resistance (MDR) phenomenon, known as a recurrent cause of chemotherapy failure.[93,94] This BCR-ABL1 independent resistance process is multifactorial and may comprise repair, drug detoxification and apoptotic resistance mechanisms. The MDR mechanism involving the expression and activity of ATP-binding-cassette (ABC) transporters, which modulates efflux transport, is the most studied one. These ABC transporters are transmembrane proteins that usually provide protections against xenobiotics. *MDR1*, for example, is overexpressed in hematopoietic cells and encodes for the drug efflux pump P-glycoprotein, forcing substances out of cells and preventing drugs, such as TKIs, from achieving an effective intracellular concentration.[95–99]

1.1.2.4 Current trends

Diagnostics

Diagnostic testing plays a key role in the management of CML and, for that purpose, has been rapidly changing over the years with the introduction of novel sensitive diagnostic tests. RT-qPCR is

probably the most sensitive technique available for detection of *BCR-ABL1* transcripts. However, detection of *BCR-ABL1* through RT-qPCR strongly depends on the quality and efficiency of RNA extraction and/or reverse transcription. False negatives may arise from RNA degradation or from repression of the *BCR-ABL1* transcript. Specific concerns include optimization of RNA extraction and real-time amplification protocols, to ensure the detection of minimal *BCR-ABL1* copies and maximal integrity of control gene; use of suitable control genes (e.g. *ABL1*, *BCR* and *GUSB*) for correct normalization of results; control RT-qPCR fluctuations over time due to technical issues; and, the stochasticity of reverse transcription and PCR amplification processes, especially when analyzing samples with low copy number.[42] Other downsides include complexity, sensitivity to contamination, lack of portability, limitations in terms of multiplexing and reporting standardization issues. These make it very difficult to shift CML molecular monitoring towards point-of-care (POC).[100]

The tight follow up of a CML patient after diagnosis increases the costs on the healthcare system, thus requiring the optimization of faster, cheaper and effective CML diagnostics methods. This is particularly important in countries in which molecular surveillance is not readily available to assist patient care. Note that the incidence of cancer is a worldwide issue, particularly impacting low-and middle-income countries, due to the increase of the population life expectancy and the lack of effective diagnostics and treatment capacity. In fact, the percentage of newly reported CML cases occurring in low-to-middle income countries has more than tripled over the past 40 years and only about 5 % of the global resources spent on cancer are deployed in these countries.[101,102]

Research on CML molecular diagnostics focuses on four key issues: i) increase detection sensitivity through robust nucleic acid amplification strategies; ii) increase the amount of information on leukemic cells status, such as type of fusion transcript, occurrence of mutations and kinase activity; iii) miniaturization towards decreasing sample volume requirements; and iv) fast and cost-effective methods for POC suitable for preliminary screening. Currently, CML diagnostics may be performed on a single microfluidic platform that uses a small volume of blood and incorporates RNA extraction, reverse transcription, qPCR and result calculation to detect the fusion transcript.[103] Though this automated microfluidic device improves sensitivity, standardization and reduces the variability from test to test, a specialized instrument is required, as well as reference material calibrated to IS and validated by the WHO.[104]

As discussed previously, detection of the t(9;22) can be performed at chromosome level through karyotyping or FISH, or at the mRNA level through reverse transcriptase coupled to nested PCR and/or qPCR. Each one of these approaches has its advantages and disadvantages, and the safest option for CML monitoring is to integrate several strategies, at different levels (Figure 1.2; Table 1.4). Due to the reported persistence of leukemic DNA even with undetectable levels of chimeric transcript, detection of *BCR-ABL1* genomic DNA using a DNA-based marker of the translocation will facilitate patient management by confirming absence/presence of the fusion gene.[105] The information on the type of transcript and its expression levels can only be provided at mRNA level, due to alternative splicing

events and consequent genetic heterogeneity. Compared with cytogenetic testing, PCR-based molecular monitoring offers an analytical sensitivity 100 to 1000 times greater than FISH or bone marrow cytogenetic analysis.[43] However, nanoparticle (NP)-related assays offer unprecedent versatility for CML diagnosis, due to their size- and shape-dependent optical properties, and their ability to be loaded with a wide range of ligands at nanoscale. These features enabled the design of novel diagnostic systems that offer significant advantages in terms of sensitivity, selectivity, reliability and practicality, which will be further discussed on sections 1.2 (*Nanomedicine*) and 1.3 (*Nanotechnology towards leukemia management*).

For BCR-ABL1 kinase domain mutation analysis, the primary technique tool to monitor patients with TKI resistance, has been Sanger sequencing. However, the presence of mutations may be identified with more sensitive techniques, such as mass spectrometry or ultra-deep sequencing. Indeed, mass spectrometry can improve the sensitivity of mutation detection by 1-log compared to standard direct sequencing.[106] A cohort study showed that next generation sequencing (NGS) detected emerging mutations, in both diagnostic and follow-up samples, earlier than Sanger sequencing in cases of therapy failure. Moreover, NGS enabled accurate identification of mutations in patients whose *BCR-ABL1* transcript level fluctuated around 0.1 % IS (MMR) or deeper molecular response. However, further studies are needed to understand the benefit of ultra-sensitive mutation screening after MMR is achieved.[107] NGS has also been applied to BCR-ABL1-independent gene mutations.[108] The large panel of 25 genes that was analyzed combined with the high sensitivity of NGS based sequencing improved mutation detection and provided novel genetic information regarding CML biology, however routine NGS data in cancer genomics is still far from implementation in all clinical settings due to its cost and computational tools requirements.[109]

Though available, other techniques for the identification of mutations are still far from routine labs: pyrosequencing, denaturing high-performance liquid chromatography (D-HPLC), double-gradient denaturing electrophoresis, multiplex-PCR and allele-specific oligonucleotide PCR.[42,110,111] These technologies may increase the level of detection for BCR-ABL1 subclones that might be underrepresented in the pool of blast cells, and consequently reduce the probability of unresponsiveness to therapy.[112]

There is still plenty of discussion among clinicians and molecular biologists on whether a negative result by karyotype analysis, FISH or RT-qPCR means that the patient is truly free of the disease. Discontinuation of IM in CML patients who have maintained DMR for at least 2 years have been subject of investigation and the first large clinical trial - the French STIM study - reported sustained treatment-free remission in 40 % of patients.[113] More recently another trial - the TWISTER study, performed by the Australasian Leukemia & Lymphoma Group (Australian New Zealand Clinical Trials Registry: ACTRN 12606000118505) - has shown that treatment-free remission may be achieved in patients testing negative by RNA-based qPCR but positive by DNA-based real-time PCR.[42] For these reasons,

there has been a continuous demand for methodologies capable to probe DNA, RNA and protein levels with enhanced sensitivity (Figure 1.2; Table 1.4).
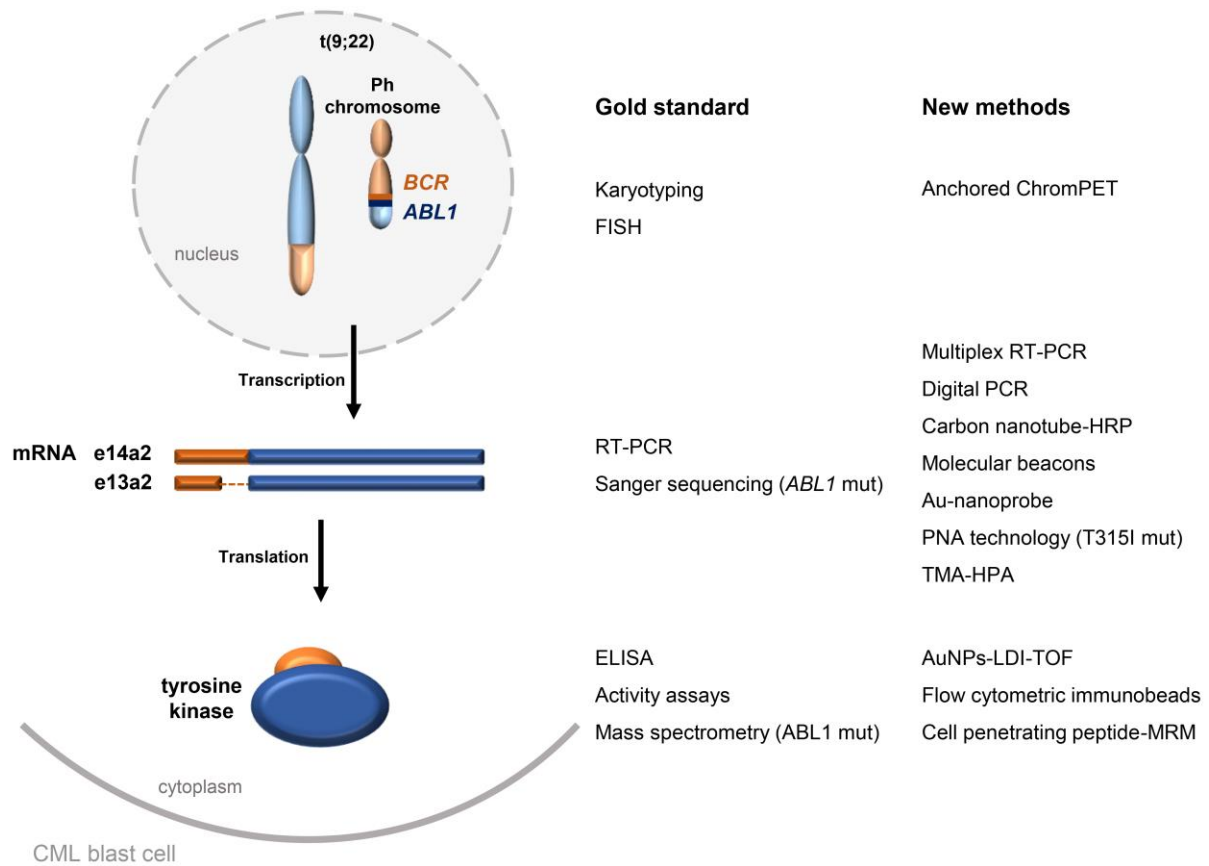
Figure 1.2 Conventional *vs* innovative methodologies for cytogenetic and molecular screening of CML, via genomic DNA, mRNA and protein. The disease-causing translocation results in a shortened chromosome 9, the Philadelphia chromosome (Ph). The two most frequent *BCR-ABL1* splicing variants (accounting for 95 % of Ph+ cases) are represented, as well as the encoded enzyme. ChromPET, chromosomal paired-end tags; ELISA, enzyme-linked immunosorbent assay; FISH, fluorescence *in situ* hybridization; HRP, horseradish peroxidase; LDI-TOF, laser desorption ionization-time of flight; MRM, multiple reaction monitoring; mut, mutations; PNA, peptide nucleic acid; RT-PCR, reverse transcription-polymerase chain reaction; TMA-HPA, transcription-mediated amplification-hybridization protection assay.

Table 1.4 Advantages and disadvantages of new approaches in CML molecular characterization.

Method	Advantages	Disadvantages	Sensitivity	Ref.
Anchored ChromPET	Analysis of multiple samples in a single assay Higher sensitivity than karyotyping, FISH or PCR	Does not detect splicing isoforms Complex implementation	10^{-4} (a)	[114]
Multiplex RT-nested PCR	Detection of multiple chromosomal translocations/breakpoints in a single reaction Suitable for minimal residual disease monitoring	Does not provide transcript quantification	10^{-4} (a)	[115–118]
Digital PCR	Lower limit of detection than RT-PCR Less prone to erroneous quantification (absolute copy number determination; no need for calibrators)	Expensive Requires a rough estimate of target copy number before testing	10^{-6} (a)	[119]
Carbon nanotube-HRP	Does not require amplification step Cheaper than RT-PCR May be extended to fluorescence/luminescent assays	Lack of standard protocol for high-purity carbon nanotubes in large scale applications	(b)	[120]
Molecular Beacon	Does not require amplification step May be used for sequence specific RT-PCR	Lower sensitivity than RT-PCR	(b)	[121,122]
Au-nanoprobe colorimetric assay	Cheap, fast and single tube Does not require amplification step Enables quantification of transcripts	Requires standardization protocol to be applied in clinical diagnostics	(b)	[123–125]

Method	Advantages	Disadvantages	Sensitivity	Ref
PNA-FISH	Analyze clonal evolution Detection at single cell level	Less information than Sanger sequencing (probes designed for specific mutations)	2 % (c)	[126]
PNA directed PCR-clamping	Fast and cheap Detection of mutations at single cell level Highly sensitive	Less information than Sanger sequencing (probes designed for specific mutation)	0.5 % (c)	[126]
TMA-HPA	Single tube method Enables quantification Reduces risk of carryover contamination and false positives	Complex design Requires specialized equipment (luminometer)	10^{-4}-10^{-5} (a)	[127]
AuNPs-LDI-TOF	Does not require purification steps Low background signals	Time consuming Requires internal standards	(b)	[128]
Immuno-beads	Detection of all isoforms of chimeric protein Higher sensitivity than karyotyping or FISH. Does not require purification step	Lower sensitivity than PCR	10^{-3} (a)	[30]
Cell penetrating peptide-MRM	Allows determination of chimeric BCR-ABL1 activity	Requires concentration step	(b)	[129]

ChromPET, chromosomal paired-end tags; FISH, fluorescence *in situ* hybridization; HRP, horseradish peroxidase; LDI-TOF, laser desorption ionization-time of flight; MRM, multiple reaction monitoring; PNA, peptide nucleic acid; TMA-HPA, transcription-mediated amplification-hybridization protection assay

(a) Sensitivity values expressed as the number of *BCR-ABL1* expressing cells in a background of *BCR-ABL1* negative cells (e.g., successful detection of one K562 cell in a background of 10 000 HL60 cells corresponds to a sensitivity value of 10^{-4}). Sensitivity of gold standard methodologies: RT-nested PCR = 10^{-6}; RTq-PCR = 10^{-5}

(b) Information not available or different scoring units were used.

(c) Sensitivity values expressed as the percentage of mutated cells/template in a wild-type background. Sensitivity of Sanger sequencing: 10-20 %

18

In myeloid neoplasms, conventional diagnostics consist of blood counts and biomarker evaluation on peripheral blood cells, complemented by morphologic examination of tumor tissues, which includes a collection of a substantial core biopsy of the bone marrow using a fine needle. Follow-up relies on peripheral blood assessment every 3 months for morphological, cytogenetic or molecular marker evaluation. Since there is a good correlation between blood and core biopsies in hematological disorders, a current debate focuses on whether bone marrow biopsies are still necessary.[130,131]

Liquid biopsies allow for non-invasive disease monitoring techniques and have been associated with circulating material originated from solid tumors, mainly circulation tumor cells (CTCs), circulating cell free DNA (cfDNA), microRNAs (miRNAs) and exosomes, that provide valuable information before and during treatment.[132–134] However, this is even more so in liquid tumors, since a direct sample of tumor cells may be retrieved from a peripheral blood collection. As a result, besides the usual counting of leukocytes, hemoglobin, lymphocytes, and platelet levels, new prognostic markers should be addressed as far as disease outcome and clinical decision-making are concerned.[135] For example, exosomes (vesicles of 30-100 nm that transport proteins, mRNAs and miRNAs) play an important role in cell communication, being able to induce some sort of transformation in receptor cells, including activation, proliferation, differentiation, or apoptosis [136,137]. In CML-derived exosomes, a specific expression pattern of miRNAs was unveiled, which might be further explored for future use as disease biomarkers.[138] In fact, higher concentrations of exosomes are found in sera of AML, CML and CLL patients with an abundant expression of surface proteins according to their cell of origin, which is rarely observed in exosomes of healthy individuals. Together, this supports the use of exosomes and miRNAs as leukemia biomarkers.

Therapeutics

Current treatment of CML patients has converted a fatal cancer into a manageable chronic disease. In fact, the 8-year survival rate of a CML patient is 87 % since 2001 and, since the advent of second-generation TKIs, the life expectancy of CML patients is now close to that observed for the general population.[139,140] The majority of patients respond very well to chemotherapy, however it is still challenging for clinicians to know when it is safe to discontinue a successful treatment and why, in some patients, leukemia recurs.[141] The recommendation is to continue medication permanently but this raises other problems, such as the development of resistance, non-compliance with treatment, fertility and pregnancy issues, and the economic burden of long-term medication. Hence, treatment cessation is currently one of the major discussion points regarding CML.[106, 113,142]

As for many other types of cancer, the way forward seems to be precision medicine, where a more specific chemotherapy strategy is conveyed to a given patient following the accurate genetic and biochemical profiling. As such, the selective delivery of a drug solely to those patients that will respond effectively to the chemotherapeutics will greatly improve the outcome. These approaches shall be made possible via the more sensitive and easy to operate detection strategies described previously which, in

conjunction with the novel molecules targeting specific subtypes of CML causing aberrations, will enable personalization of CML management.

It has been reported that transfection of siRNA against *BCR-ABL1* significantly reduced levels of corresponding mRNA and oncoprotein, with induction of apoptotic cell death in human leukemia K562 cells.[143] This approach was successfully applied using *BCR-ABL1* siRNA in a female patient with recurrent Ph+ CML, resistant to IM (Y253F mutation) and to chemotherapy with AlloSCT.[144] *BCR-ABL1* mRNA levels decreased dramatically and led to the reduction of circulating CML cells without side effects, suggesting that siRNA targeting of this gene has great potential for treatment of IM resistant CML.[145] Kim *et al* developed a DNAzyme-based strategy to specifically target and cleave both the junction sequence and the site of the T315I point mutation that confers IM resistance. The designed molecules induced apoptosis and proliferation arrest in both wild-type and T315I-mutant CML cells, in a selective manner. Moreover, *in vitro* co-treatment with the DNAzyme targeting the T315I mutation and IM resulted in enhanced inhibition of proliferation and induction of apoptosis in T315I leukemic cells as compared with IM alone, thereby abrogating IM resistance in CML cells. DNAzyme combined with IM treatment may be an alternative approach to overcome TKIs resistance in leukemic cells.[146]

Due to the genetic heterogeneity of *BCR-ABL1* and sub-optimal response to chemotherapy by some patients, one can take advantage of a personalized approach. Coupling the benefits of nanotechnology, it is possible to integrate imaging, targeting and therapeutic agents in a single vehicle – nanotheranostics, allowing real-time monitoring of disease progression/remission, minimization of off-target accumulation and side-effects, treatment specificity, reduction of therapeutic doses and repeated administrations. Linking diagnostics with targeted treatments at an early stage of the disease will benefit both patients and the economics of healthcare.[147–149] This trend will be further discussed in the following sections - 1.2 (*Nanomedicine*) and 1.3 (*Nanotechnology towards leukemia management*).

1.2 Nanomedicine

Traditional approaches for cancer management depend on centralized diagnostic platforms that can be complex, time-consuming and are set for the wide spectrum of patients and malignancies.[150] These approaches have been developed to identify suitable biomarkers and profiles, for which standard chemotherapeutics protocols are designed.[151] This has been the grounds for the development of precision oncology, in which profile data of the cancer cells enable a tailored treatment for individual patients.

Nanoscale particles have played a central role in the detection of cancer biomarkers, which is essential for the personalized assessment at the basis of precision therapeutics. These NPs versatile structural and functional properties offer the possibility for the development of rapid, specific and sensitive diagnostics, opening the door for decentralized assessment and/or ambulatory follow-up.[17] In what therapeutics are concerned, nanoconstructs' size and their ability to be tailored with specific ligands for precise delivery to the focus of disease allow for more effective strategies to cross biological barriers. Moreover, NPs can work as therapeutic/imaging agents on their own or as carriers of multiple molecules that serve a specific function: tumor targeting, cancer cells ablation (via drug or gene silencing) and real-time monitoring of cancer cells expansion or decay. This flexibility is of particular interest for theranostics strategies, offering the possibility of simultaneous cancer detection and therapy.[148]

NPs are synthesized in the range of 1-100 nm from diverse materials that, when at nanoscale, usually feature unique electronic, optical and catalytic properties, different than those of bulk materials.[152–154] There is a wide variety of NPs, including liposomes, polymers, dendrimers, carbon, metal (e.g. magnetic, gold, silver, iron oxide) and quantum dots (QDs).[155] Overall, their size is optimal for intracellular uptake and their large surface ratio permits a functionalization with different biomolecules for diagnostics and therapeutic purposes.[152–156] Among the plethora of different nanoscale devices applied to cancer diagnostics and therapeutics, this section will be focused on gold nanoparticles (AuNPs) and its advantages over the remaining NPs in cancer management.

1.2.1   Focus on gold

Nanomaterials, such as noble metal NPs, brought a fresh perspective with new possibilities to create and improve setups for biodetection of clinically relevant biomarkers[157] or genomic sequences of interest.[158,159] AuNPs, in particular, have been immensely researched for their colorimetric properties, that is, intense colors and tunable localized surface plasmon resonance (SPR), chiefly for biomolecular assays involving a colorimetric result.[158,160] SPR has been shown to be dependent on NP composition, size and shape.[161–163] A colloidal gold solution containing spherical AuNPs (<40 nm) typically presents a localized SPR absorption band with a maximum centered at approximately 520 nm, presenting a bright

red color. This localized SPR absorption band is also influenced by interparticle distance, which constitutes the foundations for most AuNP-based colorimetric assays.[164]

The chemical synthesis of AuNPs can be achieved through the reduction of gold salts to zero valence atoms, usually Au^{3+} to Au^0. The final NP size is dependent on the reaction conditions, such as nature and quantity of reducing agents, temperature, reaction time and capping agent.[165] The capping agent controls the NP growth in terms of rate, final size and morphology, and is required to increase the colloidal stability of the synthesized AuNP, either by electrostatic stabilization or by steric hindrance.[166] Electrostatic stabilization is attained through coulombic repulsion between particles possessing a layer of ions adsorbed to their surface and a second layer of counterions,[167] whereas steric hindrance stabilization relies on the use of organic molecules that restrict interactions between two independent metallic cores, preventing aggregation of the colloidal suspension.[168] Both the reduction agent as well as the capping agent should be carefully chosen to be consistent with the final application, as they may limit the solubility and subsequent derivatization of the NP. Considering a subsequent functionalization with thiolated ssDNA,[123, 160,169] these AuNPs should be hydrophilic.

One of the most common methods for the production of spherical NPs with a narrow distribution of size in aqueous medium is the citrate reduction method employed by Turkevich *et al*.[170] and later optimized by Frens[171] and Lee and Meisel.[172] This method produces hydrophilic spherical AuNPs (10–30 nm) compatible with subsequent functionalization steps. Here, the citrate molecule acts as both a reducer and a capping agent. The diameter of the produced AuNPs may be tailored, to an extent, by varying the relative ratio of citrate to gold salts. Higher concentrations of citrate yield smaller particles, while lower concentrations of citrate tend to favor the formation of larger particles.[173,174] This method yields rather stable particles with negative charge due to the weak electrostatic adsorption of citrate on the surface of the NP, which constitutes an advantage for subsequent surface modification. Other procedures can be implemented to synthesize AuNPs in a variety of sizes,[175–177] however, as explained above, the citrate reduction method is a simpler and straightforward approach for the synthesis of hydrophilic AuNPs in large quantities, with relatively low size dispersion, for subsequent modification and detection methods. For additional reading on AuNP synthesis and modifications please refer to Conde *et al*, 2015.[178]

1.2.2 Gold nanoparticle-based diagnostics

Molecular diagnostics based on screening of genomic sequences constitutes a powerful and promising way to identify genetic variations and ultimately evaluate their consequences at phenotypic level. This is particularly relevant as individual genetic variability has been associated with different multifactorial diseases[179–182] and a differential response to therapeutic agents.[183,184] To cope with this, molecular diagnostic has undergone sequential miniaturization and adaptation to medium-to-high throughput,[159,185] which has greatly benefited from the emergence of nanotechnology.[160,186]

In 1996, oligonucleotide probes were functionalized to the surface AuNPs for the first time by Mirkin and co-workers.[187] This concept utilized two different probes and generated a AuNP–DNA network, where the AuNP:oligonucleotide conjugates (Au-nanoprobes) were brought together, upon hybridization to a target complementary to both probes. In close vicinity, the Au-nanoprobe solution turns from red to blue, presenting a clear colorimetric identification of the target.[188] This crosslinking assay made a significant contribution and revealed an immense potential for colorimetric detection, when applied to clinical diagnostics.[189] For this reason, a wide number of crosslinking-like approaches have been developed for the molecular detection of nucleotide sequences, single nucleotide polymorphisms (SNPs) and other analytes.[188–190] Crosslinking systems present some drawbacks, such as the need to use two nanoprobes, a strict control of temperature to yield a successful result, and a constant need for optimization of hybridization conditions, especially when detecting long nucleotide targets (RNA or DNA), due to steric hindrance.

With this in mind, Sato and co-workers arranged a different detection scheme, relying on a single Au-nanoprobe, where aggregation was achieved by destabilizing nanoprobes in solution through an increase in ionic strength.[186] In this case, the oligonucleotide probes at the AuNP surface are required to be precisely the same length as the target aimed to detect; so, when a complementary target is present, it will fully hybridize with the Au-nanoprobe, resulting in blunt-end heteroduplexes. This phenomenon, conjugated with salt addition, is responsible for AuNPs' aggregation and, in the same way as in the crosslinking detection, the colloidal solution's color changes from red to blue. Conversely, the same ionic strength is not sufficient to destabilize Au-nanoprobes hybridized to a mismatched target; so, aggregation does not occur, and the solution retains its red color. This non-crosslinking (NCL) setup possesses some limitations, since real biological targets are usually longer than nanoprobes and cannot always confer the blunt-end heteroduplexes mandatory for aggregation, and so, for analysis of real samples, this method would always require a previous single-base extension step.[191]

Considering these limitations, Baptista and co-workers took the NCL assay one step further and designed an approach where hybridization between Au-nanoprobes and complementary targets resulted in heteroduplex formation at the nanoprobe surface, stabilizing it against salt-induced aggregation.[160] The presence of a non-complementary or mismatched target in solution would not sufficiently stabilize Au-nanoprobes, and aggregation would occur, accompanied by color change from red to blue (Figure 1.3). This design was rather simpler that the previous ones, in terms of detection. Also, it did not demand the strict temperature control required by the crosslinking assay[187,188] or present the target length limitation verified in the first NCL assay.[191] Conceptually, this method proved suitable for identification of specific nucleotide sequences in longer targets, for example, PCR products, genomic DNA, and for different applications such as detection of pathogen agents,[159,192] discrimination of single-base alterations related to blood disease [193] and semi-quantification of mRNA.[123]
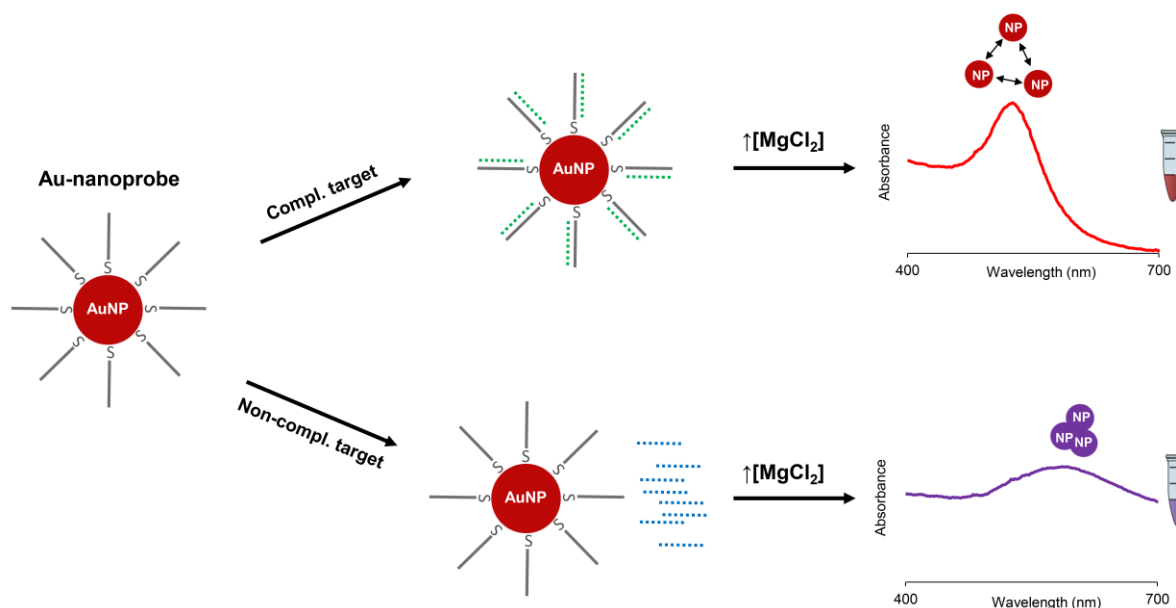
Figure 1.3 Au-nanoprobe non-crosslinking assay developed by Baptista *et al.*[160] When a complementary target is present in solution and is fully hybridized with the Au-nanoprobe, preventing aggregation upon salt induction, the colloidal solution maintains its red color. The formation of heteroduplexes resulting from hybridization between probe and complementary target bears a protective effect due to their negatively charged backbones and steric hindrance. This way, both the electrostatic repulsions and the interparticle distance between nanoprobes increase, promoting further stabilization. Conversely, the presence of non-complementary or mismatched targets does not effectively stabilize the nanoprobes, and they aggregate after salt addition with concomitant color change in the solution from red to blue/purple. AuNP, gold nanoparticle; NP, nanoparticle.

1.2.2.1 Non-cosslinking assay optimization

NCL approaches using DNA-modified AuNPs for molecular detection constitute powerful tools with potential implications in clinical diagnostics and tailored medicine. From detection of pathogenic agents to identification of specific point mutations associated with health conditions, these methods have shown remarkable versatility and simplicity.

In NCL hybridization assays, the colorimetric result is achieved by a differential aggregation of nanoprobes in solution, according to hybridization to different targets or in the absence of target. After the hybridization step, this aggregation usually occurs in response to an increase in ionic strength provided by salt addition. However, some authors have described NCL assays using pH-induced aggregation.[194,195] Functionalization of NPs with thiol-modified oligonucleotides confers a higher stability (proportional to the oligonucleotide density) against aggregation, since the electrostatic charges of the ssDNA bases increase the repulsion forces among nanoprobes in solution.[159,160,187] NaCl and

MgCl$_2$ are commonly used electrolytes for developing this colorimetric result. Divalent salts are capable of inducing aggregation at lower concentrations than monovalent salts; nevertheless, it is important to consider that divalent cations could also lead to a semi-crosslinked aggregation by coordinating phosphate groups in the nanoprobes.[196,197] Aside from this, nanoprobe concentration can also affect stability assays, for it is directly related to the interparticle distance in solution. Lower concentrations reflect larger interparticle distances and limit the probability for nanoprobes to interact with each other. So, an optimal concentration is required for extensive aggregation to occur.[198]

Strick control of pH should be considered for the development of NCL methods, namely, during DNA hybridization, since an optimal hybridization occurs in the 6.5–8 pH range. pH value directly influences hybridization efficiency and target:probe specificity: a pH of 8.0 permits discrimination between a complementary and a single-base mismatched target, since it considerably decreases non-specific bindings.[199] However, this is somewhat dependent on the setup, as some NCL hybridization approaches have shown the capability to effectively discriminate SNPs at a pH 7.[186,191] Moreover, this discrimination is improved if the mismatch is located at the 3' end of the Au-nanoprobe, as nucleotide bases near the 5' end become less available for base pairing interaction, due to stronger electrostatic interactions.[199,200]

A different feature that influences hybridization efficiency is oligonucleotide density at the Au-nanoprobe surface. By tuning the optimal conditions for stability and hybridization, differential integrity of nanoprobe:target complexes for different target complementarities (100 % complementary, noncomplementary or mismatched) may be optimized, which would be translated into distinct aggregation profiles and enhanced discrimination.

The colorimetric result, visible to the naked eye, constitutes one of the great advantages of the method. Besides this, the color change can be followed up in a ultraviolet–visible (UV-Vis) spectrophotometer in a relatively short time period after salt addition (usually 15 min is enough to reveal a colorimetric result).[159,160,193] The ratio between the absorbance at 525 nm (Abs$_{525nm}$) and at 600 nm (Abs$_{600nm}$) has been found to be a powerful analytical tool to evaluate surface plasmon resonance variations. Abs$_{525nm}$ and Abs$_{600nm}$ represent the typical absorbance maxima for the dispersed and aggregated Au-nanoprobes, respectively.[192] This ratio may not be accurate when different aggregation levels are not so pronounced (e.g., in case of mismatch target discrimination), since the noise level in the spectra increases. This can be countered by using the trapezoidal rule to calculate the area under the curve (AUC) corresponding to the disperse and aggregated fractions, and conjuring an adequate ratio between them, indicative of differential aggregation.[123,201]

1.2.2.2 Non-crosslinking assay application to biomolecular detection

Development of highly sensitive, selective and inexpensive approaches for biodetection is of great importance for clinical diagnostics of infectious diseases, genetic disorders and monitoring toxicity at both clinical and environmental levels. PCR is still considered the gold-standard technique for molecular detection associated with clinical diagnostics.[202,203] However, PCR-based techniques are generally more expensive due to reagents and enzymes, specialized personnel and equipment.[202] Colorimetric assays that use Au-nanoprobes combine several advantages in the development of new biosensors with potential implications in nanodiagnostics,[204] exhibiting rapid, simple and visible to naked eye results, with high specificity and PCR-comparable sensitivity (10–100 ng of DNA/RNA), at significantly lower costs.[123,160] The fact that Au-nanoprobe assays permit the detection of biomarkers directly on RNA samples is a major advantage, since it eliminates the stochasticity of reverse transcription and amplification processes, and enables fast and simple gene expression studies with a direct correspondence between output and biological targets.[123,124, 160,203]

Additionally, this methodology reduces carry-over contamination, since the reaction is performed in a single tube, does not require heavy implementation and is a suitable alternative to fluorescence- or radioactivity-based assays. With significant impact on cost, time, specificity and sensitivity, this detection technique is able to multi-target gene detection, is well suited for miniaturization and can be easily adapted to automated high-throughput screening.[165,204,205] As described in table 1.5, the NCL design has been applied in the detection of specific nucleotide sequences, mutations or SNPs.

Table 1.5 The different applications of the non-crosslinking nanoprobe assay: samples, targets and probes.[206]

Field	Sample	Analyte/ Amplification process	Target	Target discrimination	Nanoprobe core	Ref
Human pathogens	*Mycobacterium tuberculosis* (clinical samples)	DNA/ PCR or LAMP	*rpoB* or *gyrB* genes	Complete sequence hybridization	AuNPs	159, 192,207,208
	Drug resistance in *Mycobacterium tuberculosis* (clinical samples)	DNA/ PCR or LAMP	*rpoB* gene mutations (rifampicin resistance)	Single-base mismatch	AuNPs	207,208
		DNA/ Multiplex PCR	*rpoB* and *inhA* gene mutations (multidrug resistance)	Single-base mismatch	AuNPs	209
	Salmonella typhimurium	RNA/ NASBA	*dnaK* gene	Complete sequence hybridization	AuNPs	210
	Saccharomyces bayanus	Unamplified total RNA	*FSY1* gene	Complete sequence hybridization	AuNPs	160
	Dengue	Unamplified total RNA	5' cyclization sequence	Hybridization and DNAzyme cleavage	AuNPs	203
Cancer	Colorectal adenocarcinoma	DNA/ Single-base primer extension	*KRAS* gene	Single-base mismatch	AuNPs	191
	Multiple cancers (one-pot multiplex detection)	DNA (Forty-mer ssDNA oligonucleotides)	*TP53* gene	Complete sequence hybridization	AuAg-alloy-NPs	211
		DNA (Forty-mer ssDNA oligonucleotides)	*c-MYC* gene	Complete sequence hybridization	AuNPs	

	CML (one-pot multiplex detection)	Unamplified total RNA	*BCR-ABL1* fusion gene (e14a2 transcript)	Complete sequence hybridization	AuNPs	[123,124]
		Unamplified total RNA	*BCR-ABL1* fusion gene (e1a2 transcript)	Complete sequence hybridization	AuAg-alloy-NPs	
Other human diseases	*β*-thalassaemia	DNA/ PCR	*β-globin* gene	Single-base mismatch	AuNPs	[193]
	Obesity (clinical samples)	DNA/ PCR	*fto* gene	Single-base mismatch	AuNPs	[212]
	Diabetes	Peptide	Neurogenin 3	Antigen-antibody interaction	AuNPs	[213]
Toxicology and Metabolism	Alkylating agents	DNA adducts	Glycidamide-guanine adducts	Secondary structure between analyte and aptamer	AuNPs	[201]
	Household paints	Metal ion	Pb^{2+}	Secondary structure between analyte and aptamer	AuNPs	[214]
	Fish	Metal ion	Hg^{2+}	$T-Hg^{2+}-T$ coordination	AuNPs	[215]
	General mercury toxicity	Metal ion	Hg^{2+}	$T-Hg^{2+}-T$ coordination	AuNPs	[216]

AuAg-alloy-NPs, gold/silver alloy nanoparticles; AuNPs, gold nanoparticles; CML, chronic myeloid leukemia; LAMP, loop-mediated isothermal amplification; NASBA, nucleic acid sequence based amplification.

Genes: *c-MYC*, avian myelocytomatosis viral oncogene homolog; *dnaK*, chaperone; *FSY1*, fructose symporter 1; *fto*, α-ketoglutarate-dependent dioxygenase; *gyrB*, DNA gyrase, subunit B; *inhA*, enoyl-[acyl-carrier-protein] reductase; *KRAS*, Kirsten rat sarcoma viral oncogene homolog; *rpoB*, DNA-directed RNA polymerase, subunit B; *TP53*, tumor protein 53.

1.2.2.3 Point-of-need devices

These NCL-based biomolecular strategies are beginning to leave the test tube to integrate more complete platforms for detection, with a focus on miniaturization, portability and even envisioning a translation to the clinical setting, with a direct impact on society. The development of point-of-need devices for molecular diagnostics faces some challenges when integrating biochemical or analytical assays onto miniaturized systems, mainly in terms of automation, amount of information, reproducibility and throughput.[217,218] The NCL colorimetric assay shows great potential towards miniaturization and integration into medical diagnostic systems.[169,204] The simple principle of detection in NCL assays can readily be integrated into systems with a previous sample preparation step, for example, microfluidics, constituting rapid, inexpensive alternatives, with medium-to-high throughput capabilities, without the need for specialized personnel.

NCL Au-nanoprobe–based DNA analysis was demonstrated on a microfluidic device with a slight variation: instead of aggregating, AuNPs deposited onto the substrate made of polydimethylsiloxane (PDMS).[219] Even though this remarkable platform requires further optimization and insights into the mechanism of deposition, the outcome is very promising. The reaction on the PDMS microchip required only a small sample volume (3 µl) and discrimination of the target DNA was possible within five minutes with high sensitivity values. In a separate study, a PDMS chip has also been successfully applied for the detection of *Mycobacterium tuberculosis* using only 3 µl of DNA solution.[220] A gold-on-paper platform was developed to combine the colorimetric changes of the NCL Au-nanoprobe assay with inexpensive paper-based platforms and digital image. The wax-printed plate is impregnated with $MgCl_2$ to induce Au-nanoprobe aggregation, yielding a colorimetric discrimination dependent on the absence/presence of the complementary target. With the help of a smartphone and a simple data analysis tool, unequivocal and fast identification is possible.[221]

In a near future, routine laboratory diagnostics will be revolutionized by means of nanoscale-enabled technology. These nanoscale devices shall substitute the cumbersome equipment and biochemical reactions required for assessing genomic and transcriptomic biomarkers. One of the main impacts will be in sensitivity, where it is expected that the current limits of detection will be surpassed, and molecular diagnostics will focus on two main approaches: miniaturization of devices and platforms to assist clinicians at POC and patients in ambulatory medicine; and increase in sensitivity for low sampling and wide-ranging analytical output. These approaches will be instrumental for effective precision medicine. AuNPs, will play a key role in setting up standards in biosensing taking full advantage of portability at a low cost.

1.2.3   Gold nanoparticle-based theranostics

Significant efforts have been made in the past years towards understanding the genetic and pathophysiological processes contributing to malignant transformation and tumorigenesis. The overwhelming amount of information thus retrieved is now being translated into the field of biomarker discovery and foster cancer therapy by selective interference with cancer hallmarks. Despite these efforts, conventional cancer therapy, including surgery, chemotherapy and radiation, lack target cell specificity and are often disconnected from individual diagnosis. Also, the efficacy of conventional therapeutic strategies is often limited by the acquisition of multidrug resistance by tumor cells and by poor drug penetration into the tumor [222]. This is why several molecular targeted therapeutics have been designed to selectively target tumor cells, thus improving efficacy and decreasing toxicity.[223] These novel targeted therapeutics may be engineered to simultaneously provide information about delivery, biodistribution and diagnostics, e.g., as imaging agents allowing disease detection at its early and asymptomatic stages.[149]

Integration of diagnosis and therapy in a single platform has been termed theranostics, which has promised to significantly increase the precision and effectiveness of treatment, shifting the current clinical standard from generalized procedures to a personalized or precise approach.[224–227] Consequently, theranostics shows particular impact in heterogeneous diseases that require individualized and tailored methods of treatment and monitoring, such as cancer,[147, 149,228] rheumatoid arthritis,[229] infectious and cardiovascular diseases.[230,231] Nanotechnology has proven its capability to engineer solutions to enhance theranostics – nanotheranostics – to simultaneously diagnose a disease and monitor therapeutic efficacy noninvasively and in real-time. This tailored approach enables physicians to customize treatment based on each patient's responses and needs, thereby preventing unwanted deleterious side-effects or sub-optimal dosage that might lead to drug resistance, incomplete remission and relapse.[232,233]

Nanostructures' primary advantage is their size and their augmented surface area-to-volume ratio. They can be loaded with a plethora of (bio)molecules, such as imaging moieties (e.g., fluorophores), targeting (e.g., antibodies, peptides), therapeutic agents (e.g., chemicals/drugs, siRNA, therapeutic oligonucleotides, etc.) and stabilizers (e.g., polyethylene glycol (PEG)), which greatly favor solubility, bioavailability, and circulation half-life. These nanocarriers provide a platform for vectorization of these (bio)molecules, at high density; a protective effect upon the cargo, preventing degradation before reaching the biological target; enhancement of delivery, cancer cell uptake and deep tissue penetration, ensuring time and spatial control over imaging and/or therapeutics.[149]

Amongst the nanosized dependent properties, the optical properties of these nanocarriers have been widely explored in nanotheranostics' application. In fact, SPR resulting from photon confinement to the small particle size is a remarkable property of noble metal NPs, such as gold, which has found a multitude of biological and medical applications.[147,234,235] Indeed, these multifunctional platforms allow monitoring the route taken by the formulation, its delivery kinetics, intra-organ and/or intra-tumor

distribution, which ultimately allow evaluation of strategy and tuning of efficacy. Nevertheless, there are still some drawbacks, such as (i) the overwhelming relevance attributed to the enhanced and permeability retention (EPR) effect; (ii) the poor tumor/tissue penetration of nanoformulations that render them ineffective due to stromal modifications; (iii) the need for a more effective targeting of metastasis; and (iv) the toxicological impact on the whole organism.[222]

Despite these drawbacks, AuNPs have led the world of nanotheranostics with their unique physical and chemical properties. They can be synthesized in different shapes such as spheres, hollow, rods, diamonds, prisms, cages, either as single solid bodies or in a core shell format.[236,237] Each combination of size and shape shows slightly different properties that may be explored for theranostic purposes, such as optical properties from intense bright colors, contrast agents and photothermal capability in the infrared (IR), near infrared (NIR) and visible range, biofunctionalization potential and low toxicity.[238,239] What is more, hollow NPs and nanocages show the advantage of simultaneously acting as encapsulating vectors, allowing a higher load of agents per particle.[240]

Despite the divisive studies about AuNPs' toxicological impact *in vitro* and *in vivo*, spherical AuNPs between 10 and 60 nm in diameter are generally considered as non-toxic.[241–243] In fact, toxicity may vary with administration route, concentration and surface coverage but also with the NPs' sizes and shapes. The difficulty in standardization of the nanoconjugates, their characterization and the effect of monitorization, has strained the definition for nanosafe AuNPs.[244,245] For example, larger particles, 45 nm in size, have been demonstrated to exhibit higher cytotoxicity at a lower concentration (10 μg/mL) than those 13 nm in size (75 μg/mL).[242] Oral and intraperitoneal administration routes showed higher toxicity than tail vein injection on mice.[246] Sharp-edged NPs tend to have higher cytotoxicity than rounded ones, with several studies showing that lower concentrations are needed for stars and flowers to induce toxicity, compared to nanospheres.[247,248] On the other hand, sharp-edged conformations are more prone to endosomal escape favoring drug delivery.[249] These factors have been extensively debated in several studies.[250–253]

1.2.3.1 Targeting and delivery

AuNPs can be functionalized with molecules to provide for targeting and to enhance stability and biocompatibility *in vivo*.[243] There is a wide range of stabilizers available that may also act as therapeutic agents (e.g., miRNA, siRNA, DNA, peptides and antibodies) or to reduce NPs' immunogenicity (e.g., PEG). In fact, PEG of different molecular weights is one of the most frequently used biomolecules to increase NPs' circulation half-life and improve cellular uptake.[254,255] When referring to PEG grafting to AuNPs' surfaces, bi-functional PEGs (with a thiol group in one extremity and another group at the other end - amine, carboxylic, biotin, azide) have been widely used for direct coupling to another molecule of interest via straightforward chemistry with high yield.[256] AuNPs can be further engineered to trick the immune system, avoid removal from circulation or to cross biological barriers (e.g., blood-brain barrier), in order to increase therapeutic efficacy and allow systemic tracking.[257]

Passive targeting takes advantage of the fact that vessels surrounding solid tumors are leaky, due to incomplete endothelial linings, allowing nanomedicines to reach the tumor through the EPR effect alone. Generally, particles between 10 and 60 nm in diameter tend to passively accumulate in tumor tissues enabling, for instance, higher drug payload at the tumor site and circulating half-lives about 100 times longer than that of free anticancer drugs, with reduced systemic toxicity.[258,259] However, this strategy depends greatly on the degree of tumor vascularization and angiogenesis and on heterogeneous blood flow, which limit drug uptake and homogenous distribution within the tumor. Several approaches may overcome these limitations, for instance, using vasoconstrictive drugs. These agents cause normal vessels to constrict and blood pressure to increase, while tumor vessels do not respond to this effect because of insufficient muscular structure, thus leading to a relative increase in the input function of tumor tissues.[260] Although the EPR effect might be useful when treating confined tumor sites, it is not a factor when treating cancer cells on the bloodstream.

Another valuable strategy to increase NPs efficacy and specificity relies on attaching targeting moieties to their surface. Typically, NPs reach target cells through ligand-receptor interactions that induce receptor-mediated endocytosis and drug release inside the cell.[259] Peptide conjugation to AuNPs is one method by which active and specific targeting may be used for enhanced tumor accumulation/delivery. Chanda and collaborators used bombesin peptide-functionalized AuNPs to target the gastrin-releasing peptide (GRP) receptor which is overexpressed in breast, prostate, and small-lung carcinomas.[261] Bombesin peptide-functionalized AuNPs exhibited GRP-enhanced tumor accumulation and decreased liver uptake compared with nonspecific protein-conjugated AuNPs. In three other studies, it was possible to actively target endothelial cells of the tumor vasculature, through αvβ3 integrin, using an arginylglycylaspartic acid (RGD)-peptide conjugated to an AuNP. These RGD-functionalized AuNPs showed an increased tumor accumulation in mice xenograft studies.[262–264]

Successful targeting has also been achieved via functionalizing AuNPs with antibodies that recognize specific receptors overexpressed by cancer cells: transferrin,[265] epidermal growth factor (EGF)[243,266–271] and folate receptors.[272–275] Fernandes *et al* designed a multifunctional AuNP system composed of a monoclonal antibody against EGFR and a compound (TS265) with proven antiproliferative activity towards cancer cells. *In vivo*, the nanoformulation efficiently delivered TS265 in a controlled selective manner, boosting tumor cytotoxicity, when compared to the nontargeted counterpart or to the free compound.[243] Lu *et al* demonstrated that folate functionalized NPs were 4.7 times more directed to tumor cells and internalized by endocytosis into lysosomes when compared to non-functionalized NPs.[276] Targeting has been crucial for the development of vectorization systems capable of site specific accumulation/retention enabling NPs to deliver their cargo on site for improved therapeutic effect.[258]

Some authors have been focusing their attention on developing nanovectorization systems that mediate cargo delivery upon a particular stimulus, such as pH, increased heat, ultrasound, light and magnetic field. Tumor cells usually become hypoxic and exhibit high glycolytic activity, thus producing

carbonic and lactic acids.[277] Coating NPs with pH Low Insertion Peptides (pHLIPs) increase efficiency of targeting acidic diseased tissues. pHLIP, being a membrane peptide, has affinity to cellular membranes and targets extracellular acidity. In contrast to other pH-sensitive systems, it tracks acidity at the surface of cancer cells.[278] Antosh and collaborators reported a 34 % increase in pHLIP decorated NPs in contrast with AuNPs alone, on human lung carcinoma cell lines at pH 6.0.[279] Photothermal conversion of light into heat can increase target cells' temperature, enough to directly kill cells.[239,280] but also to release therapeutic moieties at the tumor site.[281] In a similar manner, ultrasounds and magnetic fields can locally increase temperature and precisely deliver cargo.[282] Despite the broad range of targeting approaches, there is still much more to explore in this field with many groups still looking for new effective targeting moieties that allow tumor specific accumulation and retention for improving drug release and therapeutic efficacy.[258,277]

1.2.3.2 Therapeutic agents

Drug discovery coupled with pre-clinical studies strongly focus on overcoming general issues that hamper the efficacy of drugs, such as limited solubility, high toxicity, high dosage, nonspecific delivery and short circulating half-lives.[283] Due to the advances in nanotechnology based drug delivery, the current idea has been to repackage classic drugs using targeted delivery systems to increase patient compliance, extend the product life cycle and reduce healthcare costs. Beside small drugs, these agents might be a peptide/antibody, a ribozyme, a siRNA or an antisense oligonucleotide.[256] Probably the most studied and used concept has been Doxil® (Janssen Products, Horsham, PA, USA), where doxorubicin (approved by FDA in 1974 to treat a broad range of cancer types) has shown improved efficacy when encapsulated into PEGylated liposomes. In fact, traditional chemotherapy drugs (e.g. vincristine, paclitaxel, cisplatin, etc)[284–287] and other potential anti-tumor metal compounds[288] have followed suit and been encapsulated and delivered in similar engineered vesicles.

AuNP/doxorubicin nanoformulations attempted to mimic their liposome counterpart and showed promising advantages, such as increased targeting and functionalization as well as the possibility to couple with phototherapy and to act as imaging/contrast agents.[289] Various AuNPs shapes have been functionalized with doxorubicin – stars,[262] clusters,[290] shells,[291] hollow spheres,[292] etc - showing the versatility of the nanoconstructs and their ease of functionalization. All previous examples were tested *in vivo* and have shown increased efficiency when compared with doxorubicin alone, as well as lower levels of cytotoxicity.

AuNPs have been also applied in therapeutic approaches in combination with anti-tumor drugs (e.g., platinum prodrugs,[293] 5-fluorouracil,[294] irinotecan,[276] camptothecin[295,296], Co(II) coordination compound[243]). All nanoformulations showed remarkable anticancer activity when compared with the free drug. For instance, Shi and collaborators described the use of gold hollow and nanocage shells layered with mesoporous silica and a thermosensitive polymer loaded with camptothecin. The drug is tightly packed inside the nanoconstruct with a "leakage" of only 6.8 % to the medium after 14 h in *in*

vitro conditions. NIR triggered release of the drug leading to increased tumor cell death, compared with only NIR or nanocarrier exposure.[295]

Gene therapy has been receiving increasing attention in tumor suppression due to the possibility to downregulate specific oncogene expression or to sensitize cells in an intra-cellular targeting process. In particular, small interfering RNA (siRNA) has shown potential to downregulate specific gene expression in cancer cells.[178] Since naked siRNAs show extremely short half-lives due to cellular RNases activity and poor chemical stability, the development of efficient delivery vehicles for *in vivo* applications remains a major obstacle in translating siRNA into effective therapeutics. AuNPs have been widely used as nanovectorization for gene silencing strategies.[297–300] Almost all the different shapes and sizes of AuNPs reported above have been used to vectorize gene silencing elements into cancer cells.[301,302]

Feng Yin reported the use of a light-triggered therapy using gold nanorods as nanocarriers for dual-delivery of doxorubicin and *KRAS* gene siRNA. The synergistic effect of the chemo- and gene-therapy allowed the reduction of the tumor volume rate by 90 % *in vivo*.[303] Gold spheres were described for siRNA targeting and delivery using models of increasing complexity (cells, hydra and mice), achieving effective silencing of *c-MYC* gene (~65 % reduction in expression). It was also shown that covalently bounded siRNAs were more effective silencers than siRNAs adsorbed on the surface of the NPs.[304]

Different molecular concepts for gene silencing rather than siRNA have also been used to block a particular gene. Baptista's group was pioneer in the use of hairpin ssDNA structures vectorized via AuNPs to particularly silence any possible RNA mediated pathway inside the cell.[300,305,306] In fact, the molecular actuator thus developed - gold nanobeacon (Au-nanobeacon) - is one of the most effective molecular nanotheranostics platforms, since the hairpin may be further functionalized with a fluorophore, whose fluorescence is triggered once the silencing event occurs. The potential of this system has been further characterized *in vitro* and *in vivo* with low toxicity.[241, 304,305,307] Furthermore, this system was shown to be effective *in vivo* in a promising approach to combat multidrug resistant tumors, combining in the same particle an antitumor agent (5-fluorouracil) with silencing of *MRP1*, a gene associated with acquired resistance in several tumors. *In vivo* results showed a remarkable tumor size reduction, from the synergic effect of the two agents.[294] Using gold nanobeacons, Bao *et al* were able to silence *KRAS* gene and reduce gastric tumor size in mice by 60 %, tumor vascularization by 90 % and lung metastasis by 80 %.[297]

1.2.3.3 Phototherapy

Photothermal therapy (PTT) is based on the selective sensitization of cells to thermal damage, or hyperthermia, near 45 °C. What is more, traditional PTT may be coupled to AuNPs and profit two ways: (i) the possibility to vectorize additional cargo and use the NP as scaffold for selective targeting; and (ii) enhance PTT by the AuNPs' ability to convert absorbed photons into thermal energy. By modulating the AuNPs' shape and/or shell thickness, it is possible to shift the localized SPR peak of AuNPs toward

the near-infrared (NIR), allowing deeper light penetration into tissues. Moreover, the laser energy required to achieve this transformation is far below that stipulated in medical safety standards. AuNP-mediated PTT is predominantly associated with nanorods, nanoshells and nanocages.[308,309] For example, hollow gold nanospheres (44 nm-diameter), one of the first nanotheranostics systems to be evaluated *in vivo*, have shown comparable photothermal capacity using 100 times lower concentrations to that of superparamagnetic iron oxide silica coated counterparts.[310]

Wei Lu *et al* reported in 2009 the use of hollow gold nanospheres carrying siRNA *in vivo*. After intravenous injection of the nanoconstruct and NIR laser (800 nm) irradiation, significant downregulation of the target oncogene was observed, when compared to non-exposed tumors on the same mice. Moreover, the authors proved that the escape of the NPs from the lysosomes and siRNA release in the cytosol was irradiation-dependent, coining this method as "photothermal transfection".[310] Due to their NIR band, gold rods have also been used for photothermal transfection[311] coupled to NP imaging,[312] hyperthermia,[313] or co-delivery.[303,314]

A recent study has also focused on smaller spherical AuNPs that show improved photoconversion capability from irradiation in the visible range using standard green lasers. Efficient light-to-heat conversion of AuNPs irradiated in the visible region (at the SPR peak: 530 nm) resulted in the *in vitro* elimination of laser-exposed breast cancer cells. A synergistic interaction between heat and conventional breast cancer drug doxorubicin was also observed.[239]

Another strategy that can be coupled to nanosized structures is photodynamic therapy (PTD), which involves the administration of a nontoxic agent that acts as a photosensitizer (PS) and a laser source. Photoexcitation of the photosensitizer leads to the generation of free radicals, which destroy tumor tissue.[315] Combining PDT with AuNPs has proven to be a good strategy to overcome two of its major limitations: the dark toxicity of the PS and the poor selectivity of the cellular uptake of PS between the target cells and normal tissues.[316,317]

1.2.3.4 Multimodal Imaging

The implementation of imaging techniques for diagnostic purposes enables the non-invasive assessment of anatomical, functional and molecular information, with image-guided drug delivery gaining much attention nowadays.[318] The imaging modalities most often used in the clinics are computed tomography (CT), ultrasound (US), magnetic resonance imaging (MRI), positron emission tomography (PET), single-photon emission computed tomography (SPECT), photoacoustic tomography (PAT) and fluorescence imaging.[319] When choosing an imaging technique, one should take into consideration several parameters: target tissue, resolution, sensitivity, contrast and implementation.[320–323]

AuNPs are optimal contrast agents for CT, due to the relatively high X-ray attenuation of gold and the stability of gold colloids. Since gold has higher absorption than iodine, AuNPs can achieve better contrast with lower X-ray dose.[228] On the contrary, AuNPs do not possess intrinsic properties that enable

their visualization through MRI; hence, they are usually combined with super-paramagnetic iron oxide (SPIO), gadolinium or manganese, demonstrating significant contrast enhancement in tumor models.[324] Furthermore, *in vivo* studies with gold nanorods labelled with radioactive iodine enabled photothermal therapy towards ovarian cancer and monitoring of NPs' distribution via SPECT/CT imaging. Tumor sites were clearly visualized from the SPECT images even at 24 h post-injection.[325]

Fluorescence imaging is highly suitable for high-throughput screening with high sensitivity, providing detailed molecular profiling with subcellular resolution, enabling multicolor imaging and being relatively inexpensive, but has low tissue penetration and spatial resolution, thus limiting its applications in clinical settings. Using the NIR part of the spectrum for fluorescence-based imaging, spatial resolution is improved and autofluorescence is highly reduced making the technique much more attractive for clinical applications.[272,326]

Owing to their underlying physical principles and distinct benefits/drawbacks, one can take advantage of combining two or more techniques in a single nanocarrier, avoiding a repeated challenge to the patient's immune system and providing more accurate and dependable data on the patient's condition than using a single imaging moiety.[327,328] Liu *et al* report the use of gold nanostars for multimodal imaging. Combining CT, surface-enhanced Raman scattering (SERS, of molecules adsorbing on a noble metal surface) and thermal imaging, authors could accurately detect gold stars located in the tumor and further confirm photothermal effectiveness with a thermal camera.[329] Other successful examples of combined imaging modalities using AuNPs include: a multicomponent nanocapsule used for real-time US and high-resolution MRI for image guided photothermal tumor ablation.[330]

Since the challenges of efficient tumor treatment include accurately identifying the location and size of tumors and monitoring the effectiveness of therapy after treatment, integration of contrast-enhanced diagnostic imaging capability with photothermal therapy is a winning bet in the fight against cancer.

1.2.3.5 From research lab to the clinic

The use of gold in medicine dates back to 2500 BC when Chinese and Arabic physicians used gold preparations in their practice. Medieval physicians used mixtures of colloidal gold for various ulcerative skin conditions. In the 20th century, several formulations of gold salts were used to treat tuberculosis, *Lupus vulgaris*, syphilis and rheumatism. In 1997, Guy Abraham and Peter Himmel reported the use of 20 nm AuNPs for rheumatism treatment in 10 patients.[331] Their results showed a "rapid and dramatic" positive effect on the tenderness and swelling of joints with no evidence of toxicity in any of the patients. Since then, there have been no follow-up studies on AuNPs for rheumatism in clinical settings.

Recombinant human tumor necrosis factor alpha (rhTNFα) was applied in the 80s with remarkable antitumor effects in mice, inducing apoptosis, cytolysis or cytostasis of tumor cells. However, multiple

phase II studies, with more than 156 patients, resulted in only one complete and one partial response at the maximum tolerated dose, which may correlate to a low therapeutic dose at disease site. CYT-6091(Aurimune®) from CytImmune (Rockville, MD, USA) was the first product on clinical trial using AuNPs for patients with advanced solid tumors (ClinicalTrials.gov Identifier: NCT00356980, NCT00436410). The nanoformulation is composed of PEGylated 27 nm AuNPs functionalized with rhTNF. It was administered systemically to 30 patients at doses of rhTNF that were previously shown to be toxic, without detectable side effects.[332] In addition, gold was found in breast tumor tissue but not in healthy breast tissue showing the potential of this approach. Phase II clinical trials are ongoing, aiming at understanding if this nanotechnology approach induces greater vascular leak by dynamic contrast-enhanced MRI and to evaluate the safety and efficacy of CYT-6091.

AuroLase® (Nanospectra Biosciences, Houston, TX, USA) is an FDA-approved pilot study that uses silica-gold nanoshells with a NIR laser for photothermal therapy (ClinicalTrials.gov Identifier: NCT00848042, NCT01679470). NPs called AuroShells are injected intravenously in the patient's blood stream and accumulate passively in the tumor. This clinical trial was designed to evaluate the approach's effectiveness for the treatment of advanced lung tumors resulting from either primary lung cancer or metastatic tumors in the lung. Although the trials are complete, the results have not yet been disseminated.

1.2.4 Nanotechnology commercial impact

Nanotechnology R&D continues to grow in importance both in terms of public and private funding. Indeed, global demand for nanotechnology medical products grew by 17 % from 2009 to 2014. The USA National Nanotechnology Initiative (NNI) investment in nanotechnology R&D, policy and regulation since 2001 now totals a staggering $22 billion, with the 2016 USA federal budget providing more than $1.5 billion for the NNI. The European Union (EU) and Japan are investing substantial resources in nanotechnology, with a comparable level to the USA. The returns are expected to surpass the investment, and the medical field appears to be a front runner in nanotechnology innovations.[148]

NP-based drug delivery is one of the major areas, providing a wide range of formulations that are now beginning pre-clinical or clinical trials. Besides the traditional hurdles conventional therapeutics face to enter the clinics, nanomedicines also face a lack (or the deficiency) of protocols for the characterization of these products in terms of absorption, distribution, metabolism, excretion, and toxicity. However, the FDA, in collaboration with the Nanotechnology Characterization Laboratory, has released guidelines describing how it defines a nanoscale product - specifically, as having at least one dimension between 1 and 100 nm, or as being less than a micron in size, and demonstrating size-dependent behavior. These agencies are now drafting protocols to address nanomedicines' regulatory and safety gap. The European Commission has also established several goals in terms of nanotechnology regulation, patenting and business creation, with international cooperation being a key asset to improving R&D. Bringing the EU together with countries who are active in nanotechnology

research (USA, Japan, Switzerland and Russia) could pave the way for standardized protocols and further initiatives. The fact that nanotechnology is one of the sections included in the Horizon 2020, the biggest EU Research and Innovation Program, shows the commitment to this subject and its importance in increasing Europe's competitiveness. Its main objectives include: scaling up laboratory experience to industrial settings; ensuring the safe development and application of nanotechnologies in health and the environment; and proving the significant long-term benefits provided by nanotechnology-based systems, in terms of health care and quality of life.[148]

Nanomedicines are still at an early development stage and, thus, their impact on health spending and cost effectiveness is still difficult to predict. Can these formulations compete with conventional products in the medical sector? For example, examining the cost-effectiveness of chemotherapy (gemcitabine) *versus* nanotherapy (PEGylated liposomal doxorubicin) for ovarian cancer showed that the chemotherapy pre-treatment costs were cheaper by €1285. Nonetheless, these costs were more than offset by administration and hospitalization costs, which were €2670 in favor of nanotherapy. The clinical benefit associated with nanotherapy was proven, yielding not only positive cost-effectiveness results, but also significant financial savings.[333]

Nanotheranostics innovations, specifically, can have a significant impact on health costs by reducing the number of diagnostic tests and increasing therapy efficacy. Additional savings are expected due to the overall reduction of the number of days in hospital for each patient. Hence, the global market for nanomaterials used in theranostics is anticipated to be more than $187 billion.[148] Despite these figures and expectations, those relating to AuNPs alone are just the tip of the iceberg. Another good indicator of AuNPs' increasing impact on the medical sector is the number of companies that are devoted to R&D in this area alone. Due to high competition among market players and low yield coupled with high expenditures in R&D, most companies choose to invest in specific end-use applications: diagnostic tests for the point-of-care market, biomedical imaging or photothermal therapy. Successful examples include Nanospectra (Aurolase®) and Cytimmune (Aurimune®) whose flagship products are now facing clinical trials. Although the market for gold nanomaterials is still developing, their clinical and financial benefits are undeniable. In the future, efforts should be made to improve the bridge between academia, R&D companies, regulatory agencies and the pharmaceutical industry.

1.3 Nanotechnology towards leukemia management

Nanodiagnostics

An effective treatment depends heavily on the accuracy and sensitivity of diagnosis. Traditionally, leukemia cells are detected through morphological, cytogenetic and molecular analysis of cells, that relies on the detection via fluorescent markers, FISH, PCR and/or DNA sequencing. Several nanocarriers have been researched for leukemia biosensing,[225] but for the purpose of this study and for all the reasons disclosed in section 1.2.2 (*Gold nanoparticle-based diagnostics*), this segment will focus on AuNP-based platforms.

For acute leukemia diagnostics, an anti-leukemia thiolated aptamer (sgc8c) was used to specifically recognize protein tyrosine kinase 7 (PTK7), an overexpressed transmembrane receptor in human T-cell acute lymphocytic leukemia cells. Aptamers feature a high affinity and selectivity towards their targets, and can be modified to allow the functionalization into NPs, for example, using a thiol group which permits their loading in gold surfaces through strong Au-S linkage.[334]

Since CML is associated to a unique chromosomal abnormality - *BCR-ABL1* gene - this specific target was used as a diagnostic approach using Au-nanoprobes on a NCL colorimetric assay,[123,124] and via spectral coding using Au-nanobeacons (Table 1.4).[122] Both systems enabled the distinction between the two major isoforms of *BCR-ABL1* (e14a2 *vs* e13a2), but their accuracy is yet to be tested in clinical samples.

The remaining targets for leukemia diagnostics are antigens, such as CD20, CD45 and CD19 that are overexpressed by malignant B-cells, particularly in ALL.[335] Hence, CD20 antibody (rituximab) can be used to diagnose, image and isolate malignant B-cells, through strategies involving AuNPs and SERS.[336]

Nanotherapeutics

Current treatment strategies for leukemia involve chemotherapy and radiation, which often induce long-term side-effects and multidrug resistance, or more invasive strategies like stem cell transplant that require a matching donor. Nanotechnology provides the possibility to selectively deliver a high payload of anticancer agents to malignant cells without damaging healthy cells or systemic toxicity.[337] In addition, some tissue compartments, such the bone marrow, may be inaccessible for otherwise effective drugs. Indeed, multiple studies using different types of NPs and conjugation strategies confirm this trend also for hematological diseases.[338–344]

In a 2016 study, AuNPs were functionalized with dsDNA oligonucleotides with a sequence corresponding to a gene that is overexpressed in CML cell lines (*BIRC5*), where only the antisense strand of the DNA duplex is covalently attached to the AuNP. Dasatinib, a potent TKI frequently used against CML, was conjugated to the non-covalently linked DNA strand. Targeted RNA binds to the antisense oligonucleotide and displaces the drug-conjugated DNA oligonucleotide proportionally to

BIRC5 mRNA in cells.[345] Other studies examined the efficacy of drug-coated AuNPs on AML treatment improvement, using different TKIs or fludarabine.[346–348] One of these took additional advantage of the fact that folate receptors are highly overexpressed on the surface of many tumor types and used folic acid to target AML cells.[348]

Nanotheranostics

When designing a nanotheranostics vector for hematological malignancies, one should take into consideration the following parameters: (1) choice of most suitable nanocarrier for effective delivery and cell internalization; (2) the effector molecule, usually conventional drugs or nucleic acids; (3) ensure controlled release of effector molecule; (4) an imaging component that allows for the real time monitoring of the nanoconjugate location and effect on targeted aberrant cells; (5) an active targeting agent, typically a cell-surface marker or an oligonucleotide, that maximizes specificity of the vector and minimizes damages to healthy cells, whether in peripheral blood or when targeting the bone marrow (Figure 1.4). Note that passive targeting also occurs via the EPR effect characteristic of confined tumor sites, such as the bone marrow, due to leaky vasculature, hypervascularization and lack of lymphatic drainage. This is the first and necessary step for therapeutic nanoconjugates or free drugs to accumulate in these locations, then active targeting could be achieved.[222]

The only pre-clinical study of a nanotheranostics approach used for leukemia management was done on a CML *in vivo* model, but using magnetic NPs. These were functionalized with an antineoplastic drug, paclitaxel (pac-MNP). Paclitaxel formulations can augment the anti-leukemia activity by coordinating different apoptotic signaling cascades. Pac-MNPs, acting as both drug delivery and magnetic resonance imaging contrast agent, were further functionalized with lectin glycoprotein which resulted in higher cellular uptake and lower IC$_{50}$ value suggesting the efficacy of targeted delivery of paclitaxel. Moreover, these nanoformulations showed prolonged circulation time in serum suggesting increased bioavailability and therapeutic effect of the drug *in vivo*. The nanocarrier acted as theranostic mediator, helping in early diagnosis and monitoring of leukemia, during and after treatment.[349]
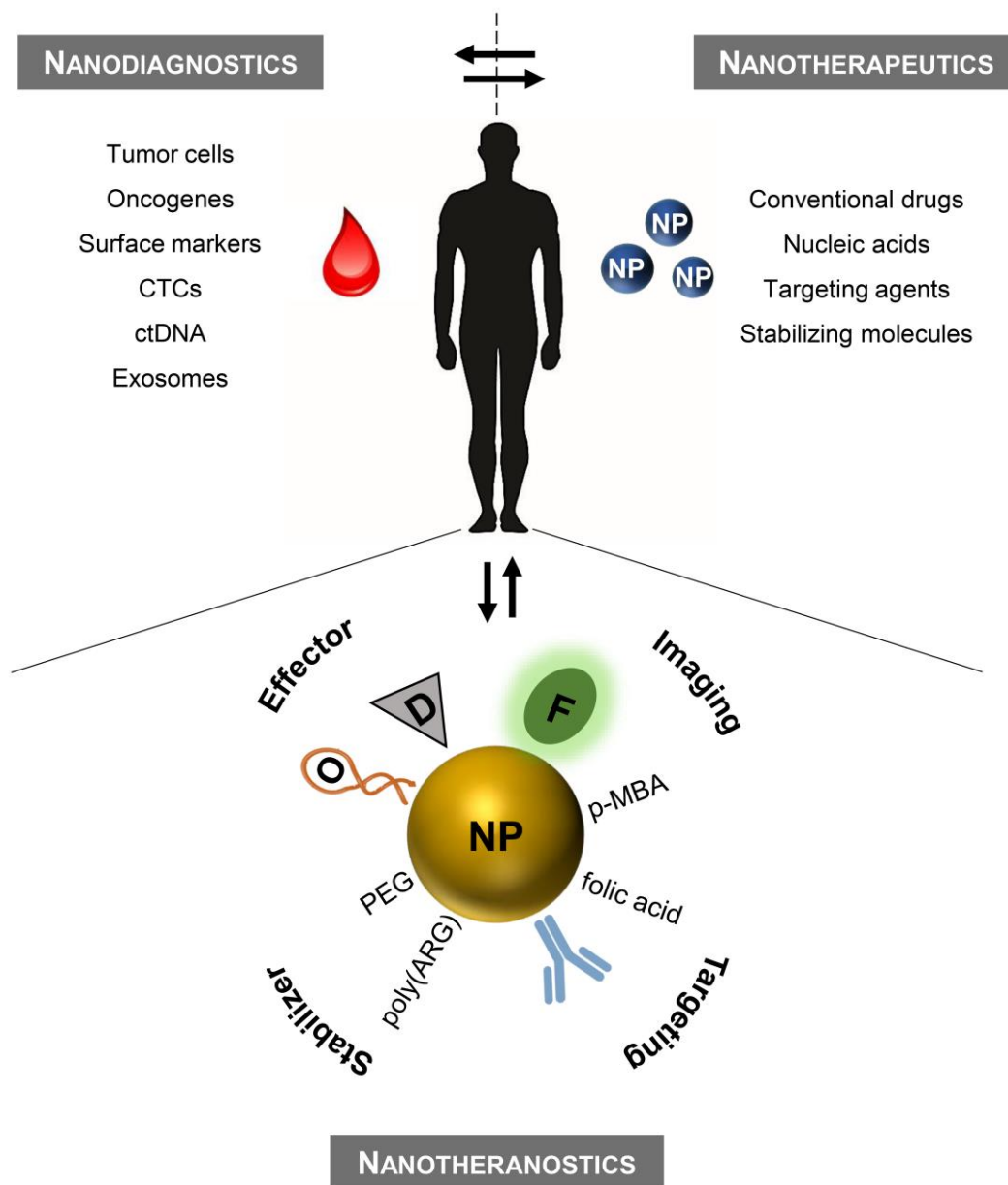
Figure 1.4 Precision nanomedicine for the management of hematological disorders. Nanodiagnostics based on liquid biopsies to assess multiple leukemia biomarkers using nanoparticles (*ex vivo* analysis). Nanotherapeutics according to the patient's molecular profile (*in vivo*). Nanotheranostics combines diagnostics and therapeutics onto a single nanomaterial. Therapeutic efficacy may be improved for standard chemotherapeutics by efficient delivery to the target that can be monitored in real-time. CTCs, circulating tumor cells; ctDNA, circulating tumor DNA; D, conventional drug; F, fluorophore; NP, nanoparticle; O, oligonucleotide; PEG, polyethylene glycol; p-MBA, p-mercaptobenzoic acid (Raman reporter); poly(ARG), poly-arginine peptide sequence.

1.3.1 Clinical trials

The described pre-clinical studies show great potential of nanomedicines in the fight against hematological malignancies but, thus far, only but a few have reached the clinical trial stage. Of these, liposomal nanoformulations seem to have some impact in blood malignancies, and recently three liposomal formulations for the treatment of leukemia have reached this milestone. In 2012, liposomal vincristine sulfate (Marqibo®, Talon Therapeutics Inc, San Francisco, CA, USA) was the first nanoformulation to get approval by the FDA to treat Ph+ ALL in adults that relapse or that do not respond to at least two anti-leukemia drugs. Vincristine inhibits microtubule formation in mitotic spindle, resulting in an arrest of dividing cells at the metaphase stage and is a standard component of chemotherapy regimens used to treat ALL and other lymphoid malignancies for over 50 years. Nevertheless, the free version of drug induces major side effects thus limiting the administered dose. Its encapsulation in a sphingomyelin/cholesterol-based liposome changed vincristine pharmacokinetics dramatically. It is now slowly released from the liposome and delivered to tissues more efficiently allowing a higher dose (ClinicalTrials.gov Identifier: NCT01439347).[350] Marqibo® has also completed phase I clinical trials for the treatment of pediatric ALL (ClinicalTrials.gov Identifier NCT01222780).[351]

CPX-351, a liposomal formulation of cytarabine and daunorubicin, has produced interesting results in phase III clinical trials for the treatment of high-risk AML. CPX-351 significantly improved overall survival, event-free survival, and response rates in comparison with the standard regimen of cytarabine and daunorubicin (ClinicalTrials.gov Identifier: NCT02286726). Annamycin, an anthracycline intended for the treatment of relapsed or refractory leukemia, has also been encapsulated in a liposome and submitted to phase I/II multi-center clinical trials. The drug was well-tolerated and showed encouraging anti-leukemic activities against ALL (ClinicalTrials.gov Identifier: NCT00271063).[352] Future studies should focus on the combination of these nanoformulations with other anti-leukemic drugs, namely TKIs, and incorporate new classes of therapeutic agents, such as, siRNA, miRs, ssDNA and gene editing.

1.4 Scope of the Thesis

Conventional chemotherapy of hematological cancers is challenged by its poor selectivity, resulting in low therapeutic efficacy and pronounced adverse side effects, which may be overturned by innovative nanomedicine approaches. Leukemia unique features have provided for the possibility of developing innovative approaches, simple and non-invasive methodologies for diagnosis and treatment using NPs. The molecular basis of each subgroup of patients is very well defined by common chromosomal translocations, shared mutations in oncogenes, gene expression profiles and immune-phenotype, which can be used as target for diagnostic testing and therapy (nanotheranostics). Moreover, a simple blood sample (liquid biopsy) provides access to the patient's full tumor profile that can support more focused therapeutic regimens. Unlike solid tumors, that require NPs to reach the site of action, liquid tumors burden is spread throughout the bloodstream. In fact, most of the barriers that NPs face to reach solid tumors are not applied in liquid tumors since circulating tumor cells are freely exposed to these agents. However, while in circulation, NPs can also be opsonized by blood proteins followed by recognition by the mononuclear phagocyte system.[353] As such, liquid tumors require slightly different diagnostic, treatment and targeting strategies.

Nanomedicine, particularly AuNP-based technology, provides several advantages for leukemia management. Concerning its therapeutic application, most studies are primarily focused on solid cancers due to the possibility to take advantage from the EPR effect experienced by tissues in the close vicinity of tumors, which enhance nanomedicine accumulation and, consequently, improve efficacy. Leukemia is addressed differently from solid tumors when nanomedicines are concerned since EPR effect is not a factor when treating bloodstream cells.

In this study, focus was given to AuNP-based nanotechnology that supports CML biomarker detection and targeted treatment. CML is a key model of leukemic hematopoiesis associated with a chromosomal translocation between the *BCR* and the *ABL1* genes. Differences in disease phenotype, prognosis and treatment are related to the qualitative and quantitative variations of the *BCR-ABL1* fusion products, thus making current CML molecular diagnostic methodologies essential to obtain the best possible outcome when it comes to treatment response. However, routine methodologies are time-consuming, expensive and some display low sensitivity. Considering the benefits of AuNPs as carriers in biological detections, the goal of this PhD project is to develop a simple method based on Au-nanoprobes able to identify a specific *BCR-ABL1* transcript type, directly in RNA samples. After validation of the assay in clinical samples, a point-of-care diagnostic device will be designed, as well as a nanotherapeutics approach for *BCR-ABL1* silencing and improvement of TKIs efficacy.

This PhD thesis will be structured around the following main stages:

i) Molecular characterization of leukemia clinical samples *(Chapter 2)*

Human bone marrow and peripheral blood samples were provided by Hospital dos Capuchos (Centro Hospitalar de Lisboa Central, CHLC, Lisboa). Samples were collected from Ph+ leukemia patients at different time points of treatment (at diagnostic and during follow-up) and from control individuals (Ph-negative leukemia patients) for posterior Au-nanoprobe assay validation in clinical samples. Particular attention was given to patients in molecular remission for sensitivity assessment.

All clinical samples (from AML, Ph+ ALL and CML patients) were routinely characterized at Hospital dos Capuchos (CHLC, Lisboa) which includes morphological, cytogenetic (karyotype analysis and FISH) and molecular analysis (RT-qPCR). At our laboratory, samples were further characterized at molecular level, including identification of transcript type and assessment of point mutations using routine methodology: RT-nested PCR[44] and Sanger sequencing. The large biological information contained in all these samples can bring new information for diagnosis, monitoring and treatment of leukemia patients and is crucial for the validation of a new nanodiagnostic system.

ii) Detection of *BCR-ABL1* transcripts in clinical samples via Au-nanoprobe assay *(Chapter 3)*

In this chapter, optimization and validation of the Au-nanoprobe colorimetric assay[123] in RNA extracted from clinical samples, not requiring retrotranscription or amplification steps, was performed. First, AuNPs were functionalized with ssDNA capable of specifically hybridizing to the most predominant *BCR-ABL1* isoform, e14a2, in biological samples. Then, the method was optimized using synthetic oligonucleotides and RNA from leukemia cell lines (HL60 or THP1, negative from *BCR-ABL1*; K562, positive for e14a2 *BCR-ABL1* transcript; BV173, positive for e13a2 *BCR-ABL1* transcript). This step allows the assessment and optimization of several features in the Au-nanoprobe assay, before moving on to clinical samples, namely probe density, selectivity, and sensitivity. Finally, the Au-nanoprobe assay was tested using fully characterized clinical samples. Comparison of the colorimetric assay outcome to the gold-standard methodology results (RT-nested PCR) should be a good indicator of the robustness of the Au-nanoprobe diagnostic assay.

iii) Development of a point-of-care device for *BCR-ABL1* RNA detection via Au-nanoprobe *(Chapter 4)*

Highly sensitive and specific biosensors based on AuNPs have opened the possibility of creating new diagnostic platforms for disease markers, especially in cancer. Based on the previous task and considering the current clinical need for a sensitive, cost-effective and fast way to diagnose CML, we intended to design a microfluidics platform for *BCR-ABL1* detection. This task was performed in collaboration with the Center of Excellence in Microelectronics Optoelectronics and Processes

(CEMOP, Universidade Nova de Lisboa), due to their expertise in the development of miniaturized biosensors.

iv) Development of a nanotheranostics approach for CML via *BCR-ABL1* gene silencing using Au-nanoconjugates *(Chapter 5)*

Based on the knowledge acquired from the previous tasks in terms of selectivity and specificity for target recognition, the aim was to develop an approach suitable for both CML nanotheranostics (diagnosis and therapy), which could lead to an effective monitoring and reduction of abnormal leukemic cells.

To achieve this goal, PEGylated AuNPs were functionalized with the same ssDNA sequence optimized in task ii), but in a hairpin conformation to potentiate the probe's selectivity to *BCR-ABL1* gene silencing, particularly the e14a2 isoform. Several parameters were assessed upon exposure of K562 cells to the Au-nanoconjugate: target and downstream gene silencing, protein expression levels, cell proliferation and apoptosis. Attention was given to the effect of the Au-nanoconjugate when combined to TKIs therapy and its efficacy on IM resistant K562 cells. Although, this Au-nanoconjugate was only tested as a nanotherapeutics approach for CML via *BCR-ABL1* gene silencing, this is the first and necessary step for the design of a successful nanotheranostics platform.

CHAPTER 2 – **MOLECULAR CHARACTERIZATION OF LEUKEMIA CLINICAL SAMPLES**

Clinical samples were kindly provided by Hospital dos Capuchos (Centro Hospitalar de Lisboa Central, CHLC, Lisbon). Hematological evaluation, cytogenetic characterization, *BCR-ABL1* gene quantification, *NMP1* and *FLT3* molecular characterization were performed at their Hematology Department, as part of their routine procedures. R. Vinhas performed *BCR-ABL1* and *CEBPA* molecular characterization, at the Research Unit on Applied Molecular Biosciences (UCIBIO, Universidade Nova de Lisboa), under the supervision of P.V. Baptista and A.R. Fernandes. Data enclosed in this chapter were originally published in the following issues:

- **Vinhas R**, Tolmatcheva A, Canto R, Ribeiro P, Lourenço A, Sousa AB, Baptista PV, Fernandes AR. 2016. A novel mutation in *CEBPA* gene in a patient with acute myeloid leukemia. Leukemia & Lymphoma. 57(3):711-713.

- **Vinhas R**, Lourenço A, Santos S, Ribeiro P, Silva M, Sousa AB, Baptista PV, Fernandes AR. A double Philadelphia chromosome-positive chronic myeloid leukemia patient, co-expressing P210$^{BCR-ABL1}$ and P195$^{BCR-ABL1}$ isoforms. [Submitted to Haematologica]

- **Vinhas R**, Lourenço A, Santos S, Lemos M, Ribeiro P, Sousa AB, Baptista PV, Fernandes AR. A novel *BCR-ABL1* mutation in a patient with Philadelphia chromosome-positive B-cell acute lymphoblastic leukemia. [Submitted to Leukemia and Lymphoma]

2.1 Abstract

Leukemia is a biologically diverse disease with a range of different chromosomal and genetic abnormalities that define subsets of the disease with prognostic relevance. Ph+ leukemia research, particularly regarding CML, was groundbreaking at several stages: it was associated to a specific chromosome abnormality, providing evidence of a genetic link to cancer for the first time; its effective genetic diagnostics allowed for an improvement on patient's overall survival; and enabled the rational drug design of the most effective agents against BCR-ABL1 expressing cells so far (TKIs).

Diagnosis of the disease plays an essential role, starting from patient's physical examination to bone marrow and peripheral blood tests that comprise hematological, cytogenetic and molecular analysis. In this chapter, focus is given to standard diagnostic procedures at molecular level: *BCR-ABL1* transcript identification, quantification and mutational analysis. A complete molecular analysis of CML, ALL and AML samples is presented.

2.2 Introduction

The Ph translocation is found in the majority of CML patients, in 25 % of patients with acute lymphoblastic leukemia (ALL), and in 1 % of newly diagnosed adults with acute myeloid leukemia (AML).[354,355] Although most CML patients present themselves in CP at diagnostics, a small but not irrelevant proportion of CML patients present in AP or even in BC when a proliferation of BCR-ABL1 positive blasts is found, making the distinction between CML, Ph+ ALL and Ph+ AML not always straightforward.[38,356] As such, full molecular characterization of chromosomal breakpoints, gene rearrangements and variations, coupled to extensive biochemical and clinical evaluation should be taken together for accurate diagnosis and treatment success.

Molecular monitoring of Ph+ hematological diseases has become an integral part of the clinical management of these patients, from diagnosis to follow-up surveillance. This is valid for transcript identification and quantification (this last is critical for monitoring minimal disease), but also for mutational analysis of the *ABL1* domain of the chimeric transcript. The latter screening is essential since it is one of the mechanisms that leads to TKI resistance, whether due to pre-existent mutations (primary resistance accounts for one third of patients) or mutations that arise from TKI treatment pressure (acquired resistance). Patients that fail to respond to IM (first generation TKI), dasatinib, nilotinib, bosutinib and ponatinib (second- and third-generation TKIs) should be administered according to results of the mutational analysis.[17] More than 100 mutations have been reported in the ABL1 kinase domain and are frequently positioned in the following regions: phosphate-binding loop (P-loop), ATP/IM binding site, catalytic domain (SH2 contact and C-loop) and the activation loop (A-loop) (Figure 2.1).[77,78]
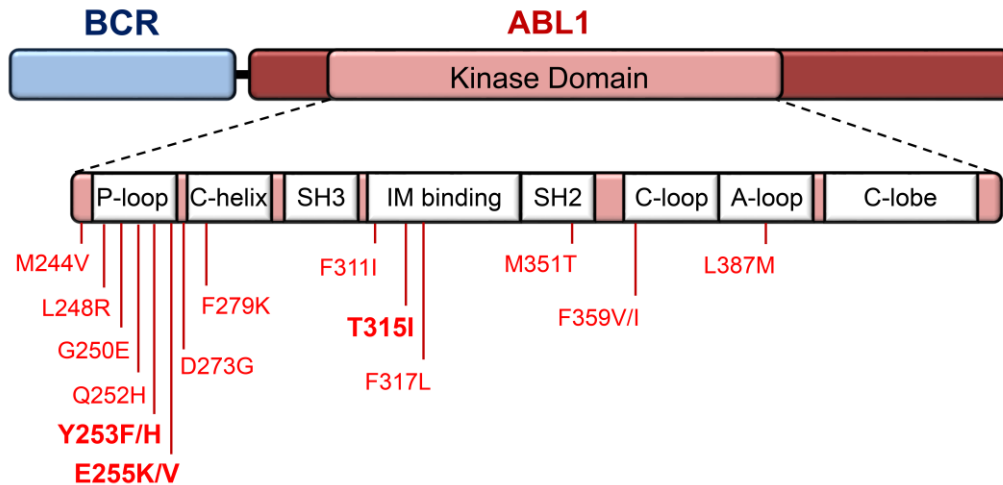
Figure 2.1 Map of the most recurrent amino acid substitutions in the BCR-ABL1 kinase domain in Ph+ clinical samples, usually associated to imatinib (IM) resistance. Highlighted mutations are the most frequent. Numbering of residues is according to normal ABL1 protein. Key structural motifs within the kinase domain are indicated: P-loop, phosphate binding loop; IM binding, ATP/IM binding region; C-loop, kinase catalytic domain; A-loop, activation loop; C-lobe, C-terminal lobe.

CML

BCR-ABL1 chimeric gene is remarkably homogenous in CML, as nearly all patients express the P210[BCRABL1] protein originated by the e14a2 or e13a2 fusion transcripts. Nevertheless, rarer isoforms of the transcript can be found in 5 % of CML cases: P190 (e1a2); P195 (e6a2); P200 (e8a2); P225 (e18a2); P230 (e19a2).[29–31] All *BCR-ABL1* isoforms encode for a constitutively active tyrosine kinase that disturbs cells proliferation, differentiation and survival, and is therefore the target for the most effective therapy against CML so far.[30,139] After the introduction of TKIs, such as IM, the annual mortality of CML has been reduced significantly, to less than 3 % per year.[139]

Several reports state that different isoforms might be associated to different prognosis, response to treatment and/or survival. Although both e13a2 and e14a2 transcripts originate the P210[BCR-ABL1] variant, they seem to represent distinct biological entities since patients with the e13a2 transcript have a slower molecular response with inferior response rates to IM and a poorer long-term outcome.[35,357,358] Moreover, P190[BCR-ABL1] results in a greater potential to induce a malignant change than P210[BCR-ABL1].[359,360] The P195[BCR-ABL1] has been described in very few CML patients and has been linked to a poor clinical outcome due to the aggressive progression of the disease.[31,361–364] This enhanced oncogenic potential of the P190/P195 isoforms is believed to result from the partial loss of BCR domains, namely, the guanine exchange factor/dbl-like domain which mediates the communication with several Ras-proteins crucial for the regulation of signaling pathways and processes such as cell proliferation, differentiation, adhesion, apoptosis, and migration.[31, 361,364,365] More recently, Reckel and collaborators

(2017) demonstrated the existence of strong differences in the interactome and tyrosine phosphoproteome between P190 and P210 signaling pathways. P190 interacts particularly with the AP2 adaptor complex involved in the regulation of clathrin-mediated endocytosis, whereas P210 interacts mostly with phosphatase Sts1. Indeed, the authors showed a stronger activation of the Stat5 transcription factor and the Erk1/2 kinases in the presence of P210, whereas P190 activates the Lyn kinase.[366]

The genetic instability of BCR-ABL1 expressing blast cells may lead to additional cytogenetic aberrations (ACAs), such as, double Ph, trisomy 8, and isochromosome 17. These are known to reduce the response to IM, the first line TKI, and are detected in less than 5 % of CML patients at diagnosis.[367] Furthermore, cytogenetic monitoring for the detection of ACAs during TKI treatment is mandatory due to the clonal evolution of the disease. It is hypothesized that the presence of a double *BCR-ABL1* chimeric gene induces stronger kinase activity and a more active blast cells proliferation.[368,369]

Ph+ ALL

ALL is very heterogenous, comprising several hematological, cytogenetic and molecular groups. The Ph chromosome is the most frequent genetic abnormality in adult ALL (Ph+ ALL), representing 20-30 % of B-lineage adult cases (B-ALL), but only 5 % of pediatric cases.[370,371] Ph+ ALL frequency increases with age representing approximately 50 % of all cases in the elderly.[371]

In Ph+ ALL, the most frequent expressed isoform of *BCR-ABL1* is the P190 in which the exon 1 of BCR is fused to exon 2 of ABL1 (e1a2), accounting for 70 % of the patients.[372,373] The remaining Ph+ ALL cases (approximately 30 %) are associated with the presence of P210$^{BCR-ABL1}$. As stated for CML cases, P190$^{BCR-ABL1}$ exhibits a higher transforming potential than P210$^{BCR-ABL1}$ and is usually linked to a higher risk of relapse.[359,360,373]

Alike CML, TKI therapy revolutionized Ph+ ALL prognosis. Complete remission can be achieved in 95 % of the cases,[373] however IM resistant Ph+ ALL patients frequently harbor the T315I mutation (ATP/IM binding site) and will only respond to ponatinib.[374,375] Several studies report the impact of ABL1 mutational screening in Ph+ ALL patients.[374,376,377]

AML

AML accounts for the majority of acute leukemia cases in adults, despite the high level of cell and molecular heterogeneity.[378] Karyotyping at diagnosis provides for the most important prognosis information in AML. Only a small percentage (~1 %) harbor the Ph chromosome and approximately 40–50 % of AML patients do not show any clonal chromosomal aberration and the most prominent sign of the disease is a blockage in granulocytic blasts differentiation. Cytogenetically normal AML patients are now classified into molecularly defined subgroups with distinct clinical outcomes. Indeed, *CEBPA*, *NPM1*, and *FLT3* mutations predict response to chemotherapy for those individuals.[379] *FLT3* and *NMP1* mutational screening is well implemented in AML diagnostics routine, however *CEBPA* molecular analysis has several technical issues and requires further optimization. *CEBPA* PCR amplification and

sequencing is difficult due to its high GC content, frequently correlating with the presence of background or sequencing artifacts. The entire gene sequencing detects all mutations, but is labor-intensive and requires expertise with unusual variants.[380]

The role of *CEBPA* in AML has gained clinical significance over recent years and is underlined by the discovery that the gene is mutated in around 11 % of patients.[381] Located on chromosome 19q13.1, *CEBPA* is a member of the basic region leucine zipper family of transcription factors. The gene encodes a 42-kDa protein with a C-terminal region (bZIP), consisting of a leucine zipper domain and an adjacent basic region, which modulates C/EBPα dimerization and DNA binding, and triggers the two transactivation domains (TAD) in the N-terminal region.[378] In hematopoiesis, C/EBPα plays a central role during granulocyte differentiation, where a diminishing activity is associated to the reduction of myeloid progenitors' differentiation potential, thus deregulating proliferation of hematopoietic cells.[378] *CEBPA* mutations affect mostly bZIP and/or TAD domains.[380]

AML patients usually exhibit biallelic *CEBPA* mutations, comprising an N-terminal and a C-terminal mutation, which result in complete abrogation of wild-type C/EBPα expression and is associated to a favorable clinical outcome.[382] Single *CEBPA* mutations also occur, in which expression of the wild-type product is retained.[383] This subgroup of patients could not be distinguished from wild-type cases as regards clinical outcome.[384] These results demonstrate significant heterogeneity within *CEBPA* mutation-positive AML with prognostic relevance.

Molecular characterization of leukemia samples (gene isoform identification and gene mutational screening) constitutes a useful tool for disease diagnostics and follow-up monitoring, particularly to detect molecular relapse and contribute to a more direct and personalized treatment. Hence, a complete molecular analysis was performed for all clinical samples provided by Hospital dos Capuchos (CHLC, Lisbon).

2.3 Patients and Methods

Patients informed consent and study approval

Patients were sent to the Hematology Department of Hospital dos Capuchos (CHLC, Lisbon, Portugal) for leukemia diagnosis. Written informed consent was obtained from all participants and the study was approved by Hospital dos Capuchos Ethics Committee. All approved ethical requirements for sample collection and assortment, processing, and analysis required by Hospital dos Capuchos Ethics Committee have been strictly followed.

Clinical samples

The presence of the Ph chromosome was confirmed by karyotype analysis and FISH. Levels of *BCR-ABL1* were assessed using RT-qPCR, according to the 2015 ELN guidelines.[38] Treatment with

TKIs was initiated immediately after diagnostics confirmation and clinical, hematological, and molecular remission was evaluated. Fresh bone marrow and peripheral blood patient samples were used immediately, or collected in RNAlater® (ThermoFisher Scientific, Waltham, MA, USA) for maximum RNA stabilization, and used directly for RNA extraction without any culture expansion and/or any cell culture method.

Karyotype banding and FISH analysis

This analysis was performed by the Hematology Department, at Hospital dos Capuchos (CHLC, Lisboa). Chromosome analysis was performed according to G-banding standard procedures on overnight cultured bone marrow cells. A total of 20 metaphases were analyzed. FISH analysis was performed in interphase cells using the LSI BCR/ABL1 Dual Color, Dual Fusion translocation probe (Abbott Molecular, Des Plaines, IL, USA), according to the manufacturer's instructions. A total of 100 and 500 nucleus were scored at diagnosis and follow-up, respectively. This analysis was carried out using a fluorescence microscope (Eclipse Ci, Nikon, Tokyo, Japan) and image capture was performed using Isis FISH Imaging System V 5.7.1 (MetaSystems, Altlussheim, Germany).

Cell culture of leukemia cell lines

Immortalized cell lines derived from CML patients in blast crisis, K562 (*BCR-ABL1* e14a2 fusion transcript positive cell line) and BV173 (*BCR-ABL1* e13a2 fusion transcript positive cell line) were cultured, respectively, in DMEM and RPMI with 10 % fetal bovine serum (FBS), at 37 °C with 5 % (v/v) CO_2. Human acute promyelocytic leukemia cell line (HL60), negative for *BCR-ABL1*, was cultured in RPMI with 10 % FBS, at 37 °C with 5 % (v/v) CO_2. These cell lines were used as positive and negative controls for the presence or absence of *BCR-ABL1* transcript.

Total RNA extraction and cDNA synthesis

Total RNA was extracted from clinical samples white cells. Briefly, 5 mL of bone marrow or peripheral blood were mixed with 10 mL of red blood cells lysis solution (5 mM $MgCL_2$, 10 mM NaCl, 10 mM Tris-HCl pH 7) and centrifuged at 400 x g for 5 min. The procedure was repeated to lyse any residual red blood cells. Total RNA extraction of white blood cells pellet was performed using the guanidine thiocyanate procedure (SV Total RNA Isolation System, Promega, Madison, WI, USA). Cell pellets were lysed in a solution containing 4 M guanidine thiocyanate, 0.1 M Tris-HCl pH 7.5, and 1 % (v/v) β-mercaptoethanol and were subsequently centrifuged at 13 000 x g for 10 min to clear the lysate of precipitated proteins and cellular debris. Nucleic acids were selectively precipitated with 30 % (v/v) ethanol; bound to the silica surface of glass fibers; and washed with 60 mM potassium acetate, 10 mM Tris-HCl pH 7.5, and 60 % (v/v) ethanol. On-column DNase I treatment lasted for 15 min at room temperature to remove genomic DNA. After several washing steps, RNA was resuspended in DEPC-treated water and stored at −80 °C until use. RNA concentration and purity (Abs_{260nm}/Abs_{230nm} and

Abs$_{260nm}$/Abs$_{280nm}$) were determined by ultraviolet (UV) spectrophotometry. As control, total RNA was also extracted from leukemia cell lines, using the same procedure.

Total RNA extracted (100 ng) was reverse transcribed into cDNA, using the NZY M-MuLV First-Strand cDNA Synthesis kit (Nzytech, Lisbon, Portugal).

Primer design

The following sequences were used to design all PCR primers described in this study: *BCR-ABL1* e14a2 (GenBank AJ131466.1); *BCR-ABL1* e13a2 (GenBank AJ131467.1); *BCR-ABL1* e1a2 (GenBank AF113911.1); *BCR-ABL1* e6a2 (GenBank AM491362.1); *BCR* (GenBank NM_004327.3); *ABL1* (GenBank NM_005157.5); *CEBPA* (GenBank NM_004364.4); *NMP1* (GenBank NM_002520.6) and *FLT3* (GenBank NM_004119.2).

BCR-ABL1 molecular analysis – Transcript identification

Nested-PCR amplification of *BCR-ABL1* from cDNA samples was performed in two separate setups: one that identifies the P210 isoforms of *BCR-ABL1* (e14a2 or e13a2) and one that identifies rarer isoforms, such as the P200 (e8a2), P195 (e6a2), P190 (e1a2).[44] Used primers are depicted in Table 2.1. PCR mixture components included 1x NH$_4$ reaction buffer (Bioline, Taunton, MA, USA), 2.5 mM MgCl$_2$, 0.15x Hi-Spec additive (Bioline), 200 µM dNTPs, 400 nM primers, and 0.02 U/µL BIOTAQ DNA polymerase (Bioline). Outer PCR was performed using 3 µL of cDNA in a 50 µL-reaction, under the following conditions: initial denaturation at 95 °C for 5 min; 30 cycles of 94 °C for 30 s, 55 °C for 30 s, 72 °C for 1 min; and a final extension step at 72 °C for 10 min. Inner PCR was performed using 1 µL of outer PCR product in a 50 µL-reaction, under the following conditions: initial denaturation at 95 °C for 5 min; 30 cycles of 94 °C for 15 s, 55 °C for 30 s, 72 °C for 1 min; and a final extension step at 72 °C for 10 min. A control PCR, for the amplification of *ABL1*, was performed using primers also depicted in Table 2.1 and the same conditions described for the outer PCR.

BCR-ABL1 molecular analysis – Mutational screening

Nested-PCR amplification of *BCR-ABL1* for mutation analysis was done using primers depicted in Table 2.2. PCR mixture components included 1x NH$_4$ reaction buffer (Bioline, Taunton, MA, USA), 2.5 mM MgCl$_2$, 0.15x Hi-Spec additive (Bioline), 200 µM dNTPs, 400 nM primers, and 0.02 U/µL BIOTAQ DNA polymerase (Bioline). Outer PCR was performed using 3 µL of cDNA in a 50 µL-reaction, under the following conditions: initial denaturation at 95 °C for 5 min; 30 cycles of 94 °C for 30 s, 55 °C for 30 s, 72 °C for 1.5 min; and a final extension step at 72 °C for 10 min. Inner PCR was performed using 1 µL of outer PCR product in a 50 µL-reaction, under the following conditions: initial denaturation at 95 °C for 5 min; 30 cycles of 94 °C for 15 s, 55 °C for 30 s, 72 °C for 1 min; and a final extension step at 72 °C for 10 min.

BCR-ABL1 molecular analysis – BCR-ABL1 levels quantification

This analysis was performed by the Hematology Department, at Hospital dos Capuchos (CHLC, Lisboa). Quantitative monitoring of *BCR-ABL1* (P210 transcript) was performed in 200 µL ethylenediaminetetraacetic acid (EDTA) peripheral blood samples using the 4-module GeneXpert platform and Xpert BCR-ABL Monitor IS G2(V1) system (Cepheid, Sunnyvale, CA, USA), according to the manufacturer's recommendations.

Mutational analysis of ABL1 on patient's genomic DNA from non-leukemic cells

Buccal epithelial cells were collected from patient 54 (Table 2.3) by twirling a swab on the inner cheeks for 1 min. The swab was separated from the stick and inserted in a microtube containing 440 µL of lysis buffer (50 mM Tris; 1 % (m/v) SDS). The tube was vortexed for several minutes to promote the release of most epithelial cells. The swab was removed, 20 µL of proteinase K (100 mg/mL dissolved in Tris-EDTA (TE) buffer: 10 mM Tris-HCl; 0.1 mM EDTA pH 8) were mixed with the cell suspension and incubated for 10 min at 50 °C. After adding 40 µL of 5 M NaCl, 500 µL of isopropanol were gently mixed with the DNA containing solution and allowed to stand for 5 min at room temperature. Sample was centrifuged for 5 min at 12 000 x g, the supernatant was removed and the dry pellet was resuspended in 100 µL of TE buffer. DNA concentration and purity (Abs_{260nm}/Abs_{230nm} and Abs_{260nm}/Abs_{280nm}) were determined by UV spectrophotometry. DNA was stored at 4 °C until use.

PCR amplification of *ABL1* exon 8 of patient's epithelial cells was performed using the following primers: forward 5'CTCAAATAATCCTCCCACTTCA and reverse 5'CCTGGAATGCCCACATATAC. PCR mixture components included 1x NH_4 reaction buffer (Bioline, Taunton, MA, USA), 2.5 mM $MgCl_2$, 0.15x Hi-Spec additive (Bioline), 200 µM dNTPs, 400 nM primers, 0.02 U/µL BIOTAQ DNA polymerase (Bioline) and 20 ng of gDNA. PCR conditions included an initial denaturation at 95 °C for 5 min; 30 cycles of 94 °C for 15 s, 55 °C for 30 s, 72 °C for 1 min; and a final extension step at 72 °C for 10 min.

NMP1 and FLT3-ITD molecular analysis

This analysis was performed by the Hematology Department, at Hospital dos Capuchos (CHLC, Lisboa). *NPM1* primers were the following: NPM1-F 5´GCGCCAGTGAAGAAATCTAT; NPM1-R 5'ACAGCCAGATATCAACTGTTAC; NPM1-Fwt 5´ATCTCTGGCAGTGGAGGAAG; NPM1-RmtA 5´CTCCACTGCCAGACAGAGA; NPM1-RmtB 5'ACTTCCTCCACTGCCATGC. PCR amplification was performed as follows: initial denaturation at 95 ˚C for 15 min; 36 cycles of 94 ˚C for 1 min, 56 ˚C for 1 min, 72 ˚C for 1 min; and a final extension step at 72 ˚C for 10 min. The amplified products were separated using electrophoresis in agarose gel. FLT3-ITD was performed as described by Lewis and collaborators.[385]

CEBPA molecular analysis – Mutational screening

PCR amplification of *CEBPA* was performed in three fragments, each one comprising a different domain of the encoded protein: TAD-1; TAD-2 and bZIP. PCR mixture components included 1x NZYLong reaction buffer (Nzytech, Lisbon, Portugal), 200 µM dNTPs, 100 nM primers and 0.05 U/µL NZYLong DNA polymerase (Nzytech). PCR was performed using 3 µL of cDNA in 25 µL-reactions. *CEBPA* primers for TAD-1 and TAD-2 regions were the following: CEBPA-1F 5′TCGCCATGCCGGGAGAACTCTAAC; CEBPA-1R 5'AGCTGCTTGGCTTCATCCTCCTC; CEBPA-2F 5'CCGCTGGTGATCAAGCAGGA; CEBPA-2R 5'CCGGTACTCGTTGCTGTTCT. PCR amplification was performed as follows: initial denaturation at 95 ˚C for 5 min; 40 cycles of 95 ˚C for 1 min, 53 ˚C for 40 s, 68 ˚C for 1 min; and a final extension step at 68 ˚C for 10 min. The C-terminal bZIP coding region of the gene was amplified using primers CEBPA-3F 5'CAAGGCCAAGAAGTCGGTGGACA and CEBPA-3R 5'CACGGCTCGGGCAAGCCTCGAGAT, and the following conditions: initial denaturation at 95 °C for 10 min; 40 cycles of 95 °C for 1 min, 61 °C for 40 s, 68 °C for 1 min; and a final extension step at 68 °C for 10 min.

PCR amplification of CEBPA in non-leukemic cells genomic DNA

The stroma of the bone marrow contains not only hematopoietic tissue, but also the yellow marrow that consists of all tissues that are not related to hematopoiesis. This fraction includes adipocytes, osteoblasts and connective fibroblasts, and are usually extracted along with hematopoietic cells during the bone marrow aspiration procedure. Hence, due to lack of additional samples (patient death; family members in the islands) and to obtain non-leukemic cells from the AML subject (patient 7; Table 2.3), the yellow marrow present in the aspirate of the AML subject was isolated and washed several times in phosphate-buffered saline (PBS) solution. Genomic DNA was extracted from these cells using the High Pure PCR Template Preparation Kit from Roche (Amadora, Portugal), according to the manufacturer's instructions. Briefly, 200 µL of cells diluted in PBS were mixed with 200 µL of binding buffer (6 M guanidine-HCL, 10 mM urea, 10 mM Tris-HCL, 20 % (v/v) Triton X-100, pH 4.4) and treated with proteinase K. The solution was mixed with 30 % (v/v) isopropanol, applied to a High Pure filter tube (polypropylene tube with two layers of glass fiber fleece), and centrifuged at 8 000 x g for 1 min. Then, 500 µL of inhibitor removal buffer (38 % (v/v) ethanol, 5 M guanidine-HCL, 20 mM Tris-HCL, pH 6.6) were added to the High Pure filter tube and centrifuged. After two washes (80 % (v/v) ethanol, 20 mM NaCL, 2 mM Tris-HCL, pH 5.5) and centrifugation steps, DNA was eluted with 100 µL of 10 mM Tris-HCL, pH 8.5 (pre-heated at 70 °C).

The bZIP coding region of the gene was amplified using primers CEBPA-3F and CEBPA-3R, described in the previous item, and the following components: 1x NZYLong reaction buffer (Nzytech, Lisbon, Portugal), 200 µM dNTPs, 100 nM primers, 0.05 U/µL NZYLong DNA polymerase (Nzytech)

and 20 ng of gDNA. PCR conditions include: initial denaturation at 95 ˚C for 10 min; 40 cycles of 95 ˚C for 15 s, 61 ˚C for 10 s, 68 ˚C for 15 s; and a final extension step at 68 ˚C for 10 min.

Sequencing and sequence alignments

PCR products were visualized via 1-2 % agarose gel electrophoresis, and subsequently analyzed by Sanger sequencing at STABVIDA (Caparica, Portugal). The Basic Local Alignment Search Tool (BLAST), from the National Center for Biotechnology Information (NCBI), was used to align all obtained sequences, via Sanger sequencing, with reference sequences specified in the *Primer design* segment of this section. Mutations are described according to the guidelines of the Human Genome Variation Society.[386]

Bioinformatics for mutation analysis

All novel gene mutations identified in this study were analyzed using three different softwares to predict their effect on the stability and structure of the encoded protein. MutationTaster predicts changes in the transcript splice sites, as well as alterations to protein features.[387] Support Vector Machine infers the stability of protein structure.[388] DISOclust provides a disorder probability score in mutated domains.[389]

Table 2.1 Nested-PCR primers for *ABL1* and *BCR-ABL1* molecular analysis of P210 and rare isoforms (P190, P195 and P200) in Ph+ hematologic malignancies.[44]

	ABL1 – Control	P210 (e14a2 or e13a2)	P200 (e8a2), P195 (e6a2) or P190 (e1a2)
Outer PCR	For 5' GGCCAGTAGCATCTGACTTTG (*ABL1* exon 2) Rev 5' ATGGTACCAGGAGTGTTTCTCC (*ABL1* exon 3)	For 5' GAAGTGTTTCAGAAGCTTCTCC (*BCR* exon 12) Rev 5' GTTTGGGCTTCACACCATTCC (*ABL1* exon 3)	For 5' GACTGCAGCTCCAATGAGAAC (*BCR* exon 1) Rev 5' GTTTGGGCTTCACACCATTC (*ABL1* exon 3)
Inner PCR	N/A	For 5' CAGATGCTGACCAACTCGTGT (*BCR* exon 13) Rev 5' TTCCCCATTGTGATTATAGCCTA (*ABL1* exon 3)	For 5' CAGAACTCGCAACAGTCCTTC (*BCR* exon 1) Rev 5' TTCCCCATTGTGATTATAGCCTA (*ABL1* exon 3)
Final PCR product size	296 bp	e14a2 - 360 bp e13a2 - 285 bp	e8a2 - 1284 bp e6a2 - 1023 bp e1a2 - 381 bp

For, forward; Rev, reverse; N/A, not applicable

Table 2.2 Primers for *BCR-ABL1* nested-PCR amplification and subsequent analysis of *ABL1* mutational status of fusion genes encoding P210 and rare *BCR-ABL1* isoforms. Adapted from van Dongen *et al*, 1999.[44]

	P210 (e14a2 or e13a2)	P200 (e8a2), P195 (e6a2) or P190 (e1a2)
Outer PCR ***BCR-ABL1* fusion**	For 5' TGCTGACCAACTCGTGTGTGA (*BCR* exon 13) Rev 5' CTTCGTCTGAGATACTGGATTCCT (*ABL1* exon 9)	For 5' CAGAACTCGCAACAGTCCTTC (*BCR* exon 1) Rev 5' CTTCGTCTGAGATACTGGATTCCT (*ABL1* exon 9)
Inner PCR ***ABL1* exons 4-7**	For 5' GCAACAAGCCCACTGTCTAT (*ABL1* exon 4) Rev 5' TGTTGTAGGCCAGGCTCTC (*ABL1* exon 7)	
Inner PCR ***ABL1* exons 7-9**	For 5' TGAGCAGGTTGATGACAGG (*ABL1* exon 7) Rev 5' TGAGATACTGGATTCCTGGAAC (*ABL1* exon 9)	

For, forward; Rev, reverse

2.4 Results and Discussion

CML diagnosis, as well as disease follow-up and treatment monitoring, is routinely assessed at the hematologic, cytogenetic and molecular level. In the current era of highly sensitive molecular assays, CML clinical samples should be submitted to the following tests: RT-nested PCR to identify the specific isoform of *BCR-ABL1*; RT-qPCR to quantify transcript levels; and transcript sequencing for mutational screening.[17] Table 2.3 summarizes the outcome for each collected sample regarding: FISH or qPCR analysis (information provided by Hospital dos Capuchos); transcript identification (*BCR-ABL1*); point mutations that are associated to disease relapse or a specific prognosis (*BCR-ABL1* and *CEBPA,* in the context of Ph+ leukemias and cytogenetically normal AML, respectively); and ACAs.

RT-nested PCR allows for the distinction of the two major isoforms of the gene due to their amplicons size difference (e14a2 *vs* e13a2) (Table 2.1). Other PCR set-ups have been designed that enable the detection of rarer isoforms, as described in Table 2.1, which was the case for samples 44 (e6a2) and 54 (e1a2) (Table 2.3). Out of 37 CML samples (collected at diagnosis and follow-up): 20 harbored the e14a2 variant (54 %); 11 harbored the e13a2 isoform (30 %); 3 co-expressed two different transcripts (8 %); and 3 follow-up samples were inconclusive (8 %). These statistics are in accordance with several studies that report the incidence of *BCR-ABL1* transcripts over several populations. Most studies describe that more than half of CML patients express the e14a2 variant and that approximately 95 % cases are associated to e14a2 and/or e13a2 *BCR-ABL1* variants.[32, 34,390–392]

Nested-PCR provides several advantages but the increase in the specificity of DNA amplification is of utmost relevance, since two sets of primers are used in two successive PCRs. Moreover, it is more sensitive than qPCR by 1-log due to the second PCR reaction.[393,394] This is important for CML diagnosis, mostly for MRD detection. In fact, AML sample 16 was found to be a case of Ph+ AML solely after RT-nested PCR analysis. Even though RT-nested PCR is often more successful in specifically amplifying long DNA fragments than conventional PCR or qPCR, it requires more detailed knowledge of the target sequences. Indeed, a nested-PCR format was also designed to enable *BCR-ABL1* mutations screening (Table 2.2) and the outcome was compiled on table 2.3. The resulting PCR products were analyzed by Sanger sequencing, the gold-standard technique for gene variations identification and mutational burden quantification, which is highly important in the characterization of clonal diseases such as CML.[395]

Due to the novelty of clinical cases corresponding to samples 44, 54 and 7 (Table 2.3), the next segments of this discussion will describe them in detail.

Table 2.3 Clinical samples cytogenetic and molecular characterization.

Type of leukemia/ Disease stage	Ref. No.	Tissue	FISH or RT-qPCR* (IS)	*BCR-ABL1* transcript identification	*BCR-ABL1* or *CEBPA* point mutations; polymorphisms; ACAs (mutational burden*)
AML at diagnosis	1	BM	-	-	-
	2	BM	-	-	-
	3	BM	-	-	-
	4	BM	-	-	-
	5	BM	-	-	-
	6	BM	-	-	-
	7	BM	-	-	CEBPA: c.1067A>T; p.N356I (50 %)
	8	BM	-	-	-
	9	BM	-	-	-
	10	BM	-	-	-
	11	BM	-	-	-
	12	BM	-	-	-
	13	BM	-	-	-
	14	BM	-	-	-
	15	BM	-	-	-
	16	BM	-	e14a2	-
CML at diagnosis	17	BM	n/a	e14a2	ABL1: c.763G>A; p.E255K (100 %)
	18	BM	n/a	e13a2	-
	19	BM	n/a	e14a2	-
	20	BM	n/a	e14a2	ABL1: c.944C>T; p.T315I (12 %)
	21	BM	n/a	e13a2	ABL1: c.943A>G; p.T315A (<10 %)

	22	BM	n/a	e14a2	-
	23	BM	FISH = 98 %	e13a2	-
	24	BM	FISH = 87 %	e14a2	-
	25	BM	FISH = 98 %	e14a2	-
	26	BM	FISH = 97 %	e14a2	-
	27	BM	FISH = 95 %	e13a2	-
	28	BM	FISH = 99 %	e13a2	-
	29	BM	FISH = 77 %	e14a2	-
	30	BM	FISH = 95 %	e14a2	-
	31	BM	FISH = 98 %	e14a2	-
	32	PB	FISH = 90 %	e13a2	-
CML at follow-up	33	PB	qPCR = 0.017 %	-	-
	34	PB	qPCR = 0.34 %	e14a2	-
	35	PB	qPCR = 0.00031 %	-	-
	36	PB	qPCR = 0.11 %	e13a2	-
	37	PB	qPCR = 1 %	-	-
	38	PB	qPCR = 3.4 %	e13a2	-
	39	PB	n/a	e13a2	-
	40	PB	n/a	e14a2 / e13a2	-
	41	PB	FISH = 33 %	e14a2	-
	42	PB	FISH = 75 %	e14a2	-
	43	PB	n/a	e14a2	BCR: c.2700T>C; p.N900N (100 %) ABL1: c.749G>A; p.G250E (75 %) ABL1: c.1052T>C; p.M351T (50 %)

	44	PB	FISH = 80 %	e14a2 / e6a2	BCR: c.2700T>C; p.N900N (100 %) ABL1 (e14a2): c.720G>A; p.T240T (50 %) ABL1 (e6a2): c.720G>A; p.T240T (100 %) Double Ph; trisomy 8
	45	PB	FISH = 6 %	e14a2	ABL1: c.875A>G; p.E292G (20 %)
	46	PB	n/a	e14a2	-
	47	PB	n/a	e13a2	-
	48	PB	n/a	e14a2	-
	49	PB	FISH = 60 %	e14a2	-
	50	PB	FISH = 6 %	e13a2	-
	51	PB	n/a	e14a2	-
	52	PB	qPCR = 0.34 %	e14a2 / e13a2	-
	53	PB	qPCR = 1.4 %	e14a2	BCR: c.2700T>C; p.N900N (100 %)
Ph+ ALL at diagnosis	54	BM	n/a	e1a2	ABL1: c.1319A>G; p.Y440C (20 %)

*Mutational burden was assessed via sequencing chromatogram peak relative quantification.

ACA, additional chromosomal aberration; ALL, acute lymphocytic leukemia; AML, acute myeloid leukemia; BM, bone marrow; CML, chronic myeloid leukemia; FISH, fluorescence *in situ* hybridization; IS, international scale; n/a; not available; PB, peripheral blood; Ph, Philadelphia chromosome; qPCR, quantitative polymerase chain reaction

Clinical case 44 - Double Ph+ CML patient, co-expressing P210$^{BCR-ABL1}$ and P195$^{BCR-ABL1}$ isoforms

In CML, BCR-ABL1 mutational events and variations on multidrug resistance transporters are probably the most frequent resistance mechanism to TKIs.[17] ACAs in Ph+ CML are also strongly associated with disease progression, however their ultimate impact on prognosis is still unclear due to their low frequency.[367]

This report is based on a previously healthy 36 years-old man, without any relevant past diseases and a one-month history of fever and night sweats. On physical examination, no hepatosplenomegaly or lymphadenopathy were found. Hemoglobin was 12.9g/dL, white blood cell count was 58300/pL (90.8 % neutrophils, 1.4 % eosinophils, 0 % basophils, 6.5 % lymphocytes, 1.3 % monocytes) and platelet count was 507 000/pL. Bone marrow aspiration showed 1% blasts and FISH for *BCR-ABL1* was 98 % positive (Table 2.4). Cytogenetic analysis of 20 mitotic bone marrow cells showed: four nuclei with one Ph chromosome; seven nuclei harboring one Ph chromosome and trisomy 8; and nine double Ph+ nuclei and trisomy 8 (Figure 2.2).

A diagnosis of CP-CML was made, with a Sokal score of 0.57, Hasford 58 and EUTOS 0. The patient initiated IM at 400 mg/day. Cytogenetic response was not achieved at three months of treatment, and not even after increase of the IM dose to 600 mg/day for two weeks (FISH=80 %) and 800 mg/day for four and half months (FISH=61 %) (Table 2.4). Due to incomplete cytogenetic response, molecular analysis of *BCR-ABL1* was performed, which linked Ph+ cells to two different isoforms of the gene: P210 (e14a2) and P195 (e6a2) (Figures 2.3 and 2.4; Appendix I - Figures I.1 and I.2). Except for two well characterized SNPs,[396–398] both transcripts exhibited no point mutations in the *ABL1* domain (Appendix I - Figures I.3-6; Table I.1).

Treatment was switched to bosutinib at month eight after diagnosis, with side effects requiring dose adjustments (grade I diarrhea, grade III elevation of liver enzymes and grade I rash). CyR was accomplished at month 13. Later, DMR was achieved for P210$^{BCR-ABL1}$, but the patient remained positive at cytogenetic level (FISH = 5 %) (Table 2.4). The patient is now referred for alloSCT.

Ph duplication is usually associated with an overexpression of BCR-ABL1 and therefore associated with an aggressive clinical outcome.[367,368] This chromosomal aberration allied to the presence of an atypical short isoform of BCR-ABL1 might explain the progression of disease in the CML patient, the lack of cytogenetic response to IM and the need for a third-generation TKI targeting the BCR-ABL1 protein. Indeed, shorter BCR-ABL1 transcripts were reported to induce an aggressive clinical phenotype due to the lack of important regulatory BCR sequences.[31, 361, 365,399]

This is the first report of a patient attaining DMR for P210 and stable cytogenetic response for P195, under treatment with bosutinib. We conclude that this CML scenario is associated with an inferior outcome to therapy with first generation TKI, and that this subset of patients need to be identified as high-risk patients and monitored closely for efficacy during chemotherapy.

Table 2.4 Disease progression for clinical case 44, including TKI treatment regimen, hematologic, cytogenetic and molecular levels.

TKI	Dosage (mg/day)	Time [months]	Disease progression
		Diagnosis	1 % blasts; FISH t(9;22) = 98 %
IM	400	[0 - 3]	Loss of HR; No CyR
	600	[3 - 3.5]	No HR; FISH = 80 % (11 % atypical pattern)
	800	[3.5 - 8]	CHR; FISH = 61 % *
Bosutinib	400	[8 – 8.5]	CHR; FISH = 68 %
	400	[8.5 - 11]	CHR; FISH = 44 %
	400	[11 - 13]	CyR; Toxicity symptoms
-	-	[13 - 15]	Toxicity fully solved
Bosutinib	300	[15 – 20]	CyR; FISH = 3.8 % (0.8 % atypical pattern); MR^{4,5} (P210)
	400	[20 - 21]	MR^{4,5} (P210)
		NOW	FISH = 5 % (2 % atypical pattern); Molecularly undetectable P210

*_BCR-ABL1_ molecular analysis linked Ph+ cells to two different variants: P210 and P195.

CHR, complete hematologic response; CyR, cytogenetic response; FISH, fluorescence _in situ_ hybridization; HR, hematologic response; IM, imatinib; MR^{4,5}, molecular response with 4.5-log reduction from IRIS baseline (_BCR-ABL1_ transcript < 0.0032 % IS); TKI, tyrosine kinase inhibitor.
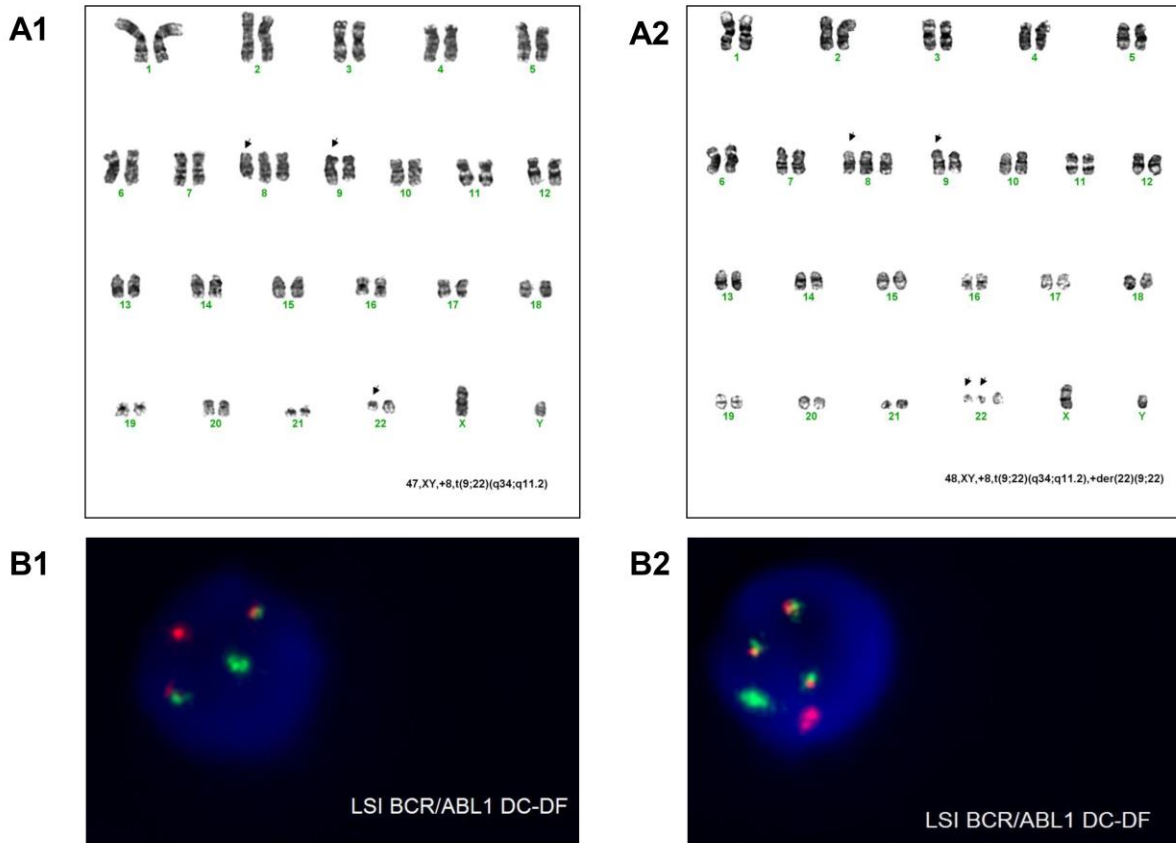
Figure 2.2 Cytogenetic analysis for clinical case 44: **A)** karyotype banding and **B)** fluorescence *in situ* hybridization (FISH) using LSI BCR/ABL1 Dual Color, Dual Fusion translocation probe (Abbott Molecular, Des Plaines, IL, USA). Chromosome G-banding showed: 4 nuclei 46,XY,t(9;22)(q34.1;q11.2); 7 nuclei 47,XY,+8,t(9;22)(q34.1;q11.2) [A1, with corresponding interphase FISH image – B1]; 9 nuclei 48,XY,+8,t(9;22)(q34.1;q11.2), +der(22)t(9;22)(q34.1;q11.2) [A2, with corresponding interphase FISH image – B2]. Images were provided by the Hematology Department from Hospital dos Capuchos (CHLC, Lisboa).
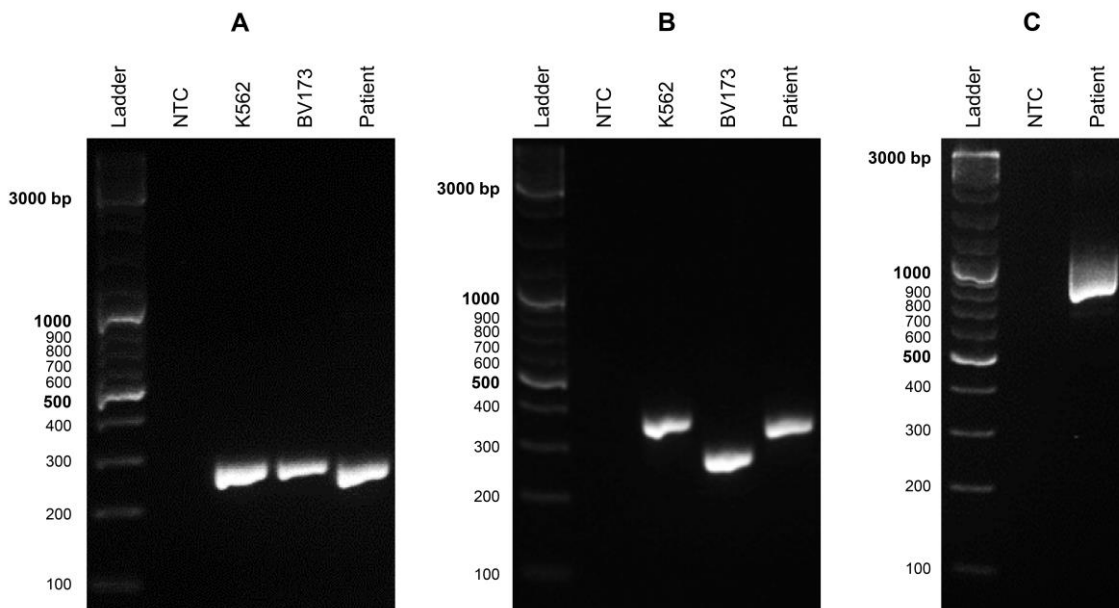
Figure 2.3 *ABL1* and *BCR-ABL1* molecular analysis. **A)** Control PCR amplification of *ABL1* from K562 cells, BV173 cells and patient 44 white blood cells. **B)** Nested-PCR amplification of P210$^{BCR-ABL1}$ isoforms from K562 cells, BV173 cells and patient 44 white blood cells. **C)** Nested-PCR amplification of rarer *BCR-ABL1* isoforms from patient 44 white blood cells. PCR products (1 µl) were resolved via 2 % (w/v) agarose gel electrophoresis. Expected PCR amplicon sizes are specified in table 2.1. NTC – non-template control; Ladder - GeneRuler DNA Ladder Mix SM0331 (Thermo Scientific, Waltham, MA, USA).
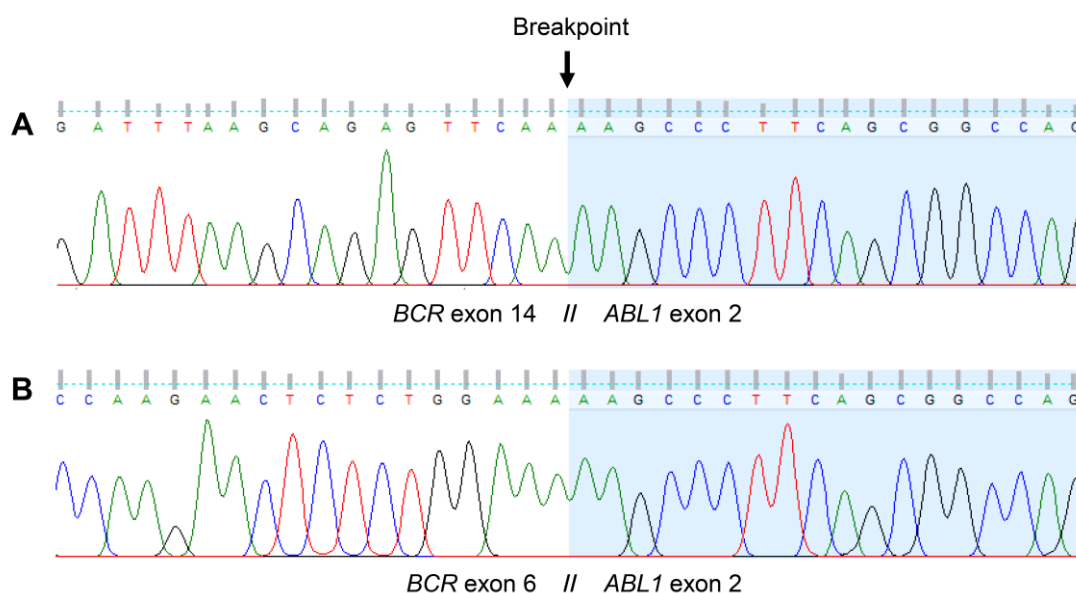
Figure 2.4 Sequence analysis of *BCR-ABL1* from patient sample 44. **A)** Sanger sequencing of PCR product represented in figure 2.3B (patient). **B)** Sanger sequencing of PCR product represented in figure 2.3C (patient).

Clinical case 54 – Ph+ B-ALL patient with a novel BCR-ABL1 mutation

The outcome of patients with Ph+ ALL has greatly benefited with TKIs therapy, however the sensitivity to each TKI must be considered in individual cases for a successful result. In parallel to what is recommended for CML, Ph+ ALL patients that do not respond to IM should undergo mutational screening for an assessment of drug resistance mechanisms.[373,376]

Here we report a 31-years old leukemia male patient. The diagnosis of B-ALL was confirmed by bone marrow morphology with cytochemistry staining and flow cytometry analysis. Further cytogenetic and molecular biology characterization was performed concluding that the patient was bearing a Ph+ B-ALL (Figure 2.5). The patient started chemotherapy according to the Dana Farber Cancer Institute consortium protocol[400] with dasatinib 140 mg/day (chosen for better central nervous system prophylaxis), which induced clinical and hematological remission. According to protocol, at day 29 after diagnosis and treatment initiation, bone marrow was collected for MRD evaluation, revealing a positive result. MRD positivity was confirmed by a second test performed four weeks later.

Patient bone marrow at day 29 was further analyzed for TKIs resistance mutations to better understand the MRD response. Molecular analysis of patient's white blood cells revealed the expression of P190[BCR-ABL1] (Figure 2.6; Appendix II – Figure II.1), the most common isoform in Ph+ ALL. The subsequent mutational analysis via Sanger sequencing showed a point mutation in the *ABL1* domain of the fusion transcript, more precisely in the region that translates for the C-terminal lobe of the kinase domain (Figure 2.7). Through quantification of sequencing chromatogram peaks, it is possible to conclude that this variation is present in 20 % of *BCR-ABL1*-expressing cells. This is recurrent in clonal hematological diseases due to the selective pressure caused by TKIs administration. In fact, the in-frame mutation in leukemic cells is not present in *ABL1* from nonleukemic cells, indicating a somatically acquired mutation rather than a germline mutation. This was confirmed by the analysis of the genomic DNA of patient's epithelial cells (Figure 2.7).

The newly described *BCR-ABL1* nucleotide substitution, c.1319A>G (codon TAC>TGC), results in the amino acid alteration p.Tyr440Cys (Figure 2.7). The substitution of a highly conserved amino acid across different species (Appendix II – Table II.1), and a shift between a large amino acid (tyrosine) into a small amino acid with a thiol side chain (cysteine), is likely to induce deviations to correct protein folding. To understand the possible effect of this mutation in the BCR-ABL1 structure, we probed the sequence through MutationTaster that predicts changes in the transcript splice sites, as well as alterations to protein features.[387] Using Support Vector Machine and sequence information there is a predicted decrease in the stability of protein structure, with a confidence score of -0.898, due to the p.Tyr440Cys mutation.[388] DISOclust software analysis also shows an increase in the disorder probability score in the mutated ABL1 domain, particularly in residues located after the Y440C mutation (Appendix II – Figure II.2).[389]

Point mutations within the C-terminal lobe region of BCR-ABL1 have been described to impair the protein´s structure. For example, the well-studied E459K substitution makes the protein inactive

conformation unstable even though the amino acid position is not near the ATP/IM binding site. Since IM only binds to the inactive conformation of BCR-ABL1, patients harboring this mutation typically do not respond to the first-line TKI, but are more sensitive to bosutinib that can bind to the active conformation of the protein.[401] Considering this information, the patient was proposed for bosutinib treatment and, ultimately, for bone marrow alloSCT.
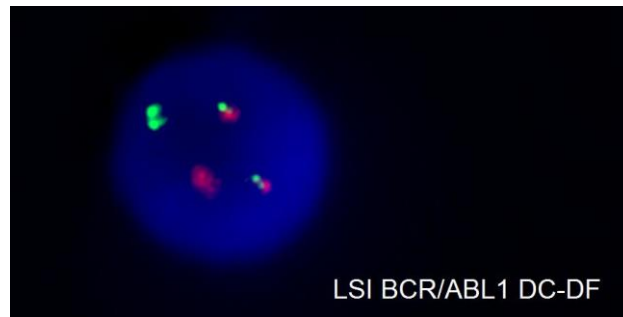
Figure 2.5 Interphase fluorescence *in situ* hybridization (FISH) analysis for clinical case 54, using LSI BCR/ABL1 Dual Color, Dual Fusion translocation probe (Abbott Molecular, Des Plaines, IL, USA). Image depicting a Ph+ nucleus, 46,XY,t(9;22)(q34.1;q11.2), was provided by the Hematology Department from Hospital dos Capuchos (CHLC, Lisboa).
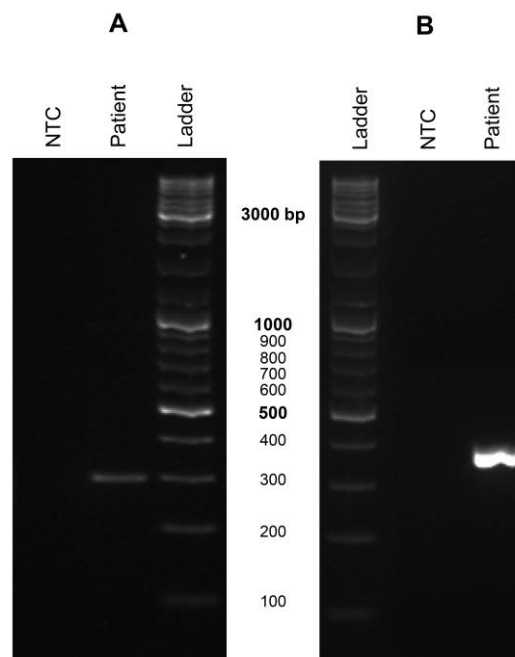
Figure 2.6 *ABL1* and *BCR-ABL1* molecular analysis of patient 54 white blood cells. **A)** Control PCR amplification of *ABL1*. Expected amplicon size is 296 bp (Table 2.1). **B)** Nested-PCR amplification of P190[BCR-ABL1] isoform. Expected amplicon size is 381 bp (Table 2.1). PCR products (1 µl) were resolved via 2 % agarose gel electrophoresis. NTC – non-template control; Ladder - GeneRuler DNA Ladder Mix SM0331 (Thermo Scientific, Waltham, MA, USA).
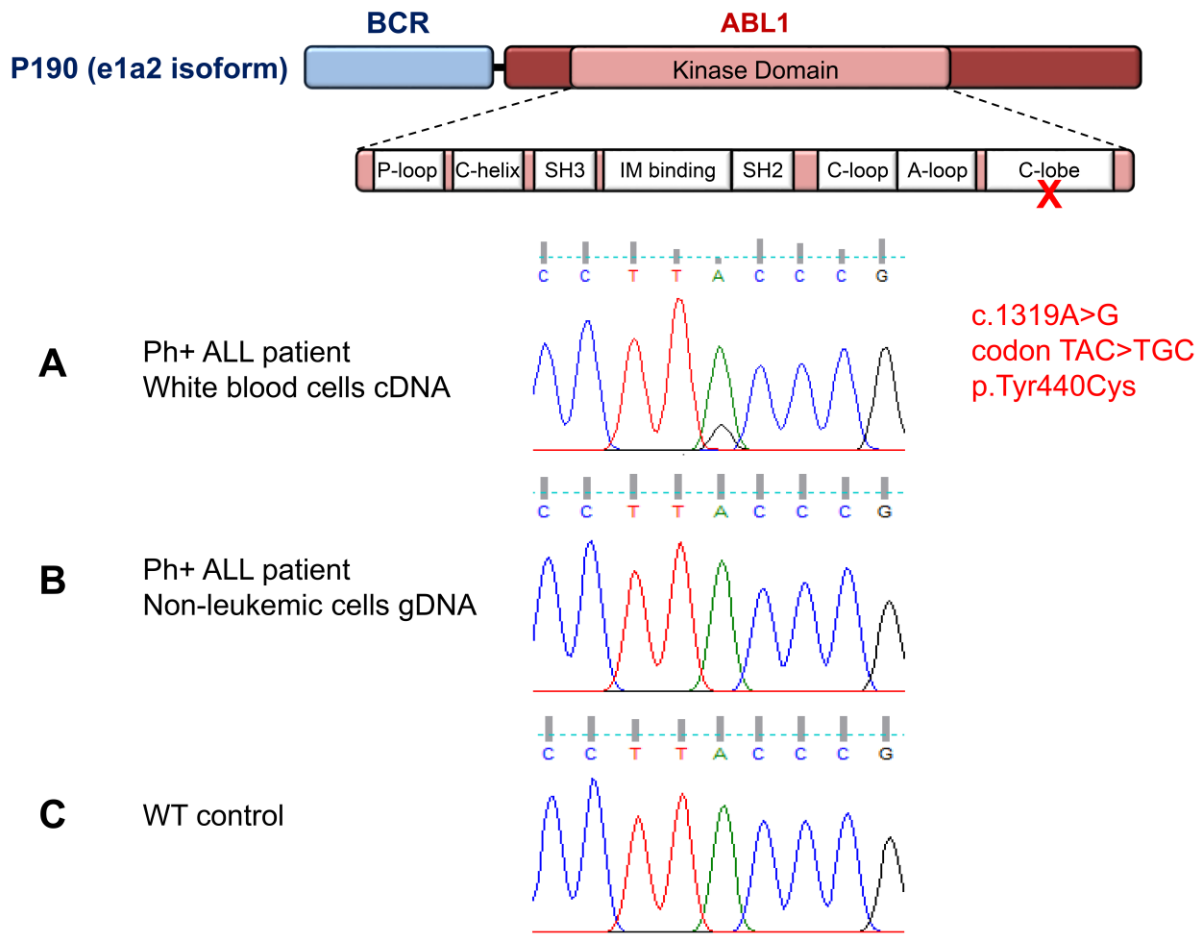
**Figure 2.7** P190^BCR-ABL1 protein structure indicating the position of the detected BCR-ABL1 point mutation. Sequencing chromatograms displaying: **A)** *BCR-ABL1* nucleotide sequence from Ph+ ALL patient 54 white blood cells. Chromatogram peak analysis indicates that the variation is present on 20 % of total Ph+ clones; **B)** *ABL1* nucleotide sequence from Ph+ ALL patient 54 epithelial cells; **C)** *ABL1* from control individual (wild-type, WT). P-loop: phosphate binding loop; IM binding: ATP/IM (imatinib) binding region; C-loop: kinase catalytic domain; A-loop: activation loop; C-lobe: C-terminal lobe.

Clinical case 7 – AML patient with a novel CEBPA mutation

The 67-year-old male patient was referred to Hospital dos Capuchos Hematology Department with generalized unspecified pain and leucocytes of 100 000/mL. Bone marrow morphology showed 96 % blast count and, together with imunophenotyping analysis, the case was classified as AML without maturation (WHO 2008). G-band karyotyping was normal. FISH for t(9;22) and molecular analysis for *NPM1* and *FLT3* mutations were negative. In contrast, *CEBPA* sequencing exposed a new nucleotide substitution: c.1067A>T (codon AAC>ATC), at a 50 % mutational burden (Figure 2.8). This *CEBPA* in-frame mutation expressed by leukemic cells was not present in non-leukemic cells, indicating a somatically acquired mutation rather than germline (confirmed by genomic DNA analysis) (Figure 2.8).

The detected variation, which has not been previously reported in the Human Genome Variations database,[386] corresponds to the following alteration of amino acid in the bZIP region of the protein: p.Asn356Ile (Figure 2.8). This mutation alters a conserved amino acid across different species (Appendix III – Table III.1) and the variance in hydrophobicity between these two amino acids (N>I) might induce deviations to correct protein folding.

To understand the possible effect of the variation on AML, we probed the sequence through MutationTaster[387] and DISOclust disorder prediction software[389] and both predict that this alteration decreases protein's stability with high scores (0.9/1 and Appendix III – Figure III.1, respectively). Using Support Vector Machine and sequence information there is a predicted disruption on the structure of the protein with a confidence score of -0.353 due to the p.N356I mutation.[388] Moreover, in frame mutations within the C-terminal bZIP region have been described to impair DNA binding and/or homo- and heterodimerization.[402,403]

Despite the range of mutations in *CEBPA* in AML patients, this is the first report on the variation c.1067A>T (p.Asn356Ile). Patients that carry a mutation in the bZIP region have a tendency towards a *CEBPA* double-mutant gene expression profile causing the complete abrogation of the transcription factor function. These mutations are associated with decreased relapse risk as well as improved survival compared to patients without a mutation.[381,384]

The patient started induction chemotherapy but complete response evaluation was not possible due to premature death by sepsis during neutropenia phase. Though mutated *CEBPA* is generally related with a favorable prognosis for cytogenetically normal AML, elevated leucocytosis at presentation is considered an adverse independent prognostic factor.
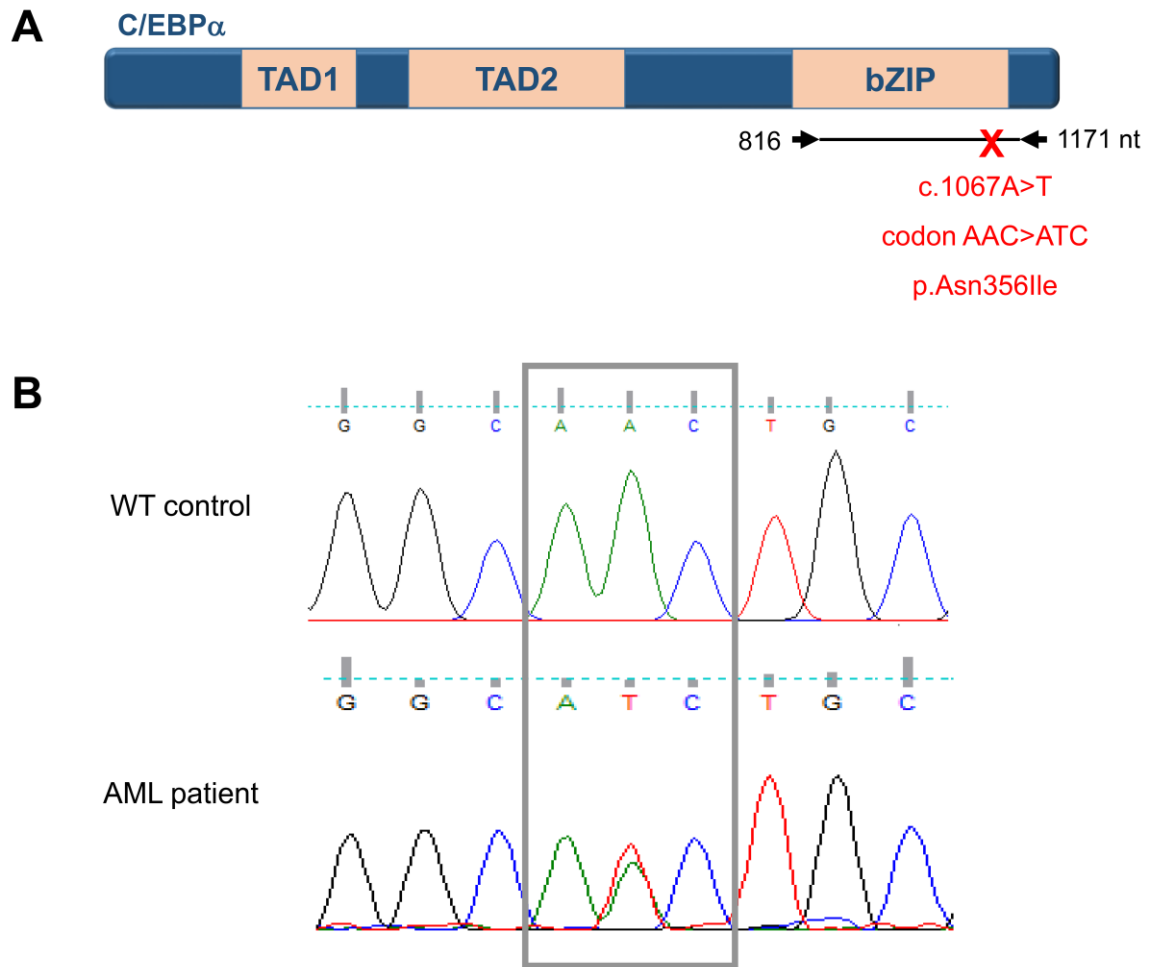
Figure 2.8 A) C/EBPα protein main domains: transactivation domains (TADs) and a leucine zipper domain (bZIP) for dimerization and DNA binding. The amplified region of the *CEBPA* gene is also represented, as well as the non-synonymous mutation detected. **B)** Normal *CEBPA* nucleotide sequence from a control individual (wild-type, WT) showing the normal c.1067A (AAC) allele and below the *CEBPA* mutation in the AML patient (clinical case 7): c.1067A>T [a substitution of AAC (Asn) to ATC (Ile)]. Chromatogram peak analysis is indicative of a heterozygous state with a mutant allele burden of over 50 %. nt, nucleotide.

2.5 Concluding Remarks

These findings demonstrate the importance of *BCR-ABL1* transcript identification and mutational screening in Ph+ leukemia patients at the time of diagnosis and in follow-up samples, particularly in individuals that do not respond to treatment or do not achieve complete remission. This is also valid for *CEBPA* mutations analysis in AML, which proved to require further optimization due to some drawbacks previously experienced by other groups, namely, difficulty in amplification and sequencing of the gene due to the presence of non-specific PCR products.[380] Other techniques should be envisaged to perform *CEBPA* analysis, which will be explored in chapter 6 (*Future perspectives* section).

Note that chapter 2 pinpoints some of the downsides of the conventional methodology for *BCR-ABL1* screening: time-consuming, complex and expensive. Thus, a complete molecular analysis of leukemia samples enables the ensuing part of this study, which aims to develop a new, fast, simple and cost-effective method for the detection of *BCR-ABL1* on clinical samples. The robustness of the new method using Au-nanoprobes will be assessed in chapter 3 and compared to gold-standard procedures used for CML diagnosis.

CHAPTER 3 – **DETECTION OF *BCR-ABL1* TRANSCRIPTS IN CLINICAL SAMPLES VIA GOLD NANOPROBES**

Clinical samples and all information on cytogenetic levels and *BCR-ABL1* gene quantification were kindly provided by Hospital dos Capuchos (Centro Hospitalar de Lisboa Central, CHLC, Lisbon). R. Vinhas performed all experiments related to *BCR-ABL1* transcript identification, nanoparticles characterization, gold-nanoprobe colorimetric assay optimization and validation, as well as data analysis, at the Research Unit on Applied Molecular Biosciences (UCIBIO, Universidade Nova de Lisboa), under the supervision of P.V. Baptista and A.R. Fernandes. The author of this thesis opted for reproduction of the resulting scientific paper, thus apologizing for any repeated content in different contexts of the document.

3.1 Abstract

AuNPs functionalized with thiolated oligonucleotides (Au-nanoprobes) have been used in a range of applications for the detection of bioanalytes of interest, from ions to proteins and DNA targets. These detection strategies are based on the unique optical properties of AuNPs, in particular, the intense color that is subject to modulation by modification of the medium dielectric. Au-nanoprobes have been applied for the detection and characterization of specific DNA sequences of interest, namely pathogens and disease biomarkers. Nevertheless, despite its relevance, only a few reports exist on the detection of RNA targets. Among these strategies, the colorimetric detection of DNA has been proven to work for several different targets in controlled samples but demonstration in real clinical bioanalysis has been elusive.

Here, we used a colorimetric method based on Au-nanoprobes for the direct detection of the e14a2 *BCR-ABL1* fusion transcript in myeloid leukemia patient samples without the need for retrotranscription. Au-nanoprobes directly assessed total RNA from 38 clinical samples, and results were validated against RT-nested PCR and RT-qPCR. The colorimetric Au-nanoprobe assay is a simple yet reliable strategy to scrutinize myeloid leukemia patients at diagnosis and evaluate progression, with obvious advantages in terms of time and cost, particularly in low- to medium income countries where molecular screening is not routinely feasible.

3.2 Introduction

Au-nanoprobes, due to their unique optical proprieties, have been widely used for nucleic acid detection with high sensibility and sensitivity at much lower costs when compared with conventional molecular methods. Disperse Au-nanoprobe solutions show a characteristic SPR band at around 525 nm (red color), which is red-shifted upon salt-induced aggregation (blue color); hybridization to a complementary nucleic acid target sequence prevents aggregation and the solution remains red.[206] This non-cross-linking colorimetric detection method has been efficiently applied to the detection of pathogens and other DNA sequences of interest, where hybridization to a specific complementary target leads to Au-nanoprobe stabilization and resistance to salt-induced aggregation.[123,164]

As mentioned earlier, CML is a clonal bone marrow stem cell disease with an annual incidence of 1–2 new cases per 100 000 adults and accounting for approximately 15 % of leukemia cases. CML is one of the rarest forms of leukemia, which is expected to become the most prevalent hematologic malignancy in the world by 2020.[37,404,405] For the past decades, management of CML therapy with TKIs has been successfully achieved.[406–408] The Ph chromosome, a reciprocal translocation of the long arms of chromosomes 9 and 22, t(9;22), is found in more than 90 % patients with CML, 15–25 % of patients with acute lymphoblastic leukemia (ALL), and 1 % of newly diagnosed adults with acute myeloid

leukemia (AML).[23,354,355] This translocation transposes the *ABL1* oncogene from chromosome 9q34 to the *BCR* gene on chromosome 22q11 (Figure 3.1).[28,30]

This reciprocal translocation during hematopoiesis combined with alternative splicing events may originate at least eight different reported *BCR-ABL1* transcripts, all encoding proteins with high tyrosine kinase activity. The vast majority of patients with CML (~95 %) express either e13a2 or e14a2 mRNAs that result from a rearrangement of the major breakpoint cluster regions (M-BCR) generating 210-kDa fusion proteins (Figure 3.1C). Several studies suggest that not only qualitative differences in the type of BCR-ABL1 proteins expressed but also quantitative variations in their total level within the cells may have an important role in determining CML phenotype.[33–35, 358,409] The fused *BCR-ABL1* gene and its gene products provide specific markers for diagnosis and disease monitoring. Currently, CML diagnosis is primarily based on clinical symptoms, complete blood count, and bone marrow biopsy. Cytogenetic analysis, such as karyotype and fluorescence in situ hybridization (FISH), may be carried out to check the presence of the Ph chromosome, and molecular tests, e.g., RT-PCR and RT-qPCR, are used for assessing type and levels of fusion transcript on RNA from bone marrow or peripheral blood specimen.[39,410] Monitoring CML by RT-qPCR and RT-nested PCR depends on local facilities and on the degree of molecular standardization of the local laboratory.[110,411,412]

Based on their size-dependent SPR absorption and the high surface-to-volume ratio allowing for surface functionalization with a variety of molecules, AuNPs are frequently used as probes in biological detections.[164,206] Baptista and colleagues developed a proof-of-concept colorimetric Au-nanoprobe method for direct detection and quantification of a *BCR-ABL1* e14a2 fusion suitable for identification of *BCR-ABL1* targets in lab-controlled conditions.[123] Contrary to the existing molecular tools for the diagnostics of CML, the Au-nanoprobe methodology requires neither retrotranscription of the sample RNA into cDNA nor its amplification in a nested-PCR format with extreme complexity. Despite several reports on the use of *BCR-ABL1* target as proof-of-concept for nanotechnology-based detection, the use of NPs for CML diagnostics in clinical samples has never been performed before.

Here, we were able to directly screen RNA extracted from blood or bone marrow samples from patients admitted to the clinics for CML or AML via the Au-nanoprobe assay and validated results against the gold standard, RT-nested PCR and qPCR, without loss of information.
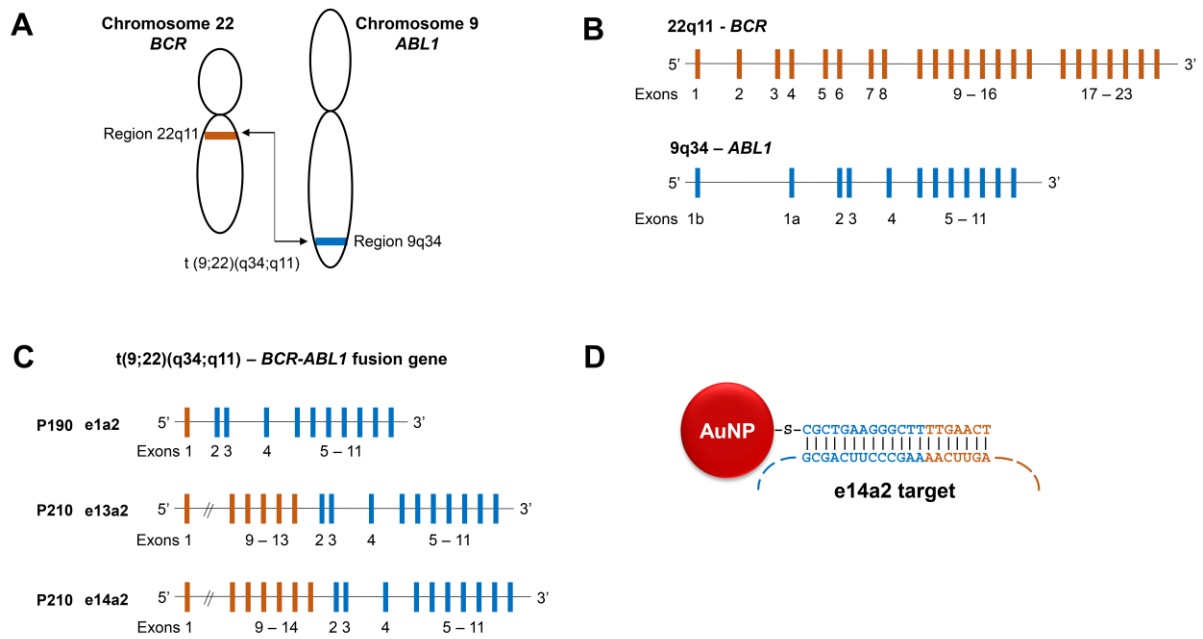
Figure 3.1 Genetics of CML. **A)** Chromosomes reciprocal translocation that originates the *BCR-ABL1* oncogene during hematopoiesis. **B)** Structure of *BCR* and *ABL1* genes. **C)** Structure of the two most common *BCR-ABL1* fusion transcripts (e14a2 and e13a2) and a rare one (e1a2). e14a2 and e13a2 isoforms encode 210 kDa fusion proteins, and the e1a2 isoform encodes a 190-kDa protein. **D)** Au-nanoprobe designed to target e14a2 mRNA.

3.3 Material and Methods

Clinical samples and control cell lines characterization

Cytogenetic and/or molecular characterization of samples was performed has described in the *Materials and Methods* section of chapter 2, including the following steps: patients informed consent and clinical samples; cytogenetic analysis; cell culture of leukemia cell lines; total RNA extraction and cDNA synthesis; *BCR-ABL1* molecular analysis.

Au-nanoprobe synthesis

The probe sequence and the complementary target derive from the *BCR-ABL1* e14a2 (also known as b3a2) chimeric protein mRNA. This target was selected because it represents the most frequent breakpoint in CML, accounting for 55 % of cases.[17,34] Probe selectivity was assessed against two other *BCR-ABL1* breakpoint regions: e13a2 and e1a2. Control oligonucleotide target sequences included *BCR*, *ABL1*, and an unrelated target (Table 3.1).

Au-nanoprobe design and synthesis were performed as previously described.[123] In brief, 14-nm AuNPs were prepared by the citrate reduction method and functionalized with the respective thiolated

oligonucleotide in an aqueous solution of AuNPs at a 1:150 (AuNP:oligonucleotide) ratio for 16 h. After centrifugation (20 min at 14 500 x g), the oily precipitate was washed with 10 mM phosphate buffer (pH 8.0), 0.1 M NaCl, centrifuged, and resuspended in the same buffer. The resulting Au-nanoprobes were stored in the dark at 4 °C.

Characterization of AuNPs and Au-nanoprobes was performed through Transmission Electron Microscopy (TEM), Dynamic Light Scattering (DLS) and UV-Vis spectroscopy.

Table 3.1 Oligonucleotide probe and synthetic oligonucleotide targets

Oligonucleotides	Sequence (5'-3')	Target sequence GeneBank Acc. No.
e14a2 probe	Thiol-CGCTGAAGGGCTTTTGAACT	AJ131466.1
e14a2 gene fusion	TGGATTTAAGCAGAGTTCAAAAGCCCTTC AGCGGCCAGTA	AJ131466.1
e13a2 gene fusion	TGACCATCAATAAGGAAGAAGCCCTTCAG CGGCCAGTAGC	AJ131467.1
e1a2 gene fusion	TCCATGGAGACGCAGAAGCCCTTCAGCGG CCAGTAGCATC	AF113911.1
***BCR* gene**	TGGATTTAAGCAGAGTTCAAATCTGTACT GCACCCTGGAG	NM_004327.3
***ABL1* gene**	CTCCAGCTGTTATCTGGAAGAAGCCCTTC AGCGGCCAGTA	NM_005157.5
***γ-actin* gene (NC)**	AGAAGAGCTACGAGCTGCCCGATGGCCAG GTCATCACCAT	NM_001199954.1

NC - Non-complementary target

Colorimetric detection with Au-nanoprobes

The Au-nanoprobe assay was performed in a total volume of 30 μL containing the Au-nanoprobe at a final concentration of 2.5 nM and the appropriate targets at a final concentration of 0.33 μM in 10 mM phosphate buffer (pH 8.0). A blank was made in the same conditions but replacing target or total RNA by an equivalent volume of 10 mM phosphate buffer (pH 8.0). Following 5 min of denaturation at 95 °C, the mixtures were cooled down to 25 °C and 80 mM MgCl$_2$ added for color revelation. Absorption spectra were run in a Tecan Infinite® M200 microplate reader (Männedorf, Switzerland).

Aggregation profiles were interpreted based on the AUC, using the trapezoidal rule:

$$rAbs = \frac{AUC\ (500\text{-}530\ nm)}{AUC\ (570\text{-}600nm)}$$

(Equation 3.1)

Au-nanoprobe aggregation is portrayed by the natural logarithm of rAbs: a value of 0 for the ln (rAbs) is considered as the threshold for distinction between non-aggregated [ln (rAbs)$\geq$ 0] and aggregated [ln (rAbs)<0] Au-nanoprobe, corresponding to a positive and a negative sample, respectively. The accuracy of the Au-nanoprobe assay was assessed calculating positive and negative predictive values (PPV and NPV, respectively), by comparison to the gold-standard methodology, RT-PCR. These proportions determine the positive results that are true positive hits (PPV) and true negatives (NPV):

$$PPV = \frac{Number\ of\ positives\ (gold-standard)}{Number\ of\ positives\ (Au-nanoprobe)}$$

(Equation 3.2)

$$NPV = \frac{Number\ of\ negatives\ (gold-standard)}{Number\ of\ negatives\ (Au-nanoprobe)}$$

(Equation 3.3)

Statistical analysis

A one-way analysis of variance (ANOVA) and a post hoc Tukey's test were carried and mean differences (P value <0.001) between groups determined with a confidence interval (CI) of 99 %.

3.4 Results and Discussion

Au-nanoprobe characterization
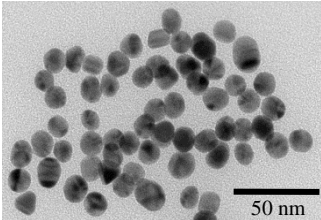
Characterization of the synthesized citrate-capped AuNPs and the Au-nanoprobe was assessed by TEM imaging, DLS measurements, and UV-Vis spectroscopy (Table 3.2). Integration of the information provided by these three techniques allows for a thorough characterization of NPs, namely size, distribution and morphology. This information is required by the Nanotechnology Characterization Laboratory for the standardization of nanomaterials intended for diagnostics or therapeutics.

TEM delivers quantitative measures of AuNPs physical size and morphology but only considers the inorganic core of the NP for size determination.[413] TEM measurements determined that the citrate-capped AuNPs used in this study present an average diameter of 14 nm (Table 3.2).

DLS enables the determination of the overall mean size of the particle considering the NPs inorganic core and the organic coating layer. Moreover, DLS is highly influenced by the presence of small populations of large particles or groups of smaller particles, which can be translated into a greater overall NP size.[414] Indeed, hydrodynamic diameter of AuNPs and the Au-nanoprobe was determined to be 20.2 nm and 28.8 nm, respectively (Table 3.2).

UV-Vis spectra can also be used to infer NPs size, by calculating the ratio of the absorbance of AuNPs at the surface plasma resonance peak (A_{spr}) to the absorbance at 450 nm (A_{450}).[415] Moreover, a characteristic red-shift from 519 (AuNP) to 524 nm (Au-nanoprobe) clearly indicates an increase in the AuNP diameter, due to bounding of the thiol-modified oligonucleotide to its surface (Table 3.2).

Table 3.2 AuNPs and Au-nanoprobe characterization through Transmission Electron Microscopy (TEM), Dynamic Light Scattering (DLS) and ultraviolet-visible (UV-Vis) spectroscopy.

	Au-core average diameter (TEM image)	Z-average (nm)	SPR peak (nm)
AuNPs	14 nm 50 nm	20.2	519
Au-nanoprobe		28.8	524

SPR – surface plasmon resonance

Au-nanoprobe calibration

Molecular diagnostics of CML usually involves the detection of the *BCR-ABL1* e14a2 fusion transcript. First, we calibrated the Au-nanoprobe to selectively identify this fusion transcript using synthetic oligonucleotides as targets for hybridization. Figure 3.2 shows that the Au-nanoprobe was able to discriminate between the fully complementary target and two other *BCR-ABL1* fusion transcripts that share the same *ABL1* region as the e14a2 transcript (e13a2 and e1a2) at 100 fmol/µl of ssDNA oligonucleotide. One can observe the selectivity of the Au-nanoprobe towards the e14a2 transcript, as the values for *BCR*, *ABL1*, and non-complementary targets are below the defined threshold.

Total RNA extracted from K562 (harboring the target e14a2 fusion transcript), BV173 (harboring the e13a2 fusion transcript), or HL60 (promyelocytic leukemia cell line without fusion transcript) was used to calibrate the assay for complex sample mixtures. The Au-nanoprobe was able to recognize the e14a2 sequence present in K562 cells, with identical specificity as that attained for synthetic oligonucleotides (Figure 3.3).

RNA extracted from HL60 and BV173 cell lines was scored as negative despite the presence of partially complementary targets: *BCR*, *ABL1*, and e13a2 mRNA (Figure 3.3B). The obtained value is clearly below the established threshold indicating that the system is capable to selectively detect only the correct target sequence even in presence of similar sequences with more than 50 % homology to the target. The colorimetric data is in clear agreement with that of the gold standard, RT-PCR.[38,44] A limit of detection (LOD) of 15 ng/µl is ideal and critical for optimal performance and sequence discrimination directly from RNA samples.
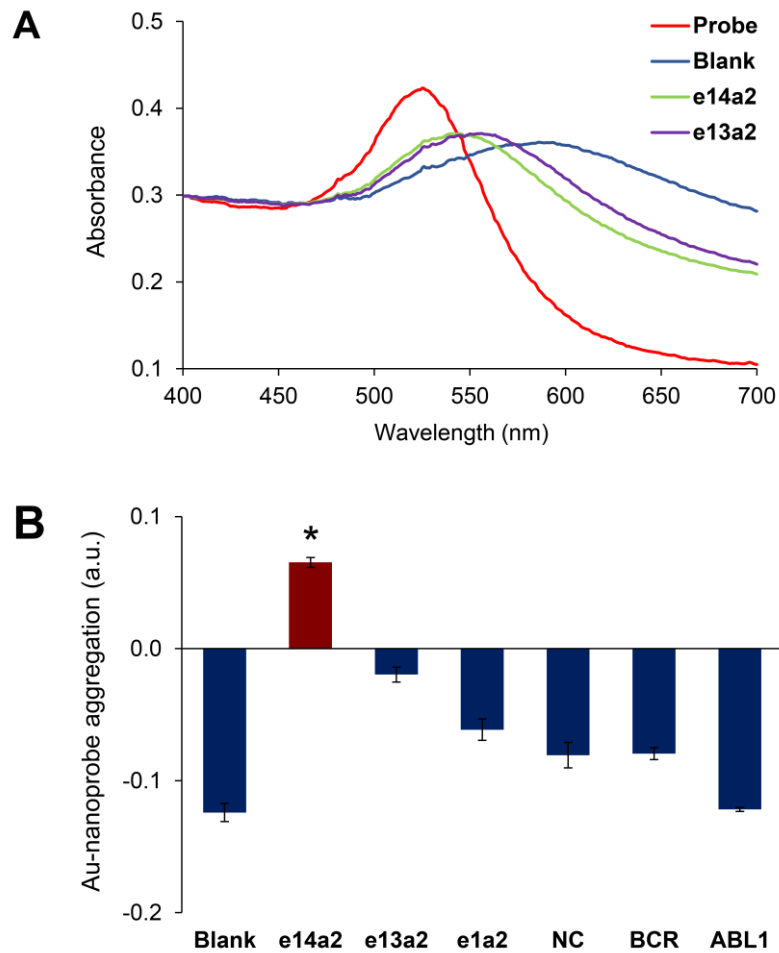
Figure 3.2 Au-nanoprobe detection of the e14a2 *BCR-ABL1* transcript variant. **A)** Visible spectra before salt addition (Probe, red); after the addition of salt in absence of any target (blank, blue), presence of the e14a2 (green) or e13a2 (purple) *BCR-ABL1* synthetic oligonucleotides. **B)** Specificity of the Au-nanoprobe towards different synthetic oligonucleotides. A threshold of 0 for Au-nanoprobe aggregation [ln (rAbs)] was considered for discrimination between positive and negative detection. The error bars represent the standard error of the mean from three independent assays. *Statistically significant difference with *P* value <0.001, in comparison to e13a2 condition (post hoc Tukey's test).
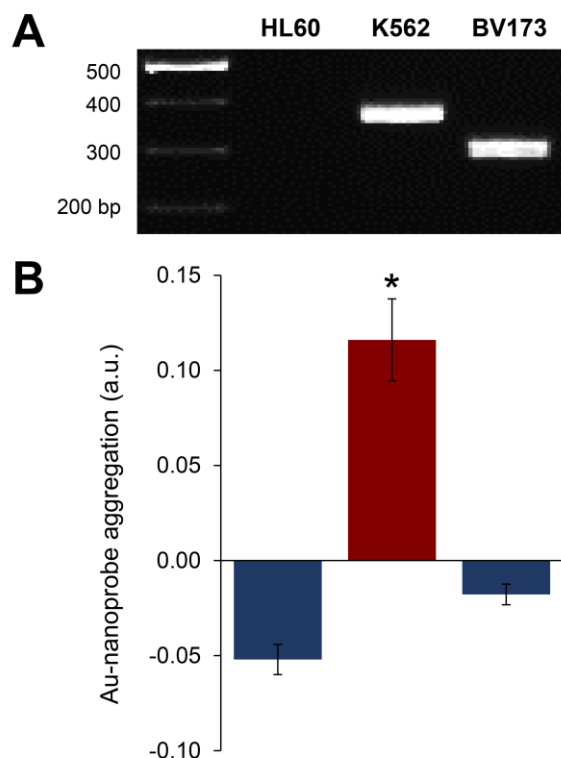
Figure 3.3 Au-nanoprobe detection of the e14a2 *BCR-ABL1* transcript variant in total RNA samples. RNA was extracted from cell lines (HL60, K562, and BV173). **A)** Agarose (2 %) gel electrophoresis showing nested-PCR products using standardized primers for the detection of the e14a2 (360 bp) and e13a2 (285 bp) transcripts. First lane is DNA ladder (GeneRuler, Fermentas). **B)** e14a2 Au-nanoprobe detection assay. A threshold of 0 for Au-nanoprobe aggregation [ln (rAbs)] was considered for discrimination between positive and negative detection. The error bars represent the standard error of the mean from at least three independent assays. *Statistically significant difference with P value <0.001, in comparison to HL60 or BV173 samples (post hoc Tukey's test)

Au-nanoprobe assay for CML diagnostics

Following calibration of the Au-nanoprobe assay, 38 myeloid leukemia samples (16 AML sample and 22 CML samples), previously characterized at the cell and molecular levels, were blindly tested via the Au-nanoprobe approach and compared to RT-nested PCR. From the attained data, we determined the sensitivity, specificity, and positive and negative predictive values (PPV and NPV, respectively) for the Au-nanoprobe assay (Figure 3.4; Table 3.3).

Samples were scored negative for e14a2 based on ln(rAbs)<0. Twelve clinical samples were correctly scored as positive for the e14a2 transcript and the remaining scored as negative. Even though all AML bone marrow samples were found negative for t(9;22) by FISH analysis, the Au-nanoprobe method was sensitive enough to detect one AML sample harboring the e14a2 fusion transcript,

confirmed by RT-nested PCR (sample 16). Moreover, the Au-nanoprobe procedure allowed to scrutinize peripheral blood follow-up samples expressing the e14a2 transcript. Sample 34, previously determined to express *BCR-ABL1* levels of 0.34 % IS, was correctly scored as positive. According to the 2015 ELN guidelines, these levels define a CCyR.[38]

Care should be taken when borderline values are obtained, as seen in samples 28 and 38, to avoid the occurrence of false positives. However, results based on ln(rAbs) are in accordance with RT-nested PCR results. PPV (12 true positive hits out of 12 positive calls) and NPV (26 true negative hits out of 26 negative calls) of 100 % indicate that the Au-nanoprobe assay under these conditions is a reliable test to scrutinize leukemia patients expressing the e14a2 fusion transcript.
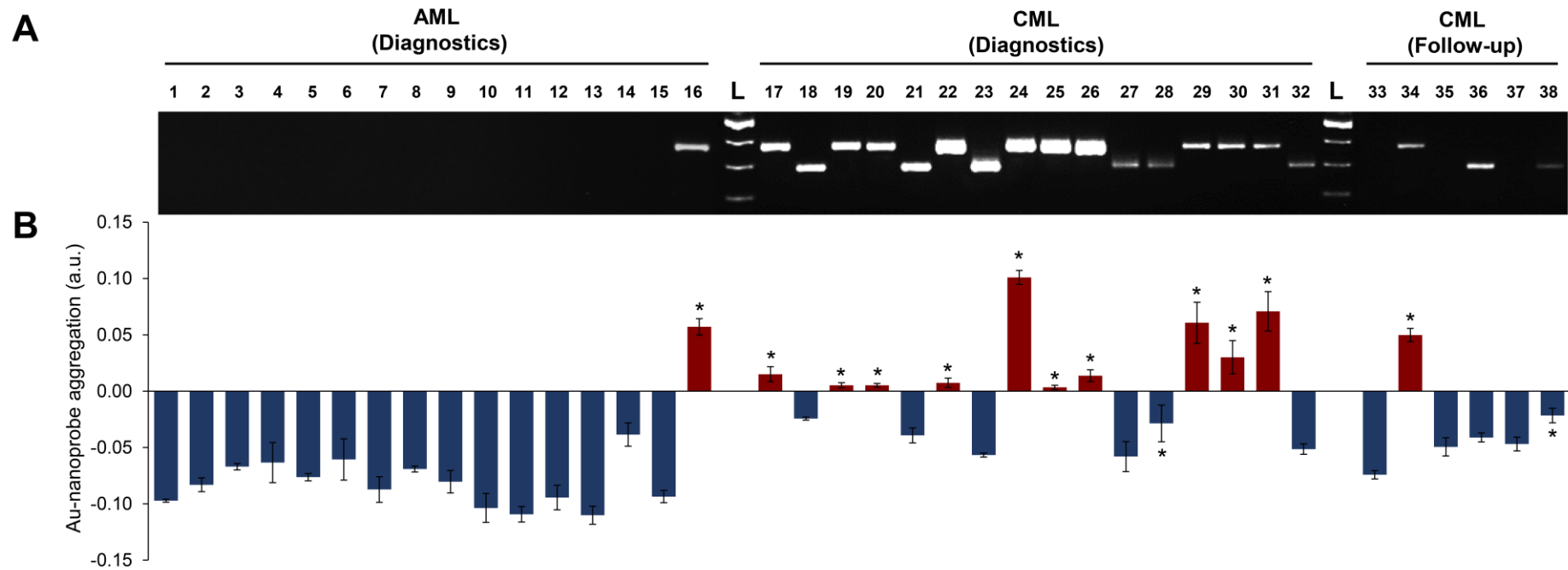
Figure 3.4 Au-nanoprobe detection of the e14a2 *BCR-ABL1* transcript variant in total RNA clinical samples. RNA extracted from bone marrow or peripheral blood samples from patients previously diagnosed with AML (1–16) or CML (17–38). **A)** Agarose (2 %) gel electrophoresis showing nested-PCR products using standardized primers for the detection of the e14a2 (360 bp) and e13a2 (285 bp) transcripts. Lanes L refer to DNA ladder (GeneRuler, Fermentas - ThermoFisher, Waltham, MA, USA): 200, 300, 400, and 500 bp (from bottom to top). **B)** e14a2 Au-nanoprobe assay. A threshold of 0 for Au-nanoprobe aggregation [ln (rAbs)] was considered for discrimination between positive and negative detection. The error bars represent the standard error of the mean from at least three independent assays. *Statistically significant difference with P value <0.001, in comparison to sample 1 (post hoc Tukey's test)

Table 3.3 Performance of Au-nanoprobe diagnostic test.

	Sample	Tissue	FISH or RT-qPCR* (IS)	RT-nested PCR	e14a2 Au-nanoprobe assay
AML at diagnostics	1	BM	n/a	No amp	-
	2	BM	n/a	No amp	-
	3	BM	n/a	No amp	-
	4	BM	n/a	No amp	-
	5	BM	n/a	No amp	-
	6	BM	n/a	No amp	-
	7	BM	n/a	No amp	-
	8	BM	n/a	No amp	-
	9	BM	n/a	No amp	-
	10	BM	n/a	No amp	-
	11	BM	n/a	No amp	-
	12	BM	n/a	No amp	-
	13	BM	n/a	No amp	-
	14	BM	n/a	No amp	-
	15	BM	n/a	No amp	-
	16	BM	n/a	**e14a2**	+
CML at diagnostics	17	BM	n/a	**e14a2**	+
	18	BM	n/a	e13a2	-
	19	BM	n/a	**e14a2**	+
	20	BM	n/a	**e14a2**	+
	21	BM	n/a	e13a2	-
	22	BM	n/a	**e14a2**	+
	23	BM	98 %	e13a2	-
	24	BM	87 %	**e14a2**	+
	25	BM	98 %	**e14a2**	+
	26	BM	97 %	**e14a2**	+
	27	BM	95 %	e13a2	-
	28	BM	99 %	e13a2	-
	29	BM	77 %	**e14a2**	+
	30	BM	95 %	**e14a2**	+
	31	BM	98 %	**e14a2**	+
	32	PB	90 %	e13a2	-
CML at follow-up	33	PB	0.017 %	No amp	-
	34	PB	0.34 %	**e14a2**	+
	35	PB	0.00031 %	No amp	-
	36	PB	0.11 %	e13a2	-
	37	PB	1 %	No amp	-

38	PB	3.4 %	e13a2	**-**

* FISH analysis for diagnostic samples (1-32) and RT-qPCR analysis for follow-up samples (33-38)

BM, bone marrow; IS, international scale; n/a, not available; No amp, no amplification; PB, peripheral blood

3.5 Concluding Remarks

The rapid and fast molecular characterization of CML patients is of utmost relevance if suitable therapy is to be initiated. Routine molecular diagnostics requires cumbersome equipment and specialized technicians to evaluate the presence of the characteristic *BCR-ABL1* fusion transcripts that constitute the hallmark of this disease. Here, we demonstrated for the first time that the Au-nanoprobe system based on the NCL mechanism may be used to rapidly identify e14a2-positive patients (Figure 3.5). Besides being able to detect a clinical sample with a *BCR-ABL1* fusion transcript, this approach allowed to discriminate between the two most frequent isoforms of this genetic abnormality - e13a2 and e14a2 - that alone account for more than 95 % of CML cases. The attained PPV and NPV indicate that the Au-nanoprobe assay is suitable for the direct screening of patients' mRNA with obvious advantages in terms of time. It should be noted that the Au-nanoprobe assay detects the fusion transcript directly from RNA extracted from patient samples and, thus, is free from the stochastic bias introduced by the standard methodologies involving enzymatic retrotranscription into cDNA followed by PCR. Because it avoids these reaction steps, the Au-nanoprobe approach is much faster and simple, reducing the detection time frame from 9 h, required for RT-nested PCR alone, to 1 h and 30 min.

Diagnostic confirmation of myeloid leukemia patients where the Ph chromosome is undetectable by chromosome banding analysis or FISH is a major concern. Results achieved with an e14a2 expressing AML sample (negative for t(9;22) negative by cytogenetic analysis) and with follow-up samples with *BCR-ABL1* levels as low as 0.34 % IS indicate the Au-nanoprobe methodology is suitable for screening patients that exhibit a CCyR but still did not achieve a MMR. Note that ELN recommends the assessment and monitoring of the disease by RT-qPCR on buffy coat blood cells every 3 months, not only after a CCyR has been achieved but also from the beginning.[38] The Au-nanoprobe methodology would be highly advantageous in these consecutive tests due to its simplicity and low cost. The assay performance suggests that it might be useful for a combined diagnostics strategy: early screening via the Au-nanoprobes for POC to quickly identify CML samples, followed by standard protocol on negative samples.

The possibility of fast and cheap screening technology based on RNA samples at admission is clearly advantageous. This is particularly relevant for countries where the economic burden of molecular diagnostics of rare diseases is way too high to allow routine testing via proposed guidelines. Considerable time would be saved from the time of admission to the start of therapy, which in turn would impact on therapy success with advantages for patients.

The overall cost of the Au-nanoprobe assay is approximately €0.20-1.00 per sample without the need of dedicated instrumentation. This is particularly relevant considering that the percentage of newly reported cases of CML occurring in low- to middle-income countries has more than tripled over the past 40 years and that only about 5 % of the global resources spent on cancer are deployed in these countries.[101] CML is one of the commonest adult leukemia in Indian population accounting for 30 to 60 % of all adult leukemia, yet little is known about the epidemiology of CML in such regions mostly due to poor registries, lack of conclusive molecular diagnosis, and the prohibitive cost of CML molecular characterization.[416,417] Indeed, the first molecular test to measure *BCR-ABL1* in sub-Saharan Africa was performed in 2011 in Ethiopia.[418] The availability of rapid and cost-effective tests should result in reducing the rate of misclassifications for leukemia and will likely improve CML incidence and mortality rates in low- to medium-income countries.

Moreover, the Au-nanoprobe colorimetric assay is highly translatable onto POC devices providing a novel platform for health diagnostics, as well as low-cost testing based on rapid low-volume sample analysis.[169, 220,221,419] This possibility will be further explored in the next chapter of this thesis, by miniaturizing the assay and integrating microfluidics and NPs to enable CML diagnostics at both clinical and remote settings.
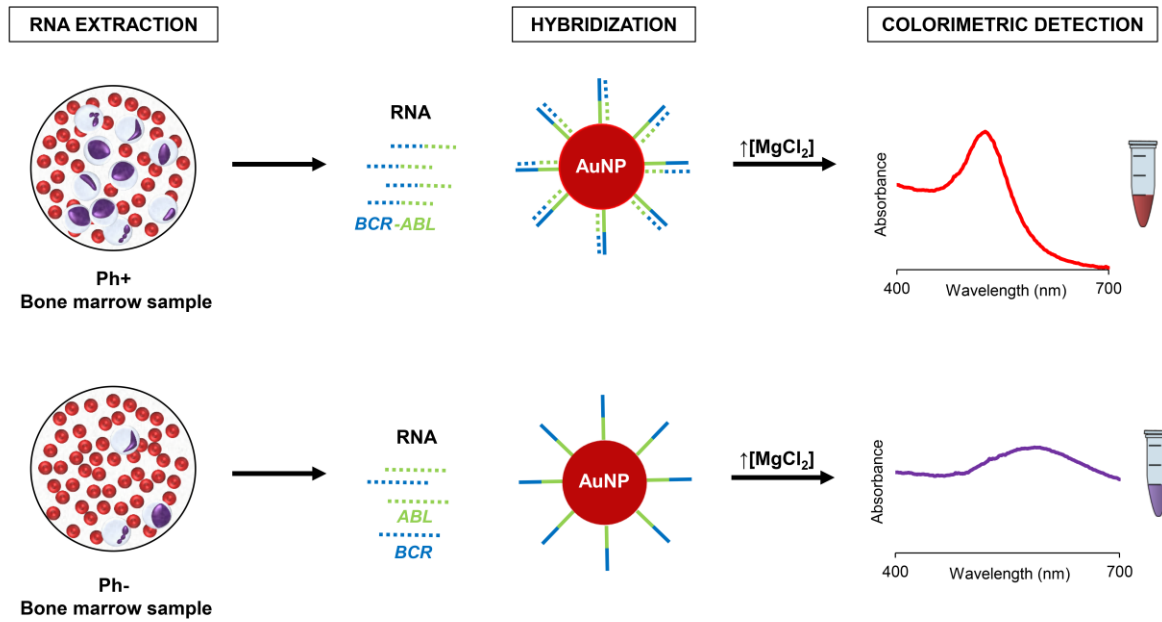
Figure 3.5 CML colorimetric detection via Au-nanoprobe assay. First, total RNA is extracted from bone marrow, or peripheral blood, samples. RNA solution is mixed with the Au-nanoprobe, designed to detect only the e14a2 *BCR-ABL1* fusion transcript. Hybridization to a complementary nucleic acid target sequence prevents salt induced aggregation and the solution remains red (surface plasmon resonance (SPR) band at 525 nm). In the absence of the e14a2 transcript, and even in the presence of partially complementary targets (*BCR* and *ABL1*), Au-nanoprobes salt induced aggregation occurs and the solution turns blue (SPR band at 600 nm).

CHAPTER 4 – **MICROFLUIDIC CHIP FOR GOLD NANOPROBE-BASED** *BCR-ABL1* **RNA DETECTION**

All microfluidic fabrication, setups and experiments were performed at the Center of Excellence in Microelectronics Optoelectronics and Processes (CEMOP, Universidade Nova de Lisboa). R. Vinhas assisted with the experiments, prepared and calibrated the Au-nanoprobe and all biological samples, performed the hybridization step before injection into the chip, and helped with data analysis, at the Research Unit on Applied Molecular Biosciences (UCIBIO, Universidade Nova de Lisboa), under the supervision of P.V. Baptista and A.R. Fernandes. The author of this thesis opted for reproduction of the resulting scientific paper, thus apologizing for any repeated content in different contexts of the document.

Alves PU, **Vinhas R**, Fernandes AR, Birol SZ, Trabzon L, Bernacka-Wojcik I, Igreja R, Lopes P, Baptista PV, Águas H, Fortunato E, Martins R. 2018. Multifunctional microfluidic chip for optical nanoprobe based RNA detection – application to Chronic Myeloid Leukemia. Scientific reports. 8(1):381.

4.1 Abstract

Many diseases have their treatment options narrowed and end up being fatal if detected during later stages. Therefore, POC devices have an increasing importance for routine screening applications in the health sector due to their portability, compactness, fast analyses and decreased costs. A multifunctional sensor, which uses Au-nanoprobes to perform RNA optical detection inside a microfluidic chip, was developed and tested. To prove the concept, this device was used for CML, a hemato-oncology disease that can be better treated in its early stages and is lacking routine fast screening tests. The chip passively mixed target RNA from samples, Au-nanoprobes and saline solution to infer a result from their final colorimetric properties. An optical fiber network was used to evaluate its transmitted spectra inside the chip. Trials provided accurate output results within 3 minutes, yielding signal-to-noise ratios up to 9 dB. When compared to actual state-of-art screening techniques, these results were, at microscale, at least 10 times faster than the reported detection methods for CML. Concerning miniaturized POC applications, this work paves the way for other new and more complex versions of optical based genosensors.

4.2 Introduction

NP-based bioanalyte detection has been at the forefront of miniaturized systems for molecular diagnostics at POC. In particular, AuNPs have been revolutionizing the molecular field of optical analysis due to their good stability, visible color change between aggregate and non-aggregate state, and affinity with biomolecules.[164, 188, 206,420] The first reports on molecular detection of DNA based on the cross-linking of AuNPs with color change have paved the way for several different approaches to circumvent limitations associated to current PCR based methods.[187] Baptista *et al* developed a NCL colorimetric method based on the differential aggregation of oligonucleotide functionalized AuNPs, and hence applied it to the detection of DNA (pathogens, human genomic, etc.). More interestingly, this system has also been used for the detection of RNA since it enables screening and characterization of transcripts, allowing gene expression studies and genetic disease studies.[123,421] Several of these systems have been further incorporated into microfluidics platforms for enhanced detection capabilities.[220, 419,422–425]

Microfluidic technology provides the means for miniaturization of chemical and biochemical analysis that may easily be made portable.[426,427] They bring several advantages when compared to standard apparatus, such as the significant decrease in volumes of reagents and samples, faster operation and reaction times, decreased analysis time and decreased costs.[428,429] These characteristics can be synergistically and simultaneously combined on microfluidic platforms,[430,431] making this type of devices promising for research purposes,[432] for high value applications in the medical and pharmaceutical industries,[433] and ideal for POC testing.[434] Optics is an effective mean for signal

transduction that can be paired with microfluidics to design highly compact and integrated devices.[435] Recent studies, which use different types of NPs to either provide or enhance optical output signals, have reported significant progress towards POC applications.[436,437] Lately, microfluidics has also burgeoned into paper-based biosensors,[438] as they provide extremely cheap cellulosic material, compatible with many chemical/biochemical/medical applications and allow the transportation of liquids without external forces due to capillary forces.[439,440] However, this technology still faces some limitations,[441] such as the sample retention within channels and sample evaporation during transport, which result in low efficiency of sample-delivery inside the device (usually less than 50 %). The LOD on paper microfluidics is also poorer when compared to conventional microfluidics due to its incapacity of analyzing samples at low concentrations.[441] Due to these constrains, and despite requiring more expensive equipment, conventional microfluidics is chosen regularly for POC applications.[442]

This work describes in detail a novel and low-cost conventional PDMS microfluidic chip which combines a short-path length micromixer and an optical circuit to perform colorimetric detection (Figure 4.1). To demonstrate the impact of this microfluidic chip for molecular diagnostics, the Au-nanoprobe assay was applied in the detection of *BCR-ABL1* fusion transcript (RNA), which is the molecular hallmark of CML.

CML is originated from the Ph chromosome - a reciprocal translocation of the long arms of chromosomes 9 and 22, t(9;22). This aberrant chromosome is found in 95 % patients with CML, 15–25 % of patients with ALL and 1 % of newly diagnosed adults with AML.[23,354,355] The Ph chromosome results from the fusion of two genes, *BCR* and *ABL1*. This fused gene leads to the transcription of the fused protein tyrosine kinase, which is constitutively active. Although several transcript isoforms have been reported, for the purpose of this study the Au-nanoprobe was designed towards the most frequent variant, e14a2, accounting for about 55 % of CML patients.[17, 29,30,34] The high treatment success rate of the disease relies not only on drug efficacy, but also on fast, accurate and early diagnostic tools.[38] Due to the scarcity of such tools, intense research has been devoted to the development of new methodologies for CML screening and management.

Following design, fabrication and characterization of the chip, three case studies with increasing complexity were performed and analyzed: one, where Au-nanoprobes were used with and without salt, for proof of concept; a second, where *BCR-ABL1* synthetic oligonucleotides were combined with Au-nanoprobes to evaluate the mixing and cross-linking behavior under mixing and optical detection inside the microchannel; and a third, where the system performance was assessed using total RNA extracted from a CML cell line, thus mimicking real clinical sample screening.

Results obtained this way were faster than the standard laboratory operation process at macroscale[421] and unprecedented at microscale. They are suitable for the fast screenings required in medical care and POC, and key to unlock new and more complex versions of optical based genosensors, either to diagnose CML or other similar diseases.
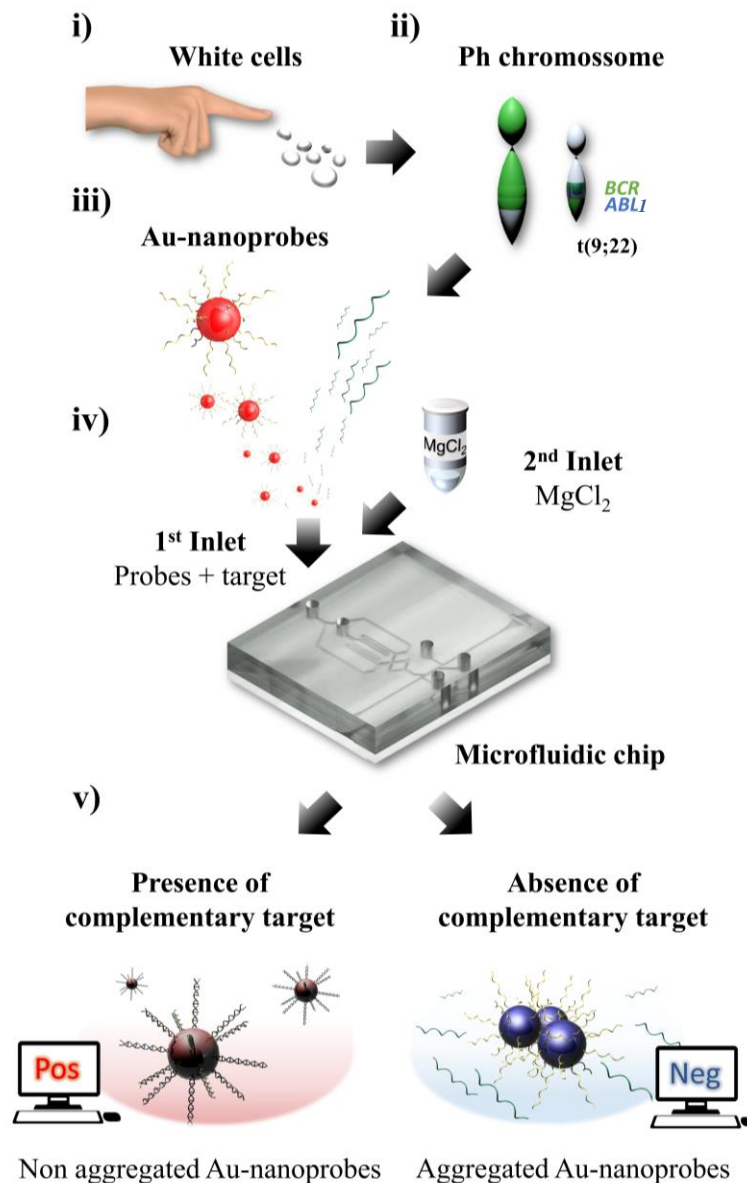
Figure 4.1 Concept of this lab-on-chip as a point-of-care application: i) White cells extracted from a small blood sample are collected to analyze gene expression; ii) This approach aims to diagnose chronic myeloid leukemia using its genetic marker, *BCR-ABL1* fusion transcript; iii) Total RNA extracted from white blood cells is then mixed with Au-nanoprobes and heated to promote hybridization. Note that Au-nanoprobes are functionalized with *BCR-ABL1* complementary sequences; iv) The resulting solution and a salt solution are infused on the two microfluidic chip inlets; v) Thorough mixing and optical detection of these components is performed inside the microfluidic chip. If the patient expresses *BCR-ABL1* transcripts complementary to the oligonucleotide sequence of Au-nanoprobes, their hybridization will cause the final solution to remain red (positive match) in the presence of salt. Otherwise, the non-hybridized Au-nanoprobes will aggregate and cause the final solution to turn blue (negative match) in the presence of salt. With the appropriate setup, and using LabView software, output results described in this step are displayed on the computer within 3 minutes.

4.3 Material and Methods

Materials

All chemicals were of molecular biology grade and purchased from Sigma-Aldrich (St. Louis, MO, USA). Ultrapure water used in these processes came from a Millipore water purification system (Merck Millipore, Billerica, MA, USA). Oligonucleotides were provided by STABVIDA (Caparica, Portugal). SU-8 2050 photoresist, propylene glycolmethyl ether acetate developer (PGMEA) and customized masks, used during the lithography process of the microchip fabrication, were obtained from Microchem (Westborough, MA, USA) and JDPhoto (Herts, UK), respectively. Epoxy resin ES562, used as a master mold for PDMS soft lithography, was ordered from Permabond (Winchester, UK). For the PDMS microchips fabrication, a Sylgard 184 Silicone Elastomer Kit was used (DowCorning, Barcelona, Spain). To improve separation between the PDMS and SU-8 mold, a silanization step was performed onto the SU-8 mold using tridecafluoro-1,1,2,2-tetrahydrooctyl trichlorosilane (Microchem). Microfluidic connections between chip and reservoirs were made using an optimized Teflon tubing kit, ordered from Elveflow (Paris, France).

Fabrication of the microfluidic chip

Microfluidic chips here presented followed standard fabrication steps.[443] A mask with the chip's pattern was designed in AutoCAD 2014. This mask was then printed on sodalime glass using chrome as ink for a precise definition. The first mold, on SU-8, was patterned by UV photolithography. SU-8 was spin-coated on silicon wafers at 1400 rpm (Karl Suss CT62, Suss MicroTec, Munich, Germany) to form a layer with approximately 125 μm, soft baked on a levelled hotplate at 65 ℃ during 5 min, followed by 25 min at 95 ℃, then left for relaxation and cool down for 10 min. Afterwards, they were exposed on a mask aligner (MA6, SussMicroTec, Germany) for 18 s with an exposure dose of 310 mJ/cm^2. The designed photolithographic mask was used in this step, together with an i-line filter to expose with the recommended wavelength of 365 nm. A post-bake took place for a duration of 5 min at 65 ℃, followed by 11 min at 95 ℃. The samples were then submerged to develop in PGMEA for approximately 12 min. A magnetic agitation at 500 rpm was used to enhance this process. In the end, samples were rinsed with isopropanol, and dried with compressed nitrogen.

A replica from the SU-8 mold was made using epoxy resin, which presents higher durability without losing the definition required to fabricate several chips. The SU-8 mold was first silanized in a vacuum desiccator to facilitate the posterior removal of PDMS. PDMS was prepared by mixing base and curing agents in a 10:1 weight proportion, stirred, degassed in a vacuum desiccator and poured over the SU-8 mold for the curing process in a levelled oven for 4 h at 65 ℃. The PDMS slab fabricated in this process, with the complementary pattern, was subsequently peeled off from the SU-8 mold and placed on top of a Petri dish with features faced up. On top of the PDMS slab, epoxy resin was poured until a layer of approximately 2 mm in thickness was formed. Another degassing step took place in the vacuum

desiccator to remove bubbles trapped in epoxy. To finish this process, epoxy was cured in the levelled oven at 120 ºC for 1 h and peeled from the PDMS. The resulting epoxy mold was then used for soft lithography fabrication of the PDMS chips. This procedure took the same steps as those described above for the PDMS slab.

For the inlets and outlet, PDMS chips were punched using a razor sharp stainless-steel biopsy puncher with 1.25 mm outer diameter. The chips were irreversibly bonded to glass slides, using oxygen plasma for 70 s at 98 mTorr with an applied power of 100 W on a Trion Minilock Phantom III RIE (TrionTech, Clearwater, FL, USA). To complete the plasma sealing, PDMS chips already bonded to glass were baked at 100 ºC for 5 min to increase the bond strength.

Samples were characterized by optical microscopy (Leitz Laborlux12MEST, Leica Microsystems, Wetzlar, Germany), confocal scanning microscopy (LSM700, Zeiss, Oberkochen, Germany), profilometry (XP-200, Ambios Technology, Santa Cruz, USA), UV-3101 PC UV/visible/NIR double beam spectrophotometry (Shimadzu, Kyoto, Japan) and scanning electron microscopy (FIB-SEM, Zeiss, Oberkochen, Germany).

Optical setup preparation

Two graded-index multimode optical fibers with 62.5 μm core diameter, 125 μm cladding diameter and 0.275 numerical aperture (GIF625, Thorlabs, Dachau, Germany) were stripped and cleaved from both sides, and inserted in the input and output optical entrances of the chip. One of the two remaining fiber tips was defined as the input fiber and connected to a SMA-ended GIF625 patch cable (Thorlabs). This cable was either coupled to a high-power green light-emitting diode (LED, M530F1, dominant wavelength: 530 nm, half width: 33 nm, typical output power: 5.1 mW, Thorlabs) or red LED (M625F1, dominant wavelength: 625 nm, half width: 18 nm, typical output power: 10.1 mW, Thorlabs). A constant current of 0.4 A was applied on both LEDs during the experiments. The other fiber tip was defined as the output fiber and was connected to a pigtailed silicon photodiode (FDSP625, Thorlabs). Connections with optical fibers were done with bare fiber terminators (BFTU, Thorlabs) and mating sleeves.

A circuit with an operation amplifier (AD549 Operational Amplifier, Analog Devices, Norwood, MA, USA) was used to enhance the photodiode output current, and convert it to a voltage signal. The photodiode was connected to the operational amplifier's inverting input (virtual ground), and a feedback network that incorporated a capacitor (1.5 nF) and a resistor (20 MΩ). The operational amplifier's noninverting input was grounded, ranging from ±12 V. Data acquisition as well as command sending were done via the computer using a LabView program (LabView 2013, National Instruments, Austin, TX, USA) with a NI USB 6008 interface (National Instruments). The same LabView program was used to operate a Legato 210P syringe pump (KD Scientific, Holliston, MA, USA), to automatically infuse and withdraw solutions from the chip.

Au-nanoprobe design and synthesis were performed as previously described in Chapter 3 (*Material and Methods* section).[421] AuNPs of 14 nm, prepared by the citrate reduction method, were functionalized with a thiolated oligonucleotide in 10 mM phosphate buffer pH 8.0, 0.1 M NaCl. The resulting Au-nanoprobes were stored in the dark at 4 °C and characterized by UV-Vis spectroscopy, TEM and DLS.

The probe sequence and the complementary target were derived from the *BCR-ABL1* e14a2 (also known as b3a2) mRNA (GenBank Accession No AJ131466.1), which is the most frequent breakpoint in CML.[17,34] Au-nanoprobe selectivity was assessed against two non-modified synthetic oligonucleotides: a complementary target corresponding to the *BCR-ABL1* e14a2 mRNA sequence, and an unrelated sequence was used as non-complementary target (as described in Table 3.1).

Immortalized human cell lines derived from a CML patient in blast crisis, K562 (*BCR-ABL1* e14a2 fusion transcript positive cell line) and from an acute monocytic leukemia patient, THP1 (*BCR-ABL1* negative) were cultured, respectively, in DMEM and RPMI with 10 % FBS, at 37 °C with 5 % (v/v) CO_2. These cell lines were used as positive and negative controls for the presence and absence of *BCR-ABL1* transcript, respectively.

Total RNA was extracted from K562 and THP1 cell pellets by the guanidine thiocyanate procedure (SV Total RNA Isolation System, Promega) as described in chapter 2 (*Material and Methods* section).[421] RNA was resuspended in DEPC-treated water and stored at -80 °C until use. RNA concentration and purity (Abs_{260nm}/Abs_{230nm} and Abs_{260nm}/Abs_{280nm}) were determined by UV spectrophotometry.

4.4 Results and Discussion

Microfluidic chip design

The microfluidic chip layout was conceived by combining 3 distinct sections (Figure 4.2A). The first section allowed infused solutions to reach the common channel simultaneously (Figure 4.2A - i). This synchronization enables a more efficient utilization since no solution will be left unmixed.

The second component of the chip had a planar micromixer incorporated to perform mixing between solutions (Figure 4.2A - ii). This micromixer was chosen over active and 3D micromixers[444,445] due to its cost efficiency and easy integration with other components of the microchannel, thus allowing low cost fabrication since it only requires a single layer of photolithography to yield the full design. Among passive planar micromixers, rhombic micromixers with obstacles[446] are suitable for this application as they fulfill the mixing requirements over a wide range of Reynold numbers and for short mixing channels (2.5 mm), thus they were implemented in the described device. The integrated mixer has one and a half rhombi, and each edge has a total of nine diamond shaped obstacles to disturb the laminar flow and force mixing between solutions (Figure 4.2B). Each rhombus is also separated by

throttles that seek to increase mixing efficiency even further by creating pressure gradients with an abrupt variation on the channel's width. These variations tend to generate vortexes, and thus, to enhance mixing.

The third and last section of the chip comprises the optical detection unit, where the nucleic acid colorimetric analysis takes place (Figure 4.2A - iii). This screening takes advantage of an extended optical path length design inside the chip,[220] which uses optical fibers to convey light between source and microfluidic chip, and between microfluidic chip and photodiode. Air lenses were incorporated at the entrance and exit, between the optical fiber grooves and the detection channel, to minimize signal losses;[419] the former collimates light coming out of the fiber tip and illuminates the microchannel content uniformly, and the latter focuses the outgoing light into the core of the output optical fiber. Two optical grooves were also integrated in the chip design to enable approximation and alignment between optical fibers and channel (this is where the optical fiber circuit crosses paths with the microfluidic channel). Built-in cleaning channels were added to allow easy removal of dust and particles before optical fiber insertion (Figure 4.2C). Green (530 nm) and red (625 nm) light emitting diodes, detector and electrical setup were kept fixed, while disposable microfluidic chips and attached optical fibers can be replaced with ease for a cleaner usage. LED wavelengths were chosen according to the absorption spectra of aggregated and non-aggregated Au-nanoprobes.[165,447] The low price, biocompatibility and optical properties of PDMS made this silicon rubber a common choice to fabricate the microfluidic chips by replica molding.[448–451] Full details on the chip design can be seen in Appendix IV – Figure IV.1.
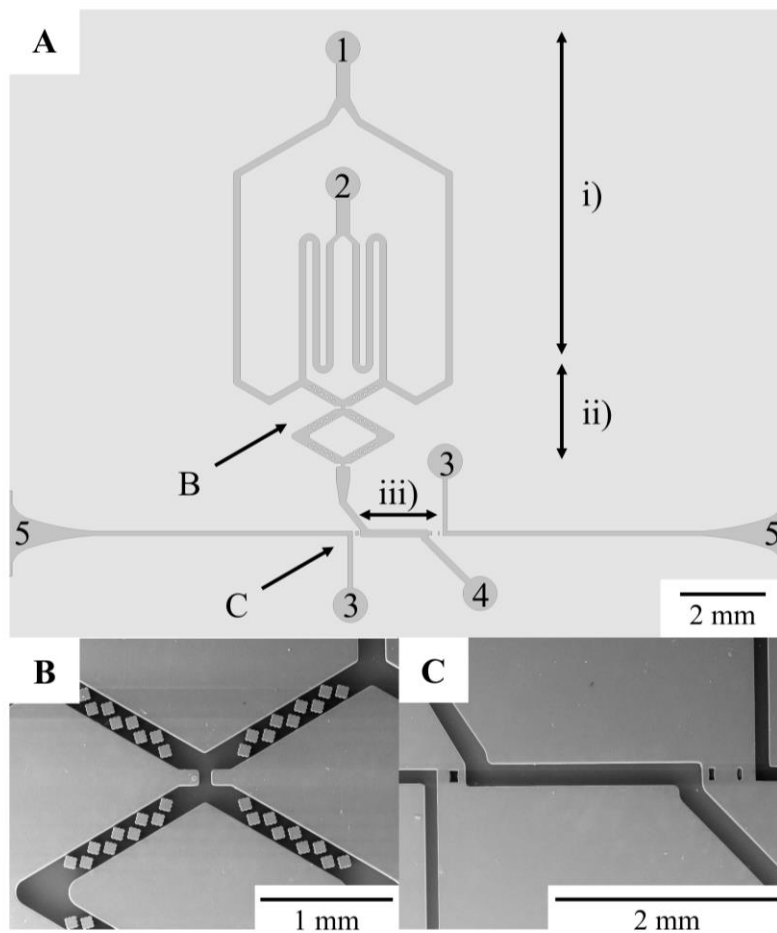
Figure 4.2 A) Microfluidic chip design. i) infusion section; ii) mixing section; iii) optical detection section; 1 – Target DNA/RNA and Au-nanoprobes solution inlet; 2 – Salt ($MgCl_2$) inlet; 3 – Optical fiber cleaning channels; 4 – Microchannel outlet; 5 – Optical fiber insertion cavity. **B)** Detailed scanning electron microscopy picture of the mixing region. The mixing region takes advantage of 1.5 rhombi, each with 36 diamond shaped obstacles and 2 throttles to perform efficient passive mixing. **C)** Detailed scanning electron microscopy picture of the detection region. A collimating lens is used between the first optical fiber groove and microchannel to align the incoming light onto the channel. Likewise, two focusing lenses are used between microchannel and the second optical fiber groove to focus the outcoming light onto the output optical fiber.

Optical setup

An optoelectronic setup was assembled to integrate the microfabricated chips and to perform optical analysis (Figure 4.3).
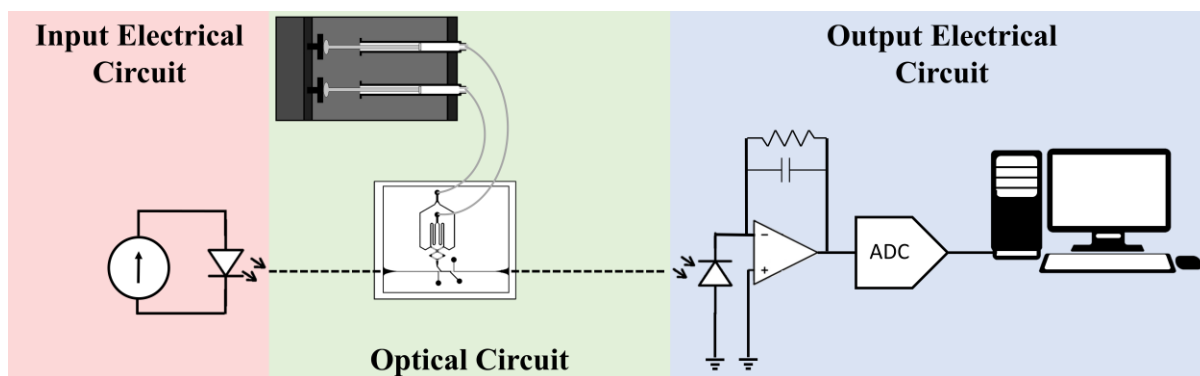
Figure 4.3 Setup scheme. Input electrical circuit: Light with one of two wavelengths (625nm; 530nm) is emitted from a powered LED through an optical fiber, represented by the dashed line. Optical circuit: The microfluidic chip is crossed by 2 optical fiber segments. The first allows incoming light to interact with solutions present in the region where optical detection occurs. The second carries the transmitted light outside the chip. A syringe pump is used to infuse these solutions inside the chip. Output electrical circuit: A photodetector transduces outcoming light to a current signal, which is amplified by an operation amplifier with a feedback network (capacitor: 1.5 nF; resistance: 20 MΩ), and converted to a voltage signal. This analog signal is then converted to digital and acquired by the computer using LabView software.

The detection response (R_s) was defined as the ratio of the digital output acquired by the computer of the red LED (dominant wavelength: 625 nm) and green LED (dominant wavelength: 530 nm) on a screened sample:
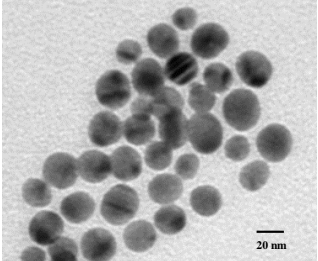
$$R_S = \frac{Sample\ V_{out}\ (625\ nm)}{Sample\ V_{out}\ (530\ nm)} \Big/ \frac{Baseline\ V_{out}\ (625\ nm)}{Baseline\ V_{out}\ (530\ nm)} \qquad \text{(Equation 4.1)}$$

This ratio was normalized to baseline sample ratio, 10 mM phosphate buffer pH 8 solution, as it eliminates the intrinsic optical properties that vary from chip to chip or with time and usage.[220,419] Baseline data were extracted prior to and after each assay in order to confirm the system reliability.

Colorimetric analysis

AuNPs of 14-nm in diameter were used and functionalized with the ssDNA probe that recognizes a unique sequence on the *BCR-ABL1* oncogene, the hallmark of CML, and fully characterized by UV-Vis spectroscopy, TEM and DLS, as described in chapter 3 (*Results and Discussion - Au-nanoprobe characterization* section) (Table 4.1).

Table 4.1 AuNPs and Au-nanoprobe characterization through Transmission Electron Microscopy (TEM), Dynamic Light Scattering (DLS) and ultraviolet-visible (UV-Vis) spectroscopy.

	Au-core average diameter (TEM image)	Z-average (nm)	SPR peak (nm)
AuNPs	14 nm 20 nm	17.4	519
Au-nanoprobe		26.3	524

SPR – surface plasmon resonance

Hybridization of Au-nanoprobes to targets was performed in 10 mM phosphate buffer pH 8, followed by a 5-minute denaturation at 95 °C. Samples were then cooled down to room temperature before injection into the chip.

The microfluidic chip was rinsed with isopropanol to increase the microchannel hydrophilicity and to avoid formation of bubbles that could otherwise affect the optical readings and increase the dead volume A syringe pump was used to infuse two different solutions of 5 µL each, one in each inlet (flowrate: 5 µL/min), according to each experiment and in a 1:1 proportion (Table 4.2). Data acquisition of electrical output signals generated from LED transmitted light started immediately after the micromixing of infused solutions, in a no-flow regime. These measurements were acquired with a sampling interval of approximately one minute.

For baseline measurements, 10 mM phosphate buffer pH 8 solution was used as the transparent medium inside the chip. It was selected as a reliable baseline source as all the tested samples are diluted in this solution. This procedure normalizes the system response for the baseline ($R_s = 1$). Sample screenings with $R_s > 1$ mean that the output voltage was higher for red light, and correspond to non-aggregated results. Likewise, sample screenings with $R_s \leq 1$ mean that the output voltage was similar or higher for green light, and correspond to aggregated results.

Microchip sensitivity (ΔR_s) was defined as the difference between the detection responses from assays with positive/non-aggregated results (R_s^+) and negative/aggregated results (R_s^-):

$$\Delta R_s = R_s^+ - R_s^-$$

(Equation 4.2)

A one-way ANOVA analysis with Tukey's Multiple Comparison test using Wolfram Mathematica 10.0 (Champaign, IL, USA) was used to validate the results.

Concentration of salt - MgCl$_2$

To achieve faster optical results, kinetic aggregation behavior inside the mixer was studied by mixing 5 nM of Au-nanoprobes and salt solutions with concentrations ranging from 0 to 1 M (1:1). Here, the mixed and final solution was studied for an Au-nanoprobe concentration of 2.5 nM, which is the optimum value for RNA detection recommended in literature.[159,421] It was optically analyzed as soon as the mixing process finished, and 15 minutes thereafter. Data showed that for salt concentrations of 0.1 M, the complete aggregation state of Au-nanoprobes could only be measured after 15 minutes of mixing (Figure 4.4). To cause immediate aggregation, at least 0.2 M of salt were needed. In both cases, 0.2 M of salt is more than enough to stabilize R$_s$.
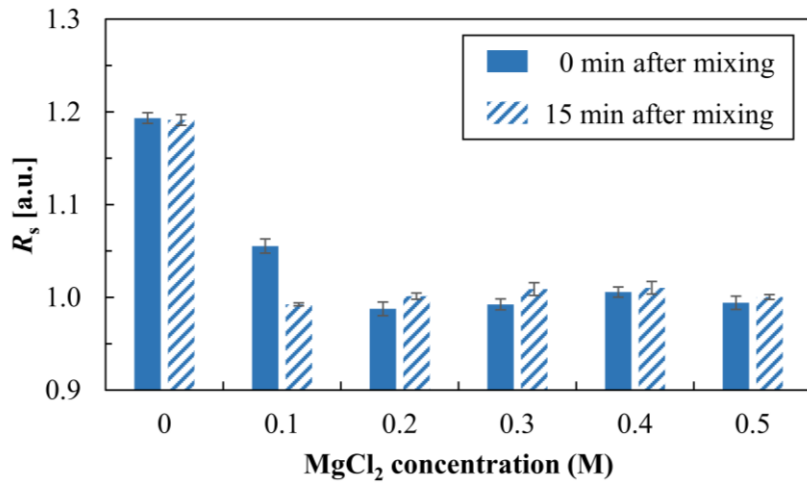
Figure 4.4 Salt saturation study for Au-nanoprobes. Ratio measurements performed immediately after mixing and repeated 15 minutes later.

LED intensity

To calibrate the signal-to-noise ratio (SNR), a cluster of trials with AuNPs with and without the predetermined salt concentration were performed, at various concentration levels (1; 3; 5 nM) and LED intensities (0.4; 0.5; 0.6 A). The device's SNR was calculated for each experimental point:

$$SNB_{dB} = 10 \, log_{10} \frac{(\Delta R_s)}{(\delta \Delta R_s)} \qquad \text{(Equation 4.3)}$$

Where ΔRs and δΔRs are the device's sensitivity and sensitivity error, respectively. Using the Hermite method on Mathematica 10.0, data points were interpolated to find an approximate SNR function within the ranges studied (Figure 4.5). Although higher concentrations present greater sensitivity, the optimum value for RNA detection recommended in literature and previously mentioned

is 2.5 nM.[159,421] This concentration was therefore used to read the highest SNR value on Figure 4.5, namely 0.4 A. Subsequent measurements were made by applying 0.4 A to both LEDs.
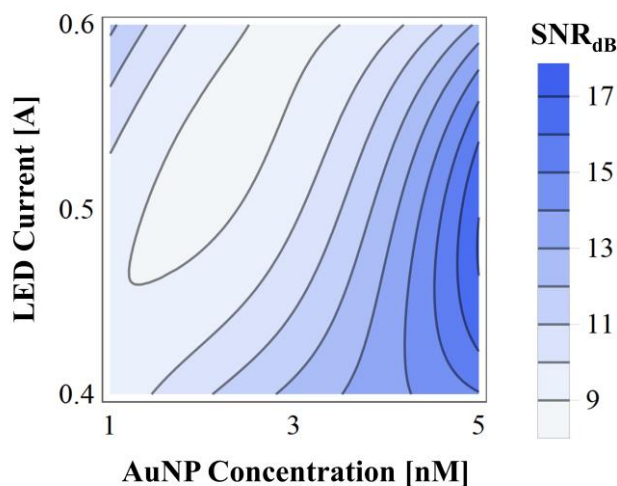
Figure 4.5 Signal-to-noise ratio (SNR) of the device, as a function of light-emitting diode (LED) applied current and gold nanoparticles (AuNPs) concentration of infused solution. Citrate capped AuNPs were used during calibration.

Case studies

The microfluidic chip was used in conjunction with the Au-nanoprobe assay to detect the specific RNA sequence associated with CML in three progressive case studies (Table 4.2). The first case study was performed to verify the colorimetric screening and reproducibility of hybridized Au-nanoprobes with/without salt (proof-of-concept). For the second case study, synthetic oligonucleotide sequences were added to Au-nanoprobes and mixed with salt to evaluate the output screening and reproducibility according to the tested sequence (complementary/noncomplementary sequence of CML). This study was done as an intermediate step towards clinical trials. The only addition to Au-nanoprobes and salt is the synthetic oligonucleotide, either complementary or non-complementary. The complementary oligonucleotide sequences have a perfect match with Au-nanoprobes and thus they represent the best-case scenario of a positive match. To mimic clinical trials, the third case study uses RNA extracted from culture cells (K562, positive for *BCR-ABL1*, or THP1, negative control), instead of synthetic DNA sequences, to evaluate the output screening and reproducibility of results. Due to the complexity of RNA solutions, positive controls extracted from cells tend to have a lower affinity to Au-nanoprobes when compared to complementary synthetic oligonucleotide sequences but constitute a better comparison to the real clinical sample.

A discriminated response between complementary (positive call) and non-complementary (negative call) assays was obtained for all 3 tested cases (Figure 4.6). Performed statistical analysis of variance (ANOVA) with Tukey's comparison test output strongly suggested that positive and negative results belong to different populations ($p < 0.05$), yielding a significant discrimination.

For the first case study, the R_s values obtained showed the least dependency on time. The absence of biological targets and other impurities was a major contributor to this consistency (Figure 4.6). The inclusion of synthetic oligonucleotides and RNA, in the second and third case studies respectively, increased the final solution density and added more variability, increasing the measurement errors. Positive measurements in these studies had R_s decrease over time. The presence of high salt concentration values may have promoted Au-nanoprobe aggregation and precipitation onto the microchannel over time, causing these losses in the ratio. Negative trials showed aggregation occurred sooner than 90 seconds, and thus, all the acquired data in these trials presented a stabilization ratio of $R_s \approx 1.00$. The R_s average values increased for the positive trials of the second and third case studies due to an increase in absorption of green light and decrease in absorption of red light, mainly caused by the non-aggregated Au-nanoprobes and respective targets.

Experimental results showed that SNR decreases both with time and complexity of experiments, i.e. species in solution. The best SNR was attained between 90 and 150 seconds, providing for the strongest outputs in the shortest frames of time (Figure 4.7). Presence of target molecules (synthetic oligonucleotides and/or total RNA) appeared to induce an increase to the detection sensitivity, even though a slight increase to the noise was also perceived.

Table 4.2 Experimental conditions used the microfluidic chip assay. Detailed description on the components used for each case study and respective concentrations.

Case study	1st (without target)		2nd (synthetic oligonucleotides)		3rd (total RNA)	
Inlet	1	2	1	2	1	2
Positive trial	[Au-nanoprobes] 5 nM	H$_2$O	[Au-nanoprobes] 5 nM + [C oligo] 200 nM	[MgCl$_2$] 0.4 M	[Au-nanoprobes] 5 nM + [K562 RNA] 120 ng/µL	[MgCl$_2$] 0.4 M
Negative trial	[Au-nanoprobes] 5 nM	[MgCl$_2$] 0.4 M	[Au-nanoprobes] 5 nM + [NC oligo] 200 nM	[MgCl$_2$] 0.4 M	[Au-nanoprobes] 5 nM + [THP1 RNA] 120 ng/µL	[MgCl$_2$] 0.4 M
After mixing (1:1)	2.5 nM (+ 0.2 M MgCl$_2$)		2.5 nM + 100 nM + 0.2 M		2.5 nM + 60 ng/µL + 0.2 M	

Hybridization of Au-nanoprobes to targets was performed in 10 mM phosphate buffer pH 8, followed by a 5-min denaturation at 95 °C. Samples were then cooled down to room temperature before injection into inlet 1 of the chip. Solutions were infused in each inlet in a 1:1 proportion.

C, complementary target; NC, non-complementary target
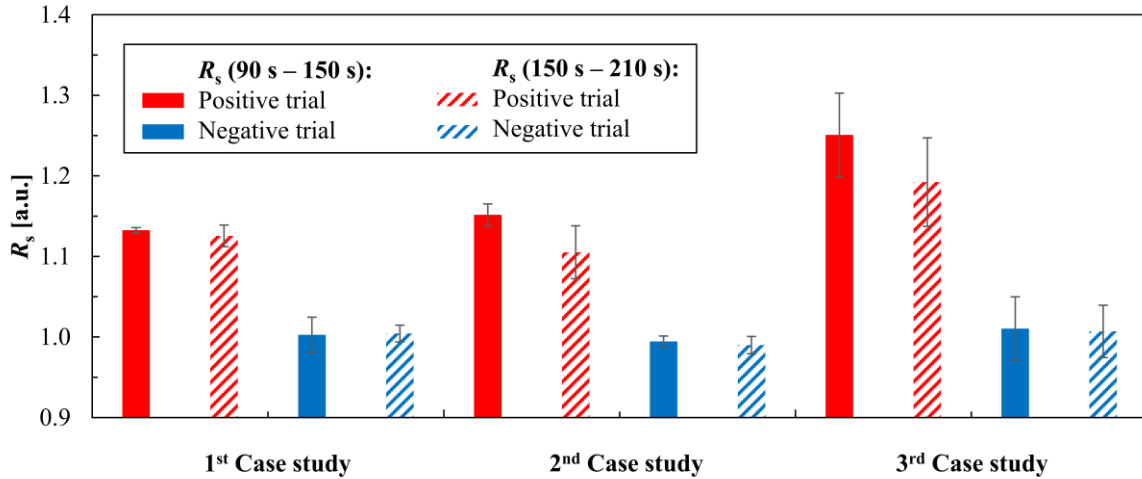
Figure 4.6 Colorimetric results via proposed microfluidic chip for each case study. Measurements were performed in 90-150 seconds (opaque bars) and 150-210 seconds (patterned bars) after filling the detection chamber. Flow was at rest during data acquisition. Bars represent the average R_s of independent measurements ($n \geq 3$) and error bars indicate standard deviations. Statistical analysis was performed with Mathematica 10.0, using one-way ANOVA and Tukey's comparison test ($p < 0.05$).
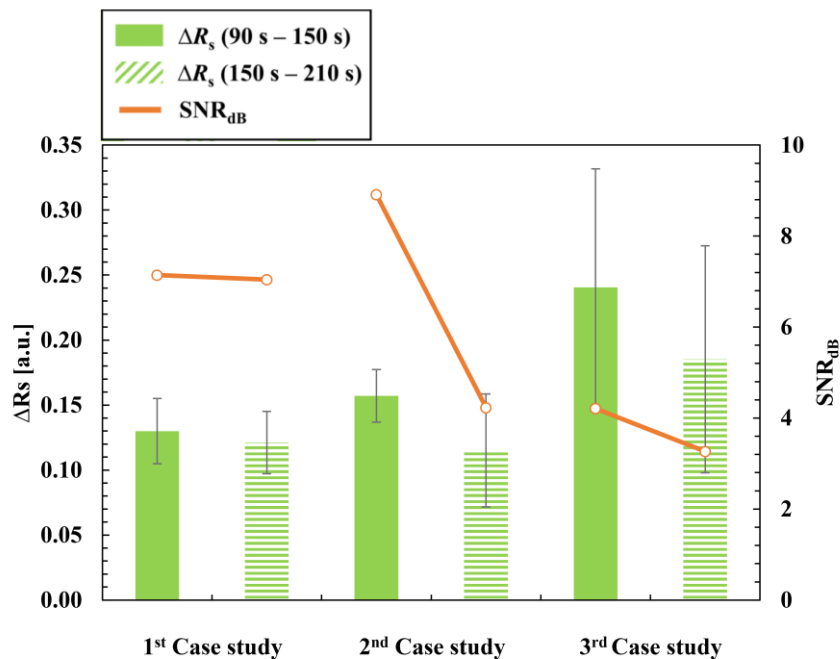
Figure 4.7 Sensitivity between positive and negative colorimetric results, within 90-150 seconds (opaque bars) and 150-210 seconds (patterned bars), and signal-to-noise ratio (SNR) trend over time (orange lines) for each case study. Bars represent the average ΔR_s of independent measurements ($n \geq 3$) and the error bars indicate their standard deviations.

The performance of the Au-nanoprobe assay off-chip was thoroughly studied in chapter 3. Au-nanoprobes could distinguish *BCR-ABL1* variants, without RT-PCR amplification, to a 100 % accuracy and a LOD of 15 ng/µL. The LOD for *BCR-ABL1* detection directly from RNA using the microfluidic setup was found at 40 ng/µL, however standard deviation is lower for 60 ng/µL of RNA (Figure 4.8). Time to data output using the microfluidic device and Au-nanoprobes is at least 10 times faster, when compared to the off-chip Au-nanoprobe assay[421] and 27 times faster when compared to conventional screening techniques for CML (RT-PCR),[38,44] or to the few existent optical screenings with Au-nanoprobes at microscale.[419] The promotion of rapid kinetics of aggregation of Au-nanoprobes is enhanced by the proposed device, which greatly improves qualitative data output.

Upon comparison of LOD values, one could argue there is a loss of sensitivity when using the microfluidic device, however results are conveyed faster using lower volumes in the latter. Though both tests need further optimization/validation, these two methodologies should be considered depending on the goal and resources available: clinics, remote settings or impoverished regions.
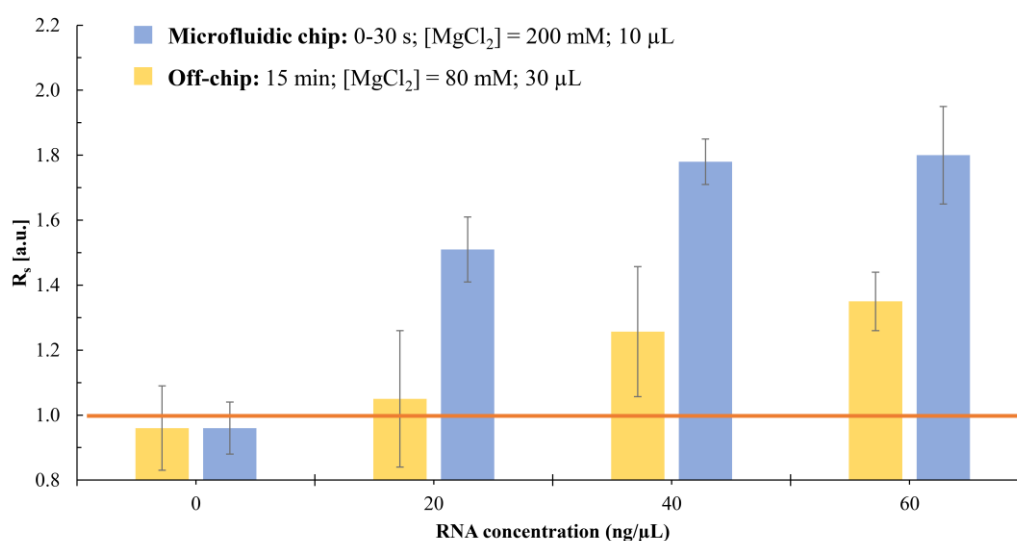
Figure 4.8 Limit of detection of *BCR-ABL1* using the corresponding Au-nanoprobes in the designed optical setup with the microfluidic chip, and same limit of detection for the off-chip version of the Au-nanoprobe assay, using a commercial microplate reader (Tecan Infinite® M200 microplate reader - Männedorf, Switzerland). The on-chip setup consumed 10 µL of total solution in a microfluidic chip, used 0.2 M of $MgCl_2$ and performed the screenings at real time. The off-chip setup consumed 30 µL of total solution in a microtube, used 80 mM of $MgCl_2$ and provided the results 15 minutes after the screening. Bars represent the average R_s of independent measurements (n ≥ 3) and error bars indicate standard deviations.

4.5 Concluding Remarks

A novel multifunctional microchip was developed and used to detect *BCR-ABL1*, the fusion transcript responsible for CML, directly from total RNA extracted from cells, via colorimetric Au-nanoprobe NCL assay. The overall design and assembly was implemented taking into account ease of scale up production and maintaining low cost fabrication. These characteristics make the device suitable for a disposable POC platform with a non-disposable host device integrating the two LED light sources, photodetector and electronic circuit with signal amplification, analogue to digital conversion and PC connectivity. Optimization of the mixing device made possible the detection of target RNA in a small sample volume (10 µL), thus reducing the amount of sample required (3× less than conventional setups).[419]

Volume might be further reduced via addition of a non-miscible buffer (mineral oil) with the sole purpose of pushing the sample solution through the mixing and optical stages, as the colorimetric detection step requires only 50 nL (volume of the filled detection channel).[452,453] The setup itself can also be optimized towards POC by miniaturizing its components, such as designing and incorporating a mechanical pump to the microfluidic chip[454] and shortening its optical path length.

The gold standard for CML detection and follow-up is RT-qPCR, with a cost of €20 per sample. Based on current costs for Au-nanoprobe colorimetric assay, the estimated cost is €0.20-1.00 per assay.[421] A microfluidic chip, integrating all steps for diagnostics, will depend on production setup that would bring costs of standalone chip operation to €10, but offering unique advantages: the microfluidic chip presented good sensitivity and was able to yield accurate results in a remarkably short period of time, due to the fast transition between mixing and detection stages provided by the chip's design, and the process becomes available anywhere due to the possibility of portability. Moreover, the total cost of each assay can be further decreased with mass production of such devices.

Since the colorimetric method for CML screening has been fully validated in mimicked clinical samples, future work shall focus on the integration of this microfluidic platform into a stand-alone device that will open the possibility to more complex, automatized and cost-effective generic DNA/RNA tests suitable for POC screening. In this specific case, it will improve the early diagnosis of CML and provide an easy to use platform for patients' follow-up.

Chapters 3 and 4 focused on the development of a new fast, simple and reliable method for CML diagnostics. As mentioned earlier, AuNPs are excellent tools for biomarker detection due to their size and remarkable optical features. However, these same properties can be applied on a nanotherapeutics approach, namely in specific gene silencing. The Au-nanoprobe-based assay provided valuable insights regarding hybridization, sequence specificity and selectivity, which were paramount for the development of an Au-nanoconstruct that effectively silences *BCR-ABL1*. This strategy is described in detail in the next chapter, aiming for the eradication of CML cells malignant phenotype.

CHAPTER 5 – GENE SILENCING USING GOLD-NANOPROBES: TOWARDS A NANOTHERANOSTICS APPROACH FOR CML

M. Cordeiro, from the Research Unit on Applied Molecular Biosciences (UCIBIO, Universidade Nova de Lisboa), designed, synthesized and characterized the Au-nanobeacon approach described at the end of this chapter. R. Vinhas performed all remaining experiments, data analysis and drafted the following manuscript, at UCIBIO (Universidade Nova de Lisboa), under the supervision of P.V. Baptista and A.R. Fernandes. The author of this thesis opted for reproduction of the resulting scientific paper, thus apologizing for any repeated content in different contexts of the document.

Vinhas R, Fernandes AR, Baptista PV. 2017. Gold nanoparticles for *BCR-ABL1* gene silencing: Improving tyrosine kinase inhibitor efficacy in chronic myeloid leukemia. Molecular Therapy - Nucleic Acids. 7:408-416.

5.1 Abstract

Introduction of TKI for CML treatment is associated with a 63 % probability of maintaining a CCyR, meaning that over 30 % patients require an alternative methodology to overcome resistance, tolerance, or side effects. Considering the potential of nanotechnology in cancer treatment and the benefits of a combined therapy with IM, a nanoconjugate was designed to achieve *BCR-ABL1* gene silencing. AuNPs were functionalized with a ssDNA oligonucleotide that selectively targets the e14a2 *BCR-ABL1* transcript expressed by K562 cells. This gold (Au)-nanoconjugate showed great efficacy in gene silencing that induced a significant increase of K562 cell death. Variation of Bcl-2 and Bax protein expression, an increase of caspase-3/7 activity, and apoptotic bodies in cells treated with the nanoconjugate demonstrate its aptitude for inducing apoptosis on K562 BCR-ABL1-expressing cells. Moreover, the combination of the silencing Au-nanoconjugate with IM prompted a decrease of IM IC$_{50}$. This Au-nanoconjugate was also capable of inducing the loss of viability of IM-resistant K562 cells. This strategy shows that combination of the nanoconstruct and IM make K562 cells more vulnerable to chemotherapy and that the Au-nanoconjugate alone may overcome IM-resistance mechanisms, thus providing an effective treatment for CML patients who exhibit drug tolerance.

5.2 Introduction

CML affects approximately 1.5 million people worldwide and is characterized by the uncontrolled proliferation of myeloid cells in the bone marrow and blood.[455] The disease hallmark results from a genetic abnormality: a reciprocal chromosomal translocation between the long arms of chromosomes 9 and 22, designated as t(9;22)(q34;q11), creating a derivative 9q+ and a shortened 22q-, the Ph chromosome. Due to different possible breakpoints on chromosome 22 and alternative splicing events, several transcripts can originate from this translocation.[17,34] However, the e14a2 and e13a2 are present in most CML patients, with the e14a2 transcript representing 55 % of Ph+ cases.[17,34] CML was the first malignancy in which a unique chromosomal abnormality was identified in approximately 95 % of cases.[23,455] All *BCR-ABL1* gene fusions described thus far encode for a constitutively active tyrosine kinase that plays a central role on leukemogenesis, since it disturbs downstream signaling pathways, causing enhanced proliferation, differentiation arrest, and resistance to cell death.[24] Hence, targeted TKIs are the standard treatment for CML, which works best on early stages of the disease, with IM being the first-line treatment. Based on the Sokal risk score at the time of diagnosis, patient age, drug cost, comorbidities, drug toxicity, and gene mutation profile, other TKIs can be administered: dasatinib, nilotinib, bosutinib, or ponatinib.[17] Although more effective than IM, these TKIs are associated with different safety profiles, and their impact on long-term overall survival remains undetermined.[456] Despite the efficacy of TKI treatment, early relapse and TKI resistance, which have been associated with BCR/ABL1-dependent or -independent mechanisms, are still major concerns.[106, 141,457]

Antisense DNA therapy is a powerful instrument for regulating the expression of genes associated with disease, with the potential to be used as an adjuvant to conventional chemotherapy.[458,459] ssDNA oligonucleotides may be delivered into cells and target specific mRNA molecules, inhibiting expression of the encoded protein.[460] AuNPs protect the antisense oligonucleotide against degradation by RNases, thus increasing circulation half-life and, therefore, the payload of therapeutic agent that is delivered to cells. The potential of AuNPs to vectorize actuators for gene silencing via simple assembly onto the NP core has been demonstrated *in vitro* and *in vivo* for a range of different nucleic acid moieties, including small interfering RNA (siRNA)[304,461–464] and antisense ssDNA.[241, 305, 307,465,466] The latter has been proven to be very specific, particularly when using stem-looped oligonucleotides, making it suitable for the real-time monitoring of gene silencing via Au-nanobeacons.[241, 305,307]

In this study, we silenced the *BCR-ABL1* chimeric gene *in vitro*, using AuNPs functionalized with an antisense oligonucleotide (Figure 5.1). The effects of the construct on BCR-ABL1 signaling pathways were further assessed through the evaluation of the changes in the expression levels of key players of cell proliferation and apoptosis/survival. Besides gene silencing evaluation, a combined therapy assay was performed to understand the role of the Au-nanoconjugate as an adjuvant to the conventional treatment for CML (IM), even in K562 cells resistant to the drug. The effect of this Au-nanoconjugate may be crucial in overcoming toxicity and resistance mechanisms related to TKI administration.
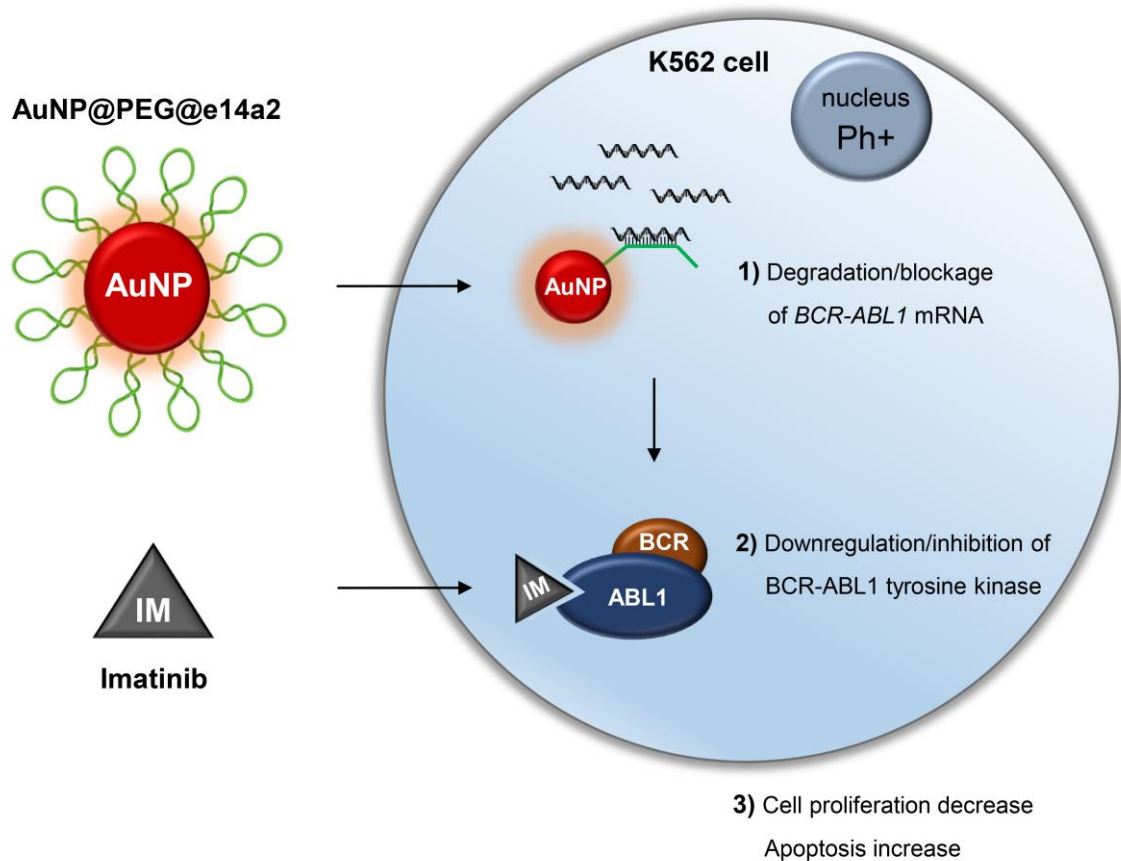
Figure 5.1 *In vitro BCR-ABL1* gene silencing via gold nanoconjugates. Gold nanoparticles (AuNPs) functionalized with a ssDNA oligonucleotide (AuNP@PEG@e14a2) selectively target the e14a2 *BCR-ABL1* transcript expressed by K562 cells. Moreover, the silencing Au-nanoconjugate improves imatinib (IM) effect on cell proliferation and apoptosis.

5.3 Material and Methods

Au-nanoconjugate synthesis and characterization

AuNPs of 14 nm were synthesized by the citrate reduction method.[172] AuNPs were first functionalized with PEG modified with a 5'-thiol group ($C_{15}H_{32}O_7S$, 356.48 Da) (AuNP@PEG), corresponding to 30 % saturation of AuNPs' surface. AuNP@PEGs were subsequently functionalized with the thiolated oligonucleotide: 5'-<u>TTTCGG</u>CGCTGAAGGGCTTTTGAACT<u>CCGAAA</u>-3' (palindromic sequence underlined; sequence targeting the fusion e14a2 *BCR-ABL1* transcript was derived from GenBank: AJ131466.1) (AuNP@PEG@e14a2 - Au-nanoconjugate).[421] A palindromic sequence was added to allow the stem-loop structure. The final ssDNA sequence was designed and analyzed using the Nucleic Acid Package (NUPACK) software.[467,468] Au-nanoconjugates were prepared at a 1:100 (AuNP:oligonucleotide) ratio and centrifuged for 40 min at 14 000 x g, and the precipitate was washed three times with diethylpyrocarbonate-treated water. The number of oligonucleotides

bonded to the AuNP surface was determined using Quant-iT OliGreen ssDNA Reagent (ThermoFisher, Waltham, MA, USA). The resulting Au-nanoconjugates were stored at 4 °C in the dark and characterized by UV-Vis spectroscopy, TEM, and DLS.

A control scrambled oligonucleotide 5'-<u>TTTCGG</u>GTTGACGTTAGCCGGATCTA<u>CCGAAA</u>-3' was also prepared and characterized under the same conditions: AuNP@PEG@scramble.

To target *c-MYC,* AuNPs were also functionalized with 30 % PEG and the following thiolated ssDNA oligonucleotide: 5'<u>GCGCCC</u>ATTTCTTCCAGATATCCTCGCT<u>GGGCGC</u> (palindromic sequence underlined; sequence targeting *c-MYC* mRNA was derived from GenBank NM_002467.5). All protocols used for AuNP@PEG@e14a2 were strictly followed for AuNP@PEG@MYC.

Cell culture and Au-nanoconjugate challenge

The immortalized cell line K562 (cell line positive for *BCR-ABL1* e14a2 fusion transcript) derived from a CML patient in blast crisis was cultured in DMEM supplemented with 10 % FBS at 37°C with 5 % CO_2 and 99 % relative humidity.

For these *in vitro* assays, cells were seeded at a density of 1 x 10^5 cells per well (24-well plates) or 5 x 10^3 cells per well (96-well plates) and challenged with 0.6 nM AuNP@PEG@e14a2, corresponding to 30 nM oligonucleotide (Au:oligonucleotide ratio = 1:50). As control, cells were exposed to 0.6 nM AuNP@PEG (control vehicle); to 0.7 nM AuNP@PEG@scramble (corresponding to 30 nM oligonucleotide; Au:oligonucleotide ratio = 1:44); or to 0.1 µM IM, and 0.01 % DMSO as control for IM. For experiments targeting *c-MYC*, cells were challenged with 0.6 nM AuNP@PEG@MYC (corresponding to 45 nM oligonucleotide; Au:oligonucleotide ratio = 1:75).

Sequence specificity was also tested using two different cell lines: an acute monocytic leukemia cell line negative for *BCR-ABL1* (THP1) and a CML cell line positive for the *BCR-ABL1* e13a2 transcript (BV173), cultured as described earlier. Incubation of cells with nanoconjugates or IM was performed at a density of 2.5 x 10^4 cells per well (96-well plate).

IM-resistant K562 cells were generated via incubation of K562-sensitive cells with increasing concentrations of IM (starting with a concentration of 0.01 µM up to 1 µM) for more the 50 passages (K562-IM). *BCR-ABL1* gene expression on K562-IM cells was evaluated via qPCR as described in the following section (*Gene expression analysis*). Data were analyzed by the comparative threshold cycle (Ct) method ($2^{-\Delta\Delta Ct}$),[469] where relative gene expression is given by quantification of *BCR-ABL1* relative to the internal control gene (*18S*), normalized to the control condition (parental K562 cells):

$$\Delta Ct = Ct_{BCR-ABL1} - Ct_{18S} \qquad \text{(Equation 5.1)}$$

$$\Delta\Delta Ct = \Delta Ct_{K562-IM} - \Delta Ct_{K562} \qquad \text{(Equation 5.2)}$$

To assess *BCR-ABL1* mutational status on K562-IM cells, a nested-PCR amplification was performed as described in chapter 2, under the *BCR-ABL1 molecular analysis – Mutational screening* section, using primers for the P210[BCR-ABL1] variant, depicted in Table 2.2. PCR products were sequenced at STABVIDA (Caparica, Portugal).

Gene expression analysis

Cells exposed to the different conditions (AuNP@PEG and Au-nanoconjugates) in 24-well plates were collected at different time points between 3 and 72 hr. Cells were centrifuged at 200 x g for 5 min at room temperature, and total RNA was extracted from cell pellets using TRIsure (Bioline, Taunton, MA, USA) according to the manufacturer's instructions. Total RNA (100 ng) was reverse transcribed using the NZY M-MuLV First-Strand cDNA Synthesis kit (NZYTech, Lisbon, Portugal).

qPCR amplification of cDNA was performed on a Corbett Rotor-Gene 6000 thermal cycler (Qiagen, Hilden, Germany) using the HOT FIREpol EvaGreen qPCR Mix which includes HOT FIREPol DNA polymerase and corresponding buffer, 2.5 mM $MgCl_2$, dNTPs and EvaGreen® dye (Solis BioDyne, Tartu, Estonia). The reaction mixture was prepared in a final volume of 20 µL with 1 µL of cDNA and the following primers, at a concentration of 100 nM each: *BCR* forward (5'-GAAGTGTTTCAGAAGCTTCTCC) and *ABL1* reverse (5'-GTTTGGGCTTCACACCATTCC); *c-MYC* forward (5'-GCTCATTTCTGAAGAGGACTTGT) and *c-MYC* reverse (5'-AGGCAGTTTACATTATGGCTAAATC); *BCL2* forward (5'-CTTCGCCGAGATGTCCAGCCA) and *BCL2* reverse (5'-CGCTCTCCACACACATGACCC); *18S* forward (5'-GTAACCCGTTGAACCCCATT) and *18S* reverse (5'-CCATCCAATCGGTAGTAGCG). qPCR conditions included an initial denaturation at 95 °C for 15 min and 40 cycles of 95 °C for 20 s, 55 °C (*BCR-ABL1, c-MYC* and *18S*) or 65 °C (*BCL-2*) for 20 s, and 72 °C for 30 s. qPCR data were analyzed by the Ct method ($2^{-\Delta\Delta Ct}$),[469] where relative gene expression is given by quantification of the gene of interest (*BCR-ABL1*, *c-MYC* or *BCL-2*) relative to internal control gene (*18S*), normalized to the control condition (cells exposed to AuNP@PEG):

$$\Delta Ct = Ct_{BCR-ABL1 \text{ or } c\text{-}MYC \text{ or } BCL\text{-}2} - Ct_{18S} \qquad \text{(Equation 5.3)}$$

$$\Delta\Delta Ct = \Delta Ct_{Au\text{-}nanoconjugate} - \Delta Ct_{AuNP@PEG} \qquad \text{(Equation 5.4)}$$

Flow cytometry

Cells were exposed to AuNP@PEG@e14a2 in 24-well plates, recovered by centrifugation at 400 x g for 5 min at 4 °C, and washed with cold PBS. Cells were resuspended in PBS and analyzed by measuring side scatter peak area (SSC-A) of 10 000 events per reading in an Attune Acoustic Focusing Cytometer (ThermoFisher, Waltham, MA, USA).

Cell proliferation assays

K562 cells were plated in 24-well plates, and growth rate was determined by counting the number of viable cells after challenge with AuNP@PEG or AuNP@PEG@e14a2 nanoconjugates using the trypan blue (0.2 %) exclusion assay (ThermoFisher, Waltham, MA, USA), where viable cells possess intact cell membranes that exclude the dye, whereas dead cells do not and appear blue.[470] Cell-doubling time was calculated as:

$$Doubling\ time = \frac{time \times log\ 2}{log\ (final\ conc.) - log\ (initial\ conc.)} \qquad \text{(Equation 5.5)}$$

Additionally, K562, THP1, and BV173 cells exposed to IM, AuNP@PEG and Au-nanoconjugates were assessed in 96-well plates using the CellTiter 96 AQueous Non-Radioactive Cell Proliferation Assay (MTS, Promega, Madison, WI, USA).[471] Absorbance at 490 nm was measured in a Tecan Infinite M200 microplate reader (Männedorf, Switzerland), and values were corrected to the respective control conditions (without cells). The IC_{50} for IM at 48 h was also determined via MTS assay by exposing K562 cells to growing IM concentrations ranging from 0.01 to 10 µM.

Apoptosis assay

K562 cells cultured in a 24-well plate were fixed with 4 % (w/v) paraformaldehyde, washed with PBS, and stained using 10 µg/mL Hoechst 33258 (ThermoFisher, Waltham, MA, USA).[472,473] At least six images per condition were collected using an AxioImager D2 fluorescence microscope (Zeiss, Oberkochen, Germany) with a 40x objective or a 100x immersion objective, a 365-nm excitation filter, and a 445/50-nm emission filter.

Western blot

Cells were washed with PBS and resuspended in lysis buffer [150 mM NaCl, 50 mM Tris (pH 8.0), 5 mM EDTA, 2 % (v/v) NP-40, 1x phosphatase inhibitor (PhosStop, Roche, Basel, Switzerland), 1x protease inhibitor (cOmplete Mini, Roche), 1 mM PMSF, and 0.1 % (w/v) DTT]. Whole-cell extracts were sonicated and centrifuged at 5000 x g for 10 min. The supernatant was recovered, and protein concentration was determined using the Pierce 660nm Protein Assay Reagent (ThermoFisher, Waltham, MA, USA) per manufacturer's specifications. Then, 25 mg total protein extracts were separated by SDS-PAGE in a 10 % (37.5:1) acrylamide-bisacrylamide gel (Merck Millipore, Billerica, MA USA). Following electrophoretic transfer onto a 0.45-mm nitrocellulose membrane (GE Healthcare, Little Chalfont, UK) and blocking with 5 % (w/v) milk solution in tris-buffered saline with 0.1 % (v/v) tween 20 (TBST), blots were incubated per manufacturer's instructions for 1 h at room temperature with primary antibodies against Bcl-2 (reference no. B3170, Sigma-Aldrich, St. Louis, MI, USA), Bax (reference no. 32503, Abcam, Cambridge, UK), and ß-actin (reference no. A5441, Sigma-Aldrich).

Membranes were washed with TBST and incubated with the appropriate secondary antibody conjugated with horseradish peroxidase (reference no. 7074 or 7076, Cell Signaling Technology, Danvers, MA, USA). WesternBright ECL (Advansta, Menlo Park, CA, USA) was applied to the membranes, and signal was acquired in a Gel Doc imager (Bio-Rad, Hercules, CA, USA).

Caspase-3/7 activity

Caspase-3/7 activity was assessed using the Caspase-3 Apoptosis Detection Kit from Santa Cruz Biotechnology (Dallas, TX, USA), as described by Luis *et al*.[474] Briefly, 50 mL cell lysates were diluted in 200 mL reaction buffer containing 10 mM DTT and 5 mL fluorometric substrate DEVD-AFC (7-amino-4-trifluoromethyl coumarin) and incubated at 37 °C for 1 h. Caspase-3/7 activity was quantified by fluorescent detection of free AFC after cleavage from DEVD peptide. The free AFC level was measured using a Varian Cary Eclipse Fluorescence Spectrophotometer (Agilent Technologies, Santa Clara, CA, USA) with a 400-nm excitation filter and a 505-nm emission filter.

Au-nanobeacon in vitro challenge and imaging

In vitro imaging of *BCR-ABL1* silencing was performed using a Au-nanobeacon combined with Förster resonance energy transfer (FRET) based spectral codification, in a strategy designed by Cordeiro *et al*, 2016.[122] Briefly, 14nm-AuNPs were first functionalized with thiolated PEG corresponding to 45 % saturation of AuNPs' surface, and subsequently with the thiolated nanobeacon. The nanobeacon hairpin was optimized to specifically detect the *BCR-ABL1* fusion region of the e14a2 isoform sequence: 5'-<u>CACCTCGAAA</u>TCTGAAGGGCTTTTGAACTCTGT<u>TTTCGAGGTG</u> (palindrome sequence underlined; sequence targeting the fusion e14a2 *BCR-ABL1* transcript was derived from GenBank: AJ131466.1). The 3' end of this sequence was coupled to sulfoindocyanine Cy3 (donor fluorophore). The sequence complementary to the palindrome sequence of the nanobeacon's hairpin (5'-CACCTCGAAA) was coupled to Dy-520XL (acceptor fluorophore).

Cells were cultured in phenol-free medium (DMEM or RPMI, depending on the cell line) on 24-well plates (1 x 10^5 cells per well) and challenged with 0.5 nM Au-nanobeacon (corresponding to 30 nM oligonucleotide; Au:oligonucleotide ratio = 1:64) and/or 25 nM acceptor (1 Au : 50 acceptor). After the stimulus, cells were transferred onto a microtube, centrifuged at 300 x g for 5 min, washed with PBS, and immediately examined by fluorescence microscopy. At least six images per condition, were collected using AxioImager D2 fluorescence microscope (Zeiss, Oberkochen, Germany) with a 40x-objective and a filter with excitation at 540-552 nm, emission at 590-4095 nm and splitter at 580 nm, with the same exposure settings. Fluorescence intensity quantification per cell, per condition, was performed after background correction, using Image J software (National Institutes of Health, Rockville, MD, USA).

All data are expressed as mean ± standard error from at least three independent experiments. Statistical significance was evaluated through one-way ANOVA followed by Tukey's multiple comparison test. Mean differences between groups were determined with a 95 % confidence interval. Statistical significance of data from Table 5.2, Figures 5.7 and 5.10, was evaluated through two-way ANOVA followed by Bonferroni's test.

5.4 Results and Discussion

Standard chemotherapy may be combined with gene silencing approaches to assist cancer cell death. For instance, ssDNA silencing oligonucleotides can recognize a specific gene product to shut down the production of a protein associated to disease, by activating RNase H that cleaves DNA/RNA hybrids; via steric blockage of translation; or by modulating alternative splicing.[460] This way, those cells harboring the selected gene marker will be selectively targeted for enhanced destruction, allowing for improvement of efficacy. In CML, the molecular hallmark of disease - *BCR-ABL1* fusion transcript - may be used to selectively target malignant cells in combination with a particular TKI, thus potentiating cell death. Gene silencing has profited from nanovectorization strategies that extend circulation half-life of therapeutic nucleic acids while improving cell uptake.[301,475] Here, we used AuNPs to deliver a specific oligonucleotide targeting the *BCR-ABL1* mRNA sequence in CML cells, where the silencing moiety was in a stem-loop configuration to improve selectivity and specificity toward target sequence.[307,476] AuNPs with 14 nm in diameter were synthesized and further functionalized with polyethylene glycol (AuNP@PEG) and with a ssDNA targeting the *BCR-ABL1* mRNA sequence (50 oligonucleotide density per NP).
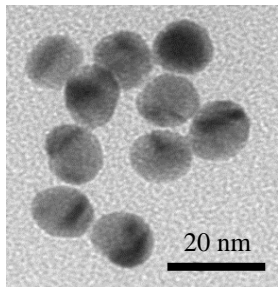
PEG functionalization is crucial to: i) increase nanoconjugate solubility both *in vivo* and *in vitro,* ii) reduce their uptake by the reticuloendothelial system, thus increasing AuNPs circulation time, and iii) decrease serum and tissue protein association.[477]

The ssDNA sequence targeting *BCR-ABL1* was designed based on several factors. The core sequence, targeting the fusion region of the e14a2 transcript, matches the one used to detect the same transcript on *ex vivo* RNA samples via the Au-nanoprobe assay (described in chapters 3 and 4). All the information concerning sequence specificity and selectivity on the previous stages of the work was paramount to potentiate the effect of the designed nanoformulation on *BCR-ABL1* gene silencing. Moreover, a palindromic sequence was added to both ends of the ssDNA oligonucleotide to induce the hairpin conformation and increase its selectivity, by ensuring that the hairpin will only open in the presence of a fully complementary target. *In silico* experiments, using NUPACK software which is ideal for the thermodynamic analysis of dilute solutions of interacting nucleic acid strands,[468] allowed to infer the best palindrome sequence for this purpose. This precise sequence was chosen to promote the formation of a perfect stem-loop structure by avoiding complementarity of the palindrome to the

BCR-ABL1 targeting sequence (internal hybridization) and evade the hybridization of the overall sequence to *BCR* or *ABL1* transcripts. Gibbs free energy variation, ΔG, also indicates that this secondary structure will likely open in the presence of a complementary target ($\Delta G_{\text{open/hybridized oligonucleotide}}$ = -45.4 kcal/mol) as opposed to a non-complementary target ($\Delta G_{\text{closed hairpin oligonucleotide}}$ = -2.9 kcal/mol).

The resulting nanoconjugates were characterized by UV-Vis spectroscopy, TEM and DLS (Table 5.1). Data related to Z-average and SPR peak shift show an increase of NPs size upon PEG functionalization and, even more, after oligonucleotide (e14a2 or scramble) loading. Although the polydispersity index (PI) slightly increases subsequently to replacement of the citrate capping (AuNPs) for thiolated ligands (PEG or oligonucleotides), all measured PI values are indicative of a monodisperse population.[478] Z-potential measures the magnitude of the electrostatic or charge repulsion/attraction between particles, which affects their stability and dispersion/aggregation status. PEG binding to the surface of AuNPs is known to induce a shift from negative to more neutral Z-potential values, as demonstrated in table 5.1. On the contrary, since ssDNA molecules have negative charge, functionalization with oligonucleotides induced a shift from -41 mV (AuNPs@PEG) to -103 mV (AuNP@PEG@scramble) or -93 mV (AuNP@PEG@e14a2).

Table 5.1 AuNPs, AuNP@PEG and AuNP@PEG@e14a2 characterization through Transmission Electron Microscopy (TEM), Dynamic Light Scattering (DLS) and ultraviolet-visible (UV-Vis) spectroscopy.

	Au-core average diameter (TEM image)	Z-average (nm)	PI	Z-potential (mV)	SPR peak (nm)
AuNPs	14 nm	17	0.211	-74	519
AuNP@PEG		27	0.380	-41	520
AuNP@PEG@scramble		54	0.346	-103	522
AuNP@PEG@e14a2	20 nm	51	0.312	-93	524-525

PI, polydispersity index; SPR, surface plasmon resonance

BCR-ABL1 gene silencing and cell fate

Real-time qPCR analysis of *BCR-ABL1* gene expression shows that, after 12 h of exposure of K562 cells to 0.6 nM AuNP@PEG@e14a2, expression of the fusion transcript decreases till it reaches a minimum at 24 h (Figure 5.2). After 72 h, *BCR-ABL1* expression is completely restored, possibly due to oligonucleotide degradation and/or cell expansion over time, which increases the number of cells per NP applied in cell medium, but in line with what has been previously observed for other targets.[301,479] Together, these data show efficient gene silencing by the designed nanoconjugates.

Once effective gene silencing of *BCR-ABL1* was achieved, we investigated downstream control points for apoptosis/survival. A comparable transient effect was observed for *BCL-2*, a downstream target gene of *BCR-ABL1*, which followed a similar reduction profile (Figure 5.2). This result further corroborates the overall cell effect of silencing *BCR-ABL1*, since Bcl-2 expression levels are strongly regulated by BCR-ABL1 in cancer cells. In fact, in the signaling pathway that ultimately culminates in increased survival and unregulated proliferation of Ph+ cells, BCR-ABL1 prevents apoptosis by inducing Bcl-2 through a cascade of responses involving constitutive *RAS* activation and *BCL-2* gene regulation.[480]
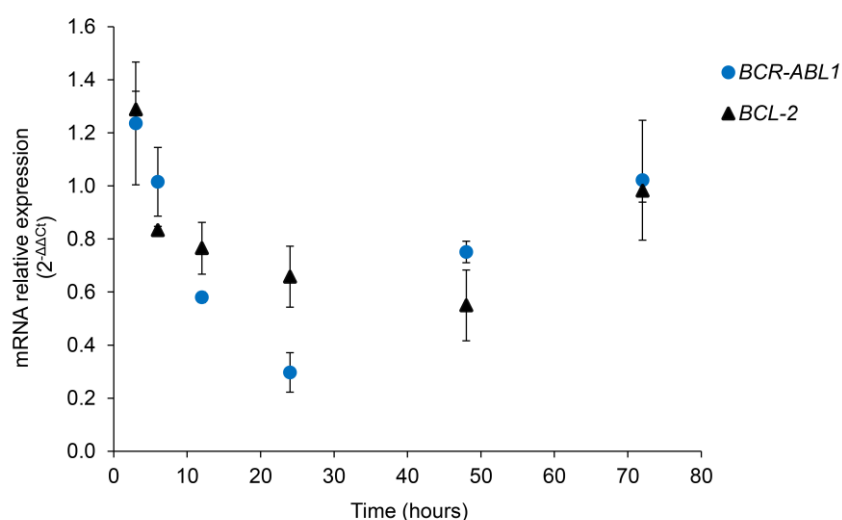
Figure 5.2 Au-nanoconjugate AuNP@PEG@e14a2 effectively silence *BCR-ABL1*. *BCR-ABL1* (blue full circle) and *BCL-2* (black full triangle) mRNA relative expression after treatment of K562 cells with AuNP@PEG and AuNP@PEG@e14a2. Data were normalized to the *18S* gene and then to cells exposed to AuNP@PEG. Ct, threshold cycle. Error bars represent the standard error of the mean of at least three independent experiments.

Flow cytometry data also corroborate these trends for K562 cells treated with AuNP@PEG@e14a2 (Figure 5.3). Measurement of side scatter intensity (SSC) in flow cytometry is an efficient way to study cell interaction with AuNPs associated with their strong scattering.[481] SSC values increased for cells treated with the Au-nanoconjugate, peaking at 24 h (Figure 5.3).
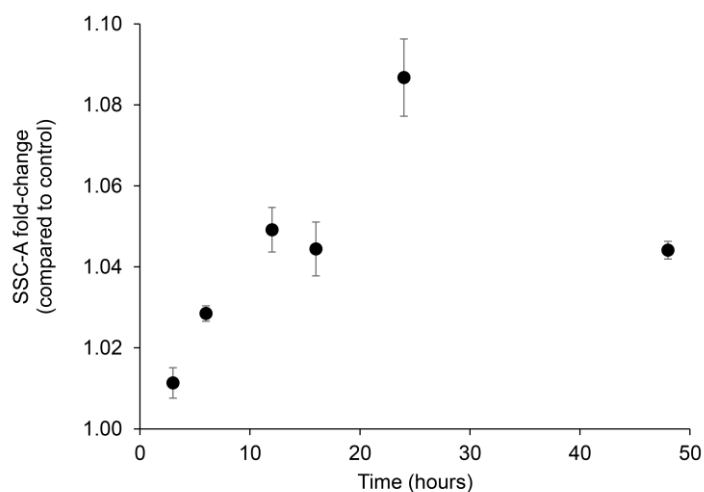
Figure 5.3 Side scattering analysis of K562 cells after exposure to AuNP@PEG@e14a2. Side scattering peak area (SSC-A) was measured via flow cytometry and raw values were normalized against control condition (cells without treatment). Error bars represent the standard error of the mean of three independent experiments.

In CML, BCR-ABL1 induces the deregulation of cell proliferation with the inhibition of apoptosis and an increased survival rate. Exposure of K562 cells to the Au-nanoconjugate significantly delayed cell growth, particularly for the 24-48 h period (Figure 5.4A). In that period, cell-doubling time was *circa* 116 h, which is much slower than control (PBS) or control vehicle (AuNP@PEG): 17 h and 20 h, respectively. These data are in accordance with gene expression studies discussed earlier, where the window of silencing effectiveness was between 24 h and 48 h. Cell-viability studies by the MTS assay also show a decrease of cell viability of 25 % at 48 h (Figure 5.4B). The short-term effect induced by the construct might be associated with the increase in cell numbers after 48 h, skewing the most efficient cell:Au-nanoconjugate ratio. The Au-nanoconjugate functionalized with a scrambled oligonucleotide showed no effect on cell viability. As such, the previously observed reduction in cell viability (25 %; Figure 5.4B) was due to the oligonucleotide effect by targeting the fusion e14a2 *BCR-ABL1* transcript.

The Au-nanoconjugate specificity toward cells expressing the e14a2 *BCR-ABL1* transcript was confirmed by assessing cell viability on THP1 (*BCR-ABL1*-negative cell line derived from an acute monocytic leukemia patient) and BV173 (CML cell line derived from an e13a2-positive patient). The silencing nanoconjugate, specific for the e14a2 *BCR-ABL1* isoform, solely promoted cell-viability reduction on K562 cells, indicating that the construct is highly specific, since the e14a2 and e13a2 transcripts share the *ABL1* part of the sequence (Figure 5.4C). This high-sequence specificity had been previously demonstrated for *in vitro* CML diagnostics in clinical samples using AuNPs.[421] Because the sequence only targets the isoform of interest, it acts as a molecular marker for targeted therapy. As expected, IM had no effect on THP1 but decreased cell viability on BV173 and K562, since it was designed to bind specifically to the active site of BCR-ABL1 proteins.[89]
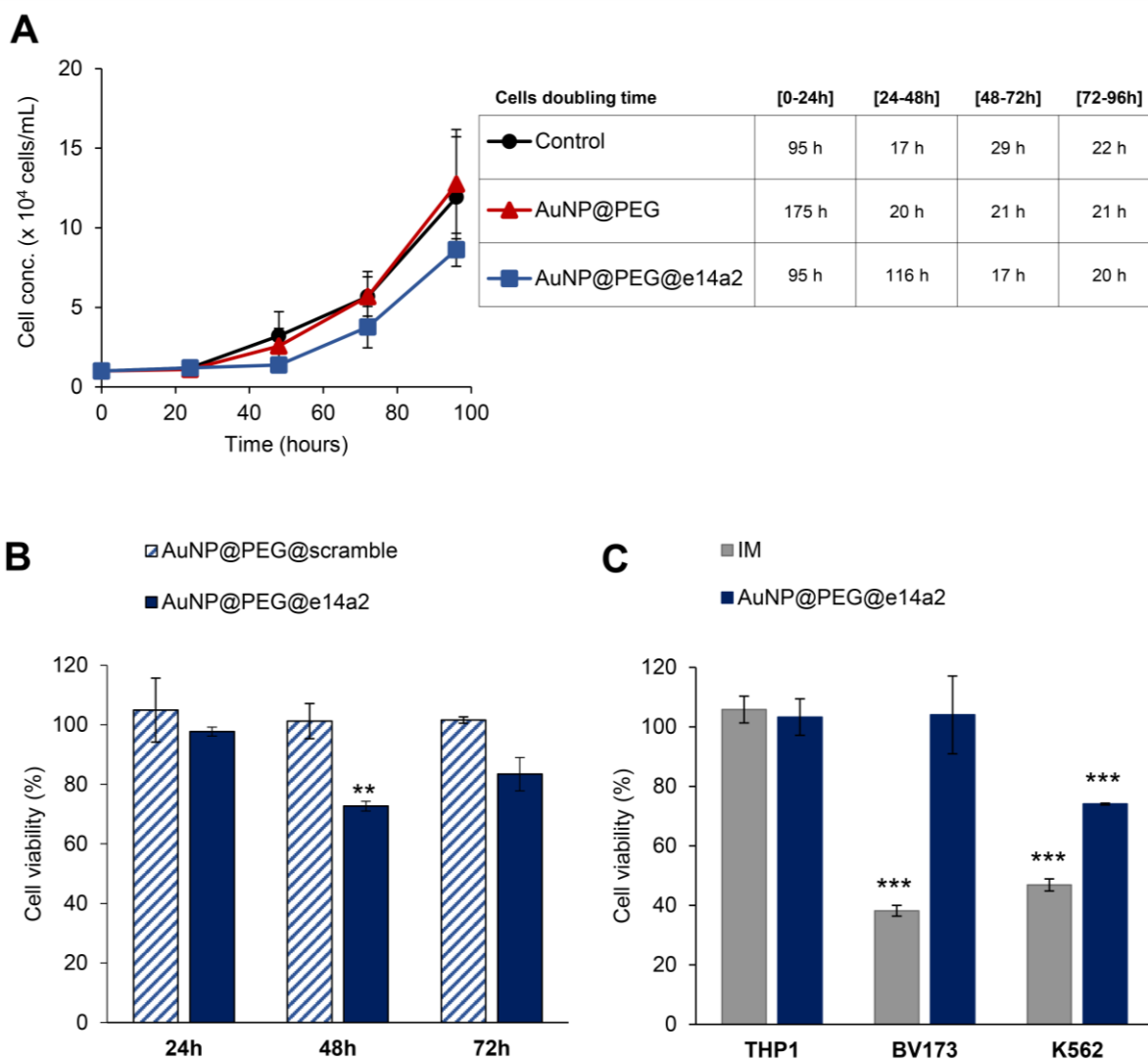
Figure 5.4 Cell proliferation assays upon exposure to AuNP@PEG@e14a2. **A)** Cell viability count via trypan blue exclusion assay on untreated K562 cells (black circles), cells exposed to AuNP@PEG (red triangles), and silencing nanoconjugate (blue squares). Cells' doubling time was also calculated (embedded table). conc., concentration. **B)** Cell viability over time on K562 cells challenged with AuNP@PEG@e14a2 (silencing nanoconjugate) and AuNP@PEG@scramble. **C)** Sequence specificity of AuNP@PEG@e14a2 toward *BCR-ABL1* measured by impact on cell viability on THP1, BV173, and K562 cells; cells were also challenged with 0.1 µM imatinib (IM), which is specific for BCR-ABL1. Data on plots (B) and (C) were normalized to AuNP@PEG. **p < 0.01; ***p < 0.001, Tukey's test statistical significance versus first column.

The IM mechanism of action involves blocking the active site of BCR-ABL1 tyrosine kinase, that subsequently induces cancer cell death via apoptosis.[482,483] We investigated the triggering of apoptotic pathways by cells challenged with our silencing nanoconjugate, AuNP@PEG@e14a2. Cells nuclei undergo several morphological changes even at early apoptosis, including chromatin condensation, nuclear fragmentation, and the presence of apoptotic bodies, which can be visualized using a fluorescent DNA dye (Hoechst) (Figure 5.5).[484] The silencing nanoconjugates were shown to induce an increase on the number of apoptotic cells at 48 h, when compared to normal cells, cells exposed to AuNP@PEG@scramble, or cells exposed to AuNP@PEG, which does not induce apoptosis (Appendix V – Figure V.1).
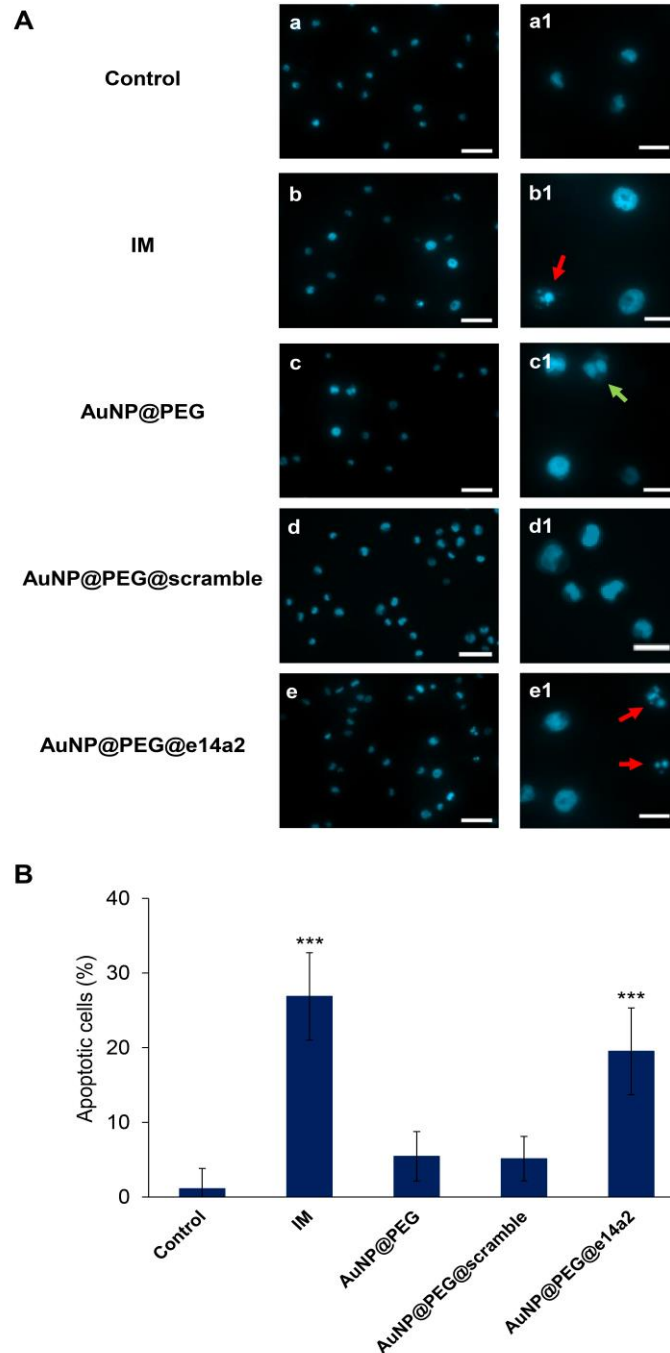
Figure 5.5 Silencing nanoconjugate AuNP@PEG@e14a2 induces apoptosis. **A)** Hoechst staining on non-treated (control) cells (a and a1) or cells treated for 48 h with 0.1 µM IM (b and b1), 0.6 nM AuNP@PEG (c and c1), 0.7 nM AuNP@PEG@scramble (d and d1), or 0.6 nM AuNP@PEG@e14a2 (corresponding to 30 nM of oligonucleotide) (e and e1). Representative fluorescence microscopy images are shown in (a)–(e); scale bars, 50 µm. Zoomed images for each condition are shown at right, in (a1)–(e1), for better visualization between apoptotic (red arrows) or mitotic (green arrow) cell morphology; scale bars, 20 µm. **B)** Apoptotic events count based on nucleus morphology and formation of apoptotic bodies after Hoechst staining. ***p < 0.001, Tukey's test statistical significance when compared to control and AuNP@PEG.

The anti-apoptotic protein Bcl-2 and pro-apoptotic protein Bax are important regulators in the mitochondrial apoptotic pathway, particularly in BCR-ABL1-expressing cells. Inhibition of apoptosis is thought to result from activation of the phosphoinositide 3-kinase and Ras pathways, with induction through Akt of c-Myc and Bcl-2, and variation of their expression levels is of great importance for regulating apoptosis.[485] Many chemotherapeutic agents, including TKIs, trigger apoptotic cell death by activating caspases. Upon an apoptotic stimulus, initiator caspases (e.g., caspase-8 and caspase-9) cleave and activate executioner caspases (e.g., caspase-3), inducing proteolytic cleavage of specific apoptotic substrates that culminate in cell death.[486] To further confirm the downstream events triggered by direct silencing of BCR-ABL1 that ultimately induce apoptosis, we evaluated the actual expression of these two canonical apoptotic pathways: the Bcl-2/Bax and caspase activation (Figure 5.6).

The observed pro-apoptotic effect of our silencing nanoconjugate corroborated data attained from the gene silencing experiments (Figure 5.2), where *BCL-2* gene expression was downregulated. Silencing of *BCR-ABL1* using AuNP@PEG@e14a2 not only downregulated Bcl-2 but also upregulated Bax expression, shifting K562 cells from the anti-apoptotic setting characteristic of BCR-ABL1-expressing cells to pro-apoptotic (Figures 5.6A and 5.6B). A 2-fold change on the Bax/Bcl-2 ratio was obtained for AuNP@PEG@e14a2, higher than that of IM, the gold standard of CML chemotherapeutics (Figure 5.6C). Caspase-3/7 activity was then measured at 24 and 48 h and, although no effect was observed at the shorter time point, there was an increase in caspase activity at 48 h, mimicking the effect induced by IM (Figure 5.6D). The time-dependent profile observed with this assay also highlights the delay observed between gene silencing (higher effect at 24 h) and protein expression/activation (higher effect at 48 h).
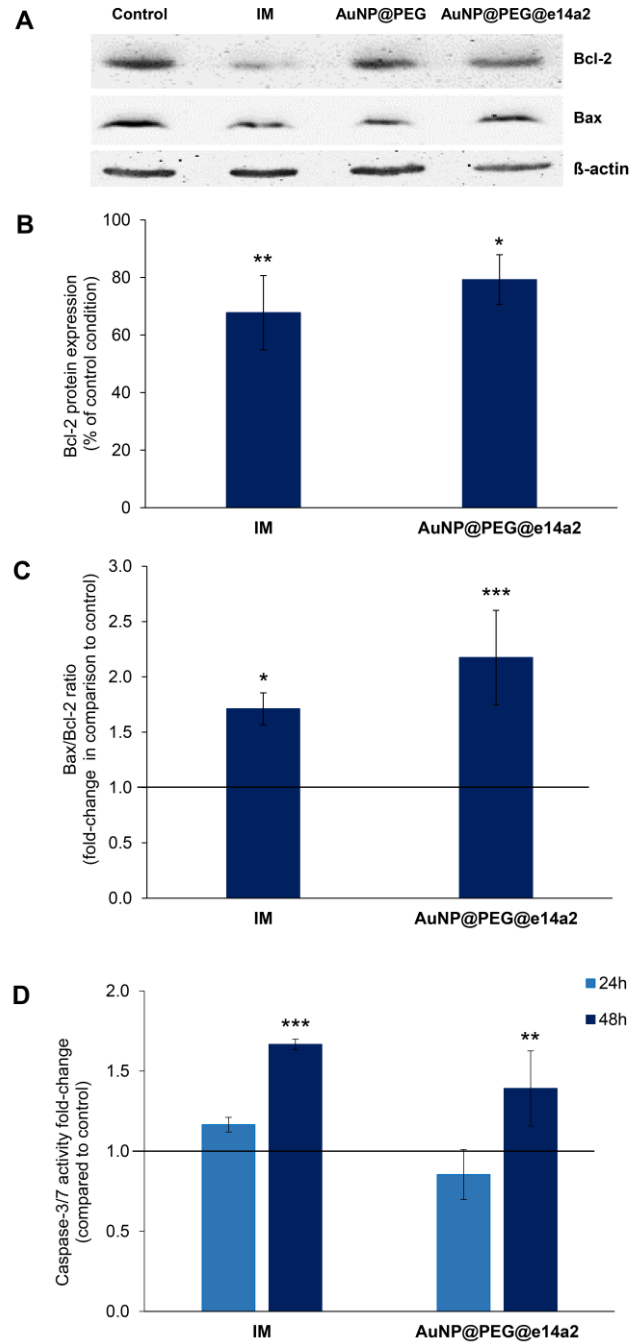
Figure 5.6 Triggering of apoptotic cascade via AuNP@PEG@e14a2. **A)** Expression of K562 cells Bcl-2 and Bax after exposure to the Au-nanoconjugate. Bcl-2 (26 kDa) and Bax (21 kDa) protein quantification was performed via western blotting on cell extracts after a 48 h exposure to 0.1 µM imatinib (IM) or 0.6 nM AuNP@PEG@e14a2. Band quantification was first normalized against ß-actin (42 kDa) and, subsequently, to the control condition: cells without treatment or cells exposed to 0.6 nM AuNP@PEG. **B)** Bcl-2 protein expression (control as 100 %). **C)** Apoptotic index of K562 cells, based on Bax/Bcl-2 ratio. **D)** Caspase-3/7 activity on K562 cells after exposure to 0.1 µM IM or 0.6 nM AuNP@PEG@e14a2. Values were normalized against cells without treatment (value represented by the threshold). $*p < 0.05$; $**p < 0.01$; $***p < 0.001$, Tukey's test statistical significance.

Improving CML cell death by a combination of IM and silencing nanoconjugates

Recently, the use of combinatory strategies for effective therapy has been the focus of numerous studies to overcome the consequences of TKI resistance and long-term treatments in CML. In fact, TKI resistance affects nearly 30 % of CML patients and is related to the overexpression of BCR-ABL1, mutational events, drug metabolism, transport and intracellular influx, and patient non-compliance.[456] The efficacy of the Au-nanoconjugate as an adjuvant to conventional therapy was assessed by measuring cell viability after a combined 48 h-challenge with the silencing nanoconjugate and increasing concentrations of IM (0.01–10 µM). AuNP@PEG@e14a2 combined with IM increased efficacy by 23 % when compared to the drug alone, demonstrating the ability of the nanoconjugate to enhance the effect of IM on cell proliferation. It should be mentioned that challenging cells with AuNP@PEG seem to slightly increase cell viability. When compared to IM + AuNP@PEG, the combinatory approach of IM + silencing nanoconjugate was 30 % more effective (Table 5.2).

Table 5.2 Imatinib's (IM) IC_{50} when combined with silencing nanoconjugate AuNP@PEG@e14a2. IC_{50} were calculated for the 48 h-stimuli.

	IM	IM + AuNP@PEG	IM + AuNP@PEG@e14a2
Imatinib IC_{50} (nM)	220	240	170***

* Bonferroni's test statistical significance, compared to IM or IM+AuNP@PEG: $p < 0.001$ (***).

Concentration-response plots, from which these IC_{50} values were computed, are represented in Appendix V – Figure V.2.

The effect of the Au-nanoconjugate on IM-resistant cells was also analyzed (Figure 5.7). To obtain this *in vitro* model, K562 cells were exposed to increasing concentrations of IM up to 1 µM. Several studies show potential resistance mechanisms that arise from this exposure and correlate to CML disease progression *in vivo*: incidence of point mutations in *BCR-ABL1* that impair TKIs binding to the encoded protein; overexpression of *BCR-ABL1*; and/or overexpression of genes involved in drug transport or redistribution.[97,487,488] Although it was not possible to analyze the expression of efflux pumps at mRNA or protein level in these cells (e.g. MDR1), their tolerance to IM was associated to an increase of *BCR-ABL1* expression rather than mutations to *ABL1* (Appendix V – Figure V.3).

Figure 5.7 demonstrates that IM-resistant K562 cells do not respond to the concentration of the drug corresponding to the half maximal inhibitory concentration (IC_{50}) of sensitive parental K562 cells (as shown in Figure 5.4C). Remarkably, AuNP@PEG@e14a2 induced a significant reduction (30 %) of viability in K562-IM-resistant cells.
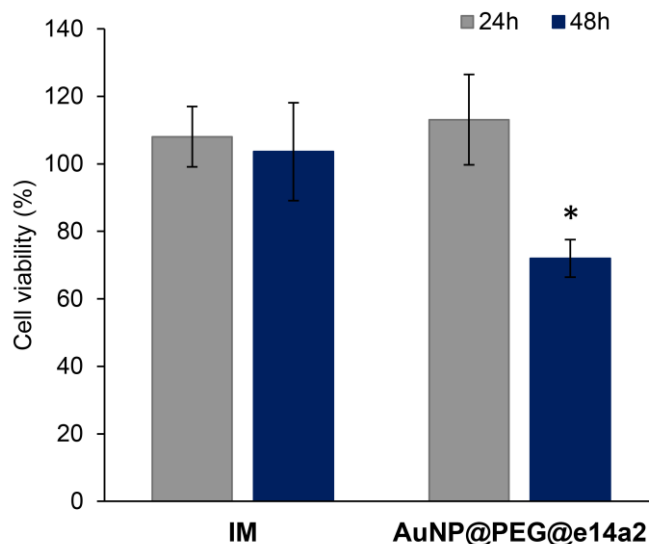
Figure 5.7 Viability via MTS assay of K562 cells resistant to imatinib (IM). Cells were challenged with 0.1 µM imatinib or 0.6 nM AuNP@PEG@e14a2 for 24 or 48 h. $*p < 0.05$, Bonferroni's test statistical significance, compared to the control condition AuNP@PEG.

5.5 Concluding Remarks

Here, we show that using a sequence-selective silencing nanoconjugate, AuNP@PEG@e14a2, may be used to regulate CML cell proliferation and apoptosis (Figure 5.8). Such silencing potential is exerted with great sequence selectivity that may be used to selectively target those cells harboring a particular gene/gene isoform. This strategy may provide an additional wave of destruction to current TKIs, particularly in patients that display TKI toxicity and/or resistance and frequently relapse. It is clearly aligned with the recent recommendations of the ELN, due to the high cost to CML patients and public institutions of long-term treatment and the occurrence of adverse effects.[38,489] Our procedure might open the way for the development of specific and selective molecular targeting approaches that should impact how we perceive chemotherapy and provide for enhanced precision for a range of drugs that have already proven their tremendous efficacy in the clinics.
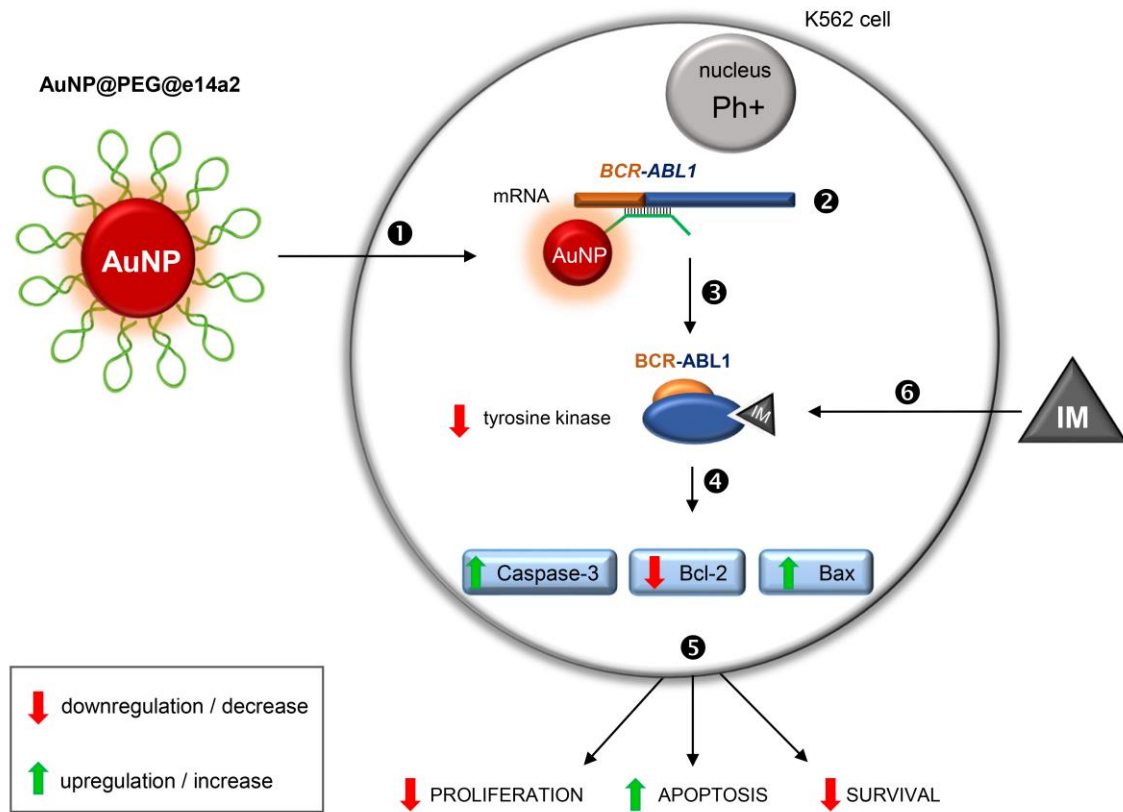
Figure 5.8 Gold nanoparticle (AuNP)-based *BCR-ABL1* gene silencing. (1–6) In (1), AuNPs functionalized with the e14a2 antisense hairpin ssDNA oligonucleotide (AuNP@PEG@e14a2) are internalized by K562 cells, a CML *in vitro* model. (2) The Au-nanoconjugate recognizes *BCR-ABL1* mRNA expressed by these cells. The hairpin opens in the presence of the complementary *BCR-ABL1* sequence, silencing gene expression and triggering mRNA degradation and (3) leading to the translation inhibition of the encoded tyrosine kinase and to (4) the downregulation of Bcl-2 and the upregulation of Bax and caspase-3/7 activity. (5) The apoptotic pathway increases CML cell apoptosis and decreases proliferation and survival, ultimately killing BCR-ABL1 leukemic cells. (6) Conjugation of tyrosine kinase inhibitors (IM) with the gene-silencing Au-nanoconjugate should be an effective way to overcome chemotherapy resistance.

After effective *BCR-ABL1* silencing using gold nanoformulations, a few other lines of research were pursued to potentiate leukemia cells elimination. CML treatment relies mostly on its central player, BCR-ABL1, however this oncogenic pathway offers other targets to fight the deregulated proliferation, differentiation and apoptosis characteristic of Ph+ cells. For instance, the well-studied protooncogene *c-MYC* is one of the targets of BCR-ABL1 and is expressed at high level in CML cells.[490] Indeed, i*n vitro* inhibition of *c-MYC* with antisense oligonucleotides can inhibit BCR-ABL1 transformation or leukemogenesis.[491] Our preliminary results show stable *c-MYC* inhibition after 24 h of exposure of K562 cells to AuNPs functionalized with 30 % PEG and an hairpin-shaped ssDNA oligonucleotide that targets *c-MYC* mRNA (AuNP@PEG@MYC). *In vitro* cells viability was also decreased to approximately 75 % after a 48 h-stimulus with the Au-nanoconjugate (Figure 5.9). The next stages of this project should include combination of *c-MYC* silencing with *BCR-ABL1* silencing and/or inhibition with TKIs therapy. This collective strategy should be extremely advantageous since these agents will act on distinct molecules of the same pathway therefore increasing the chances of regulating CML cells activity and overcoming the burden of TKIs resistance mutations.
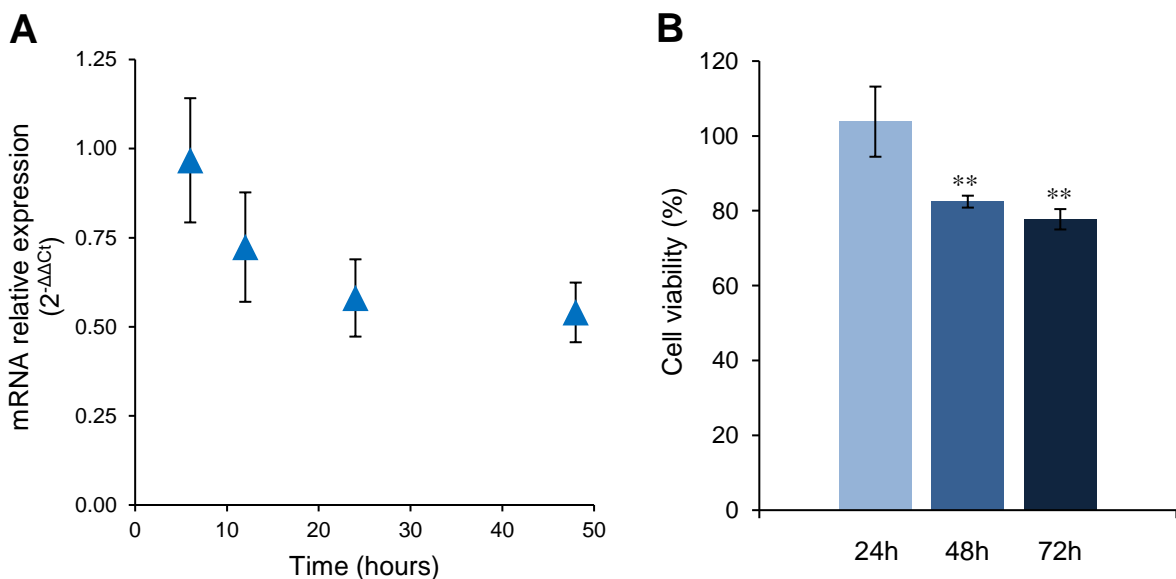
Figure 5.9 *In vitro c-MYC* gene silencing on K562 cells using AuNP@PEG@MYC. **A)** Au-nanoconjugate targeting *c-MYC* effectively silences the gene expressed by K562 cells. Plot represents mRNA relative expression after treatment of K562 cells with 0.6 nM AuNP@PEG@MYC (corresponding to 40 nM oligonucleotide). Data were normalized to the 18S gene and then to cells exposed to AuNP@PEG. Ct, threshold cycle. **B)** Cell viability over time on K562 cells challenged with the silencing nanoconjugate (MTS assay). Data were normalized to cells exposed to AuNP@PEG. Error bars represent the standard error of the mean of at least three independent experiments. **p < 0.01, Tukey's test statistical significance versus first column.

Although AuNPs can act as imaging agents on their own, which could be used to locate them *in vivo*, several imaging components/strategies can be loaded onto the NP to monitor its effect on cells, e.g., gene silencing. Thus, we tested a nanotheranostics approach based on AuNPs functionalized with beacons.[122,240,304,306] Our strategy coupled a fluorescent molecule to the distal end (3') of the hairpin-shaped silencing oligonucleotide (Au-nanobeacons) combined with FRET based spectral codification for the detection of *BCR-ABL1* fusion sequence (e14a2 isoform). In the absence of a complementary sequence, the hairpin should be in closed conformation and the AuNP acts as a fluorescence quencher due to its proximity to the fluorophore. Presence of a complementary target (e14a2 mRNA) opens the hairpin structure and enables fluorescence recovery. Additionally, this fluorophore acts as a donor for FRET to an acceptor fluorophore on a second oligonucleotide sequence that will hybridize in the vicinity of the donor upon target recognition.[122] The existing array of available fluorescent molecules makes it possible to develop a range of Au-nanoconjugates suitable for monitoring each *BCR-ABL1* isoform silencing. The specific spectral signature of donor and acceptor pairs formed provides an additional level of information of the hybridization events occurring in solution.

The described approach has been previously tested for *BCR-ABL1* detection using synthetic oligonucleotide solutions as a platform for CML diagnostics.[122] We have now tested it on K562 cells for the real-time monitoring of *BCR-ABL1* silencing, using fluorescence microscopy (Figure 5.10). These preliminary data show that the strategy is highly specific for cells that express the e14a2 transcript, even when using the Au-nanobeacon alone. Several other experiments should be envisaged to understand the FRET phenomenon, and its advantages, under these conditions. Since fluorescence microscopy filters are very broad and generic, these same *in vitro* tests should be performed on a fluorescence spectrophotometer for a more fine control over excitation/emission wavelengths, and better distinction between fluorophores (donor *vs* acceptor) and their separate contributions to the detected signal. Because cells were examined over discrete periods of time (6, 12 and 24 h), one could perform a live cell imaging experiment to better control this Au-nanobeacon-based methodology over time.

While the described results using AuNPs are very promising for CML theranostics, numerous parameters should be optimized, which will be discussed in more detail in the next chapter of this thesis (*Futures perspectives* section).
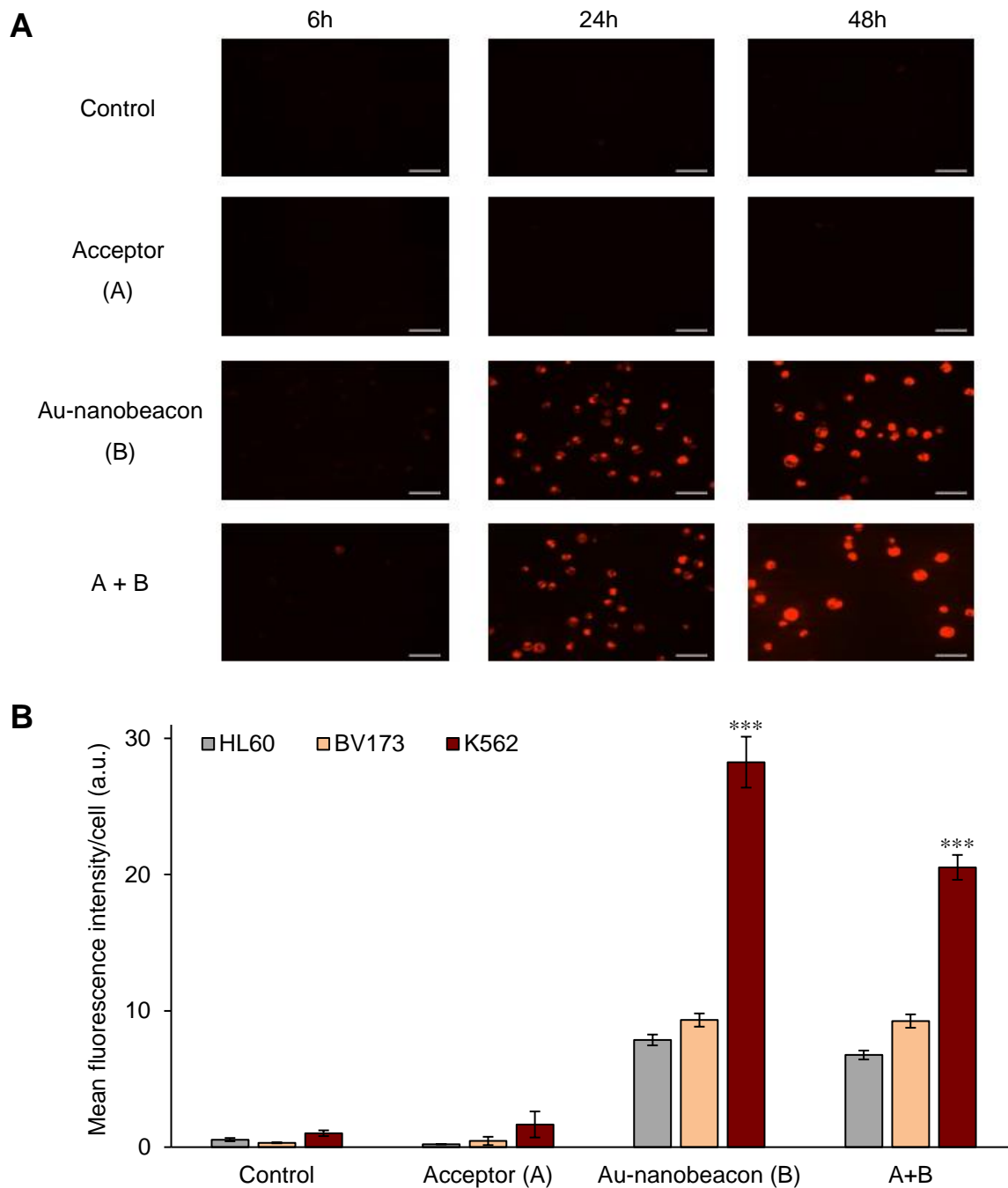
Figure 5.10 *In vitro* real-time imaging of *BCR-ABL1* silencing. **A)** Fluorescence microscopy of K562 cells challenged with e14a2 targeting Au-nanobeacon (donor molecule, sulfoindocyanine Cy3) and/or acceptor (Dy-520XL). Representative fluorescence microscopy images are shown with corresponding scale bars (50 µm). **B)** Fluorescence intensity quantification per cell, per condition, after background correction. Three different cell lines (HL60, BV173 and K562) were used to evaluate the specificity of the Au-nanobeacon/acceptor (48 h-stimulus). Error bars represent the standard error of the mean of at least three independent experiments. For additional information on this strategy design, please refer to Cordeiro *et al*, 2016.[122] ***p < 0.001, Bonferroni's test statistical significance, compared to control.

CHAPTER 6 – **CONCLUSIONS AND FUTURE PERSPECTIVES**

6.1 Final considerations

Cancer nanomedicine has been deeply focused on two main vectors: solutions for accurate molecular characterization of tumors and new approaches for improved chemotherapy. However, most of these advances are still in the pre-clinical stage of research and far from substituting or assisting traditional cancer management procedures. Moreover, the vast majority of these nanoformulations have been designed and directed at solid tumors, due to their well-studied architecture, invasiveness and distinctive confined localization, in detriment of liquid tumors.

Nevertheless, several factors inherent to hematological malignancies, particularly leukemia, show their potential as targets of smart nanomaterials and how much these diseases would benefit from a more personalized approach than current diagnostics and treatment regimens. First and foremost, leukemia requires less invasive techniques to obtain hematological, cytogenetic and molecular information on the tumor, since a simple blood withdraw is enough to collect these data and correlates perfectly with bone marrow levels. Although leukemia is a very diverse disease, all subgroups hallmarks are well-defined, which is essential for biomarker detection and specific abnormal cells ablation. Attention was given to CML, since it is associated to a unique chromosomal abnormality that results in the fusion of *BCR* and *ABL1* genes, present in virtually all patients; also, molecular characterization of this genetic alteration is essential for treatment success. Moreover, the disease has got a local environment to target (e.g. bone marrow) but most of its malignant cells are circulating through the body, thus requiring smarter approaches for tackling these cancer cells with increased efficacy. Many features of NPs have been described in this thesis that make them entirely suitable candidates towards CML nanotheranostics, a central approach in precision oncology as it allows the integration of diagnostics and therapeutics in a single material through NPs engineering.

Cytogenetic and molecular monitoring plays an essential role in the management of leukemia patients at diagnosis and during disease progression. Indeed, chapter 2 of this thesis was paramount for medical decision making in cases harboring known genetic variations, but also disclosed new clinical cases and provided an integrated analysis between patient's molecular profile, disease treatment and progression. This was particularly relevant for the three cases described in more detail in that chapter (clinical cases 44, 54 and 7). Although further bioinformatic studies are still needed, for instance on mutation modelling, protein mutagenesis, structure and function, these reports are likely to improve the knowledge on leukemia pathogenesis and, in the future, aid patients harboring similar genetic aberrations.

Several issues related to cytogenetic and molecular characterization of leukemia samples were encountered. Cytogenetic testing lacks sensitivity for CML follow-up, since *BCR-ABL1* transcripts remain detectable far beyond samples testing negative for t(9;22) via FISH. Molecular monitorization using RT-PCR overcomes this limitation, due to its well-known sensitivity and specificity, however it

is time-consuming, complex, error-prone and expensive. Thus, new solutions should be envisaged to mitigate these issues.

Another issue relates to *BCR-ABL1* transcript identification which is highly important, not only for suitable disease monitoring since transcript levels should be compared to the correct standard, but also for prognosis evaluation given that different transcripts are associated to distinct disease progression and treatment responses. Indeed, recent recommendations from ELN state that transcript variant identification should be performed at diagnosis. However, most routine tests done in hospital settings only quantify the most frequent *BCR-ABL1* isoforms (e14a2 or e13a2), and these distinct molecular entities are usually regarded as the same phenotypical group.

For all these reasons, samples described on chapter 2 were used for proof-of-concept of emerging molecular technologies to advance monitoring in CML. Note that the process of implementing a molecular genetic test for diagnostic use is complex and involves many levels of assessment, and most methodologies do not leave pre-clinical stages due to lack of appropriate samples for clinical validation.

Numerous biosensing platforms have been proposed relying on the optical properties of AuNPs. Thus, chapter 3 focused on CML diagnosis and enabled the optimization of a new methodology for CML detection, based on Au-nanoprobes. This colorimetric approach was previously optimized using total RNA from leukemia cell lines,[123,124] however, we present for the first time the validation of NCL method using samples derived from leukemia patients, and compare its sensitivity and specificity to standardized clinical procedures for CML detection and characterization. Though the test was performed on a small sample size, one must considerer the incidence of Ph+ diseases and the time frame of this project.

The results obtained using Au-nanoprobes and total RNA from clinical samples show the robustness of the test, namely PPV and NPV values (100 %). The assay, not only detected *BCR-ABL1*-positive samples, but also enabled distinction between the most frequent isoforms (e14a2 *vs* e13a2). The outcome is particularly attractive taking into consideration that the extracted RNA was mixed directly with Au-nanoprobes, without amplification via RT-PCR or other methodology, thus reducing time and complexity when compared to routine molecular diagnostics.

The features of the Au-nanoprobe assay are ideal for CML molecular diagnostics, since according to the ELN and NCCN guidelines, *BCR-ABL1* molecular monitoring is required every 3 months after disease diagnosis and until DMR is achieved. Although RT-PCR has been highly optimized in terms of transcript quantification and international harmonization of results, the procedural aspects of the technique are still complex and time-consuming. Due to the inherent simplicity of the Au-nanoprobe assay at a very small scale, the test is suitable for a fast an accurate preliminary screening of CML, thus assisting routine methodologies such as RT-qPCR. Sensitivity levels of the assay are also promising since it was able to detect the e14a2 transcript in a sample that exhibited levels as low as 0.34 % *BCR-*

ABL1 IS. However, additional optimization is needed to achieve the sensitivity values required by ELN or NCCN guidelines for CML molecular tests (0.01 % *BCR-ABL1* IS; corresponding to DMR).[38] After complete cytogenetic response is attained, patient molecular stratification is the cornerstone of CML monitoring due to the advent of highly effective TKIs, sophisticated molecular tools and automated analytical solutions. Moreover, the Au-nanoprobe assay seems to be highly dependent on total RNA quantity, since samples with RNA concentration below 15 ng/µL constantly scored as negative, independently of their transcript type. These issues, and potential solutions, will be further explored in the *Future perspectives* section.

Au-nanoprobe assays offer the additional possibility of incorporation into chip-based detection devices. Indeed, the previous CML diagnostic method, optimized to detect *BCR-ABL1* directly from total RNA extracted from cells, was successfully translated onto a microfluidic platform, integrating the mixing of the system components and optic detection (chapter 4). This new design allowed to achieve faster and accurate results using lower volumes than its off-chip version, mostly due to the scale of the device and the fast transition between injection of samples, mixing and photodetection.

Both versions of the Au-nanoprobe assay described in this thesis (off-chip or on-chip) can offer solutions for different clinical settings. The microfluidics chip may be a suitable solution for CML healthcare worldwide, since it is made of a disposable cheap POC platform with a non-disposable component integrating the light sources and photodetector, for a fast low-volume screening. However, its cost, though lower than conventional methodologies, might still be unaffordable for some countries. In these cases, the simple off-chip version of the assay can be an appropriate solution, since it requires fewer resources. AuNP-based diagnostics may bring molecular diagnostics to remote and impoverished countries where monitoring strategies are strict and limited, enabling worldwide efforts to diagnose and control CML. Many patients and clinicians still do not have access to reproducible and standardized BCR-ABL1 testing. Shipping reference samples to smaller facilities located in isolated regions, or even perform any kind of molecular testing, may not always be feasible or cost-effective.

Nevertheless, proper comparison between these methodologies can only occur after completion of the microfluidic device to include the hybridization step of the Au-nanoprobe colorimetric assay and, possibly, an upstream module for automatized RNA extraction in a closed system, as way to decrease the differences in performance between sites, operators, days, and prevent contaminations. Differences between methodologies (Off-chip Au-nanoprobe assay *vs* microfluidic device *vs* RT-PCR) should then be assessed using clinical samples and IS standards.

On the last part of this thesis, focus was given to CML therapeutics and its challenges (chapter 5). All the information gathered and optimized for the design of a specific Au-nanoprobe, targeting the most frequent *BCR-ABL1* transcript, was used to develop a Au-nanoconjugate intended to silence the

e14a2 isoform of the gene. The sequence-selective silencing nanoconjugate, AuNP@PEG@e14a2, regulated CML cells proliferation and apoptotic pathways *in vitro*. Even though this was a transient effect, the nanoformulation enabled a decrease on imatinib's IC_{50}, meaning a lower dose was required to achieve the same result, and induced a viability decrease on IM-resistant cells. This NP-based treatment strategy is particularly relevant for patients that exhibit aggressive side effects and/or do not respond to TKIs. ELN guidelines show the importance of discontinuing TKI therapy, achieving DMR and maintaining the operational cure, due to the associated cost of CML management and the burden caused to patients.[489] Novel therapy options should be researched in order to enhance TKI precision in the clinics, but also to avoid allogeneic transplantation (salvage therapy) in case of complete unresponsiveness to chemotherapy.

Other studies have shown that silencing of *c-MYC* in various *BCR-ABL1* positive cell lines causes significant downregulation of BCR-ABL1, decreases proliferation rate and induces cell death in CML cells. Hence, based on the same strategy applied for *BCR-ABL1* gene silencing using AuNPs, a second Au-nanoconjugate was designed targeting *c-MYC,* as to achieve a higher effect on K562 cells viability. Though more stable over time, the effect obtained using this nanoconstruct was very similar to the one obtained when using the one targeting *BCR-ABL1*, which might be due to the close interplay of these two oncogenes. However, several other conditions should be tested, namely, a combined stimulus with both agents. One should also keep in mind *c-MYC* primary oncogenic role across several tumors, meaning the designed construct (AuNP@PEG@MYC) may be used against other malignancies thus attaining a more versatile function than that of AuNP@PEG@e14a2.

After accomplishing effective Au-nanotherapeutics based on gene silencing, a nanotheranostics strategy for CML was considered. Gold nanotheranostics opens a new venue for complex differential diagnostics, and therapy of the disease. The ability of AuNPs to specifically target and probe tumor cells makes them a useful delivery system for anticancer agents. The type of formulation additives used can also improve visualization and control over the effects of these agents *in vitro* and *in vivo*. The tested approach enabled the real-time monitoring of specific gene-silencing events on K562 cells, however it requires a deeper analysis and further experiments to understand all underlying mechanisms: route of AuNPs internalization; cellular localization and distribution; antisense oligonucleotide/target hybridization dynamics; and fluorescence/FRET events. Besides, a more complete version of this nanoconstruct should be envisaged to enhance its efficacy and specificity, which will be discussed on the *Future perspectives* section.

This work allowed a better understanding on the molecular basis of leukemia and the way it defines prognosis and treatments options. However, it mostly contributed to the development of new tools for CML management, at both point-of-care diagnostics and early development of a nanotheranostics approach to selectively eliminate malignant cells, and help conventional therapies.

6.2 Future perspectives

Although the line of research of this thesis answered several questions regarding leukemogenesis and provided novel solutions for biomarker detection and therapeutics, much remains to be done for these nanomedicines to be more effective, standardized, certified and reach clinical settings. Hence, potential future stages on this project will be discussed in this section.

Leukemia molecular monitoring

The way several biomarkers influence leukemia prognosis is of utmost importance. For instance, mutations on *CEBPA*, *NPM1*, and *FLT3* genes are among the most common and bear important prognostic significance for AML. However, diagnostic testing for *CEBPA* mutations in cytogenetically normal AML is hindered by technical challenges associated with the GC content of the gene, the complex nature of the mutations, including frequent expansions or contractions of homopolymer sequences and the large number of different insertions and deletions, and the complexity of the sequence analysis and variant interpretation. Suitable alternatives for detection of all *CEBPA* mutations should be designed: iPLEX-MassArray®, next generation sequencing or high-resolution melting.

On the contrary, molecular monitoring of Ph+ diseases, namely transcript identification, quantification and mutational screening, is highly standardized in clinical laboratories. Nevertheless, there is still room for improvement in terms of methodologies complexity, time required to obtain results, increase the amount of information provided by fewer tests and the invasiveness of sample collection (e.g., bone marrow biopsy *vs* peripheral blood withdraw).

Alternate approaches for molecular response assessment are currently being explored to investigate whether enhanced sensitivity may help achieving treatment-free remission and TKI discontinuation in a greater proportion of CML patients, and to widen the access to reliable and standardized monitoring, namely by probing different key players of the disease (e.g., *BCR-ABL1* gDNA, mRNA, protein or different molecules on the BCR-ABL1 signaling pathway).[492] NPs are excellent tools to probe the disease at different stages: early-phase, chronic-phase, accelerated phase, or remission. Indeed, the same Au-nanoprobe used to monitor *BCR-ABL1* transcripts is suitable to detect the same sequence in gDNA, after DMR is achieved. Furthermore, these nanostructures can be functionalized with specific antibodies to probe for disease biomarkers at protein level in more complex fluids, such as serum, in a similar strategy designed by Weerkamp *et al* (2009).[30] By using AuNPs functionalized with antibodies that recognize BCR epitopes in the most upstream part of the BCR protein and another set that recognizes the ABL1 epitope located downstream of exon 3, the assay enables the detection of all BCR-ABL1 isoforms. A crosslinking approach should be the most appropriate solution for this assay, since only the presence of a complementary target to both antibodies (BCR-ABL1 fusion protein) will decrease interparticle distance and produce a colorimetric shift.

BCR-ABL1 isoforms complete screening

Although the e14a2 *BCR-ABL1* isoform accounts for more than half of CML cases, the optimized Au-nanoprobe assay should target other transcripts: the common isoform e13a2 and rare variants. All the information collected for the e14a2 isoform biosensing using Au-nanoprobes, namely sequence design and test conditions, should aid on the development of an array test for additional *BCR-ABL1* isoforms. This would enable a high throughput molecular screening of all Ph+ patients.

The method can be further adapted to allow *BCR-ABL1* mutational screening and the associated TKIs resistance mechanisms (at least for the most common TKI resistance mutations). In fact, the Au-nanoprobe assay has been successfully optimized to detect single nucleotide variations for other diseases.[193, 199, 207, 419,493]

BCR-ABL1 transcript quantification

The optimized Au-nanoprobe assay was proven to be very effective as a qualitative method for CML biosensing. Transcript identification at the time of diagnosis is in accordance to recent ELN and NCCN guidelines, since it is imperative for correct follow-up and can help choosing a suitable therapeutic regimen. Nevertheless, *BCR-ABL1* quantification is required for disease monitoring throughout the course of the disease. The AuNPs colorimetric method can in fact be adapted for gene quantification. This was demonstrated by Conde *et al*, where the Au-nanoprobe assay showed a linear correlation for *BCR-ABL1* detection within the range of 10-60 ng/µl of total RNA.[123,124]

Nevertheless, if *BCR-ABL1* quantification using Au-nanoprobes is to be pursued, several parameters should be considered. The novel methodology for measuring *BCR-ABL1* transcript levels in patients with CML should be compared to IS values to allow comparison to RT-qPCR sensitivity and accuracy, as well as results harmonization between individual laboratories. Moreover, the method robustness and sensitivity can be improved by using an isothermal amplification technique, such as rolling circle amplification (RCA). Indeed, a recent study using RCA on K562 RNA samples allowed for the direct quantification of *BCR-ABL1* genes at room temperature, eliminating the requirement for external temperature controllers and overall complexity of the molecular diagnostic approach, thus making it more suitable for integration on a biomolecular recognition device for POC.[494]

On-chip BCR-ABL1 detection

The microfluid version of the colorimetric method has been fully validated using RNA samples from leukemia cell lines, however results should be corroborated using patient-derived samples as previously done for the off-chip setting. Future work shall also focus on the integration of a hybridization module on the microfluidic platform, upstream the mixing and photodetection components. Although the inclusion of a temperature-controlled chamber in the device raises several technical issues, it unlocks the possibility for a more complex, automatized and cost-effective CML detection assay, thus enabling a fast screening of diagnostic and follow-up samples.

The final version of the lab-on-chip is envisaged to include a complete setup for blood analysis, from RNA extraction to biomarker detection. The micro-scale of the complete device should provide an output faster than existing automatized equipment (Genexpert®) using smaller sample volumes.[220, 419,422]

CML gene silencing

By targeting *BCR-ABL1*, our designed Au-nanoconjugate provided for an effective solution to overcome TKI resistance in CML. Yet, these resistance mechanisms can also be BCR-ABL1 independent. Overexpression of *MDR1*, the gene encoding for a drug efflux pump, has been identified as a mechanism of resistance to IM.[33,94] CML resistance reversal can be achieved by silencing the *MDR1* gene therefore increasing IM intracellular levels.

A different strategy might be related to miRNAs. miRNA expression profiles can clearly distinguish CML patients from healthy individuals, CML phases, and between patients either responding or not responding to TKI therapy.[495,496] Identification of miRNAs that directly target the expression of BCR-ABL1 may play a role in the miRNA-based therapy in CML. In effect, miR-17/92 cluster has been well characterized in the context of CML, with specific molecular mechanisms. Upregulation of this miRNAs cluster has been described as the result of a transactivation by the BCR-ABL1-MYC pathway in early chronic phase.

Note that AuNPs provide an appropriate vector to convey all the mentioned alternatives to tackle CML, as it was demonstrated with AuNP@PEG@e14a2. Furthermore, they can be functionalized with distinct silencing oligonucleotides in a multifunctional strategy, targeting different key players on CML pathogenesis: *BCR-ABL1*, *MDR1*, miRNAs or anti-apoptotic genes. Yet, other nanoscale vehicles can be used to achieve effective gene therapy: liposomes, cationic polymers, dendrimers and exosomes.[462,497,498] These vectors protect nucleic acids from rapid degradation in plasma and cellular cytoplasm, thus increasing their short half-life. However, all of them seem to possess the same drawback, as they are only able to induce a transient gene-silencing effect, most likely due to the dilution of the effector molecule upon cell division and its degradation upon intracellular release. To achieve prolonged gene silencing, a controlled release approach should be considered. One can also combine the advantages of the mentioned vehicles in a single system. For instance, the unique physicochemical and optical properties of AuNPs can be encapsulated onto a cationic liposomes or dendrimers to enhance the stability of negatively charged nucleic acids in the bloodstream and improve their cellular delivery.[499,500]

Although I have demonstrated the efficacy of *in vitro* gene silencing using AuNPs towards CML therapeutics, a few parameters remain to be tested, namely, a complete comparison between the effect of the nanoformulation (AuNP@PEG@e14a2) against the effect of the silencing moiety alone or in combination to other vehicles. Moreover, one can apply the same strategy but using siRNA technology. Antisense ssDNA oligonucleotides and siRNAs share important similarities as gene expression

modulators. However, their design and mechanism are quite different: an antisense ssDNA oligonucleotide must function as a single strand; on the contrary, siRNA duplexes cooperate with the RNA-induced silencing complex (RISC) to bind complementary RNA. This basic difference may lower cost and simplify delivery, in favor of the antisense ssDNA technology. Still, siRNAs have been more thoroughly studied in cell culture, however it is not clear whether this efficacy translates to *in vivo* trials. Different gene therapy technologies have different strengths and weaknesses, nevertheless the main problem is that most have not crossed the pre-clinical stages of research.

Nanotheranostics for CML

Even though the results shown in chapter 5 of this thesis are very promising for the development of a nanotheranostics platforms towards personalized management of CML, other components need to be added to the silencing Au-nanoconjugate/Au-nanobeacon for it to be exceedingly effective.

In what concerns leukemia, passive targeting via EPR might be an aspect to consider when treating the core of the disease (bone marrow),[501] however the bulk of malignant cells is spread through peripheral blood. Hence, active targeting is particularly important when treating blood-borne diseases to enhance the effect on circulating abnormal cells without damaging healthy ones. Adding folic acid to the Au-nanoconjugate will likely improve tumor cell selectivity and the uptake efficiency of the nanoformulation, since folate receptors are highly overexpressed on the surface of many tumor types, including CML. Folate and folate conjugates can bind to its receptor with high affinity and be internalized by cells via receptor-mediated endocytosis, while avoiding normal cells that express low levels of these surface proteins.[502] Interleukin-3 receptor is also overexpressed in CML blasts compared to normal hematopoietic cells and thus is able to act as a receptor target in a cancer drug delivery system.[503]

Finally, one can take advantage of the nanocarrier to deliver IM to CML cells. Combining the TKI and the *BCR-ABL1* silencing moiety in the same particle should enhance their separate effects for two main reasons: it ensures a higher payload of the drug into cells, when compared to the free drug, and that both therapeutic functions would be synchronized in time and space. This approach would be highly beneficial from a clinical point of view, since it would decrease the off-target effects of IM, by using a controlled release mechanism and active targeting, and it would avoid a repeated challenge to the patient's bloodstream. Though this new strategy is foreseen to mitigate the well-studied TKIs resistance mechanisms, one should contemplate the occurrence of new tolerance mechanisms against the proposed nanoconjugates. Further focus on pharmacokinetic, pharmacodynamic and toxicology status of nanoformulations needs to be clarified, as well as the economic viability of the end use product.

Considering that these additional changes will improve the Au-nanoconjugate/Au-nanobeacon efficacy, a more complete version of the nanoformulation should be tested in pre-clinical models of CML.

Leukemia in vitro and in vivo models

We have developed an *in vitro* model for IM resistance CML. The results we obtained suggest that cells respond to IM increasing concentrations by overexpressing *BCR-ABL1*, but after prolonged exposure and for higher doses of TKI, other mechanisms may take place.[97] Further studies are needed to assess this model: BCR-ABL1 protein and drug transporters expression profile, and whether resistance to IM is stable or can in fact be overturned. Note that the problem of drug resistance cannot be solved solely by circumventing *BCR-ABL1* expression, but also the expression of drug transporters or anti-apoptotic proteins involved in the complex CML network. This model is relevant to establish the possible mechanisms of resistance in CML and open the way for more effective pharmacological intervention.

The success of nanomedicines development at a pre-clinical stage depends greatly on the availability of *in vivo* tumor models that can mimic the real human tumor environment. Leukemia models show several obstacles, namely related to the fact that the pathogenesis of the disease in murine models is not relevant to most human cases; also, they fail to replicate the complex microenvironment from which these human cancers arise, and do not embody their genetic and molecular heterogeneity.[504,505] Xenografts mitigate some of these issues, but because they are usually conducted on immunocompromised mice to avoid immune rejection of the human cells, they eliminate the effects of the immune system on tumor expansion and on NPs efficacy and targeting.[505] The variability of experimental conditions between the different pre-clinical studies using NPs to tackle leukemia also contribute to their reduced clinical impact. Protocols for standardization of experiments should be implemented to mitigate this issue.

Clinical translation

Though the potential of nanomedicines is huge, much remains to be done to translate nanoformulations into clinical practice. Numerous parameters must be studied: pharmacokinetics (including internalization, biodistribution, clearance and toxicity), efficacy, classification, standardization, scalability and safety guidelines. FDA, EMA and the Nanotechnology Characterization Laboratory are gathering relevant information to mitigate some of these issues. However, theranostics still exists in a grey area since most information refers exclusively to therapeutics or to diagnostics. The mentioned issues should be urgently tackled since nanomedicines are now entering a decisive phase of clinical trials. Being cancer the main target when designing nanotheranostics approaches, one can speculate that nanomedicines clinical research is ahead of regulatory protocols establishment because most clinical trials are conducted in late-stage cancer patients, when cutting edge treatments might be the only option.

REFERENCES

1. Siegel RL, Miller KD, Jemal A. Cancer statistics. *CA Cancer J Clin* 2016; **66**: 7–30.

2. Hu D, Shilatifard A. Epigenetics of hematopoiesis and hematological malignancies. *Genes Dev* 2016; **30**: 2021–2041.

3. Den Boer ML, van Slegtenhorst M, De Menezes RX *et al.* A subtype of childhood acute lymphoblastic leukaemia with poor treatment outcome: a genome-wide classification study. *Lancet Oncol* 2009; **10**: 125–134.

4. Freeman CL, Gribben JG. Immunotherapy in Chronic Lymphocytic Leukaemia (CLL). *Curr Hematol Malig Rep* 2016; **11**: 29–36.

5. Tiacci E, Park JH, De Carolis L *et al.* Targeting mutant BRAF in relapsed or refractory hairy-cell leukemia. *N Engl J Med* 2015; **373**: 1733–1747.

6. Arber DA, Orazi A, Hasserjian R *et al.* Editorial introduction to a review series : the 2016 revision of the WHO classification of tumors of hematopoietic and lymphoid tissues. *Blood* 2016; **127**: 2361–2365.

7. Greaves M. Leukaemia 'firsts' in cancer research and treatment. *Nat Rev Cancer* 2016; **16**: 163–172.

8. Jabbour E, Kantarjian H. Chronic myeloid leukemia: 2012 update on diagnosis, monitoring, and management. *Am J Hematol* 2012; **87**: 1037–1045.

9. Wierda WG, Zelenetz AD, Gordon LI *et al.* NCCN guidelines insights: Chronic Lymphocytic Leukemia / Small Lymphocytic Leukemia, version 1.2017. *J Natl Compr Canc Netw* 2017; **15**: 293–311.

10. Keeney M, Hedley BD, Chin-Yee IH. Flow cytometry - Recognizing unusual populations in leukemia and lymphoma diagnosis. *Int J Lab Hematol* 2017; **39**: 86–92.

11. Taylor J, Xiao W, Abdel-Wahab O. Diagnosis and classification of hematologic malignancies on the basis of genetics. *Blood* 2017; **130**: 410–423.

12. Tasian SK, Hunger SP. Genomic characterization of paediatric acute lymphoblastic leukaemia: an opportunity for precision medicine therapeutics. *Br J Haematol* 2017; **176**: 867–882.

13. Fasan A, Haferlach C, Alpermann T *et al.* The role of different genetic subtypes of CEBPA mutated AML. *Leukemia* 2014; **28**: 794–803.

14. Döhner H, Estey E, Grimwade D *et al.* Diagnosis and management of AML in adults: 2017 ELN recommendations from an international expert panel. *Blood* 2017; **129**: 424–447.

15. Roe J-S, Vakoc CR. C/EBPα: critical at the origin of leukemic transformation. *J Exp Med* 2014;

211: 1–4.

16. Wang ML, Bailey NG. Acute myeloid leukemia genetics risk stratification and implications for therapy. *Arch Pathol Lab Med* 2015; **139**: 1215–1223.

17. Vinhas R, Cordeiro M, Pedrosa P *et al.* Current trends in molecular diagnostics of chronic myeloid leukemia. *Leuk Lymphoma* 2017; **58**: 1791–1804.

18. Patel AB, Wilds BW, Deininger MW. Treating the chronic-phase chronic myeloid leukemia patient: which TKI, when to switch and when to stop? *Expert Rev Hematol* 2017; **10**: 659–674.

19. Campiotti L, Suter MB, Guasti L *et al.* Imatinib discontinuation in chronic myeloid leukaemia patients with undetectable BCR-ABL transcript level: A systematic review and a meta-analysis. *Eur J Cancer* 2017; **77**: 48–56.

20. Yohe S, Ustun C, Godley LA. Molecular genetic markers in acute myeloid leukemia. *J Clin Med* 2015; **4**: 460–478.

21. Goldman JM. Chronic Myeloid Leukemia: A historical perspective. *Semin Hematol* 2010; **47**: 302–311.

22. Mughal TI, Radich JP, Deininger MW *et al.* Chronic myeloid leukemia: Reminiscences and dreams. *Haematologica* 2016; **101**: 541–558.

23. Rowley JD. A new consistent chromosomal abnormality in chronic myelogenous leukaemia identified by quinacrine fluorescence and giemsa staining. *Nature* 1973; **243**: 290–293.

24. Quintas-Cardama A, Cortes J. Molecular biology of bcr-abl1 – positive chronic myeloid leukemia. *Blood* 2009; **113**: 1619–1630.

25. Melo J V, Barnes DJ. Chronic myeloid leukaemia as a model of disease evolution in human cancer. *Nat Rev Cancer* 2007; **7**: 441–453.

26. Chen Y, Peng C, Li D *et al.* Molecular and cellular bases of chronic myeloid leukemia. *Protein Cell* 2010; **1**: 124–132.

27. Chen M, Gallipoli P, Degeer D *et al.* Targeting primitive chronic myeloid leukemia cells by effective inhibition of a new AHI-1-BCR-ABL-JAK2 complex. *J Natl Cancer Inst* 2013; **105**: 405–423.

28. Heisterkamp N, Groffen J. Philadelphia-positive leukemia: a personal perspective. *Oncogene* 2002; **21**: 8536–8540.

29. Melo JV. The diversity of BCR-ABL fusion proteins and their relationship to leukemia phenotype. *Blood* 1996; **88**: 1697–1702.

30. Weerkamp F, Dekking E, Ng YY *et al.* Flow cytometric immunobead assay for the detection of

BCR-ABL fusion proteins in leukemia patients. *Leukemia* 2009; **23**: 1106–1117.

31. Torres F, Ivanova-Dragoeva A, Pereira M *et al.* An e6a2 BCR-ABL fusion transcript in a CML patient having an iliac chloroma at initial presentation. *Leuk Lymphoma* 2007; **48**: 1034–1037.

32. Arun AK, Senthamizhselvi A, Mani S *et al.* Frequency of rare BCR-ABL1 fusion transcripts in chronic myeloid leukemia patients. *Int J Lab Hematol* 2016; **16**: 1–8.

33. Balatzenko G, Vundinti BR, Margarita G. Correlation between the type of bcr-abl transcripts and blood cell counts in chronic myeloid leukemia - A possible influence of mdr1 gene expression. *Hematol Rep* 2011; **3**: 5–9.

34. Hanfstein B, Lauseker M, Hehlmann R *et al.* Distinct characteristics of e13a2 versus e14a2 BCR-ABL1 driven chronic myeloid leukemia under first-line therapy with imatinib. *Haematologica* 2014; **99**: 1441–1447.

35. Castagnetti F, Gugliotta G, Breccia M *et al.* The BCR-ABL1 transcript type influences response and outcome in Philadelphia chromosome-positive chronic myeloid leukemia patients treated frontline with imatinib. *Am J Hematol* 2017; **92**: 797–805.

36. Santos FPS, Kantarjian H, Quintás-Cardama A *et al.* Evolution of therapies for chronic myelogenous leukemia. *Cancer J* 2011; **17**: 465–76.

37. Jabbour EJ, Kanterjian H. Chronic myeloid leukemia: 2014 update on diagnosis, monitoring, and management. *Am J Hematol* 2014; **89**: 547–56.

38. Baccarani M, Castagnetti F, Gugliotta G *et al.* A review of the European LeukemiaNet recommendations for the management of CML. *Ann Hematol* 2015; **94**: 141–147.

39. Ou J, Vergilio J-A, Bagg A. Molecular diagnosis and monitoring in the clinical management of patients with chronic myelogenous leukemia treated with tyrosine kinase inhibitors. *Am J Hematol* 2008; **83**: 296–302.

40. Diger Hehlmann R. How I treat CML blast crisis. *Blood* 2012; **120**: 737–748.

41. Perrotti D, Jamieson C, Goldman J *et al.* Chronic myeloid leukemia: Mechanisms of blastic transformation. *J Clin Invest* 2010; **120**: 2254–2264.

42. Soverini S, Rosti G, Baccarani M *et al.* Molecular monitoring. *Curr Hematol Malig Rep* 2014; **9**: 1–8.

43. Press RD, Kamel-Reid S, Ang D. BCR-ABL1 RT-qPCR for monitoring the molecular response to tyrosine kinase inhibitors in chronic myeloid leukemia. *J Mol Diagnostics* 2013; **15**: 565–576.

44. van Dongen JJ, Macintyre EA, Gabert JA *et al.* Standardized RT-PCR analysis of fusion gene

transcripts from chromosome aberrations in acute leukemia for detection of minimal residual disease. Report of the BIOMED-1 Concerted Action: investigation of minimal residual disease in acute leukemia. *Leukemia* 1999; **13**: 1901–1928.

45. Baccarani M, Cortes J, Pane F *et al.* Chronic myeloid leukemia: An update of concepts and management recommendations of European LeukemiaNet. *J Clin Oncol* 2009; **27**: 6041–6051.

46. Zhen C, Wang YL. Molecular monitoring of chronic myeloid leukemia: International standardization of BCR-ABL1 quantitation. *J Mol Diagnostics* 2013; **15**: 556–564.

47. Bolufer P. Standardized quantitative assessment of BCR-ABL1 transcripts on an international scale. *Clin Chem* 2013; **59**: 874–875.

48. Hughes TP, Kaeda J, Branford S *et al.* Frequency of major molecular responses to imatinib or interferon alfa plus cytarabine in newly diagnosed chronic myeloid leukemia. *N Engl J Med* 2003; **349**: 1423–1432.

49. Soverini S, Hochhaus A, Nicolini FE *et al.* BCR-ABL kinase domain mutation analysis in chronic myeloid leukemia patients treated with tyrosine kinase inhibitors : recommendations from an expert panel on behalf of European LeukemiaNet. *Blood* 2011; **118**: 1208–1215.

50. Bonifazi F, de Vivo A, Rosti G *et al.* Chronic myeloid leukemia and interferon-alpha: a study of complete cytogenetic responders. *Blood* 2001; **98**: 3074–81.

51. Hehlmann R, Heimpel H, Hasford J *et al.* Randomized comparison of interferon-alpha with busulfan and hydroxyurea in chronic myelogenous leukemia. *Blood* 1994; **84**: 4063–4077.

52. Hansen JA, Gooley TA, Martin PJ *et al.* Bone marrow transplants from unrelated donors for patients with chronic myeloid leukemia. *N Engl J Med* 1998; **338**: 962–8.

53. Silver BRT, Woolf SH, Appelbaum FR *et al.* An evidence-based analysis of the effect of busulfan, hydroxyurea, interferon, and allogeneic bone marrow transplantation in treating the chronic phase of chronic myeloid leukemia: Developed for the American Society of Hematology. *Blood* 1999; **94**: 1517–1536.

54. O'Brien SG, Guilhot F, Larson RA *et al.* Imatinib compared with interferon and low-dose cytarabine for newly diagnosed chronic-phase chronic myeloid leukemia. *N Engl J Med* 2003; **348**: 994–1004.

55. Druker BJ, Guilhot F, O'Brien SG *et al.* Five-year follow-up of patients receiving imatinib for chronic myeloid leukemia. *N Engl J Med* 2006; **355**: 2408–2417.

56. Giles FJ, Cortes JE, Kantarjian HM. Targeting the kinase activity of the BCR-ABL fusion protein in patients with chronic myeloid leukemia. *Curr Mol Med* 2005; **5**: 615–623.

57. Sweet K, Pinilla-Ibarz J, Zhang L. Clinical advances in the management of chronic myelogenous

leukemia: Focus on bosutinib and patient considerations. *Patient Prefer Adherence* 2014; **8**: 981–986.

58.   O'Brien S, Radich JP, Abboud CN *et al.* Chronic Myelogenous Leukemia, Version 1.2014. *J Natl Compr Canc Netw* 2013; **11**: 1327–1340.

59.   Mathisen MS, Kantarjian HM, Cortes J *et al.* Practical issues surrounding the explosion of tyrosine kinase inhibitors for the management of chronic myeloid leukemia. *Blood Rev* 2014; **28**: 179–187.

60.   Miller GD, Bruno BJ, Lim CS. Resistant mutations in CML and Ph+ALL - Role of ponatinib. *Biol Targets Ther* 2014; **8**: 243–254.

61.   Kantarjian HM, Cortes JE, Kim DW *et al.* Bosutinib safety and management of toxicity in leukemia patients with resistance or intolerance to imatinib and other tyrosine kinase inhibitors. *Blood* 2014; **123**: 1309–1318.

62.   Hill BG, Kota VK, Khoury HJ. Bosutinib: A third generation tyrosine kinase inhibitor for the treatment of chronic myeloid leukemia. *Expert Rev Anticancer Ther* 2014; **14**: 765–770.

63.   Leach B. In CML, next-generation TKIs aim to boost outcomes. 2012. http://www.onclive.com/publications/oncology-live/2012/november-2012/in-cml-next-generation-tkis-aim-to-boost-outcomes (accessed 31 May 2016).

64.   Druker BJ, Lydon NB. Lessons learned from the development of an Abl tyrosine kinase inhibitor for chronic myelogenous leukemia. *J Clin Invest* 2000; **105**: 3–7.

65.   Manley PW, Cowan-Jacob SW, Mestan J. Advances in the structural biology, design and clinical development of Bcr-Abl kinase inhibitors for the treatment of chronic myeloid leukaemia. *Biochim Biophys Acta - Proteins Proteomics* 2005; **1754**: 3–13.

66.   O'Hare T, Zabriskie MS, Eiring AM *et al.* Pushing the limits of targeted therapy in chronic myeloid leukaemia. *Nat Rev Cancer* 2012; **12**: 513–526.

67.   Lin H, Chen M, Rothe K *et al.* Selective JAK2/ABL dual inhibition therapy effectively eliminates TKI-insensitive CML stem/progenitor cells. *Oncotarget* 2014; **5**: 1–15.

68.   Khan AM, Bixby DL. BCR-ABL inhibitors: Updates in the management of patients with chronic-phase chronic myeloid leukemia. *Hematology* 2013; **19**: 249–258.

69.   Baccarani M, Castagnetti F, Gugliotta G *et al.* Treatment recommendations for chronic myeloid leukemia. *Mediterr J Hematol Infect Dis* 2014; **6**: e2014005.

70.   Ernst T, Hochhaus A. Chronic myeloid leukemia: Clinical impact of BCR-ABL1 mutations and other lesions associated with disease progression. *Semin Oncol* 2012; **39**: 58–66.

71. O'Hare T, Walters DK, Stoffregen EP *et al.* In vitro activity of Bcr-Abl inhibitors AMN107 and BMS-354825 against clinically relevant imatinib-resistant Abl kinase domain mutants. *Cancer Res* 2005; **65**: 4500–4505.

72. Tokarski JS, Newitt JA, Chang CYJ *et al.* The structure of dasatinib (BMS-354825) bound to activated ABL kinase domain elucidates its inhibitory activity against imatinib-resistant ABL mutants. *Cancer Res* 2006; **66**: 5790–5797.

73. Jabbour E, Kantarjian HM, Saglio G *et al.* Early response with dasatinib or imatinib in chronic myeloid leukemia: 3-year follow-up from a randomized phase 3 trial (DASISION). *Blood* 2014; **123**: 494–500.

74. Larson RA, Hochhaus A, Hughes TP *et al.* Nilotinib vs imatinib in patients with newly diagnosed Philadelphia chromosome-positive chronic myeloid leukemia in chronic phase: ENESTnd 3-year follow-up. *Leukemia* 2012; **26**: 2197–2203.

75. Fausel C. Targeted chronic myeloid leukemia therapy: Seeking a cure. *Am J Heal Pharm* 2007; **64**: S9-15.

76. Gorre ME. Clinical resistance to STI-571 cancer therapy caused by BCR-ABL gene mutation or amplification. *Science* 2001; **293**: 876–880.

77. Vaidya S, Ghosh K, Vundinti BR. Recent developments in drug resistance mechanism in chronic myeloid leukemia: A review. *Eur J Haematol* 2011; **87**: 381–393.

78. Bixby D, Talpaz M. Mechanisms of resistance to tyrosine kinase inhibitors in chronic myeloid leukemia and recent therapeutic strategies to overcome resistance. *Hematology Am Soc Hematol Educ Program* 2009; 461–476.

79. Hughes T, Saglio G, Branford S *et al.* Impact of baseline BCR-ABL mutations on response to nilotinib in patients with chronic myeloid leukemia in chronic phase. *J Clin Oncol* 2009; **27**: 4204–4210.

80. Müller MC, Cortes JE, Kim DW *et al.* Dasatinib treatment of chronic-phase chronic myeloid leukemia: Analysis of responses according to preexisting BCR-ABL mutations. *Blood* 2009; **114**: 4944–4953.

81. Bethelmie-Bryan B, Lord K, Holloway S *et al.* Bosutinib treatment for Philadelphia chromosome-positive leukemias. *Futur Oncol* 2014; **10**: 179–185.

82. Khoury HJ, Cortes JE, Kantarjian HM *et al.* Bosutinib is active in chronic phase chronic myeloid leukemia after imatinib and dasatinib and/or nilotinib therapy failure. *Blood* 2012; **119**: 3403–3412.

83. Cortes JE, Kim DW, Pinilla-Ibarz J *et al.* A phase 2 trial of ponatinib in philadelphia

chromosome-positive leukemias. *N Engl J Med* 2013; **369**: 1783–1796.

84. O'Hare T, Shakespeare WC, Zhu X *et al.* AP24534, a pan-BCR-ABL inhibitor for chronic myeloid leukemia, potently inhibits the T315I mutant and overcomes mutation-based resistance. *Cancer Cell* 2009; **16**: 401–412.

85. Jabbour E, Branford S, Saglio G *et al.* Practical advice for determining the role of BCR-ABL mutations in guiding tyrosine kinase inhibitor therapy in patients with chronic myeloid leukemia. *Cancer* 2011; **117**: 1800–1811.

86. Nicolini FE, Ibrahim AR, Soverini S *et al.* The BCR-ABL T315I mutation compromises survival in chronic phase chronic myelogenous leukemia patients resistant to tyrosine kinase inhibitors, in a matched pair analysis. *Haematologica* 2013; **98**: 1510–1516.

87. Radich JP. Monitoring response to tyrosine kinase inhibitor therapy, mutational analysis, and new treatment options in chronic myelogenous leukemia. *J Natl Compr Canc Netw* 2013; **11**: 663–6.

88. Jabbour E, Cortes J, Santos FPS *et al.* Results of allogeneic hematopoietic stem cell transplantation for chronic myelogenous leukemia patients who failed tyrosine kinase inhibitors after developing BCR-ABL1 kinase domain mutations. *Blood* 2011; **117**: 3641–3647.

89. Larson RA, Druker BJ, Guilhot F *et al.* Imatinib pharmacokinetics and its correlation with response and safety in chronic-phase chronic myeloid leukemia: A subanalysis of the IRIS study. *Blood* 2008; **111**: 4022–4028.

90. Gréen H, Skoglund K, Rommel F *et al.* CYP3A activity influences imatinib response in patients with chronic myeloid leukemia: A pilot study on in vivo CYP3A activity. *Eur J Clin Pharmacol* 2010; **66**: 383–386.

91. White DL, Dang P, Engler J *et al.* Functional activity of the OCT-1 protein is predictive of long-term outcome in patients with chronic-phase chronic myeloid leukemia treated with imatinib. *J Clin Oncol* 2010; **28**: 2761–2767.

92. White DL, Saunders VA, Dang P *et al.* Most CML patients who have a suboptimal response to imatinib have low OCT-1 activity: Higher doses of imatinib may overcome the negative impact of low OCT-1 activity. *Blood* 2007; **110**: 4064–4072.

93. Gottesman MM. Mechanisms of cancer drug resistance. *Annu Rev Med* 2002; **53**: 615–627.

94. Burger H, Van Tol H, Brok M *et al.* Chronic imatinib mesylate exposure leads to reduced intracellular drug accumulation by induction of the ABCG2 (BCRP) and ABCB1 (MDR1) drug transport pumps. *Cancer Biol Ther* 2005; **4**: 747–752.

95. Dohse M, Scharenberg C, Shukla S *et al.* Comparison of ATP-binding cassette transporter

interactions with the tyrosine kinase inhibitors imatinib, nilotinib, and dasatinib. *Drug Metab Dispos* 2010; **38**: 1371–1380.

96. Stromskaya TP, Rybalkina EY, Kruglov SS *et al.* Role of P-glycoprotein in evolution of populations of chronic myeloid leukemia cells treated with imatinib. *Biochem* 2008; **73**: 29–37.

97. Gromicho M, Dinis J, Magalhaes M *et al.* Development of imatinib and dasatinib resistance: dynamics of expression of drug transporters ABCB1, ABCC1, ABCG2, MVP, and SLC22A1. *Leuk Lymphoma* 2011; **52**: 1980–1990.

98. Gromicho M, Magalhaes M, Torres F *et al.* Instability of mRNA expression signatures of drug transporters in chronic myeloid leukemia patients resistant to imatinib. *Oncol Rep* 2013; **29**: 741–750.

99. Naka K, Hoshii T, Hirao A. Novel therapeutic approach to eradicate tyrosine kinase inhibitor resistant chronic myeloid leukemia stem cells. *Cancer Sci* 2010; **101**: 1577–1581.

100. Rosi NL, Mirkin CA. Nanostructures in biodiagnostics. *Chem Rev* 2005; **105**: 1547–1562.

101. Farmer P, Frenk J, Knaul FM *et al.* Expansion of cancer care and control in countries of low and middle income: A call to action. *Lancet* 2010; **376**: 1186–1193.

102. Kanavos P. The rising burden of cancer in the developing world. *Ann Oncol* 2006; **17**: viii15-viii23.

103. Winn-Deen ES, Helton B, Van Atta R *et al.* Development of an integrated assay for detection of BCR-ABL RNA. *Clin Chem* 2007; **53**: 1593–1600.

104. Cayuela JM, Macintyre E, Darlington M *et al.* Cartridge-based automated BCR-ABL1 mRNA quantification: Solving the issues of standardization, at what cost? *Haematologica* 2011; **96**: 664–671.

105. Mattarucchi E, Spinelli O, Rambaldi A *et al.* Molecular monitoring of residual disease in chronic myeloid leukemia by genomic DNA compared with conventional mRNA analysis. *J Mol Diagn* 2009; **11**: 482–7.

106. Carella AM, Branford S, Deininger M *et al.* What challenges remain in chronic myeloid leukemia research? *Haematologica* 2013; **98**: 1168–1172.

107. Machova Polakova K, Kulvait V, Benesova A *et al.* Next-generation deep sequencing improves detection of BCR-ABL1 kinase domain mutations emerging under tyrosine kinase inhibitor treatment of chronic myeloid leukemia patients in chronic phase. *J Cancer Res Clin Oncol* 2015; **141**: 887–899.

108. Schmidt M, Rinke J, Schäfer V *et al.* Molecular-defined clonal evolution in patients with chronic myeloid leukemia independent of the BCR-ABL status. *Leukemia* 2014; **28**: 2292–2299.

109. Becich M, Santana-Santos L, Gullapalli R *et al.* Next generation sequencing in clinical medicine: Challenges and lessons for pathology and biomedical informatics. *J Pathol Inform* 2012; **3**: 40.

110. Hughes T, Deininger M, Hochhaus A *et al.* Monitoring CML patients responding to treatment with tyrosine kinase inhibitors: Review and recommendations for harmonizing current methodology for detecting BCR-ABL transcripts and kinase domain mutations and for expressing results. *Blood* 2006; **108**: 28–37.

111. Soverini S, De Benedittis C, Polakova KM *et al.* Unraveling the complexity of tyrosine kinase inhibitor-resistant populations by ultra-deep sequencing of the BCR-ABL kinase domain. *Blood* 2013; **122**: 1634–1648.

112. Parker WT, Ho M, Scott HS *et al.* Poor response to second-line kinase inhibitors in chronic myeloid leukemia patients with multiple low-level mutations, irrespective of their resistance profile. *Blood* 2012; **119**: 2234–2238.

113. Mahon FX, Réa D, Guilhot J *et al.* Discontinuation of imatinib in patients with chronic myeloid leukaemia who have maintained complete molecular remission for at least 2 years: the prospective, multicentre Stop Imatinib (STIM) trial. *Lancet Oncol* 2010; **11**: 1029–1035.

114. Shibata Y, Malhotra A, Dutta A. Detection of DNA fusion junctions for BCR-ABL translocations by Anchored ChromPET. *Genome Med* 2010; **2**: 70.

115. Salto-Tellez M, Shelat SG, Benoit B *et al.* Multiplex RT-PCR for the detection of leukemia-associated translocations: validation and application to routine molecular diagnostic practice. *J Mol Diagn* 2003; **5**: 231–236.

116. Park JS, Yi JW, Jeong SH *et al.* Comparison of multiplex reverse transcription polymerase chain reaction and conventional cytogenetics as a diagnostic strategy for acute leukemia. *Int J Lab Hematol* 2008; **30**: 513–518.

117. Choi H-J, Kim H-R, Shin M-G *et al.* Spectra of chromosomal aberrations in 325 leukemia patients and implications for the development of new molecular detection systems. *J Korean Med Sci* 2011; **26**: 886–92.

118. Song M-J, Kim H-J, Park C-H *et al.* Diagnostic utility of a multiplex RT-PCR assay in detecting fusion transcripts from recurrent genetic abnormalities of acute leukemia by WHO 2008 classification. *Diagnostic Mol Pathol* 2012; **21**: 40–44.

119. Jennings LJ, George D, Czech J *et al.* Detection and quantification of BCR-ABL1 fusion transcripts by droplet digital PCR. *J Mol Diagnostics* 2014; **16**: 174–179.

120. Lee AC, Du D, Chen B *et al.* Electrochemical detection of leukemia oncogenes using enzyme-

loaded carbon nanotube labels. *Analyst* 2014; **139**: 4223–4230.

121. Liu A, Sun Z, Wang K *et al.* Molecular beacon-based fluorescence biosensor for the detection of gene fragment and PCR amplification products related to chronic myelogenous leukemia. *Anal Bioanal Chem* 2012; **402**: 805–812.

122. Cordeiro M, Giestas L, Lima JC *et al.* BioCode gold-nanobeacon for the detection of fusion transcripts causing chronic myeloid leukemia. *J Nanobiotechnology* 2016; **14**: 38.

123. Conde J, de la Fuente JM, Baptista PV. RNA quantification using gold nanoprobes - Application to cancer diagnostics. *J Nanobiotechnology* 2010; **8**: 5.

124. Conde J, Doria G, De La Fuente JM *et al.* RNA quantification using noble metal nanoprobes: Simultaneous identification of several different mrna targets using color multiplexing and application to cancer diagnostics. *Methods Mol Biol* 2012; **906**: 71–87.

125. Baptista PV. RNA quantification with gold nanoprobes for cancer diagnostics. *Clin Lab Med* 2012; **32**: 1–13.

126. Rosso V, Bracco E, Pedrola R *et al.* Detection of BCR-ABL T315I mutation by peptide nucleic acid directed PCR clamping and by peptide nucleic acid FISH. *Biomark Res* 2015; **3**: 15.

127. Langabeer SE, Gale RE, Harvey RC *et al.* Transcription-mediated amplification and hybridisation protection assay to determine BCR-ABL transcript levels in patients with chronic myeloid leukaemia. *Leukemia* 2002; **16**: 393–399.

128. Hong S-H, Kim J Il, Kang H *et al.* Detection and quantification of the Bcr/Abl chimeric protein on biochips using LDI-TOF MS. *Chem Commun* 2014; **50**: 4831.

129. Yang TY, Eissler CL, Hall MC *et al.* A multiple reaction monitoring (MRM) method to detect Bcr-Abl kinase activity in CML using a peptide biosensor. *PLoS One* 2013; **8**: 1–10.

130. Tong WG, Sandhu VK, Wood BL *et al.* Correlation between peripheral blood and bone marrow regarding FLT3-ITD and NPM1 mutational status in patients with acute myeloid leukemia. *Haematologica* 2015; **100**: e97-8.

131. Rezaei A, Adib M, Mokarian F *et al.* Leukemia markers expression of peripheral blood vs bone marrow blasts using flow cytometry. *Med Sci Monit* 2003; **9**: CR359-62.

132. Ranuncolo SM. Liquid biopsy in liquid tumors. *J Cancer Ther* 2017; **8**: 302–320.

133. Zhang W, Xia W, Lv Z *et al.* Liquid biopsy for cancer: Circulating tumor cells, circulating free DNA or exosomes? *Cell Physiol Biochem* 2017; **41**: 755–768.

134. Buder A, Tomuta C, Filipits M. The potential of liquid biopsies. *Curr Opin Oncol* 2016; **28**: 130–134.

135. Gomes LC, Evangelista FCG, Sousa LP de *et al.* Prognosis biomarkers evaluation in chronic lymphocytic leukemia. *Hematol Oncol Stem Cell Ther* 2017; **10**: 57–62.

136. Boyiadzis M, Whiteside TL. The emerging roles of tumor-derived exosomes in hematological malignancies. *Leukemia* 2017; **31**: 1259–1268.

137. Kumar B, Garcia M, Murakami JL *et al.* Exosome-mediated microenvironment dysregulation in leukemia. *Biochim Biophys Acta - Mol Cell Res* 2016; **1863**: 464–470.

138. Raimondo S, Corrado C, Raimondi L *et al.* Role of extracellular vesicles in hematological malignancies. *Biomed Res Int* 2015; **2015**: 821613.

139. Kantarjian H, O'Brien S, Jabbour E *et al.* Improved survival in chronic myeloid leukemia since the introduction of imatinib therapy: A single-institution historical experience. *Blood* 2012; **119**: 1981–1987.

140. Björkholm M, Ohm L, Eloranta S *et al.* Success story of targeted therapy in chronic myeloid leukemia: A population-based study of patients diagnosed in Sweden from 1973 to 2008. *J Clin Oncol* 2011; **29**: 2514–2520.

141. Mahon F-X. Is going for cure in chronic myeloid leukemia possible and justifiable? *ASH Educ Progr B* 2012; **2012**: 122–128.

142. Ross DM, Branford S, Seymour JF *et al.* Safety and efficacy of imatinib cessation for CML patients with stable undetectable minimal residual disease: Results from the TWISTER study. *Blood* 2013; **122**: 515–522.

143. Wilda M, Fuchs U, Wössmann W *et al.* Killing of leukemic cells with a BCR/ABL fusion gene by RNA interference (RNAi). *Oncogene* 2002; **21**: 5716–5724.

144. Koldehoff M, Elmaagacli AH. Therapeutic targeting of gene expression by siRNAs directed against BCR-ABL transcripts in a patient with imatinib-resistant chronic myeloid leukemia. *Methods Mol Biol* 2009; **487**: 451–466.

145. Guo J, Cahill MR, McKenna SL *et al.* Biomimetic nanoparticles for siRNA delivery in the treatment of leukaemia. *Biotechnol Adv* 2014; **32**: 1396–1409.

146. Kim JE, Yoon S, Choi B-R *et al.* Cleavage of BCR–ABL transcripts at the T315I point mutation by DNAzyme promotes apoptotic cell death in imatinib-resistant BCR–ABL leukemic cells. *Leukemia* 2013; **27**: 1650–1658.

147. Cabral RM, Baptista PV. Anti-cancer precision theranostics : A focus on multifunctional gold nanoparticles. *Expert Rev Mol Diagn* 2014; **14**: 1041–1052.

148. Pedrosa P, Vinhas R, Fernandes A *et al.* Gold nanotheranostics: Proof-of-concept or clinical tool? *Nanomaterials* 2015; **5**: 1853–1879.

149. Vinhas R, Cordeiro M, Mendo S *et al.* Gold nanoparticle-based theranostics: disease diagnostics and treatment using a single nanomaterial. *Nanobiosensors Dis Diagnosis* 2015; **4**: 11–23.

150. Friedman AA, Letai A, Fisher DE *et al.* Precision medicine for cancer with next-generation functional diagnostics. *Nat Rev Cancer* 2015; **15**: 747–756.

151. Zaimy M, Saffarzadeh N, Mohammadi A *et al.* New methods in the diagnosis of cancer and gene therapy of cancer based on nanoparticles. *Cancer Gene Ther* 2017; **24**: 233–243.

152. Hasan S. A review on nanoparticles: Their synthesis and types. *Res J Recent Sci* 2015; **4**: 9–11.

153. Tatar AS, Nagy-Simon T, Tomuleasa C *et al.* Nanomedicine approaches in acute lymphoblastic leukemia. *J Control Release* 2016; **238**: 123–138.

154. Nikalje AP. Nanotechnology and its applications in medicine. *Med Chem* 2015; **5**: 81–89.

155. Mendes R, Carreira B, Baptista PV *et al.* Non-small cell lung cancer biomarkers and targeted therapy - Two faces of the same coin fostered by nanotechnology. *Expert Rev Precis Med Drug Dev* 2016; **1**: 155–168.

156. Tinkle S, Mcneil SE, Mühlebach S *et al.* Nanomedicines: Addressing the scientific and regulatory gap. *Ann N Y Acad Sci* 2014; **1313**: 35–56.

157. Perfézou M, Turner A, Merkoçi A. Cancer detection using nanoparticle-based sensors. *Chem Soc Rev* 2012; **41**: 2606–2622.

158. Thaxton CS, Georganopoulou DG, Mirkin CA. Gold nanoparticle probes for the detection of nucleic acid targets. *Clin Chim Acta* 2006; **363**: 120–126.

159. Baptista PV, Koziol-Montewka M, Paluch-Oles J *et al.* Gold-nanoparticle-probe-based assay for rapid and direct detection of Mycobacterium tuberculosis DNA in clinical samples. *Clin Chem* 2006; **52**: 1433–1434.

160. Baptista P, Doria G, Henriques D *et al.* Colorimetric detection of eukaryotic gene expression with DNA-derivatized gold nanoparticles. *J Biotechnol* 2005; **119**: 111–117.

161. Hutter E, Fendler JH. Exploitation of localized surface plasmon resonance. *Adv Mater* 2004; **16**: 1685–1706.

162. Murphy CJ, Sau TK, Gole AM *et al.* Anisotropic metal nanoparticles: Synthesis, assembly, and optical applications. *J Phys Chem B* 2005; **109**: 13857–13870.

163. Liz-Marzán LM. Tailoring surface plasmons through the morphology and assembly of metal nanoparticles. *Langmuir* 2006; **22**: 32–41.

164. Doria G, Conde J, Veigas B *et al.* Noble metal nanoparticles for biosensing applications. *Sensors* 2012; **12**: 1657–1687.

165. Baptista P, Pereira E, Eaton P *et al.* Gold nanoparticles for the development of clinical diagnosis methods. *Anal Bioanal Chem* 2008; **391**: 943–950.

166. Richards R, Bönnemann H. Synthetic Approaches to Metallic Nanomaterials. In: *Nanofabrication Towards Biomedical Applications: Techniques, Tools, Applications, and Impact*. 2005, pp 1–32.

167. Ghosh SK, Pal T. Interparticle coupling effect on the surface plasmon resonance of gold nanoparticles: From theory to applications. *Chem Rev* 2007; **107**: 4797–4862.

168. Bönnemann H, Richards RM. Nanoscopic metal particles - Synthetic methods and potential applications. *Eur J Inorg Chem* 2001; **2001**: 2455–2480.

169. Veigas B, Fortunato E, Baptista PV. Mobile based gold nanoprobe TB diagnostics for point-of-need. *Methods Mol Biol* 2015; **1256**: 41–56.

170. Turkevich J, Stevenson PC, Hillier J. A study of the nucleation and growth processes in the synthesis of colloidal gold. *Discuss Faraday Soc* 1951; **11**: 55.

171. Frens G. Controlled nucleation for the regulation of the particle size in monodisperse gold suspensions. *Nat Phys Sci* 1973; **241**: 20–22.

172. Lee PC, Meisel D. Adsorption and surface-enhanced Raman of dyes on silver and gold sols. *J Phys Chem* 1982; **86**: 3391–3395.

173. Ji X, Song X, Li J *et al.* Size control of gold nanocrystals in citrate reduction: The third role of citrate. *J Am Chem Soc* 2007; **129**: 13939–13948.

174. Kumar D, Meenan BJ, Mutreja I *et al.* Controlling the size and size distribution of gold nanoparticles: A design of experiment study. *Int J Nanosci* 2012; **11**: 1250023.

175. Brust M, Walker M, Bethell D *et al.* Synthesis of thiol-derivatised gold nanoparticles in a two-phase Liquid–Liquid system. *J Chem Soc, Chem Commun* 1994; **7**: 801–802.

176. Ackerson CJ, Jadzinsky PD, Kornberg RD. Thiolate ligands for synthesis of water-soluble gold clusters. *J Am Chem Soc* 2005; **127**: 6550–6551.

177. Jana NR, Gearheart L, Murphy CJ. Seeding growth for size control of 5-40 nm diameter gold nanoparticles. *Langmuir* 2001; **17**: 6782–6786.

178. Conde J, Ambrosone A, Hernandez Y *et al.* 15 years on siRNA delivery: Beyond the State-of-the-Art on inorganic nanoparticles for RNAi therapeutics. *Nano Today* 2015; **10**: 421–450.

179. Silva SN, Gil OM, Oliveira VC *et al.* Association of polymorphisms in ERCC2 gene with non-familial thyroid cancer risk. *Cancer Epidemiol Biomarkers Prev* 2005; **14**: 2407–2412.

180. Hung RJ, Hall J, Brennan P *et al.* Genetic polymorphisms in the base excision repair pathway

and cancer risk: A HuGE review. *Am J Epidemiol* 2005; **162**: 925–942.

181.   Kavvoura FK, Ioannidis JPA. CTLA-4 gene polymorphisms and susceptibility to type 1 diabetes mellitus: A HuGE review and meta-analysis. *Am J Epidemiol* 2005; **162**: 3–16.

182.   Szolnoki Z, Melegh B. Gene-gene and gene-environment interplay represent specific susceptibility for different types of ischaemic stroke and leukoaraiosis. *Curr Med Chem* 2006; **13**: 1627–1634.

183.   Yong WP, Innocenti F, Ratain MJ. The role of pharmacogenetics in cancer therapeutics. *Br J Clin Pharmacol* 2006; **62**: 35–46.

184.   Wang L, McLeod HL, Weinshilboum RM. Genomics and drug response. *N Engl J Med* 2011; **364**: 1144–1153.

185.   Leroy Q, Raoult D. Review of microarray studies for host-intracellular pathogen interactions. *J Microbiol Methods* 2010; **81**: 81–95.

186.   Sato K, Hosokawa K, Maeda M. Rapid aggregation of gold nanoparticles induced by non-cross-linking DNA hybridization. *J Am Chem Soc* 2003; **125**: 8102–8103.

187.   Mirkin CA, Letsinger RL, Mucic RC *et al.* A DNA-based method for rationally assembling nanoparticles into macroscopic materials. *Nature* 1996; **382**: 607–609.

188.   Storhoff JJ, Elghanian R, Mucic RC *et al.* One-pot colorimetric differentiation of polynucleotides with single base imperfections using gold nanoparticle probes. *J Am Chem Soc* 1998; **120**: 1959–1964.

189.   Larguinho M, Baptista PV. Gold and silver nanoparticles for clinical diagnostics - From genomics to proteomics. *J Proteomics* 2012; **75**: 2811–2823.

190.   Liu J, Lu Y. Fast colorimetric sensing of adenosine and cocaine based on a general sensor design involving aptamers and nanoparticles. *Angew Chemie - Int Ed* 2005; **45**: 90–94.

191.   Sato K, Hosokawa K, Maeda M. Non-cross-linking gold nanoparticle aggregation as a detection method for single-base substitutions. *Nucleic Acids Res* 2005; **33**: e4.

192.   Costa P, Amaro A, Botelho A *et al.* Gold nanoprobe assay for the identification of mycobacteria of the Mycobacterium tuberculosis complex. *Clin Microbiol Infect* 2010; **16**: 1464–1469.

193.   Doria G, Franco R, Baptista P. Nanodiagnostics: fast colorimetric method for single nucleotide polymorphism/mutation detection. *IET Nanobiotechnol* 2007; **1**: 53–57.

194.   Padmavathy B, Vinoth Kumar R, Jaffar Ali BM. A direct detection of Escherichia coli genomic DNA using gold nanoprobes. *J Nanobiotechnology* 2012; **10**: 8.

195.   Liandris E, Gazouli M, Andreadou M *et al.* Direct detection of unamplified DNA from

pathogenic mycobacteria using DNA-derivatized gold nanoparticles. *J Microbiol Methods* 2009; **78**: 260–264.

196. Stakenborg T, Peeters S, Reekmans G *et al.* Increasing the stability of DNA-functionalized gold nanoparticles using mercaptoalkanes. *J Nanoparticle Res* 2008; **10**: 143–152.

197. Duguid JG, Bloomfield VA. Aggregation of melted DNA by divalent metal ion-mediated cross-linking. *Biophys J* 1995; **69**: 2642–2648.

198. Doria G. *DNA Nanoprobes for Molecular Detection [PhD thesis]*. Universidade Nova de Lisboa 2010.

199. Doria G, Baumgartner BG, Franco R *et al.* Optimizing Au-nanoprobes for specific sequence discrimination. *Colloids Surf B Biointerfaces* 2010; **77**: 122–124.

200. Lytton-Jean AKR, Mirkin CA. A thermodynamic investigation into the binding properties of DNA functionalized gold nanoparticle probes and molecular fluorophore probes. *J Am Chem Soc* 2005; **127**: 12754–12755.

201. Larguinho M, Santos S, Almeida J *et al.* DNA adduct identification using gold-aptamer nanoprobes. *IET Nanobiotechnology* 2015; **9**: 95–101.

202. Baca JT, Severns V, Lovato D *et al.* Rapid detection of Ebola virus with a reagent-free, point-of-care biosensor. *Sensors* 2015; **15**: 8605–8614.

203. Carter JR, Balaraman V, Kucharski CA *et al.* A novel dengue virus detection method that couples DNAzyme and gold nanoparticle approaches. *Virol J* 2013; **10**: 201.

204. Baptista PV. Nanodiagnostics: leaving the research lab to enter the clinics? *Diagnosis* 2014; **1**: 305–309.

205. Veigas B, Branquinho R, Pinto JV *et al.* Ion sensing (EIS) real-time quantitative monitorization of isothermal DNA amplification. *Biosens Bioelectron* 2014; **52**: 50–55.

206. Larguinho M, Canto R, Cordeiro M *et al.* Gold nanoprobe-based non-crosslinking hybridization for molecular diagnostics. *Expert Rev Mol Diagn* 2015; **15**: 1355–1368.

207. Veigas B, Machado D, Perdigão J *et al.* Au-nanoprobes for detection of SNPs associated with antibiotic resistance in Mycobacterium tuberculosis. *Nanotechnology* 2010; **21**: 415101.

208. Veigas B, Pedrosa P, Couto I *et al.* Isothermal DNA amplification coupled to Au-nanoprobes for detection of mutations associated to Rifampicin resistance in Mycobacterium tuberculosis. *J Nanobiotechnology* 2013; **11**: 1–6.

209. Pedrosa P, Veigas B, Machado D *et al.* Gold nanoprobes for multi loci assessment of multi-drug resistant tuberculosis. *Tuberculosis* 2014; **94**: 332–337.

210. Mollasalehi H, Yazdanparast R. Non-crosslinking gold nanoprobes for detection of nucleic acid sequence-based amplification products. *Anal Biochem* 2012; **425**: 91–95.

211. Doria G, Larguinho M, Dias JT *et al.* Gold-silver-alloy nanoprobes for one-pot multiplex DNA detection. *Nanotechnology* 2010; **21**: 255101.

212. Carlos FF, Flores O, Doria G *et al.* Characterization of genomic SNP via colorimetric detection using a single gold nanoprobe. *Anal Biochem* 2014; **12**: 2–5.

213. Yuan Y, Zhang J, Zhang H *et al.* Label-free colorimetric immunoassay for the simple and sensitive detection of neurogenin3 using gold nanoparticles. *Biosens Bioelectron* 2011; **26**: 4245–4248.

214. Mazumdar D, Liu J, Lu G *et al.* Easy-to-use dipstick tests for detection of lead in paints using non-cross-linked gold nanoparticle-DNAzyme conjugates. *Chem Commun* 2010; **46**: 1416–1418.

215. Wu J, Li L, Zhu D *et al.* Colorimetric assay for mercury (II) based on mercury-specific deoxyribonucleic acid-functionalized gold nanoparticles. *Anal Chim Acta* 2011; **694**: 115–119.

216. Gao ZF, Song WW, Luo HQ *et al.* Detection of mercury ions (II) based on non-cross-linking aggregation of double-stranded DNA modified gold nanoparticles by resonance Rayleigh scattering method. *Biosens Bioelectron* 2015; **65**: 360–365.

217. Kiechle FL, Holland CA. Point-of-Care testing and molecular diagnostics: Miniaturization required. *Clin Lab Med* 2009; **29**: 555–560.

218. Ríos Á, Zougagh M, Avila M. Miniaturization through lab-on-a-chip: Utopia or reality for routine laboratories? A review. *Anal Chim Acta* 2012; **740**: 1–11.

219. Sato Y, Hosokawa K, Maeda M. Detection of non-cross-linking interaction between DNA-modified gold nanoparticles and a DNA-modified flat gold surface using surface plasmon resonance imaging on a microchip. *Colloids Surf B Biointerfaces* 2008; **62**: 71–76.

220. Bernacka-Wojcik I, Lopes P, Catarina Vaz A *et al.* Bio-microfluidic platform for gold nanoprobe based DNA detection-application to Mycobacterium tuberculosis. *Biosens Bioelectron* 2013; **48**: 87–93.

221. Veigas B, Jacob JM, Costa MN *et al.* Gold on paper–paper platform for Au-nanoprobe TB detection. *Lab Chip* 2012; **12**: 4802–4808.

222. Lammers T, Kiessling F, Hennink WE *et al.* Drug targeting to tumors: Principles, pitfalls and (pre-) clinical progress. *J Control Release* 2012; **161**: 175–187.

223. Martins P, Marques M, Coito L *et al.* Organometallic compounds in cancer therapy: past lessons and future directions. *Anticancer Agents Med Chem* 2014; **14**: 1199–1212.

224. Cole JT, Holland NB. Multifunctional nanoparticles for use in theranostic applications. *Drug Deliv Transl Res* 2015; **5**: 295–309.

225. Sharma H, Mishra PK, Talegaonkar S *et al.* Metal nanoparticles: A theranostic nanotool against cancer. *Drug Discov Today* 2015; **20**: 1143–1151.

226. Kojima R, Aubel D, Fussenegger M. Novel theranostic agents for next-generation personalized medicine: Small molecules, nanoparticles, and engineered mammalian cells. *Curr Opin Chem Biol* 2015; **28**: 29–38.

227. Hee J, Lee S, Son S *et al.* Theranostic nanoparticles for future personalized medicine. *J Control Release* 2014; **190**: 477–484.

228. Dreifuss T, Betzer O, Shilo M *et al.* A challenge for theranostics: Is the optimal particle for therapy also optimal for diagnostics? *Nanoscale* 2015; **7**: 15175–15184.

229. Kim HJ, Lee SM, Park KH *et al.* Drug-loaded gold/iron/gold plasmonic nanoparticles for magnetic targeted chemo-photothermal treatment of rheumatoid arthritis. *Biomaterials* 2015; **61**: 95–102.

230. Prabhu P, Patravale V. The upcoming field of theranostic nanomedicine: An overview. *J Biomed Nanotechnol* 2012; **8**: 859–882.

231. Sharma PA, Maheshwari R, Tekade M *et al.* Nanomaterial based approaches for the diagnosis and therapy of cardiovascular diseases. *Curr Pharm Des* 2015; **21**: 4465–4478.

232. Muthu MS, Mei L, Feng S-S. Nanotheranostics: advanced nanomedicine for the integration of diagnosis and therapy. *Nanomedicine* 2014; **9**: 1277–1280.

233. Frank D, Tyagi C, Tomar L *et al.* Overview of the role of nanotechnological innovations in the detection and treatment of solid tumors. *Int J Nanomedicine* 2014; **9**: 589–613.

234. Baptista P. Could gold nanoprobes be an important tool in cancer diagnostics? *Expert Rev Mol Diagn* 2012; **12**: 541–543.

235. Shah M, Badwaik VD, Dakshinamurthy R. Biological applications of gold nanoparticles. *J Nanosci Nanotechnol* 2014; **14**: 344–362.

236. Grzelczak M, Pérez-Juste J, Mulvaney P *et al.* Shape control in gold nanoparticle synthesis. *Chem Soc Rev* 2008; **37**: 1783–1791.

237. Kawamura G, Nogami M, Matsuda A. Shape-controlled metal nanoparticles and their assemblies with optical functionalities. *J Nanomater* 2013; **2013**: 631350.

238. Sajanlal PR, Sreeprasad TS, Samal AK *et al.* Anisotropic nanomaterials: structure, growth, assembly, and functions. *Nano Rev* 2011; **2**: 5883.

239. Mendes R, Pedrosa P, Lima JC *et al.* Photothermal enhancement of chemotherapy in breast cancer by visible irradiation of Gold Nanoparticles. *Sci Rep* 2017; **7**: 10872.

240. You J, Zhang G, Li C. Exceptionally high payload of doxorubicin in hollow gold nanospheres for near-infrared light-triggered drug release. *ACS Nano* 2010; **4**: 1033–1041.

241. Conde J, Larguinho M, Cordeiro A *et al.* Gold-nanobeacons for gene therapy: evaluation of genotoxicity, cell toxicity and proteome profiling analysis. *Nanotoxicology* 2014; **8**: 521–532.

242. Mironava T, Hadjiargyrou M, Simon M *et al.* Gold nanoparticles cellular toxicity and recovery: Effect of size, concentration and exposure time. *Nanotoxicology* 2010; **4**: 120–137.

243. Fernandes AR, Jesus J, Martins P *et al.* Multifunctional gold-nanoparticles: A nanovectorization tool for the targeted delivery of novel chemotherapeutic agents. *J Control Release* 2017; **245**: 52–61.

244. Soenen SJ, Parak WJ, Rejman J *et al.* (Intra)cellular stability of inorganic nanoparticles: Effects on cytotoxicity, particle functionality, and biomedical applications. *Chem Rev* 2015; **115**: 2109–2135.

245. Nazarenus M, Zhang Q, Soliman MG *et al.* In vitro interaction of colloidal nanoparticles with mammalian cells: What have we learned thus far? *Beilstein J Nanotechnol* 2014; **5**: 1477–1490.

246. Zhang XD, Wu HY, Wu D *et al.* Toxicologic effects of gold nanoparticles in vivo by different administration routes. *Int J Nanomedicine* 2010; **5**: 771–781.

247. Favi PM, Gao M, Johana Sepúlveda Arango L *et al.* Shape and surface effects on the cytotoxicity of nanoparticles: Gold nanospheres versus gold nanostars. *J Biomed Mater Res A* 2015; **103**: 3449–3462.

248. Sultana S, Djaker N, Boca-Farcau S *et al.* Comparative toxicity evaluation of flower-shaped and spherical gold nanoparticles on human endothelial cells. *Nanotechnology* 2015; **26**: 55101.

249. Chu Z, Zhang S, Zhang B *et al.* Unambiguous observation of shape effects on cellular fate of nanoparticles. *Sci Rep* 2015; **4**: 4495.

250. Gerber A, Bundschuh M, Klingelhofer D *et al.* Gold nanoparticles: recent aspects for human toxicology. *J Occup Med Toxicol* 2013; **8**: 32.

251. Yildirimer L, Thanh NTK, Loizidou M *et al.* Toxicological considerations of clinically applicable nanoparticles. *Nano Today* 2011; **6**: 585–607.

252. Nel AE, Parak WJ, Chan WCW *et al.* Where are we heading in nanotechnology environmental health and safety and materials characterization? *ACS Nano* 2015; **9**: 5627–5630.

253. Alkilany AM, Murphy CJ. Toxicity and cellular uptake of gold nanoparticles: What we have

learned so far? *J Nanoparticle Res* 2010; **12**: 2313–2333.

254. Maldiney T, Richard C, Seguin J *et al.* Effect of core diameter, surface coating, and PEG chain length on the biodistribution of persistent luminescence nanoparticles in mice. *ACS Nano* 2011; **5**: 854–862.

255. Zhao J, Feng SS. Effects of PEG tethering chain length of vitamin E TPGS with a Herceptin-functionalized nanoparticle formulation for targeted delivery of anticancer drugs. *Biomaterials* 2014; **35**: 3340–3347.

256. Conde JJ, Dias JT, Grazú V *et al.* Revisiting 30 years of biofunctionalization and surface chemistry of inorganic nanoparticles for nanomedicine. *Front Chem* 2014; **2**: 48.

257. Yu MMK, Park J, Jon S. Targeting strategies for multifunctional nanoparticles in cancer imaging and therapy. *Theranostics* 2012; **2**: 3–44.

258. Dreaden EC, Austin LA, Mackey M a *et al.* Size matters: gold nanoparticles in targeted cancer drug delivery. *Ther Deliv* 2012; **3**: 457–478.

259. Kobayashi H, Watanabe R, Choyke PL. Improving conventional enhanced permeability and retention (EPR) effects; What is the appropriate target? *Theranostics* 2014; **4**: 81–89.

260. Maeda H. Macromolecular therapeutics in cancer treatment: The EPR effect and beyond. *J Control Release* 2012; **164**: 138–144.

261. Chanda N, Kattumuri V, Shukla R *et al.* Bombesin functionalized gold nanoparticles show in vitro and in vivo cancer receptor specificity. *Proc Natl Acad Sci* 2010; **107**: 8760–8765.

262. Chen H, Zhang X, Dai S *et al.* Multifunctional gold nanostar conjugates for tumor imaging and combined photothermal and chemo-therapy. *Theranostics* 2013; **3**: 633–649.

263. Ruan S, He Q, Gao H. Matrix metalloproteinase triggered size-shrinkable gelatin-gold fabricated nanoparticles for tumor microenvironment sensitive penetration and diagnosis of glioma. *Nanoscale* 2015; **7**: 9487–9496.

264. Conde J, Tian F, Hernández Y *et al.* In vivo tumor targeting via nanoparticle-mediated therapeutic siRNA coupled to inflammatory response in lung cancer mouse models. *Biomaterials* 2013; **34**: 7744–7753.

265. Choi CHJ, Alabi CA, Webster P *et al.* Mechanism of active targeting in solid tumors with transferrin-containing gold nanoparticles. *Proc Natl Acad Sci USA* 2010; **107**: 1235–40.

266. Ahmed M, Pan DW, Davis ME. Lack of in vivo antibody dependent cellular cytotoxicity with antibody containing gold nanoparticles. *Bioconjug Chem* 2015; **26**: 812–816.

267. Qian Y, Qiu M, Wu Q *et al.* Enhanced cytotoxic activity of cetuximab in EGFR-positive lung

cancer by conjugating with gold nanoparticles. *Sci Rep* 2014; **4**: 7490.

268. Kao H-W, Lin Y-Y, Chen C-C *et al.* Biological characterization of cetuximab-conjugated gold nanoparticles in a tumor animal model. *Nanotechnology* 2014; **25**: 295102.

269. Conde J, Bao C, Cui D *et al.* Antibody-drug gold nanoantennas with Raman spectroscopic fingerprints for in vivo tumour theranostics. *J Control Release* 2014; **183**: 87–93.

270. Lukianova-Hleb EY, Ren X, Sawant RR *et al.* On-demand intracellular amplification of chemoradiation with cancer-specific plasmonic nanobubbles. *Nat Med* 2014; **20**: 778–784.

271. Van De Broek B, Devoogdt N, Dhollander A *et al.* Specific cell targeting with nanobody conjugated branched gold nanoparticles for photothermal therapy. *ACS Nano* 2011; **5**: 4319–4328.

272. Topete A, Alatorre-Meda M, Iglesias P *et al.* Fluorescent drug-loaded, polymeric-based, branched gold nanoshells for localized multimodal therapy and imaging of tumoral cells. *ACS Nano* 2014; **8**: 2725–2738.

273. Topete A, Alatorre-Meda M, Villar-Alvarez EM *et al.* Polymeric-gold nanohybrids for combined imaging and cancer therapy. *Adv Healthc Mater* 2014; **3**: 1309–1325.

274. Zhong J, Wen L, Yang S *et al.* Imaging-guided high-efficient photoacoustic tumor therapy with targeting gold nanorods. *Nanomedicine Nanotechnology, Biol Med* 2015; **11**: 1499–1509.

275. Cheng J, Gu Y-J, Cheng SH *et al.* Surface functionalized gold nanoparticles for drug delivery. *J Biomed Nanotechnol* 2013; **9**: 1362–1369.

276. Lu W, Zhang G, Zhang R *et al.* Tumor site-specific silencing of NF-κB p65 by targeted hollow gold nanosphere-mediated photothermal transfection. *Cancer Res* 2010; **70**: 3177–3188.

277. Chiche J, Brahimi-Horn MC, Pouysségur J. Tumour hypoxia induces a metabolic shift causing acidosis: A common feature in cancer. *J Cell Mol Med* 2010; **14**: 771–794.

278. Arachchige MCM, Reshetnyak YK, Andreev OA. Advanced targeted nanomedicine. *J Biotechnol* 2015; **202**: 88–97.

279. Antosh MP, Wijesinghe DD, Shrestha S *et al.* Enhancement of radiation effect on cancer cells by gold-pHLIP. *Proc Natl Acad Sci* 2015; **112**: 5372–5376.

280. Chen J, Glaus C, Laforest R *et al.* Gold nanocages as photothermal transducers for cancer treatment. *Small* 2010; **6**: 811–817.

281. Yavuz MS, Cheng Y, Chen J *et al.* Gold nanocages covered by smart polymers for controlled release with near-infrared light. *Nat Mater* 2009; **8**: 935–939.

282. Lee JH, Chen KJ, Noh SH *et al.* On-demand drug release system for in vivo cancer treatment

through self-assembled magnetic nanoparticles. *Angew Chemie - Int Ed* 2013; **52**: 4384–4388.

283. Hughes JP, Rees SS, Kalindjian SB *et al.* Principles of early drug discovery. *Br J Pharmacol* 2011; **162**: 1239–1249.

284. Silverman JA, Deitcher SR. Marqibo® (vincristine sulfate liposome injection) improves the pharmacokinetics and pharmacodynamics of vincristine. *Cancer Chemother Pharmacol* 2013; **71**: 555–564.

285. Koudelka S, Turánek J. Liposomal paclitaxel formulations. *J Control Release* 2012; **163**: 322–334.

286. Stathopoulos GP. Liposomal cisplatin: a new cisplatin formulation. *Anticancer Drugs* 2010; **21**: 732–736.

287. Slingerland M, Guchelaar HJ, Gelderblom H. Liposomal drug formulations in cancer therapy: 15 years along the road. *Drug Discov Today* 2012; **17**: 160–166.

288. Corvo MLL, Mendo AS, Figueiredo S *et al.* Liposomes as delivery system of a Sn(IV) complex for cancer therapy. *Pharm Res* 2016; **33**: 1351–1358.

289. Zhang X, Teodoro JG, Nadeau JL. Intratumoral gold-doxorubicin is effective in treating melanoma in mice. *Nanomedicine Nanotechnology, Biol Med* 2015; **11**: 1365–1375.

290. Chen H, Li S, Li B *et al.* Folate-modified gold nanoclusters as near-infrared fluorescent probes for tumor imaging and therapy. *Nanoscale* 2012; **4**: 6050.

291. Jing L, Liang X, Li X *et al.* Mn-porphyrin conjugated Au nanoshells encapsulating doxorubicin for potential magnetic resonance imaging and light triggered synergistic therapy of cancer. *Theranostics* 2014; **4**: 858–871.

292. You J, Zhang R, Xiong C *et al.* Effective photothermal chemotherapy using doxorubicin-loaded gold nanospheres that target EphB4 receptors in tumors. *Cancer Res* 2012; **72**: 4777–4786.

293. Dhar S, Daniel WL, Giljohann DA *et al.* Polyvalent oligonucleotide gold nanoparticle conjugates as delivery vehicles for platinum(IV) warheads. *J Am Chem Soc* 2009; **131**: 14652–14653.

294. Conde J, Oliva N, Artzi N. Implantable hydrogel embedded dark-gold nanoswitch as a theranostic probe to sense and overcome cancer multidrug resistance. *Proc Natl Acad Sci* 2015; **112**: E1278–E1287.

295. Shi P, Liu Z, Dong K *et al.* A smart 'sense-act-treat' system: combining a ratiometric pH sensor with a near infrared therapeutic gold nanocage. *Adv Mater* 2014; **26**: 6635–6641.

296. Svenson S, Wolfgang M, Hwang J *et al.* Preclinical to clinical development of the novel

camptothecin nanopharmaceutical CRLX101. *J Control Release* 2011; **153**: 49–55.

297. Bao C, Conde J, Curtin J *et al.* Bioresponsive antisense DNA gold nanobeacons as a hybrid in vivo theranostics platform for the inhibition of cancer cells and metastasis. *Sci Rep* 2015; **5**: 12297.

298. Huang X, Hu Q, Braun GB *et al.* Light-activated RNA interference in human embryonic stem cells. *Biomaterials* 2015; **63**: 70–79.

299. Chen Z, Zhang L, He Y *et al.* Enhanced shRNA delivery and ABCG2 silencing by charge-reversible layered nanocarriers. *Small* 2015; **11**: 952–962.

300. Conde J, Rosa J, Baptista P. Gold-Nanobeacons as a theranostic system for the detection and inhibition of specific genes. *Protoc Exch* 2013; : 1–35.

301. Ding Y, Jiang Z, Saha K *et al.* Gold nanoparticles for nucleic acid delivery. *Mol Ther* 2014; **22**: 1075–1083.

302. Webb JA, Bardhan R. Emerging advances in nanomedicine with engineered gold nanostructures. *Nanoscale* 2014; **6**: 2502–2530.

303. Yin F, Yang C, Wang Q *et al.* A light-driven therapy of pancreatic adenocarcinoma using gold nanorods-based nanocarriers for co-delivery of doxorubicin and siRNA. *Theranostics* 2015; **5**: 818–833.

304. Conde JJ, Ambrosone A, Sanz V *et al.* Design of multifunctional gold nanoparticles for in vitro and in vivo gene silencing. *ACS Nano* 2012; **6**: 8316–8324.

305. Conde J, Rosa J, de la Fuente JM *et al.* Gold-nanobeacons for simultaneous gene specific silencing and intracellular tracking of the silencing events. *Biomaterials* 2013; **34**: 2516–2523.

306. Rosa J, Conde J, de la Fuente JM *et al.* Gold-nanobeacons for real-time monitoring of RNA synthesis. *Biosens Bioelectron* 2012; **36**: 161–167.

307. Cordeiro M, Carvalho L, Silva J *et al.* Gold nanobeacons for tracking gene silencing in zebrafish. *Nanomaterials* 2017; **7**: E10.

308. Cabral RM, Baptista PV. The chemistry and biology of gold nanoparticle-mediated photothermal therapy: Promises and challenges. *Nano Life* 2013; **3**: 1330001.

309. Liu Y, Xu M, Chen Q *et al.* Gold nanorods/mesoporous silica-based nanocomposite as theranostic agents for targeting near-infrared imaging and photothermal therapy induced with laser. *Int J Nanomedicine* 2015; **10**: 4747–4761.

310. Lu W, Xiong C, Zhang G *et al.* Targeted photothermal ablation of murine melanomas with melanocyte-stimulating hormone analog - conjugated hollow gold nanospheres. *Clin Cancer*

Res 2009; **15**: 876–886.

311. Bonoiu AC, Bergey EJ, Ding H *et al.* Gold nanorod-siRNA induces efficient in vivo gene silencing in the rat hippocampus. *Nanomedicine (Lond)* 2011; **6**: 617–630.

312. Taruttis A, Lozano N, Nunes A *et al.* siRNA liposome-gold nanorod vectors for multispectral optoacoustic tomography theranostics. *Nanoscale* 2014; **6**: 13451–13456.

313. Shen J, Kim HC, Mu C *et al.* Multifunctional gold nanorods for siRNA gene silencing and photothermal therapy. *Adv Healthc Mater* 2014; **3**: 1629–1637.

314. Bishop CJ, Tzeng SY, Green JJ. Degradable polymer-coated gold nanoparticles for co-delivery of DNA and siRNA. *Acta Biomater* 2015; **11**: 393–403.

315. Lim CK, Heo J, Shin S *et al.* Nanophotosensitizers toward advanced photodynamic therapy of Cancer. *Cancer Lett* 2013; **334**: 176–187.

316. Meyers JD, Cheng Y, Broome A-M *et al.* Peptide-targeted gold nanoparticles for photodynamic therapy of brain cancer. *Part Part Syst Charact* 2015; **32**: 448–457.

317. Yu J, Hsu C-H, Huang C-C *et al.* Development of therapeutic Au-methylene blue nanoparticles for targeted photodynamic therapy of cervical cancer cells. *ACS Appl Mater Interfaces* 2015; **7**: 432–441.

318. Willmann JK, van Bruggen N, Dinkelborg LM *et al.* Molecular imaging in drug development. *Nat Rev Drug Discov* 2008; **7**: 591–607.

319. Janib SM, Moses AS, MacKay JA. Imaging and drug delivery using theranostic nanoparticles. *Adv Drug Deliv Rev* 2010; **62**: 1052–1063.

320. Hong H, Zhang Y, Sun J *et al.* Molecular imaging and therapy of cancer with radiolabeled nanoparticles. *Nano Today* 2009; **4**: 399–413.

321. Lusic H, Grinstaff MW. X - ray-Computed Tomography Contrast Agents. *Chem Rev* 2013; **113**: 1641–1666.

322. Hasebroock KM, Serkova NJ. Toxicity of MRI and CT contrast agents. *Expert Opin Drug Metab Toxicol* 2009; **5**: 403–416.

323. Wang LV, Hu S. Photoacoustic tomography: in vivo imaging from organelles to organs. *Science* 2012; **335**: 1458–1462.

324. Blasiak B, Van Veggel FCJM, Tomanek B. Applications of nanoparticles for MRI cancer diagnosis and therapy. *J Nanomater* 2013; **2013**: 148578.

325. Jang B, Park S, Kang SH *et al.* Gold nanorods for target selective SPECT/CT imaging and photothermal therapy in vivo. *Quant Imaging Med Surg* 2012; **2**: 1–11.

326. Kosaka N, Ogawa M, Choyke PL *et al.* Clinical implications of near-infrared fluorescence imaging in cancer. *Futur Oncol* 2009; **5**: 1501–1511.

327. Kievit FM, Zhang M. Cancer nanotheranostics: Improving imaging and therapy by targeted delivery across biological barriers. *Adv Mater* 2011; **23**: 1–31.

328. Louie A. Multimodality imaging probes: Design and challenges. *Chem Rev* 2010; **110**: 3146–3195.

329. Liu Y, Ashton JR, Moding EJ *et al.* A plasmonic gold nanostar theranostic probe for in vivo tumor imaging and photothermal therapy. *Theranostics* 2015; **5**: 946–960.

330. Ke H, Wang J, Tong S *et al.* Gold nanoshelled liquid perfluorocarbon magnetic nanocapsules: A nanotheranostic platform for bimodal ultrasound/magnetic resonance imaging guided photothermal tumor ablation. *Theranostics* 2014; **4**: 12–23.

331. Abraham GE, Himmel PB. Management of rheumatoid arthritis: Rationale for the use of colloidal metallic gold. *J Nutr Environ Med* 1997; **7**: 295–305.

332. Libutti SK, Paciotti GF, Byrnes AA *et al.* Phase I and pharmacokinetic studies of CYT-6091, a novel PEGylated colloidal gold-rhTNF nanomedicine. *Clin Cancer Res* 2010; **16**: 6139–6149.

333. Bosetti R, Ferrandina G, Marneffe W *et al.* Cost–effectiveness of gemcitabine versus PEGylated liposomal doxorubicin for recurrent or progressive ovarian cancer: comparing chemotherapy with nanotherapy. *Nanomedicine* 2014; **9**: 2175–2186.

334. Khoshfetrat SM, Mehrgardi MA. Amplified detection of leukemia cancer cells using an aptamer-conjugated gold-coated magnetic nanoparticles on a nitrogen-doped graphene modified electrode. *Bioelectrochemistry* 2017; **114**: 24–32.

335. Tazi I, Nafil H, Mahmal L. Monoclonal antibodies in hematological malignancies: past, present and future. *J Cancer Res Ther* 2011; **7**: 399–407.

336. Sahoo SL, Liu C-H, Wu W-C. Lymphoma cell isolation using multifunctional magnetic nanoparticles: antibody conjugation and characterization. *RSC Adv* 2017; **7**: 22468–22478.

337. Chen H, Zhang W, Zhu G *et al.* Rethinking cancer nanotheranostics. *Nat Rev Mater* 2017; **2**: 17024.

338. Huang B, Liu H, Huang D *et al.* Apoptosis induction and imaging of cadmium-telluride quantum dots with wogonin in multidrug-resistant leukemia K562/A02 cell. *J Nanosci Nanotechnol* 2016; **16**: 2499–2503.

339. Silva EL, Lima FA, Carneiro G *et al.* Improved in vitro antileukemic activity of all-trans retinoic acid loaded in cholesteryl butyrate solid lipid nanoparticles. *J Nanosci Nanotechnol* 2016; **16**: 1291–1300.

340.   Knapp CM, He J, Lister J *et al.* Lipidoid nanoparticle mediated silencing of Mcl-1 induces apoptosis in mantle cell lymphoma. *Exp Biol Med* 2016; **241**: 1–7.

341.   Dorrance AM, Neviani P, Ferenchak GJ *et al.* Targeting leukemia stem cells in vivo with antagomiR-126 nanoparticles in acute myeloid leukemia. *Leukemia* 2015; **29**: 2143–53.

342.   Huang B, Abraham WD, Zheng Y *et al.* Active targeting of chemotherapy to disseminated tumors using nanoparticle-carrying T cells. *Sci Transl Med* 2015; **7**: 291ra94.

343.   Zong H, Sen S, Zhang G *et al.* In vivo targeting of leukemia stem cells by directing parthenolide-loaded nanoparticles to the bone marrow niche. *Leukemia* 2016; **30**: 1582–1586.

344.   Krishnan V, Xu X, Kelly D *et al.* CD19-targeted nanodelivery of doxorubicin enhances therapeutic efficacy in B-cell acute lymphoblastic leukemia. *Mol Pharm* 2015; **12**: 2101–2111.

345.   Gossai NP, Naumann JA, Li N-S *et al.* Drug conjugated nanoparticles activated by cancer cell specific mRNA. *Oncotarget* 2014; **7**: 38243–38256.

346.   Simon T, Tomuleasa C, Bojan A *et al.* Design of FLT3 inhibitor-gold nanoparticle conjugates as potential therapeutic agents for the treatment of acute myeloid leukemia. *Nanoscale Res Lett* 2015; **10**: 466.

347.   Petrushev B, Simon T, Berce C *et al.* Gold nanoparticles enhance the effect of tyrosine kinase inhibitors in acute myeloid leukemia therapy. *Int J Nanomedicine* 2016; **11**: 641–660.

348.   Song S, Hao Y, Yang X *et al.* Using gold nanoparticles as delivery vehicles for targeted delivery of chemotherapy drug fludarabine phosphate to treat hematological cancers. *J Nanosci Nanotechnol* 2016; **16**: 2582–2586.

349.   Singh A, Dilnawaz F, Sahoo SK. Long circulating lectin conjugated paclitaxel loaded magnetic nanoparticles: A new theranostic avenue for leukemia therapy. *PLoS One* 2011; **6**: e26803.

350.   Douer D. Efficacy and safety of vincristine sulfate liposome injection in the treatment of adult acute lymphocytic leukemia. *Oncologist* 2016; **21**: 840–847.

351.   Shah NN, Merchant MS, Cole DE *et al.* Vincristine sulfate liposomes injection (VSLI, Marqibo®): Results from a phase I study in children, adolescents, and young adults with refractory solid tumors or leukemias. *Pediatr Blood Cancer* 2016; **63**: 997–1005.

352.   Wetzler M, Thomas DA, Wang ES *et al.* Phase I/II trial of nanomolecular liposomal annamycin in adult patients with relapsed/refractory acute lymphoblastic leukemia. *Clin Lymphoma Myeloma Leuk* 2013; **13**: 430–434.

353.   Sriraman SK, Aryasomayajula B, Torchilin VP. Barriers to drug delivery in solid tumors. *Tissue Barriers* 2014; **2**: e29528.

354. Burmeister T, Schwartz S, Taubald A *et al.* Atypical BCR-ABL mRNA transcripts in adult acute lymphoblastic leukemia. *Haematologica* 2007; **92**: 1699–1702.

355. Keung Y-K, Beaty M, Powell BL *et al.* Philadelphia chromosome positive myelodysplastic syndrome and acute myeloid leukemia - Retrospective study and review of literature. *Leuk Res* 2004; **28**: 579–586.

356. Nacheva EP, Grace CD, Brazma D *et al.* Does BCR/ABL1 positive Acute Myeloid Leukaemia Exist? *Br J Haematol* 2013; **161**: 541–550.

357. Rostami G, Hamid M, Jalaeikhoo H. Impact of the BCR-ABL1 fusion transcripts on different responses to Imatinib and disease recurrence in Iranian patients with Chronic Myeloid Leukemia. *Gene* 2017; **627**: 202–206.

358. Jain P, Kantarjian H, Patel KP *et al.* Impact of BCR-ABL transcript type on response and survival in patients with chronic phase chronic myeloid leukemia treated with tyrosine kinase inhibitors. *Blood* 2016; **127**: 1269–1276.

359. Lichty BD, Keating A, Callum J *et al.* Expression of p210 and p190 BCR-ABL due to alternative splicing in chronic myelogenous leukaemia. *Br J Haematol* 1998; **103**: 711–715.

360. Score J, Calasanz MJ, Ottman O *et al.* Analysis of genomic breakpoints in p190 and p210 BCR–ABL indicate distinct mechanisms of formation. *Leukemia* 2010; **24**: 1742–1750.

361. Rohon P, Divoka M, Calabkova L *et al.* Identification of e6a2 BCR-ABL fusion in a philadelphia-positive CML with marked basophilia: Implications for treatment strategy. *Biomed Pap* 2011; **155**: 187–190.

362. Beel KA, Lemmens J, Vranckx H *et al.* CML with e6a2 BCR-ABL1 transcript: An aggressive entity? *Ann Hematol* 2011; **90**: 1241–1243.

363. Zagaria A, Anelli L, Coccaro N *et al.* BCR–ABL1 e6a2 transcript in chronic myeloid leukemia: biological features and molecular monitoring by droplet digital PCR. *Virchows Arch* 2015; **467**: 357–363.

364. Vefring HK, Gruber FXE, Wee L *et al.* Chronic myelogenous leukemia with the e6a2 bcr-abl and lacking imatinib response: Presentation of two cases. *Acta Haematol* 2009; **122**: 11–16.

365. Schultheis B, Wang L, Clark RE *et al.* BCR-ABL with an e6a2 fusion in a CML patient diagnosed in blast crisis. *Leukemia* 2003; **17**: 2054–5.

366. Reckel S, Hamelin R, Georgeon S *et al.* Differential signaling networks of Bcr–Abl p210 and p190 kinases in leukemia cells defined by functional proteomics. *Leukemia* 2017; **31**: 1502–1512.

367. Fabarius A, Leitner A, Hochhaus A *et al.* Impact of additional cytogenetic aberrations at

diagnosis on prognosis of CML: Long-term observation of 1151 patients from the randomized CML Study IV. *Blood* 2011; **118**: 6760–6768.

368. Otero L, Ornellas MH, Dobbin J *et al.* Double Philadelphia-chromosome: a resistance factor on the imatinib mesylate therapy for chronic myeloid leukemia. *Int J Lab Hematol* 2008; **30**: 346–348.

369. Tohda S, Sakashita C, Fukuda T *et al.* Establishment of a double Philadelphia chromosome-positive acute lymphoblastic leukemia-derived cell line, TMD5: Effects of cytokines and differentiation inducers on growth of the cells. *Leuk Res* 1999; **23**: 255–261.

370. Forghieri F, Luppi M, Potenza L. Philadelphia chromosome-positive Acute Lymphoblastic Leukemia. *Hematology* 2015; **20**: 618–619.

371. Chiaretti S, Foa R. Management of adult Ph-positive acute lymphoblastic leukemia. *Hematology* 2015; **2015**: 406–413.

372. Dombret H, Gabert J, Boiron J-M *et al.* Outcome of treatment in adults with Philadelphia chromosome-positive acute lymphoblastic leukemia - Results of the prospective multicenter LALA-94 trial. *Blood* 2002; **100**: 2357–2366.

373. Thomas X, Heiblig M. The development of agents targeting the BCR-ABL tyrosine kinase as Philadelphia chromosome-positive acute lymphoblastic leukemia treatment. *Expert Opin Drug Discov* 2016; **11**: 1061–1070.

374. Nicolini FE, Basak GW, Kim DW *et al.* Overall survival with ponatinib versus allogeneic stem cell transplantation in Philadelphia chromosome-positive leukemias with the T315I mutation. *Cancer* 2017; **123**: 2875–2880.

375. Sanford DS, Kantarjian H, O'Brien S *et al.* The role of ponatinib in Philadelphia chromosome-positive acute lymphoblastic leukemia. *Expert Rev Anticancer Ther* 2015; **15**: 365–373.

376. Molinos-Quintana A, Aquino V, Montero I *et al.* Emerging BCR/ABL1 mutations under treatment with tyrosine kinase inhibitors in paediatric acute lymphoblastic leukaemia. *Acta Haematol* 2015; **134**: 71–75.

377. Pfeifer H, Lange T, Wystub S *et al.* Prevalence and dynamics of bcr-abl kinase domain mutations during imatinib treatment differ in patients with newly diagnosed and recurrent bcr-abl positive acute lymphoblastic leukemia. *Leukemia* 2012; **26**: 1475–1481.

378. Pabst T, Mueller BU. Complexity of CEBPA dysregulation in human acute myeloid leukemia. *Clin Cancer Res* 2009; **15**: 5303–5307.

379. Schlenk RF, Döhner K, Krauter J *et al.* Mutations and treatment outcome in cytogenetically normal acute myeloid leukemia. *N Engl J Med* 2008; **358**: 1909–1918.

380. Mannelli F, Ponziani V, Bencini S *et al.* CEBPA–double-mutated acute myeloid leukemia displays a unique phenotypic profile: A reliable screening method and insight into biological features. *Haematologica* 2017; **102**: 529–540.

381. Pulikkan JA, Tenen DG, Behre G. C/EBPα deregulation as a paradigm for leukemogenesis. *Leukemia* 2017; **31**: 2279–2285.

382. Renneville A, Boissel N, Gachard N *et al.* The favorable impact of CEBPA mutations in patients with acute myeloid leukemia is only observed in the absence of associated cytogenetic abnormalities and FLT3 internal duplication. *Blood* 2009; **113**: 5090–5093.

383. Hollink I, van den Heuvel-Eibrink M, Arentsen-Peters S *et al.* Characterization of CEBPA mutations and promoter hypermethylation in pediatric acute myeloid leukemia. *Haematologica* 2011; **96**: 384–392.

384. Wouters BJ, Löwenberg B, Erpelinck-Verschueren CAJ *et al.* Double CEBPA mutations, but not single CEBPA mutations, define a subgroup of acute myeloid leukemia with a distinctive gene expression profile that is uniquely associated with a favorable outcome. *Blood* 2009; **113**: 3088–3091.

385. Levis M, Smith BD, Garrett E *et al.* The clinical outcome of patients with acute myeloid leukemia expressing FLT3 internal tandem duplication mutations could be altered by treatment regimen. *J Appl Res* 2003; **3**: 296–303.

386. den Dunnen JT, Dalgleish R, Maglott DR *et al*. HGVS recommendations for the description of sequence variants: 2016 update. *Hum Mutat* 2016; **37**: 564-569.

387. Schwarz JM, Cooper DN, Schuelke M *et al.* MutationTaster2: mutation prediction for the deep-sequencing age. *Nat Methods* 2014; **11**: 361–362.

388. Cheng J, Randall A, Baldi P. Prediction of protein stability changes for single-site mutations using support vector machines. *Proteins Struct Funct Bioinforma* 2005; **62**: 1125–1132.

389. Mcguffin LJ. Intrinsic disorder prediction from the analysis of multiple protein fold recognition models. *Bioinformatics* 2008; **24**: 1798–1804.

390. Chakrabarti P, Chakrabarty S, Aich R *et al.* Incidence of BCR-ABL transcript variants in patients with chronic myeloid leukemia: Their correlation with presenting features, risk scores and response to treatment with imatinib mesylate. *Indian J Med Paediatr Oncol* 2014; **35**: 26.

391. Osman EAI, Hamad K, Elmula IMF *et al.* Frequencies of BCR-ABL1 fusion transcripts among Sudanese chronic myeloid leukaemia patients. *Genet Mol Biol* 2010; **33**: 229–231.

392. Yaghmaie M, Ghaffari SH, Ghavamzadeh A *et al.* Frequency of BCR-ABL fusion transcripts in Iranian patients with chronic myeloid leukemia. *Arch Iran Med* 2008; **11**: 247–251.

393. Bartley PA, Ross DM, Latham S *et al.* Sensitive detection and quantification of minimal residual disease in chronic myeloid leukaemia using nested quantitative PCR for BCR-ABL DNA. *Int J Lab Hematol* 2010; **32**: e222-8.

394. Guo JQ, Lin H, Kantarjian H *et al.* Comparison of competitive-nested PCR and real-time PCR in detecting BCR-ABL fusion transcripts in chronic myeloid leukemia patients. *Leukemia* 2002; **16**: 2447–2453.

395. Baccarani M, Soverini S, De Benedittis C. Molecular monitoring and mutations in chronic myeloid leukemia: how to get the most out of your tyrosine kinase inhibitor. *Am Soc Clin Oncol Educ B* 2014; **2014**: 167–175.

396. Nandagopalan SR, Kuila N, Biswas S *et al.* Dual transcripts of BCR-ABL & different polymorphisms in chronic myeloid leukaemia patients. *Indian J Med Res Suppl* 2016; **143**: 136–141.

397. Shweta S, Sarjana D. Imatinib mesylate resistance and mutations: An Indian experience. *Indian J Med Paediatr Oncol* 2013; **34**: 213–220.

398. Ernst T, Hoffmann J, Erben P *et al.* ABL single nucleotide polymorphisms may masquerade as BCR-ABL mutations associated with resistance to tyrosine kinase inhibitors in patients with chronic myeloid leukemia. *Haematologica* 2008; **93**: 1389–1393.

399. Verma D, Kantarjian HM, Jones D *et al.* Chronic myeloid leukemia (CML) with P190BCR-ABL: Analysis of characteristics, outcomes, and prognostic significance. *Blood* 2009; **114**: 2232–2235.

400. DeAngelo DJ, Stevenson KE, Dahlberg SE *et al.* Long-term outcome of a pediatric-inspired regimen used for adults aged 18–50 years with newly diagnosed acute lymphoblastic leukemia. *Leukemia* 2015; **29**: 526–534.

401. Kim D, Kim DW, Cho BS *et al.* Structural modeling of V299L and E459K Bcr-Abl mutation, and sequential therapy of tyrosine kinase inhibitors for the compound mutations. *Leuk Res* 2009; **33**: 1260–1265.

402. Asou H, Gombart AF, Takeuchi S *et al.* Establishment of the acute myeloid leukemia cell line Kasumi-6 from a patient with a dominant-negative mutation in the DNA-binding region of the C/EBPα gene. *Genes Chromosom Cancer* 2003; **36**: 167–174.

403. Gombart AF. Mutations in the gene encoding the transcription factor CCAAT/enhancer binding protein alpha in myelodysplastic syndromes and acute myeloid leukemias. *Blood* 2002; **99**: 1332–1340.

404. Jemal A, Siegel R, Xu J *et al.* Cancer statistics, 2010. *CA Cancer J Clin* 2010; **60**: 277–300.

405. Hehlmann R, Hochhaus A, Baccarani M. Chronic myeloid leukaemia. *Lancet* 2007; **370**: 342–350.

406. Tang M, Gonen M, Quintas-Cardama A *et al.* Dynamics of chronic myeloid leukemia response to long-term targeted therapy reveal treatment effects on leukemic stem cells. *Blood* 2011; **118**: 1622–1631.

407. Stein AM, Bottino D, Modur V *et al.* BCR-ABL transcript dynamics support the hypothesis that leukemic stem cells are reduced during imatinib teatment. *Clin Cancer Res* 2011; **17**: 6812–6821.

408. Hehlmann R, Lauseker M, Jung-Munkwitz S *et al.* Tolerability-adapted imatinib 800 mg/d versus 400 mg/d versus 400 mg/d plus interferon-alpha in newly diagnosed chronic myeloid leukemia. *J Clin Oncol* 2011; **29**: 1634–1642.

409. Kantarjian H, O'Brien S, Cortes J *et al.* Sudden onset of the blastic phase of chronic myelogenous leukemia: Patterns and implications. *Cancer* 2003; **98**: 81–85.

410. Branford S, Hughes TP, Rudzki Z. Monitoring chronic myeloid leukaemia therapy by real-time quantitative PCR in blood is a reliable alternative to bone marrow cytogenetics. *Br J Haematol* 1999; **107**: 587–599.

411. Baccarani M, Deininger MW, Rosti G *et al.* European LeukemiaNet recommendations for the management of chronic myeloid leukemia: 2013. *Blood* 2013; **122**: 872–884.

412. Branford S, Fletcher L, Cross NCP *et al.* Desirable performance characteristics for BCR-ABL measurement on an international reporting scale to allow consistent interpretation of individual patient response and comparison of response rates between clinical trials. *Blood* 2008; **112**: 3330–3338.

413. Rice SB, Chan C, Brown SC *et al.* Particle size distributions by transmission electron microscopy: an interlaboratory comparison case study. *Metrologia* 2013; **50**: 663–678.

414. Hinterwirth H, Wiedmer SK, Moilanen M *et al.* Comparative method evaluation for size and size-distribution analysis of gold nanoparticles. *J Sep Sci* 2013; **36**: 2952–2961.

415. Haiss W, Thanh NTK, Aveyard J *et al.* Determination of size and concentration of gold nanoparticles from UV-Vis spectra. *Anal Chem* 2007; **79**: 4215–4221.

416. Tekinturhan E, Audureau E, Tavolacci M-PP *et al.* Improving access to care in low and middle-income countries: Institutional factors related to enrollment and patient outcome in a cancer drug access program. *BMC Heal Serv Res* 2013; **13**: 304.

417. Ganesan P, Kumar L. Chronic Myeloid Leukemia in India. *J Glob Oncol* 2017; **3**: 64–71.

418. Garcia-Gonzalez P, Boultbee P, Epstein D. Novel humanitarian aid program: The Glivec

International Patient Assistance Program - Lessons learned from providing access to breakthrough targeted oncology treatment in low- and middle-income countries. *J Glob Oncol* 2015; **1**: 37–45.

419. Bernacka-Wojcik I, Águas H, Carlos FF *et al.* Single nucleotide polymorphism detection using gold nanoprobes and bio-microfluidic platform with embedded microlenses. *Biotechnol Bioeng* 2015; **112**: 1210–1219.

420. Sun J, Xianyu Y, Jiang X. Point-of-care biochemical assays using gold nanoparticle-implemented microfluidics. *Chem Soc Rev* 2014; **43**: 6239–6253.

421. Vinhas R, Correia C, Ribeiro P *et al.* Colorimetric assessment of BCR-ABL1 transcripts in clinical samples via gold nanoprobes. *Anal Bioanal Chem* 2016; **408**: 5277–5284.

422. Hosokawa K, Sato K, Ichikawa N *et al.* Power-free poly(dimethylsiloxane) microfluidic devices for gold nanoparticle-based DNA analysis. *Lab Chip* 2004; **4**: 181–185.

423. Hsu M-H, Fang W-F, Lai Y-H *et al.* Enhanced mobile hybridization of gold nanoparticles decorated with oligonucleotide in microchannel devices. *Lab Chip* 2010; **10**: 2583–2587.

424. Huang CT, Jen CP, Chao TC *et al.* A novel design of grooved fibers for fiber-optic localized plasmon resonance biosensors. *Sensors* 2009; **9**: 6456–6470.

425. Silva LB, Veigas B, Doria G *et al.* Portable optoelectronic biosensing platform for identification of mycobacteria from the Mycobacterium tuberculosis complex. *Biosens Bioelectron* 2011; **26**: 2012–2017.

426. Weibel DB, Whitesides GM. Applications of microfluidics in chemical biology. *Curr Opin Chem Biol* 2006; **10**: 584–591.

427. Liu CN, Toriello NM, Mathies RA. Multichannel PCR-CE microdevice for genetic analysis. *Anal Chem* 2006; **78**: 5474–5479.

428. Mir M, Homs A, Samitier J. Integrated electrochemical DNA biosensors for lab-on-a-chip devices. *Electrophoresis* 2009; **30**: 3386–3397.

429. Lei KF. Recent developments and patents on biological sensing using nanoparticles in microfluidic systems. *Recent Pat Nanotechnol* 2013; **7**: 81–90.

430. Viskari PJ, Landers JP. Unconventional detection methods for microfluidic devices. *Electrophoresis* 2006; **27**: 1797–1810.

431. Zhou F, Lu M, Wang W *et al.* Electrochemical immunosensor for simultaneous detection of dual cardiac markers based on a poly(dimethylsiloxane)-gold nanoparticles composite microfluidic chip: A proof of principle. *Clin Chem* 2010; **56**: 1701–1707.

432. Lisowski P, Zarzycki PK. Microfluidic paper-based analytical devices (μPADs) and micro total analysis systems (μTAS): Development, applications and future trends. *Chromatographia* 2013; **76**: 1201–1214.

433. Whitesides GM. The origins and the future of microfluidics. *Nature* 2006; **442**: 368–373.

434. Gan W, Zhuang B, Zhang P *et al.* A filter paper-based microdevice for low-cost, rapid, and automated DNA extraction and amplification from diverse sample types. *Lab Chip* 2014; **14**: 3719–3728.

435. Psaltis D, Quake SR, Yang C. Developing optofluidic technology through the fusion of microfluidics and optics. *Nature* 2006; **442**: 381–386.

436. Marques AC, Santos L, Costa MN *et al.* Office paper platform for bioelectrochromic detection of electrochemically active bacteria using tungsten trioxide nanoprobes. *Sci Rep* 2015; **5**: 9910.

437. Karabchevsky A, Mosayyebi A, Kavokin A V. Tuning the chemiluminescence of a luminol flow using plasmonic nanoparticles. *Light Sci Appl* 2016; **5**: e16164.

438. Ahmed S, Bui MPN, Abbas A. Paper-based chemical and biological sensors: Engineering aspects. *Biosens Bioelectron* 2016; **77**: 249–263.

439. Cate DM, Adkins JA, Mettakoonpitak J *et al.* Recent developments in paper-based microfluidic devices. *Anal Chem* 2015; **87**: 19–41.

440. Liana DD, Raguse B, Justin Gooding J *et al.* Recent advances in paper-based sensors. *Sensors* 2012; **12**: 11505–11526.

441. Li X, Ballerini DR, Shen W. A perspective on paper-based microfluidics: Current status and future trends. *Biomicrofluidics* 2012; **6**: 11301–1130113.

442. Choi S. Powering point-of-care diagnostic devices. *Biotechnol Adv* 2016; **34**: 321–330.

443. Whitesides GM, Ostuni E, Takayama S *et al.* Soft lithography in biology and biochemistry. *Annu Rev Biomed Eng* 2001; **3**: 335–373.

444. Nguyen N-T, Wu Z. Micromixers - A review. *J Micromechanics Microengineering* 2005; **15**: R1–R16.

445. Lee CY, Chang CL, Wang YN *et al.* Microfluidic mixing: A review. *Int J Mol Sci* 2011; **12**: 3263–3287.

446. Bernacka-Wojcik I, Ribeiro S, Wojcik PJ *et al.* Experimental optimization of a passive planar rhombic micromixer with obstacles for effective mixing in a short channel length. *RSC Adv* 2014; **4**: 56013–56025.

447. Elghanian R, Storhoff JJ, Mucic RC *et al.* Selective colorimetric detection of polynucleotides

based on the distance-dependent optical properties of gold nanoparticles. *Science* 1997; **277**: 1078–1081.

448.   Mcdonald JC, Duffy DC, Anderson JR *et al.* Fabrication of microfluidic systems in poly (dimethylsiloxane). *Electrophoresis* 2000; **21**: 27–40.

449.   Campo A del, Greiner C. SU-8: a photoresist for high-aspect-ratio and 3D submicron lithography. *J Micromechanics Microengineering* 2007; **17**: R81–R95.

450.   Desai SP, Freeman DM, Voldman J. Plastic masters - Rigid templates for soft lithography. *Lab Chip* 2009; **9**: 1631.

451.   Hammacher J, Fuelle A, Flaemig J *et al.* Stress engineering and mechanical properties of SU-8-layers for mechanical applications. *Microsyst Technol* 2008; **14**: 1515–1523.

452.   Wen N, Zhao Z, Fan B *et al.* Development of droplet microfluidics enabling high-throughput single-cell analysis. *Molecules* 2016; **21**: E881.

453.   Wang DS, Fan SK. Microfluidic surface plasmon resonance sensors: From principles to point-of-care applications. *Sensors* 2016; **16**: E1175.

454.   Gong MM, MacDonald BD, Vu Nguyen T *et al.* Hand-powered microfluidics: A membrane pump with a patient-to-chip syringe interface. *Biomicrofluidics* 2012; **6**: 44102.

455.   Jabbour E, Kantarjian H. Chronic myeloid leukemia: 2016 update on diagnosis, therapy, and monitoring. *Am J Hematol* 2016; **91**: 252–265.

456.   Rosti G, Castagnetti F, Gugliotta G *et al.* Tyrosine kinase inhibitors in chronic myeloid leukaemia: which, when, for whom? *Nat Rev Clin Oncol* 2016; **14**: 141–154.

457.   Helgason G V, Mukhopadhyay A, Karvela M *et al.* Autophagy in chronic myeloid leukaemia: stem cell survival and implication in therapy. *Curr Cancer Drug Targets* 2013; **13**: 724–34.

458.   Szczylik C, Skorski T, Nicolaides N *et al.* Selective inhibition of leukemia cell proliferation by BCR-ABL antisense oligodeoxynucleotides. *Science* 1991; **253**: 562–565.

459.   Moreno PM, Pêgo AP. Therapeutic antisense oligonucleotides against cancer: hurdling to the clinic. *Front Chem* 2014; **2**: 87.

460.   Watts J, Corey D. Gene silencing by siRNAs and antisense oligonucleotides in the laboratory and the clinic. *J Pathol* 2012; **226**: 365–379.

461.   Wu J, Liu B, Wu H *et al.* A gold nanoparticle platform for the delivery of functional TGF-β1 siRNA into cancer cells. *J Biomed Nanotechnol* 2016; **12**: 800–810.

462.   Lee SK, Tung CH. siRNA nanoparticles for ultra-long gene silencing in vivo. *Methods Mol Biol* 2016; **1372**: 113–120.

463. Heinemann D, Schomaker M, Kalies S *et al.* Gold nanoparticle mediated laser transfection for efficient siRNA mediated gene knock down. *PLoS One* 2013; **8**: e58604.

464. Lee SK, Han MS, Asokan S *et al.* Effective gene silencing by multilayered siRNA-coated gold nanoparticles. *Small* 2011; **7**: 364–370.

465. Huschka R, Barhoumi A, Liu Q *et al.* Gene silencing by gold nanoshell-mediated delivery and laser-triggered release of antisense oligonucleotide and siRNA. *ACS Nano* 2012; **6**: 7681–7691.

466. Jiwaji M, Sandison ME, Reboud J *et al.* Quantification of functionalised gold nanoparticle-targeted knockdown of gene expression in HeLa cells. *PLoS One* 2014; **9**: e99458.

467. Wolfe BR, Pierce NA. Sequence design for a test tube of interacting nucleic acid strands. *ACS Synth Biol* 2015; **4**: 1086–1100.

468. Zadeh JN, Steenberg CD, Bois JS *et al.* NUPACK: Analysis and design of nucleic acid systems. *J Comput Chem* 2011; **32**: 170–173.

469. Livak KJ, Schmittgen TD. Analysis of relative gene expression data using real-time quantitative PCR and the $2^{-\Delta\Delta CT}$ method. *Methods* 2001; **25**: 402–408.

470. Strober W. Trypan blue exclusion test of cell viability. *Curr Protoc Immunol* 2015; **111**: A3.B.1-3.

471. Tipping AJ, Mahon FX, Zafirides G *et al.* Drug responses of imatinib mesylate-resistant cells: synergism of imatinib with other chemotherapeutic drugs. *Leukemia* 2002; **16**: 2349–2357.

472. Silva A, Luís D, Santos S *et al.* Biological characterization of the antiproliferative potential of Co(II) and Sn(IV) coordination compounds in human cancer cell lines: A comparative proteomic approach. *Drug Metabol Drug Interact* 2013; **28**: 167–176.

473. Sutradhar M, Fernandes AR, Silva J *et al.* Water soluble heterometallic potassium-dioxidovanadium(V) complexes as potential antiproliferative agents. *J Inorg Biochem* 2016; **155**: 17–25.

474. Luís DV, Silva J, Tomaz AI *et al.* Insights into the mechanisms underlying the antiproliferative potential of a Co(II) coordination compound bearing 1,10-phenanthroline-5,6-dione: DNA and protein interaction studies. *J Biol Inorg Chem* 2014; **19**: 787–803.

475. Vigderman L, Zubarev ER. Therapeutic platforms based on gold nanoparticles and their covalent conjugates with drug molecules. *Adv Drug Deliv Rev* 2013; **65**: 663–676.

476. Kuang T, Chang L, Peng X *et al.* Molecular beacon nano-sensors for probing living cancer cells. *Trends Biotechnol* 2017; **35**: 347–359.

477. Jokerst JV, Lobovkina T, Zare RN *et al.* Nanoparticle PEGylation for imaging and therapy.

Nanomedicine 2011; **6**: 715–728.

478. Bogatyrev VA, Dykman LA, Khlebtsov BN *et al.* Measurement of mean size and evaluation of polydispersity of gold nanoparticles from spectra of optical absorption and scattering. *Opt Spectrosc* 2004; **96**: 128–135.

479. Chen J, Xie J. Progress on RNAi-based molecular medicines. *Int J Nanomedicine* 2012; **7**: 3971–3980.

480. Sanchez Garcia I, Martin Zanca D. Regulation of Bcl-2 gene expression by BCR-ABL is mediated by Ras. *J Mol Biol* 1997; **267**: 225–228.

481. Paino IMM, Marangoni VS, de Oliveira R de CS *et al.* Cyto and genotoxicity of gold nanoparticles in human hepatocellular carcinoma and peripheral blood mononuclear cells. *Toxicol Lett* 2012; **215**: 119–125.

482. Druker BJ. Translation of the Philadelphia chromosome into therapy for CML. *Blood* 2008; **112**: 4808–4817.

483. Drullion C, Trégoat C, Lagarde V *et al.* Apoptosis and autophagy have opposite roles on imatinib-induced K562 leukemia cell senescence. *Cell Death Dis* 2012; **3**: e373.

484. Elmore S. Apoptosis: A review of programmed cell Death. *Toxicol Pathol* 2007; **35**: 495–516.

485. Hata AN, Engelman JA, Faber AC. The BCL2 family: Key mediators of the apoptotic response to targeted anticancer therapeutics. *Cancer Discov* 2015; **5**: 475–487.

486. Kurokawa M, Ito T, Yang C-S *et al.* Engineering a BCR-ABL-activated caspase for the selective elimination of leukemic cells. *Proc Natl Acad Sci* 2013; **110**: 2300–2305.

487. Azam M, Latek RR, Daley GQ. Mechanisms of autoinhibition and STI-571/imatinib resistance revealed by mutagenesis of BCR-ABL. *Cell* 2003; **112**: 831–843.

488. Arunasree KM, Roy KR, Anilkumar K *et al.* Imatinib-resistant K562 cells are more sensitive to celecoxib, a selective COX-2 inhibitor: Role of COX-2 and MDR-1. *Leuk Res* 2008; **32**: 855–864.

489. Usui N. Updated European leukemianet recommendations for the management of CML. In: *Molecular Pathogenesis and Treatment of Chronic Myelogenous Leukemia*. 2015, pp 81–100.

490. Abraham SA, Hopcroft LEM, Carrick E *et al.* Dual targeting of p53 and c-MYC selectively eliminates leukaemic stem cells. *Nature* 2016; **534**: 341–346.

491. Lucas CM, Harris RJ, Giannoudis A *et al.* C-MYC inhibition decreases CIP2A and reduces BCR-ABL1 tyrosine kinase activity in chronic myeloid leukemia. *Haematologica* 2015; **100**: e179–e182.

492.   Soverini S, De Benedittis C, Mancini M *et al.* Present and future of molecular monitoring in chronic myeloid leukaemia. *Br J Haematol* 2016; **173**: 337–349.

493.   Carlos FF, Flores O, Doria G *et al.* Characterization of genomic single nucleotide polymorphism via colorimetric detection using a single gold nanoprobe. *Anal Biochem* 2014; **465**: 1–5.

494.   Veigas B, Pinto J, Vinhas R *et al.* Quantitative real-time monitoring of RCA amplification of cancer biomarkers mediated by a flexible ion sensitive platform. *Biosens Bioelectron* 2017; **91**: 788–795.

495.   Litwińska Z, Machaliński B. miRNAs in chronic myeloid leukemia: Small molecules, essential function. *Leuk Lymphoma* 2017; **58**: 1297–1305.

496.   Weidhaas JB. Expression patterns of microRNAs associated with CML phases and their disease related targets. *Mol Cancer* 2011; **10**: 41.

497.   Dawidczyk CM, Russell LM, Searson PC. Nanomedicines for cancer therapy: state-of-the-art and limitations to pre-clinical studies that hinder future developments. *Front Chem* 2014; **2**: 69.

498.   Babu A, Muralidharan R, Amreddy N *et al.* Nanoparticles for siRNA-based gene silencing in tumor therapy. *IEEE Trans Nanobioscience* 2016; **15**: 849–863.

499.   Hou W, Wei P, Kong L *et al.* Partially PEGylated dendrimer-entrapped gold nanoparticles: a promising nanoplatform for highly efficient DNA and siRNA delivery. *J Mater Chem B* 2016; **4**: 2933–2943.

500.   Kong L, Wu Y, Alves CS *et al.* Efficient delivery of therapeutic siRNA into glioblastoma cells using multifunctional dendrimer-entrapped gold nanoparticles. *Nanomedicine* 2016; **11**: 3103–3115.

501.   Benito J, Zeng Z, Konopleva M *et al.* Targeting hypoxia in the leukemia microenvironment. *Int J Hematol Oncol* 2013; **2**: 279–288.

502.   Ledermann JA, Canevari S, Thigpen T. Targeting the folate receptor: Diagnostic and therapeutic approaches to personalize cancer treatments. *Ann Oncol* 2015; **26**: 2034–2043.

503.   Bellavia D, Raimondo S, Calabrese G *et al.* Interleukin 3- receptor targeted exosomes inhibit in vitro and in vivo chronic myelogenous Leukemia cell growth. *Theranostics* 2017; **7**: 1333–1345.

504.   Cook GJ, Pardee TS. Animal models of leukemia: Any closer to the real thing? *Cancer Metastasis Rev* 2013; **32**: 63–76.

505.   Kohnken R, Porcu P, Mishra A. Overview of the use of murine models in leukemia and lymphoma research. *Front Oncol* 2017; **7**: 22.

APPENDICES

Appendix I – Clinical case 44 *BCR-ABL1* transcript identification and mutational analysis

```
Seq 1    1    TTCCGCTGACCATCAACAAGGAAGATGATGAGTCTCCGGGGCTCTATGGGTTTCTGAATG    60
              ||||||||||||||||*|||||||||||||||||||||||||||||||||||||||||||
Seq 2    275  TTCCGCTGACCATCAATAAGGAAGATGATGAGTCTCCGGGGCTCTATGGGTTTCTGAATG    334

Seq 1    61   TCATCGTCCACTCAGCCACTGGATTTAAGCAGAGTTCAAAAGCCCTTCAGCGGCCAGTAG    120
              ||||||||||||||||||||||||||||||||||||||||| ||||||||||||||||||
Seq 2    335  TCATCGTCCACTCAGCCACTGGATTTAAGCAGAGTTCAAAAGCCCTTCAGCGGCCAGTAG    394

Seq 1    121  CATCTGACTTTGAGCCTCAGGGTCTGAGTGAAGCCGCTCGTTGGAACTCCAAGGAAAACC    180
              ||||||||||||||||||||||||||||||||||||||||||||||||||||||||||||
Seq 2    395  CATCTGACTTTGAGCCTCAGGGTCTGAGTGAAGCCGCTCGTTGGAACTCCAAGGAAAACC    454

Seq 1    181  TTCTCGCTGGACCCAGTGAAAATGACCCCAACCTTTTCGTTGCACTGTATGATTTTGTGG    240
              ||||||||||||||||||||||||||||||||||||||||||||||||||||||||||||
Seq 2    455  TTCTCGCTGGACCCAGTGAAAATGACCCCAACCTTTTCGTTGCACTGTATGATTTTGTGG    514

Seq 1    241  CCAGTGGAGATAACACTCTAAGCATAACTAAAGGTGAAAAGCTCCGGGTCTTAGGCTATA    300
              ||||||||||||||||||||||||||||||||||||||||||||||||||||||||||||
Seq 2    515  CCAGTGGAGATAACACTCTAAGCATAACTAAAGGTGAAAAGCTCCGGGTCTTAGGCTATA    574

Seq 1    301  ATC   303
              |||
Seq 2    575  ATC   577
```

Figure I.1 Alignment of CML patient (sample 44) e14a2 nucleotide sequence [Seq 1] with *BCR-ABL1* e14a2 reference sequence from GenBank AJ131466.1 [Seq 2]. *Detected SNP on *BCR* exon 13, c.2700T>C. Arrow indicates the breakpoint in this *BCR-ABL1* isoform.

```
Seq 1    1    CGCCGCAGTGCCATAAGCGGCACCGGCACTGCCCGGTTGTCGTGTCCGAGGCCACCATCG    60
              ||||||||||||||||||||||||||||||||||||||||||||||||||||||||||||
Seq 2    330  CGCCGCAGTGCCATAAGCGGCACCGGCACTGCCCGGTTGTCGTGTCCGAGGCCACCATCG    389

Seq 1    61   TGGGCGTCCGCAAGACCGGGCAGATCTGGCCCAACGATGGCGAGGGCGCCTTCCATGGAG    120
              ||||||||||||||||||||||||||||||||||||||||||||||||||||||||||||
Seq 2    390  TGGGCGTCCGCAAGACCGGGCAGATCTGGCCCAACGATGGCGAGGGCGCCTTCCATGGAG    449

Seq 1    121  ACGCAGATGGCTCGTTCGGAACACCACCTGGATACGGCTGCGCTGCAGACCGGGCAGAGG    180
              ||||||||||||||||||||||||||||||||||||||||||||||||||||||||||||
Seq 2    450  ACGCAGATGGCTCGTTCGGAACACCACCTGGATACGGCTGCGCTGCAGACCGGGCAGAGG    509

Seq 1    181  AGCAGCGCCGGCACCAAGATGGGCTGCCCTACATTGATGACTCGCCCTCCTCATCGCCCC    240
              ||||||||||||||||||||||||||||||||||||||||||||||||||||||||||||
Seq 2    510  AGCAGCGCCGGCACCAAGATGGGCTGCCCTACATTGATGACTCGCCCTCCTCATCGCCCC    569

Seq 1    241  ACCTCAGCAGCAAGGGCAGGGGCAGCCGGGATGCGCTGGTCTCGGGAGCCCTGGAGTCCA    300
              ||||||||||||||||||||||||||||||||||||||||||||||||||||||||||||
Seq 2    570  ACCTCAGCAGCAAGGGCAGGGGCAGCCGGGATGCGCTGGTCTCGGGAGCCCTGGAGTCCA    629

Seq 1    301  CTAAAGCGAGTGAGCTGGACTTGGAAAAGGGCTTGGAGATGAGAAAATGGGTCCTGTCGG    360
              ||||||||||||||||||||||||||||||||||||||||||||||||||||||||||||
Seq 2    630  CTAAAGCGAGTGAGCTGGACTTGGAAAAGGGCTTGGAGATGAGAAAATGGGTCCTGTCGG    689
```

```
Seq 1    361  GAATCCTGGCTAGCGAGGAGACTTACCTGAGCCACCTGGAGGCACTGCTGCTGCCCATGA  420
              ||||||||||||||||||||||||||||||||||||||||||||||||||||||||||||
Seq 2    690  GAATCCTGGCTAGCGAGGAGACTTACCTGAGCCACCTGGAGGCACTGCTGCTGCCCATGA  749

Seq 1    421  AGCCTTTGAAAGCCGCTGCCACCACCTCTCAGCCGGTGCTGACGAGTCAGCAGATCGAGA  480
              ||||||||||||||||||||||||||||||||||||||||||||||||||||||||||||
Seq 2    750  AGCCTTTGAAAGCCGCTGCCACCACCTCTCAGCCGGTGCTGACGAGTCAGCAGATCGAGA  809

Seq 1    481  CCATCTTCTTCAAAGTGCCTGAGCTCTACGAGATCCACAAGGAGTTCTATGATGGGCTCT  540
              ||||||||||||||||||||||||||||||||||||||||||||||||||||||||||||
Seq 2    810  CCATCTTCTTCAAAGTGCCTGAGCTCTACGAGATCCACAAGGAGTTCTATGATGGGCTCT  869

Seq 1    541  TCCCCCGCGTGCAGCAGTGGAGCCACCAGCAGCGGGTGGGCGACCTCTTCCAGAAGCTGG  600
              ||||||||||||||||||||||||||||||||||||||||||||||||||||||||||||
Seq 2    870  TCCCCCGCGTGCAGCAGTGGAGCCACCAGCAGCGGGTGGGCGACCTCTTCCAGAAGCTGG  929

Seq 1    601  CCAGCCAGCTGGGTGTGTACCGGGCCTTCGTGGACAACTACGGAGTTGCCATGGAAATGG  660
              ||||||||||||||||||||||||||||||||||||||||||||||||||||||||||||
Seq 2    930  CCAGCCAGCTGGGTGTGTACCGGGCCTTCGTGGACAACTACGGAGTTGCCATGGAAATGG  989

Seq 1    661  CTGAGAAGTGCTGTCAGGCCAATGCTCAGTTTGCAGAAATCTCCGAGAACCTGAGAGCCA  720
              ||||||||||||||||||||||||||||||||||||||||||||||||||||||||||||
Seq 2    990  CTGAGAAGTGCTGTCAGGCCAATGCTCAGTTTGCAGAAATCTCCGAGAACCTGAGAGCCA  1049

Seq 1    721  GAAGCAACAAAGATGCCAAGGATCCAACGACCAAGAACTCTCTGGAAAAAGCCCTTCAGC  780
              ||||||||||||||||||||||||||||||||||||||||||||||||||||||||||||
Seq 2   1050  GAAGCAACAAAGATGCCAAGGATCCAACGACCAAGAACTCTCTGGAAAAAGCCCTTCAGC  1109

Seq 1    781  GGCCAGTAGCATCTGACTTTGAGCCTCAGGGTCTGAGTGAAGCCGCTCGTTGGAACTCCA  840
              ||||||||||||||||||||||||||||||||||||||||||||||||||||||||||||
Seq 2   1110  GGCCAGTAGCATCTGACTTTGAGCCTCAGGGTCTGAGTGAAGCCGCTCGTTGGAACTCCA  1169

Seq 1    841  AGGAAAACCTTCTCGCTGGACCCAGTGAAAATGACCCCAACCTTTTCGTTGCACTGTATG  900
              ||||||||||||||||||||||||||||||||||||||||||||||||||||||||||||
Seq 2   1170  AGGAAAACCTTCTCGCTGGACCCAGTGAAAATGACCCCAACCTTTTCGTTGCACTGTATG  1229

Seq 1    901  ATTTTGTGGCCAGTGGAGATAACACTCTAAGCATAACTAAAGGTGAAAAGCTCCGGGTCT  960
              ||||||||||||||||||||||||||||||||||||||||||||||||||||||||||||
Seq 2   1230  ATTTTGTGGCCAGTGGAGATAACACTCTAAGCATAACTAAAGGTGAAAAGCTCCGGGTCT  1289
```

Figure I.2 Alignment of CML patient (sample 44) e6a2 nucleotide sequence [Seq 1] with *BCR-ABL1* e6a2 (GenBank AM491362.1), *BCR* (GenBank NM_004327.3) and *ABL1* (GenBank NM_005157.5) consensus sequence [Seq 2]. Arrow indicates the breakpoint in this *BCR-ABL1* isoform.

```
Seq 1    1     GCAACAAGCCCACTGTCTATGGTGTGTCCCCCAACTACGACAAGTGGGAGATGGAACGCA  60
               ||||||||||||||||||||||||||||||||||||||||||||||||||||||||||||
Seq 2    851   GCAACAAGCCCACTGTCTATGGTGTGTCCCCCAACTACGACAAGTGGGAGATGGAACGCA  910

Seq 1    61    CGGACATCACCATGAAGCACAAGCTGGGCGGGGGCCAGTACGGGGAGGTGTACGAGGGCG  120
               ||||||||||||||||||||||||||||||||||||||||||||||||||||||||||||
Seq 2    911   CGGACATCACCATGAAGCACAAGCTGGGCGGGGGCCAGTACGGGGAGGTGTACGAGGGCG  970

Seq 1    121   TGTGGAAGAAATACAGCCTGACGGTGGCCGTGAAGACCTTGAAGGAGGACACCATGGAGG  180
               ||||||||||||||||||||||||||||||||||||||||||||||||||||||||||||
Seq 2    971   TGTGGAAGAAATACAGCCTGACGGTGGCCGTGAAGACCTTGAAGGAGGACACCATGGAGG  1030

Seq 1    181   TGGAAGAGTTCTTGAAAGAAGCTGCAGTCATGAAAGAGATCAAACACCCTAACCTGGTGC  240
               ||||||||||||||||||||||||||||||||||||||||||||||||||||||||||||
Seq 2   1031   TGGAAGAGTTCTTGAAAGAAGCTGCAGTCATGAAAGAGATCAAACACCCTAACCTGGTGC  1090

Seq 1    241   AGCTCCTTGGGGTCTGCACCCGGGAGCCCCCGTTCTATATCATCACTGAGTTCATGACCT  300
               ||||||||||||||||||||||||||||||||||||||||||||||||||||||||||||
Seq 2   1091   AGCTCCTTGGGGTCTGCACCCGGGAGCCCCCGTTCTATATCATCACTGAGTTCATGACCT  1150

Seq 1    301   ACGGGAACCTCCTGGACTACCTGAGGGAGTGCAACCGGCAGGAGGTGAACGCCGTGGTGC  360
               ||||||||||||||||||||||||||||||||||||||||||||||||||||||||||||
Seq 2   1151   ACGGGAACCTCCTGGACTACCTGAGGGAGTGCAACCGGCAGGAGGTGAACGCCGTGGTGC  1210
```

```
Seq 1    361  TGCTGTACATGGCCACTCAGATCTCGTCAGCCATGGAGTACCTGGAGAAGAAAAACTTCA  420
              ||||||||||||||||||||||||||||||||||||||||||||||||||||||||||||
Seq 2   1211  TGCTGTACATGGCCACTCAGATCTCGTCAGCCATGGAGTACCTGGAGAAGAAAAACTTCA  1270

Seq 1    421  TCCACAGAGATCTTGCTGCCCGAAACTGCCTGGTAGGGGAGAACCACTTGGTGAAGGTAG  480
              ||||||||||||||||||||||||||||||||||||||||||||||||||||||||||||
Seq 2   1271  TCCACAGAGATCTTGCTGCCCGAAACTGCCTGGTAGGGGAGAACCACTTGGTGAAGGTAG  1330

Seq 1    481  CTGATTTTGGCCTGAGCAGGTTGATGACAGGGGACACCTACACAGCCCATGC   532
              ||||||||||||||||||||||||||||||||||||||||||||||||||||
Seq 2   1331  CTGATTTTGGCCTGAGCAGGTTGATGACAGGGGACACCTACACAGCCCATGC   1382
```

Figure I.3 Alignment of CML patient (sample 44) *ABL1* nucleotide sequence (exons 4-7), from the e14a2 isoform [Seq 1], with *ABL1* reference sequence from GenBank NM_005157.5 [Seq 2].

```
Seq 1      1  TGAGCAGGTTGATGACAGGGGACACCTACACAGCCCATGCTGGAGCCAAGTTCCCCATCA  60
              ||||||||||||||||||||||||||||||||||||||||||||||||||||||||||||
Seq 2   1343  TGAGCAGGTTGATGACAGGGGACACCTACACAGCCCATGCTGGAGCCAAGTTCCCCATCA  1402

Seq 1     61  AATGGACTGCACCCGAGAGCCTGGCCTACAACAAGTTCTCCATCAAGTCCGACGTCTGGG  120
              ||||||||||||||||||||||||||||||||||||||||||||||||||||||||||||
Seq 2   1403  AATGGACTGCACCCGAGAGCCTGGCCTACAACAAGTTCTCCATCAAGTCCGACGTCTGGG  1462

Seq 1    121  CATTTGGAGTATTGCTTTGGGAAATTGCTACCTATGGCATGTCCCCTTACCCGGGAATTG  180
              ||||||||||||||||||||||||||||||||||||||||||||||||||||||||||||
Seq 2   1463  CATTTGGAGTATTGCTTTGGGAAATTGCTACCTATGGCATGTCCCCTTACCCGGGAATTG  1522

Seq 1    181  ACCTGTCCCAGGTGTATGAGCTGCTAGAGAAGGACTACCGCATGGAGCGCCCAGAAGGCT  240
              ||||||||||||||||||||||||||||||||||||||||||||||||||||||||||||
Seq 2   1523  ACCTGTCCCAGGTGTATGAGCTGCTAGAGAAGGACTACCGCATGGAGCGCCCAGAAGGCT  1582

Seq 1    241  GCCCAGAGAAGGTCTATGAACTCATGCGAGCATGTTGGCAGTGGAATCCCTCTGACCGGC  300
              ||||||||||||||||||||||||||||||||||||||||||||||||||||||||||||
Seq 2   1583  GCCCAGAGAAGGTCTATGAACTCATGCGAGCATGTTGGCAGTGGAATCCCTCTGACCGGC  1642

Seq 1    301  CCTCCTT  307
              |||||||
Seq 2   1643  CCTCCTT  1649
```

Figure I.4 Alignment of CML patient (sample 44) *ABL1* nucleotide sequence (exons 7-9), from the e14a2 isoform [Seq 1], with *ABL1* reference sequence from GenBank NM_005157.5 [Seq 2].

```
Seq 1      1  GTGGGAGATGGAACGCACAGACATCACCATGAAGCACAAGCTGGGCGGGGGCCAGTACGG  60
              |||||||||||||||||||||*||||||||||||||||||||||||||||||||||||||
Seq 2    894  GTGGGAGATGGAACGCACAGACATCACCATGAAGCACAAGCTGGGCGGGGGCCAGTACGG  953

Seq 1     61  GGAGGTGTACGAGGGCGTGTGGAAGAAATACAGCCTGACGGTGGCCGTGAAGACCTTGAA  120
              ||||||||||||||||||||||||||||||||||||||||||||||||||||||||||||
Seq 2    954  GGAGGTGTACGAGGGCGTGTGGAAGAAATACAGCCTGACGGTGGCCGTGAAGACCTTGAA  1013

Seq 1    121  GGAGGACACCATGGAGGTGGAAGAGTTCTTGAAAGAAGCTGCAGTCATGAAAGAGATCAA  180
              ||||||||||||||||||||||||||||||||||||||||||||||||||||||||||||
Seq 2   1014  GGAGGACACCATGGAGGTGGAAGAGTTCTTGAAAGAAGCTGCAGTCATGAAAGAGATCAA  1073
```

```
Seq 1     181   ACACCCTAACCTGGTGCAGCTCCTTGGGGTCTGCACCCGGGAGCCCCCGTTCTATATCAT   240
                |||||||||||||||||||||||||||||||||||||||||||||||||||||||||||||
Seq 2    1074   ACACCCTAACCTGGTGCAGCTCCTTGGGGTCTGCACCCGGGAGCCCCCGTTCTATATCAT   1133

Seq 1     241   CACTGAGTTCATGACCTACGGGAACCTCCTGGACTACCTGAGGGAGTGCAACCGGCAGGA   300
                |||||||||||||||||||||||||||||||||||||||||||||||||||||||||||||
Seq 2    1134   CACTGAGTTCATGACCTACGGGAACCTCCTGGACTACCTGAGGGAGTGCAACCGGCAGGA   1193

Seq 1     301   GGTGAACGCCGTGGTGCTGCTGTACATGGCCACTCAGATCTCGTCAGCCATGGAGTACCT   360
                |||||||||||||||||||||||||||||||||||||||||||||||||||||||||||||
Seq 2    1194   GGTGAACGCCGTGGTGCTGCTGTACATGGCCACTCAGATCTCGTCAGCCATGGAGTACCT   1253

Seq 1     361   GGAGAAGAAAAACTTCATCCACAGAGATCTTGCTGCCCGAAACTGCCTGGTAGGGGAGAA   420
                |||||||||||||||||||||||||||||||||||||||||||||||||||||||||||||
Seq 2    1254   GGAGAAGAAAAACTTCATCCACAGAGATCTTGCTGCCCGAAACTGCCTGGTAGGGGAGAA   1313

Seq 1     421   CCACTTGGTGAAGGTAGCTGATTTTGGCCTGAGCAGGTTGATGACAGGGGACACCTACAC   480
                |||||||||||||||||||||||||||||||||||||||||||||||||||||||||||||
Seq 2    1314   CCACTTGGTGAAGGTAGCTGATTTTGGCCTGAGCAGGTTGATGACAGGGGACACCTACAC   1373

Seq 1     481   AGCCCATGCTGGAGCCAAGTTCCCCATCAAATGGACTGCACCCGAGAGCCTGGCCTACAA   540
                |||||||||||||||||||||||||||||||||||||||||||||||||||||||||||||
Seq 2    1374   AGCCCATGCTGGAGCCAAGTTCCCCATCAAATGGACTGCACCCGAGAGCCTGGCCTACAA   1433
```

Figure I.5 Alignment of CML patient (sample 44) *ABL1* nucleotide sequence (exons 4-7), from the e6a2 isoform [Seq 1], with *ABL1* reference sequence from GenBank NM_005157.5 [Seq 2]. *Detected SNP on *ABL1* exon 4, c.720G>A.

```
Seq 1       1   AGTTCCCCATCAAATGGACTGCACCCGAGAGCCTGGCCTACAACAAGTTCTCCATCAAGT   60
                |||||||||||||||||||||||||||||||||||||||||||||||||||||||||||||
Seq 2    1391   AGTTCCCCATCAAATGGACTGCACCCGAGAGCCTGGCCTACAACAAGTTCTCCATCAAGT   1450

Seq 1      61   CCGACGTCTGGGCATTTGGAGTATTGCTTTGGGAAATTGCTACCTATGGCATGTCCCCTT   120
                |||||||||||||||||||||||||||||||||||||||||||||||||||||||||||||
Seq 2    1451   CCGACGTCTGGGCATTTGGAGTATTGCTTTGGGAAATTGCTACCTATGGCATGTCCCCTT   1510

Seq 1     121   ACCCGGGAATTGACCTGTCCCAGGTGTATGAGCTGCTAGAGAAGGACTACCGCATGGAGC   180
                |||||||||||||||||||||||||||||||||||||||||||||||||||||||||||||
Seq 2    1511   ACCCGGGAATTGACCTGTCCCAGGTGTATGAGCTGCTAGAGAAGGACTACCGCATGGAGC   1570

Seq 1     181   GCCCAGAAGGCTGCCCAGAGAAGGTCTATGAACTCATGCGAGCATGTTGGCAGTGGAATC   240
                |||||||||||||||||||||||||||||||||||||||||||||||||||||||||||||
Seq 2    1571   GCCCAGAAGGCTGCCCAGAGAAGGTCTATGAACTCATGCGAGCATGTTGGCAGTGGAATC   1630

Seq 1     241   CCTCTGACCGGCCCTCCTTTGCTGAAATCCACCAAGCCTTTGAAACAATGTTCCAGGAAT   300
                |||||||||||||||||||||||||||||||||||||||||||||||||||||||||||||
Seq 2    1631   CCTCTGACCGGCCCTCCTTTGCTGAAATCCACCAAGCCTTTGAAACAATGTTCCAGGAAT   1690

Seq 1     301   CCAGTATCTCA   311
                |||||||||||
Seq 2    1691   CCAGTATCTCA   1701
```

Figure I.6 Alignment of CML patient (sample 44) *ABL1* nucleotide sequence (exons 7-9), from the e6a2 isoform [Seq 1], with *ABL1* reference sequence from GenBank NM_005157.5 [Seq 2].
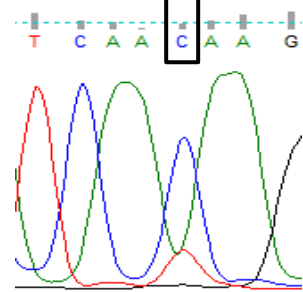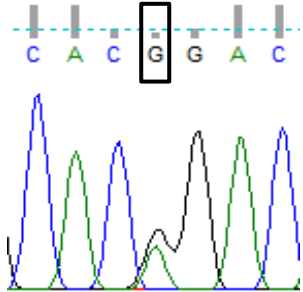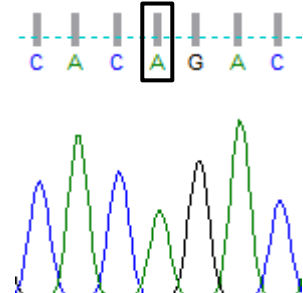
Table I.1 Single nucleotide polymorphisms detected by Sanger sequencing on patient P210 and P195 isoforms (sample 44).

BCR-ABL1 isoform (transcript)	Exon	cDNA sequence	Protein sequence	Ratio	Sequencing chromatogram
P210 (e14a2)	BCR ex.13	c.2700T>C	N900N	75 %	
P210 (e14a2)	ABL1 ex.4	c.720G>A	T240T	50 %	
P195 (e6a2)	ABL1 ex.4	c.720G>A	T240T	100 %	

Appendix II – Clinical case 54 *BCR-ABL1* transcript identification and protein structure analysis

```
Seq 1    1    CGCCGCAGTGCCATAAGCGGCACCGGCACTGCCCGGTTGTCGTGTCCGAGGCCACCATCG    60
              ||||||||||||||||||||||||||||||||||||||||||||||||||||||||||||
Seq 2    330  CGCCGCAGTGCCATAAGCGGCACCGGCACTGCCCGGTTGTCGTGTCCGAGGCCACCATCG    389

Seq 1    61   TGGGCGTCCGCAAGACCGGGCAGATCTGGCCCAACGATGGCGAGGGCGCCTTCCATGGAG    120
              ||||||||||||||||||||||||||||||||||||||||||||||||||||||||||||
Seq 2    390  TGGGCGTCCGCAAGACCGGGCAGATCTGGCCCAACGATGGCGAGGGCGCCTTCCATGGAG    449

Seq 1    121  ACGCAGAAGCCCTTCAGCGGCCAGTAGCATCTGACTTTGAGCCTCAGGGTCTGAGTGAAG    180
              ||||||||||||||||||||||||||||||||||||||||||||||||||||||||||||
Seq 2    450  ACGCAGAAGCCCTTCAGCGGCCAGTAGCATCTGACTTTGAGCCTCAGGGTCTGAGTGAAG    509

Seq 1    181  CCGCTCGTTGGAACTCCAAGGAAAACCTTCTCGCTGGACCCAGTGAAAATGACCCCAACC    240
              ||||||||||||||||||||||||||||||||||||||||||||||||||||||||||||
Seq 2    510  CCGCTCGTTGGAACTCCAAGGAAAACCTTCTCGCTGGACCCAGTGAAAATGACCCCAACC    569

Seq 1    241  TTTTCGTTGCACTGTATGATTTTGTGGCCAGTGGAGATAACACTCTAAGCATAACTAAAG    300
              ||||||||||||||||||||||||||||||||||||||||||||||||||||||||||||
Seq 2    570  TTTTCGTTGCACTGTATGATTTTGTGGCCAGTGGAGATAACACTCTAAGCATAACTAAAG    629

Seq 1    301  GTGAAAAGCTCCGGGTCTTAGGCTATAATC    330
              ||||||||||||||||||||||||||||||
Seq 2    630  GTGAAAAGCTCCGGGTCTTAGGCTATAATC    659
```

Figure II.1 Alignment of CML patient (sample 54) e1a2 nucleotide sequence [Seq 1] with *BCR-ABL1* e1a2 reference sequence from GenBank AF113911.1 [Seq 2]. Arrow indicates the breakpoint in this *BCR-ABL1* isoform.
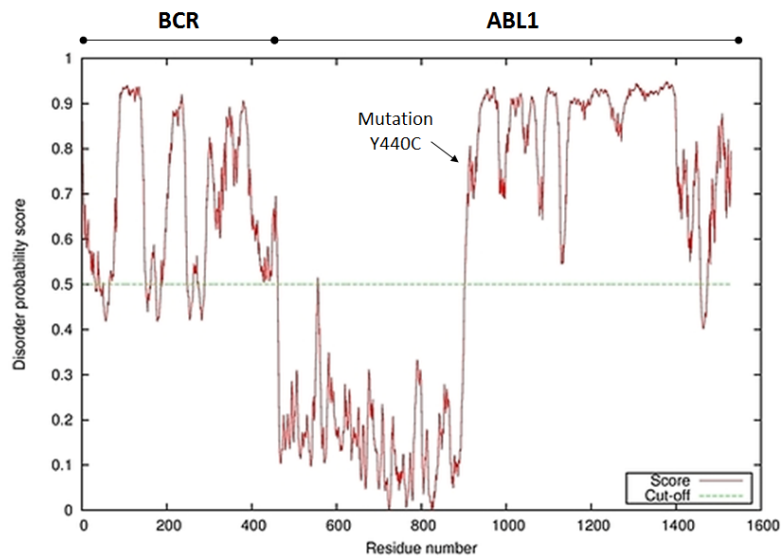

Figure II.2 DISOclust disorder prediction results. Disorder probability score by residue number in BCR-ABL1 protein harboring the Y440C on the ABL1 domain.

Table II.1 ABL1 protein alignment between different species demonstrates the conservation of the affected amino acid.

Species	AA position	Alignment
H. sapiens mutated (Ph+ LLA patient)	440	LWEIATYGMSP**C**PGIDLSQVYEL
H. sapiens wild-type	440	LWEIATYGMSP**Y**PGIDLSQVYEL
P. troglodytes	459	LWEIATYGMSP**Y**PGIDLS
M. mulatta	168	LWEIATYGMSP**Y**PGIDLSQVYEL
F. catus	459	LWEIATYGMSP**Y**PGIDLS
M. musculus	459	LWEIATYGMSP**Y**PGIDLS
G. gallus	440	LWEIATYGMSP**Y**PGIDLSQVYEL
T. rubripes	801	LWEIATYGMSP**Y**PGIDL
D. rerio	459	LWEIATYGMSP**Y**PGIDLSQ
D. melanogaster	587	LWEIATYGMSP**Y**PAIDLTDVYHK
C. elegans	509	LWEIATYGMAP**Y**PGVELSNVYGL

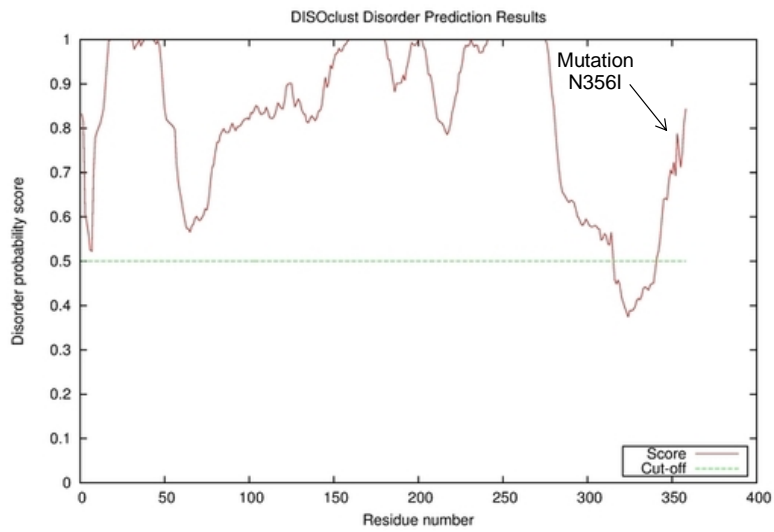**Appendix III – Clinical case 7 *BCR-ABL1* transcript identification and protein structure analysis**

Figure III.1 DISOclust disorder prediction results. Disorder probability score by residue number in C/EBPα protein harboring the N356I mutation.

Table III.1 C/EBPα protein alignment between different species demonstrates the conservation of the affected amino acid.

Species	AA position	Alignment
H. sapiens mutated (AML patient)	356	LDTLRGIFRQLPESSLVKAMGI**I**CA
H. sapiens wild-type	356	LDTLRGIFRQLPESSLVKAMG**N**CA
C. sabaeus	354	LDTLRGIFRQLPESSLVKAMG**N**CA
P. alecto	354	LDTLRGIFRQLPESSLVKAMG**N**CA
M. auratus	367	LDTLRGIFRQLPESSLVKAMG**N**CA
C. jacchus	356	LDTLRGIFRQLPESSLVKAMG**N**CA
S. scrofa	352	LDTLRGIFRQLPESSLVKAMG**N**CA
R. norvegicus	356	LDTLRGIFRQLPESSLVKAMG**N**CA
M. musculus	357	LDTLRGIFRQLPESSLVKAMG**N**CA
C. porcellus	314	IFRQLPESSLVKAMS**N**CA
B. taurus	351	FRQLPESSLVKAMG**N**CA

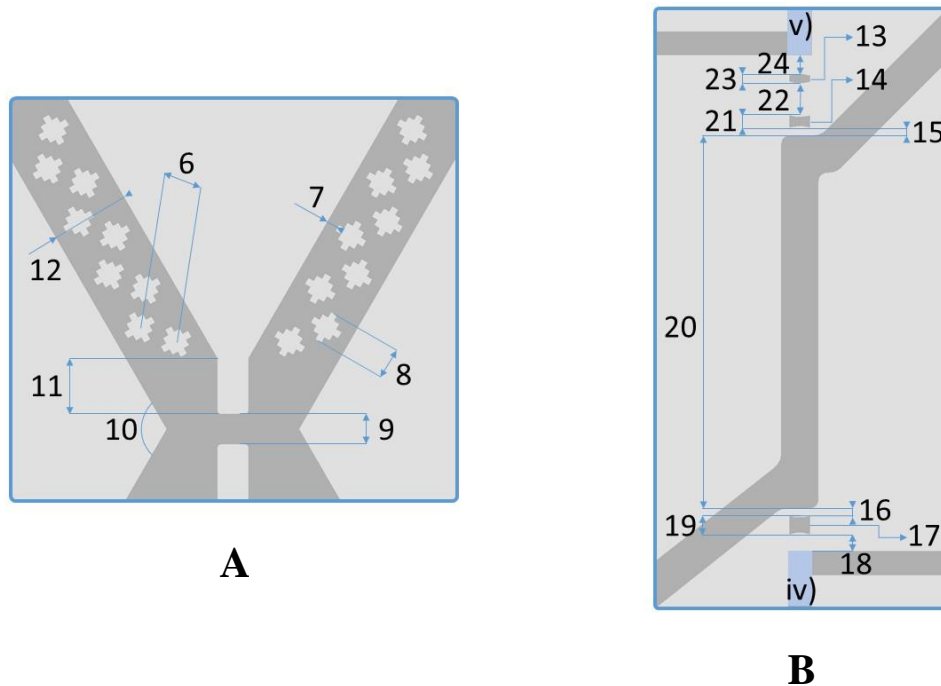**Appendix IV – Detailed microfluidic chip design**

Figure IV.1 Microfluidic chip – Mixing and detection design.

A) Mixing microchannel - detailed view. 6- distance between diamond shaped obstacles: 128μm; 7- distance between diamond shaped obstacles and wall: 40μm; 8- diamond shaped obstacle width: 100μm; 9- throttle width: 100μm; 10- Rhombi angle: 120º; 11- Gap between throttle and channel: 12- 180μm; mixer channel width: 260μm.

B) Optical detection microchannel – detailed view. 13- 3rd lens curvature radius/width: 180μm/110μm; 14- 2nd lens curvature radius/width: 210μm/110μm; 15- minimum (min.) distance between 2nd lens and channel: 42.5μm; 16- min. distance between 1st lens and channel: 41μm; 17- 1st lens curvature radius/width: 175μm/110μm; 18- min. distance between 1st lens and optical fiber: 91μm; 19- 1st lens maximum (max.) thickness: 98μm; 20- Optical path length inside the channel: 2mm; 21- 2nd lens max. thickness: 65μm; 22- min. distance between 2nd and 3rd lenses: 173μm; 23-3rd lens max. thickness: 50μm; 24- distance between 3rd lens and optical fiber: 100μm. iv) and v) mark the spot of input and output optical fibers, respectively, with a groove width of 127μm.
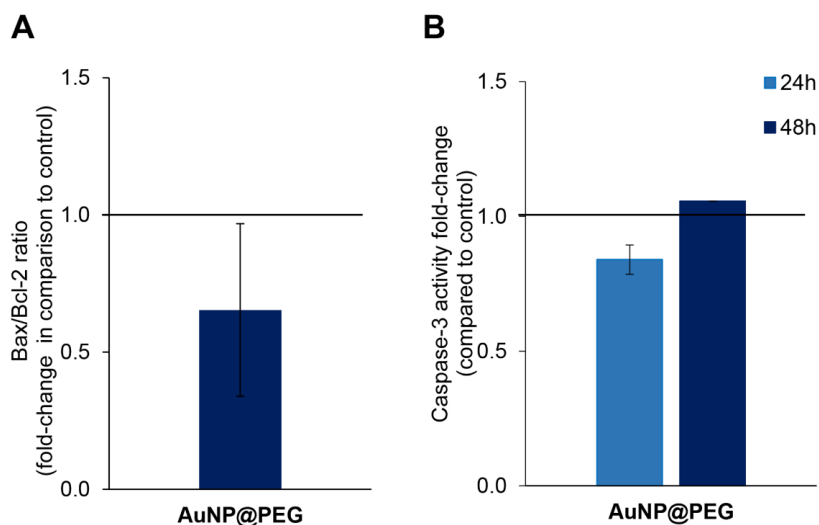
Figure V.1 Effect of AuNP@PEG (0.6 nM) on K562 apoptotic index (Bax/Bcl-2 ratio) (A) and on caspase-3/7 activity (B). Threshold represents control condition (untreated cells). Error bars represent the standard error of the mean of three independent experiments.
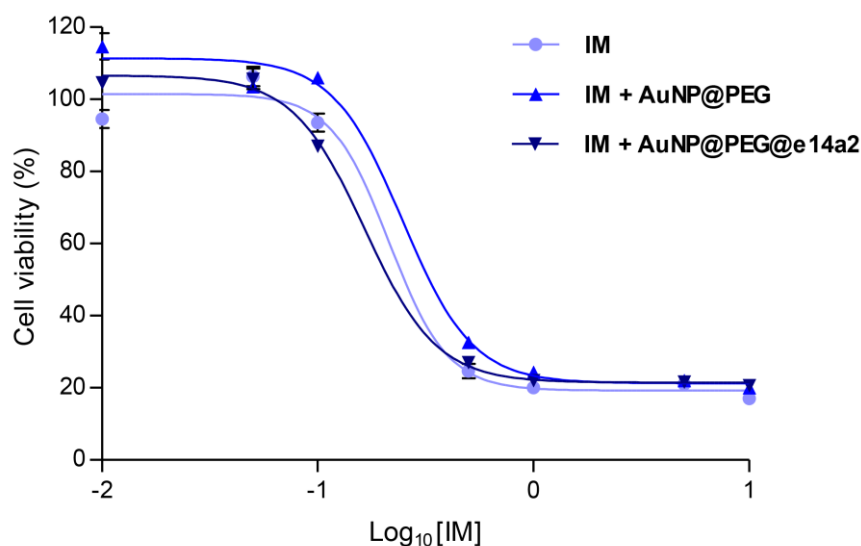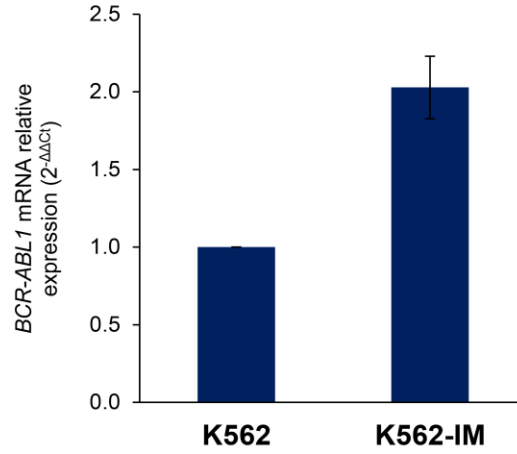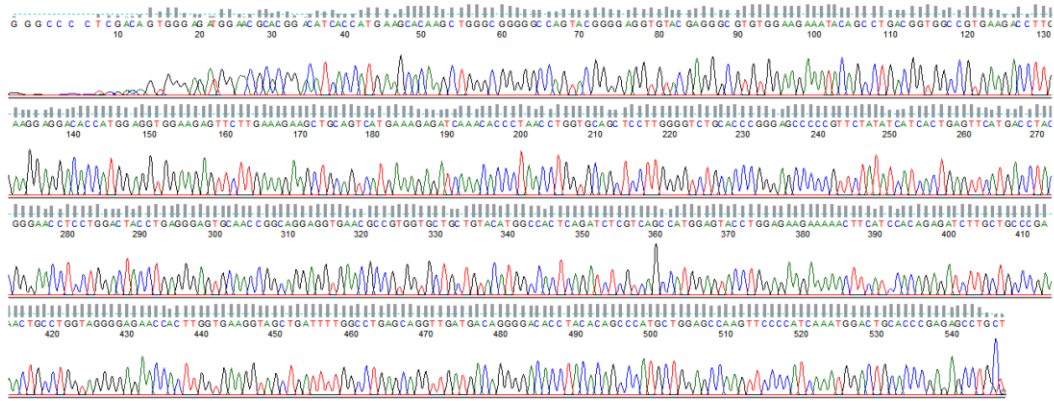

Figure V.2 Concentration-response plots obtained after a 48 h-exposure of K562 cells to IM alone (0.01-10 µM) or combined with nanoconjugates (0.6 nM). Cell viability was measured via MTS assay. Error bars represent the standard error of the mean of three independent experiments.
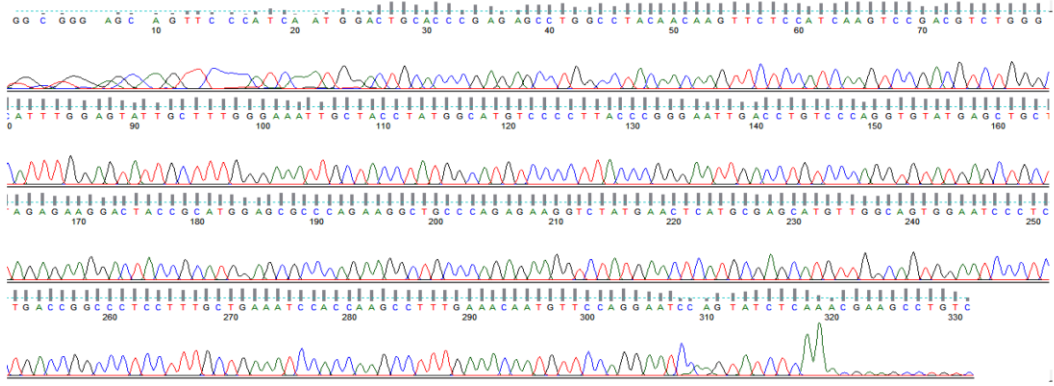
A

BCR-ABL1 mRNA relative expression (2^{-\Delta\Delta Ct})

2.5
2.0
1.5
1.0
0.5
0.0

K562   K562-IM

B

C

B1

```
Query  1     AGTGGGAGATGGAACGCACGGACATCACCATGAAGCACAAGCTGGGCGGGGGCCAGTACG   60
             ||||||||||||||||||||||||||||||||||||||||||||||||||||||||||||
Sbjct  893   AGTGGGAGATGGAACGCACGGACATCACCATGAAGCACAAGCTGGGCGGGGGCCAGTACG   952

Query  61    GGGAGGTGTACGAGGGCGTGTGGAAGAAATACAGCCTGACGGTGGCCGTGAAGACCTTGA   120
             ||||||||||||||||||||||||||||||||||||||||||||||||||||||||||||
Sbjct  953   GGGAGGTGTACGAGGGCGTGTGGAAGAAATACAGCCTGACGGTGGCCGTGAAGACCTTGA   1012

Query  121   AGGAGGACACCATGGAGGTGGAAGAGTTCTTGAAAGAAGCTGCAGTCATGAAAGAGATCA   180
             ||||||||||||||||||||||||||||||||||||||||||||||||||||||||||||
Sbjct  1013  AGGAGGACACCATGGAGGTGGAAGAGTTCTTGAAAGAAGCTGCAGTCATGAAAGAGATCA   1072

Query  181   AACACCCTAACCTGGTGCAGCTCCTTGGGGTCTGCACCCGGGAGCCCCCGTTCTATATCA   240
             ||||||||||||||||||||||||||||||||||||||||||||||||||||||||||||
Sbjct  1073  AACACCCTAACCTGGTGCAGCTCCTTGGGGTCTGCACCCGGGAGCCCCCGTTCTATATCA   1132

Query  241   TCACTGAGTTCATGACCTACGGGAACCTCCTGGACTACCTGAGGGGAGTGCAACCGGCAGG   300
             |||||||||||||||||||||||||||||||||||||||||||||||||||||||||||
Sbjct  1133  TCACTGAGTTCATGACCTACGGGAACCTCCTGGACTACCTGAGGGGAGTGCAACCGGCAGG   1192

Query  301   AGGTGAACGCCGTGGTGCTGCTGTACATGGCCACTCAGATCTCGTCAGCCATGGGAGTACC   360
             ||||||||||||||||||||||||||||||||||||||||||||||||||||||||||||
Sbjct  1193  AGGTGAACGCCGTGGTGCTGCTGTACATGGCCACTCAGATCTCGTCAGCCATGGGAGTACC   1252

Query  361   TGGAGAAGAAAAACTTCATCCACAGAGATCTTGCTGCCCGAAACTGCCTGGTAGGGGGAGA   420
             ||||||||||||||||||||||||||||||||||||||||||||||||||||||||||||
Sbjct  1253  TGGAGAAGAAAAACTTCATCCACAGAGATCTTGCTGCCCGAAACTGCCTGGTAGGGGGAGA   1312

Query  421   ACCACTTGGTGAAGGTAGCTGATTTTGGCCTGAGCAGGGTTGATGACAGGGGACACCTACA   480
             ||||||||||||||||||||||||||||||||||||||||||||||||||||||||||||
Sbjct  1313  ACCACTTGGTGAAGGTAGCTGATTTTGGCCTGAGCAGGGTTGATGACAGGGGACACCTACA   1372

Query  481   CAGCCCATGCTGGAGCCAAGTTCCCCATCAAATGGACTGCACCCGAGAGCCTG   533
             ||||||||||||||||||||||||||||||||||||||||||||||||||||
Sbjct  1373  CAGCCCATGCTGGAGCCAAGTTCCCCATCAAATGGACTGCACCCGAGAGCCTG   1425
```

C1

```
Query  1     AATGGACTGCACCCGAGAGCCTGGCCTACAACAAGTTCTCCATCAAGTCCGACGTCTGGG   60
             ||||||||||||||||||||||||||||||||||||||||||||||||||||||||||||
Sbjct  1403  AATGGACTGCACCCGAGAGCCTGGCCTACAACAAGTTCTCCATCAAGTCCGACGTCTGGG   1462

Query  61    CATTTGGAGTATTGCTTTGGGAAATTGCTACCTATGGCATGTCCCCTTACCCGGGAATTG   120
             ||||||||||||||||||||||||||||||||||||||||||||||||||||||||||||
Sbjct  1463  CATTTGGAGTATTGCTTTGGGAAATTGCTACCTATGGCATGTCCCCTTACCCGGGAATTG   1522

Query  121   ACCTGTCCCAGGTGTATGAGCTGCTAGAGAAGGACTACCGCATGGAGCGCCCAGAAGGCT   180
             ||||||||||||||||||||||||||||||||||||||||||||||||||||||||||||
Sbjct  1523  ACCTGTCCCAGGTGTATGAGCTGCTAGAGAAGGACTACCGCATGGAGCGCCCAGAAGGCT   1582

Query  181   GCCCAGAGAAGGTCTATGAACTCATGCGAGCATGTTGGCAGTGGAATCCCTCTGACCGGC   240
             ||||||||||||||||||||||||||||||||||||||||||||||||||||||||||||
Sbjct  1583  GCCCAGAGAAGGTCTATGAACTCATGCGAGCATGTTGGCAGTGGAATCCCTCTGACCGGC   1642

Query  241   CCTCCTTTGCTGAAATCCACCAAGCCTTTGAAACAATGTTCCAGGAATCCAGTATCTCA   299
             |||||||||||||||||||||||||||||||||||||||||||||||||||||||||||
Sbjct  1643  CCTCCTTTGCTGAAATCCACCAAGCCTTTGAAACAATGTTCCAGGAATCCAGTATCTCA   1701
```

195

Figure V.3 Assessment of *BCR-ABL1* gene expression and mutational status of K562 cells exposed to increasing concentrations of IM (K562-IM). **A)** *BCR-ABL1* gene expression on K562-IM cells was evaluated via qPCR. Data was analyzed by the comparative threshold cycle (Ct) method ($2^{-\Delta\Delta Ct}$), where relative gene expression is given by quantification of *BCR-ABL1* relative to internal control gene (*18S*), normalized to control condition (parental K562 cells). Error bars represent the standard error of the mean of three independent experiments. **B)** Sequencing chromatogram of *ABL1* of K562-IM cells: exons 4-7. **B1)** Exons 4-7 query sequence alignment against *ABL1* reference mRNA sequence (GenBank NM_005157.5) **C)** Sequencing chromatogram of *ABL1* of K562-IM cells: exons 7-9. **C1)** Exons 7-9 query sequence alignment against *ABL1* reference mRNA sequence (GenBank NM_005157.5).